



Application of Dimethyl Ether in Compression Ignition Engines

Hansen, Kim Rene

Publication date:
2013

Document Version
Publisher's PDF, also known as Version of record

[Link back to DTU Orbit](#)

Citation (APA):
Hansen, K. R. (2013). *Application of Dimethyl Ether in Compression Ignition Engines*. Technical University of Denmark.

General rights

Copyright and moral rights for the publications made accessible in the public portal are retained by the authors and/or other copyright owners and it is a condition of accessing publications that users recognise and abide by the legal requirements associated with these rights.

- Users may download and print one copy of any publication from the public portal for the purpose of private study or research.
- You may not further distribute the material or use it for any profit-making activity or commercial gain
- You may freely distribute the URL identifying the publication in the public portal

If you believe that this document breaches copyright please contact us providing details, and we will remove access to the work immediately and investigate your claim.

Application of Dimethyl Ether in Compression Ignition Engines

Kim Rene Hansen

October 2012

Application of Dimethyl Ether in Compression Ignition Engines

2012

By
Kim Rene Hansen

Copyright: Reproduction of this publication in whole or in part must include the customary bibliographic citation, including author attribution, report title, etc.

Published by: Department of Mechanical Engineering, Nils Koppels Allé, Building 403, DK-2800 Kgs. Lyngby, Denmark

Request re-

port from: www.mek.dtu.dk

ISSN: [0000-0000] (electronic version)

ISBN: [000-00-0000-000-0] (electronic version)

ISSN: [0000-0000] (printed version)

ISBN: [000-00-0000-000-0] (printed version)

Preface

This thesis is submitted in partial fulfillment of the requirements for the PhD degree at the Technical University of Denmark.

The study was carried out at the Department of Mechanical Engineering, Section of Thermal Energy from September 2007 to October 2012. Supervisor was Associate Professor Jesper Schramm, DTU Mekanik and co-supervisors Professor Emeritus Spencer Sorenson, DTU Mekanik and Associate Professor Ion Marius Sivebæk, DTU Mekanik.

The PhD study was funded by the Technical University of Denmark and included membership of the research school DCAMM (Danish Center for Applied Mathematics and Mechanics).

I would like to thank my supervisors and the other members of the internal combustion engine group at DTU for the invaluable guidance and support throughout the project. Special thanks go to Jakob Duus Dolriis and Christoffer Hansson for the excellent engine design work they carried out while, during their master project, they built the final prototype that became test engine for this study. Thanks also to Jacob Jeppesen who did the calculations that resulted in a correction to the cylinder volume function for the test engine during his bachelor project. Finally, a thank you to the technical staff at the department who helped manufacture parts for the experimental work.

Kim Rene Hansen
Lyngby, October 2012

Abstract

This study has its roots in two separate events at the Department of Mechanical Engineering at DTU. In 1995 the first attempt to operate a diesel engine on dimethyl ether (DME) was successfully concluded. In 2004 the department decided to compete in the vehicle fuel efficiency competition Shell Eco-Marathon.

The diesel engine test results from 1995 showed that DME is a superb diesel fuel. DME is easy to ignite by compression ignition and it has a molecular structure that results in near-zero emission of particulates when burned. These are features of a fuel that are highly desirable in a diesel engine. The challenges with DME as a diesel engine fuel are mainly related to poor lubricity and incompatibility with a range of elastomers commonly used for seals in fuel injection systems. This means that although DME burns well in a diesel engine designing a fuel injection system for DME is challenging. Since then studies have revealed that the injection pressure for DME does not have to be as high as with diesel to achieve satisfactory performance. This opens for a larger range of possibilities when designing injection systems.

In the period from 2004 to 2009 the DME engine was perfected for use in the car DTU was racing in the Shell Eco-Marathon. The car won the competition in 2007 and 2009. The concept was to use a direct injected two-stroke engine operating with an injection pressure of only 150 bars. A piston pump operating without metal-to-metal contact had been developed to supply that pressure. The elastomer seals that provided the sealing instead of the metal-to-metal contact could do that because of the low injection pressure.

The engine developed in this way was based on a 50cc Peugeot two-stroke engine. The fuel injector used was a Bosch HDEV originally developed for direct injection of gasoline in automotive engines at up to 200 bars pressure. This injector was too large to provide for normal diesel engine operation on an engine of only 50cc. Although DME ignites easily all the fuel was injected before combustion started due to the high flow rate. Attempts to find a smaller injector that was also able to deal with the required injection pressure and also DME were not fruitful. Despite the fact that this combustion mode was more a result of necessity than choice the engine efficiency was higher than 30% which is good for an engine of this size. Up until this stage engine design and testing work was done with a focus on efficiency not emissions.

The objective of this study was to investigate the combustion mode and the emissions of the engine and to investigate possible improvements. It has been

shown that the engine operates in a partially premixed mode. It does so with emissions of NO_x that are an order of magnitude lower than for traditional automotive diesel engines. Emissions of carbon monoxide and unburned hydrocarbons were quite high though. Experiments with an oxidation catalyst revealed that carbon monoxide could effectively be converted to carbon dioxide but the low exhaust temperature did not allow for full oxidation of the unburned hydrocarbons.

Resumé

Dette studie har sin oprindelse i to separate hændelser på Institut for Mekanisk Teknologi på DTU. I 1995 blev en dieselmotor for første gang kørt på DME, og med succes. I 2004 besluttede instituttet at deltage i Shells konkurrence for brændstoføkonomi: Shell Eco-Marathon.

Testresultaterne fra forsøgene i 1995 viste at DME er et fremragende dieselmotorbrændstof. DME antændes nemt ved kompressionstænding og det har en molekylær struktur, der gør, at der praktisk taget ikke kommer partikler fra forbrænding af DME. Dette er egenskaber, der er meget ønskelige for et dieselmotorbrændstof. Udfordringerne ved anvendelse af DME i dieselmotorer er den ringe smøreevne og inkompatibilitet med en række af de elastomerer, der typisk anvendes som tætningselementer i brændstofindsprøjtningssystemer. Dette betyder, at selvom DME brænder fint i en dieselmotor, så er det en udfordring at designe et pålideligt brændstofindsprøjtningssystem. Siden da har studier vist, at det ikke er nødvendigt at bruge samme høje indsprøjtningstryk, som man gør i dieselmotorer, til DME. Dette åbner en række muligheder, hvad angår design af indsprøjtningssystemet.

I perioden 2004-2009 blev DME-motoren optimeret til brug i den bil, som DTU deltog med ved Shell Eco-Marathon. Bilen vandt konkurrencen i 2007 og 2009. Konceptet var baseret på en direkte indsprøjtet totaktsmotor med et indsprøjtningstryk på kun 150 bar. En stempelpumpe uden direkte metal-metal kontakt var blevet udviklet til at levere indsprøjtningstrykket. De elastomértætninger, der blev anvendt i stedet for metal-metal kontakt, fungerede pga. det lave indsprøjtningstryk.

Motoren var baseret på en 50cc Peugeot totaktsmotor. Brændstofindsprøjtningssydysen der blev anvendt var en Bosch HDEV 5, som oprindeligt var udviklet til direkte indsprøjtning af benzin i bilmotorer ved op til 200 bar. Denne indsprøjtningssydse var for stor til at opnå en almindelig dieselforbrændingsproces i en motor på kun 50cc. Selvom DME antænder let, så blev alt brændstoffet indsprøjtet før forbrændingen påbegyndte, pga. den høje indstrømningsrate. Forsøg på at finde en mindre indsprøjtningssydse, der også kunne klare det nødvendige indsprøjtningstryk, lykkedes ikke.

På trods af, at den resulterende forbrændingsproces mere var et resultat af nødvendighed end design, så var motorvirkningsgraden over 30%, hvilket er godt for en motor af denne størrelse. Indtil dette tidspunkt var alt udviklings- og testarbejde gjort med fokus på virkningsgrad og ikke emissioner.

Formålet med dette studie er, at undersøge forbrændingsprocessen og emissionerne fra motoren, og undersøge mulige forbedringer. Det er påvist, at motoren kører med en delvist forblandet forbrændingsproces. Dette resulterer i NO_x emissioner der er en størrelsesorden lavere end traditionelle dieselmotorer til biler. Udslippet af kulmonoxid og uforbrændte kulbrinter er ret højt. Eksperimenter med en oxydationskatalysator viste, at kulmonoxiden effektivt kunne omdannes til kuldioxid, men den lave udstødstemperatur gjorde det ikke muligt at omsætte alle kulbrinterne.

Content

| | |
|---|------------|
| ABSTRACT..... | 4 |
| RESUMÉ..... | 6 |
| 1. INTRODUCTION | 10 |
| 1.1 OUTLINE OF THESIS..... | 10 |
| 1.2 CONTEXT | 12 |
| 1.3 DME AS AN ENERGY CARRIER..... | 14 |
| 1.4 COMMERCIALIZATION OF DME..... | 22 |
| 1.5 STATE OF THE ART - DME AS AN ENGINE FUEL | 24 |
| 1.6 MOTIVATION AND OBJECTIVES..... | 28 |
| 1.7 METHODS..... | 28 |
| 2. COMBUSTION REGIME | 29 |
| 3. EXPERIMENTAL SETUP..... | 37 |
| 4. FLAME TEMPERATURES | 38 |
| 5. CYCLE SIMULATION | 41 |
| 6. PERFORMANCE AND EMISSIONS | 55 |
| 7. OPTICAL ACCESS CYLINDER HEAD | 60 |
| 8. INDIRECT INJECTION | 66 |
| 9. EGR..... | 72 |
| 9.1 THEORY | 72 |
| 9.2 EXPERIMENTS | 74 |
| 10. AFTERTREATMENT..... | 76 |
| 10.1 PERFORMANCE OF AN OXIDATION CATALYSTS | 76 |
| 10.2 EXPERIMENTAL SETUP..... | 76 |
| 10.3 RESULTS | 77 |
| 11. HEAT TRANSFER | 80 |
| 11.1 EXPERIMENTAL RESULTS FOR MOTORING | 80 |
| 11.2 CFD..... | 83 |
| 12. COMBUSTION NOISE | 106 |
| 12.1 PEAK PRESSURE RISE RATE (PPRR)..... | 106 |
| 13. ESTIMATION OF PASSENGER CAR PERFORMANCE..... | 109 |
| 13.1 NEDC CYCLE SIMULATIONS..... | 109 |
| 14. DME FUEL PUMP | 115 |
| 14.1 CONCEPT | 115 |
| 14.2 DESIGN..... | 115 |
| 14.3 PERFORMANCE..... | 116 |

| | | |
|------|---------------------------|------------|
| 14.4 | DURABILITY | 117 |
| 15. | CONCLUSION | 118 |
| 16. | NOMENCLATURE | 119 |

1. Introduction

1.1 Outline of Thesis

A short description of the role of the individual chapters is given below.

1.1.1 Chapter 1

Introduces the field of energy to the reader. It then goes on to explain the possibilities and challenges with DME as a fuel. A review of earlier work related to the application of DME in compression ignition engines is given. Motivation, objectives and methods conclude the chapter.

1.1.2 Chapter 2

Reviews the possible ways to burn fuel in an internal combustion engine and places the current study in relation to those.

1.1.3 Chapter 3

Describes the engine and test setup being used.

1.1.4 Chapter 4

Presents flame temperature calculations for traditional fuels and DME in order to clarify if DME deviates in a way that could have an effect on emissions.

1.1.5 Chapter 5

Describes and shows results from a cycle simulation made during the study. The cycle simulation is used in later chapters to represent the ideal premixed compression ignition two-stroke engine compared to the results of the experiments.

1.1.6 Chapter 6

Compares the performance and emissions of the test engine with the cycle simulation.

1.1.7 Chapter 7

Describes the design and test results with an optically accessible cylinder made to gain knowledge about the fuel distribution in the combustion chamber of the test engine.

1.1.8 Chapter 8

Shows the design and test results of an indirect injection cylinder head that was made to improve the mixing of fuel and air.

1.1.9 Chapter 9

Describes test results with increased internal exhaust gas recirculation by means of throttling.

1.1.10 Chapter 10

Explains the performance of an oxidation catalyst that was added to the exhaust system.

1.1.11 Chapter 11

Presents CFD calculations that investigate the effect of engine size and combustion chamber shape on heat transfer rates and blowby.

1.1.12 Chapter 12

Gives an assessment of the engines noise level and harshness of operation based on measured peak pressure rise rates.

1.1.13 Chapter 13

Estimates the performance of an engine of this type in a car.

1.1.14 Chapter 14

Gives a summary of the progress made at DTU towards a reliable fuel pump for DME.

1.2 Context

Modern societies are strongly dependent on easy access to cheap and reliable energy. In principle there are only two ways in which energy is made available for human exploitation.

1. Energy from the Sun
2. Energy existing in the Earth-Moon system at its creation

The energy in the direct sunlight that hits the Earth's surface is more than enough to cover human needs but at the current state of technological development it is impractical and expensive to collect and distribute direct solar energy for all human purposes. Solar energy that is converted by natural processes into kinetic energy, potential energy and into chemical bonds is denser and can be easier to use.

Tidal energy is an example of energy existing in the Earth-Moon system at its creation. Tidal energy can be extracted from water motion caused by the periodic variations in gravitational attraction between the Earth and the Moon. Another example is geothermal energy. Most of the geothermal energy is released by on-going radioactive decay in the Earth's core. Both tidal and geothermal energy are being actively researched and some installations are in use but the contribution to the total energy use is small.

Energy release by radioactive processes can also be realized on the Earth's surface. This is currently done in nuclear fission reactors of which there exist more than 400 worldwide. Unfortunately the use of radioactivity involves the risk of radiation leaking to the environment which represents a real risk to both humans and other forms of life. Nuclear fusion is an alternative technology that involves a significantly smaller risk but it is still a developing technology. Both fission and fusion reactors also utilize energy stored in the Earth-Moon system at its creation.

As mentioned, sunlight transformed into other types of energy can be easier to use than direct sunlight. These types of energy are:

- Wind
- Wave
- Hydro
- Fossil fuels
- Bio fuels

Fossil fuels have been in use for more than a century. Indeed the development of fossil fuel resources has driven the industrial development for the last 150 years. Fossil fuels constitute the type of cheap and reliable energy that promotes business and industry. This is mainly because fossil fuels are energy dense and can be easily stored. Actually storage of energy in any other form than hydrocarbons is difficult to achieve. With the notable exception of the potential energy in the dams behind hydro power plants human civilization has so far been incapable of storing large amounts of energy for later use. This is one of the reasons that wind and wave power have not played a major role in the energy sector until recently. The availability of wind and wave energy is periodic in nature and the lack of a suitable way of storing energy for periods of no wind or wave activity is a hindrance to more widespread exploitation. The fact that wind power has gotten some success recently is due to careful administration of the electrical grids that allow for some integration of periodic production. Coal fired power plants, nuclear power plants and hydroelectric power plants can be regulated up and down corresponding to variations in wind power production.

Coal, oil and gas are all fossil fuels that consist primarily of hydrogen and carbon in different combinations. They originate from carbon fixation in plant material by photosynthesis that occurred in earlier geological periods, either in the form of plant material directly or organisms that feed upon the plant material. Burning fossil fuels to release energy thus releases carbon to the atmosphere, in the form of CO_2 , which was captured millions of years ago. This increases the concentration of CO_2 in the atmosphere and changes the radiation properties of it leading to higher surface temperatures on Earth. This so-called greenhouse effect has been heavily debated but is now considered a reality by the majority of scientists in the field.

This is one of the primary reasons for the interest in biofuels. Biofuels are hydrocarbons that have been produced from plant material, also called biomass, which has recently captured carbon from the atmosphere. In this way there is no net contribution to atmospheric CO_2 when they are burned. Another reason for the interest in biofuels is the fact that fossil fuel reservoirs are distributed unevenly on Earth. Many industrialized nations are not able to meet their demands without importing fossil fuels which makes their industry production vulnerable. Most countries could supply at least part of their energy needs by producing biofuels and in this way reduce their dependency on foreign fossil fuels. The challenge with biofuels is that a significant portion of the biomass that is available is already used for other purposes most notably food. Initial progress in biofuels production also quickly resulted in increased food prices [1], a result that is clearly not desirable. Following this, focus has turned towards so-called second generation biofuels that are made from the non-food parts of biomass. Dimethyl ether belongs to this category. In fact, DME can be made from a variety of sources including waste, so although DME is also a second generation biofuel it is more correct to simply state that DME is a synthetic fuel.

Transportation represents a special challenge when it comes to energy supply. Because the energy required to propel a vehicle has to be brought along in the vehicle only a few

energy storage and conversion options are practical. By far the most common method is to use a liquid fossil fuel that is converted to mechanical work in an internal combustion engine. Using a liquid makes it easy to transport the fuel inside the vehicle and also to refuel the vehicle. The commercial success of the internal combustion engine as the energy conversion unit is related to its low weight, low price and its durability. The compression ignition engine is the most energy efficient of the internal combustion engines and this thesis presents an alternative way to use the synthetic fuel dimethyl ether in a compression ignition engine.

1.3 DME as an Energy Carrier

DME has been in use for many years as an aerosol propellant. It is a colorless, odorless and non-toxic gas with a vapor pressure suitable for driving for example hair lacquer out of a can. It is also a byproduct that is formed during the production of methanol. In the early 1990's the Danish company Haldor Topsøe A/S, who designs methanol production plants, considered if it was possible to use this byproduct as an engine fuel. This was tested at DTU and in 1995 a paper was published with the first experimental results using a diesel engine [2]. The results showed that DME was an excellent diesel engine fuel with respect to engine efficiency and emissions. With respect to engine durability there were problems because of the very low lubricity of DME and incompatibility with a range of polymers.

These first results generated much interest in the scientific community and the use of DME as a fuel has been explored globally since. Japan, South Korea and China have been at the forefront of this development. The main conclusions regarding the use of DME in engines have not changed much since the original paper from 1995. Significant progress has been made with respect to compatible materials and fuel system design but an off-the-shelf cheap and durable high pressure fuel injection system for pure DME is still not available.

This situation is one of the primary motivations for the studies described in this thesis: Is it possible to design an engine that can use DME as efficiently as a diesel engine but without the need for a costly high pressure fuel injection system?

At this point the reader may argue: Why bother with engines in the first place? The future belongs to electric and fuel cell vehicles!

1.3.1 Electricity and Hydrogen vs. Hydrocarbons

The energy density of liquid hydrocarbons is much higher than what can be attained with batteries. Energy density is also low for hydrogen which is the best fuel for fuel cells. See Figure 1.

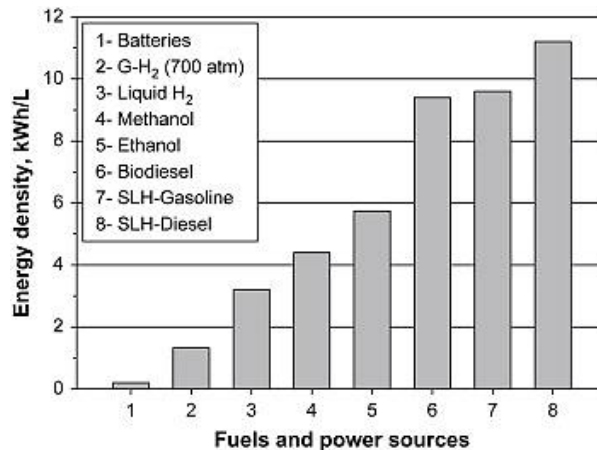


Figure 1 - Volumetric energy densities of selected energy carriers [3]

This makes hydrocarbons a good choice for vehicles and it is one of the main reasons for them being successful in transportation for the last 100 years. But hydrocarbons from fossil sources are a finite resource and the contribution of CO₂ to the atmosphere from their use is a problem in terms of climate change. On top of this there are problems with other harmful emissions when burning hydrocarbons in an engine such as NO_x and particulates. But these problems are not an unavoidable result of the use of the hydrocarbons themselves. If hydrocarbons could be produced in a sustainable, CO₂-neutral way and burned in engines without significant harmful emissions they would still be a very efficient way of storing energy in a vehicle. In fact, the high energy density of hydrocarbons contributes to a lower weight of the vehicle and thereby a lower energy consumption to drive it forward compared to a vehicle powered by for example electrical batteries. Three different ways of supplying energy to the transportation sector are illustrated in the following figures.

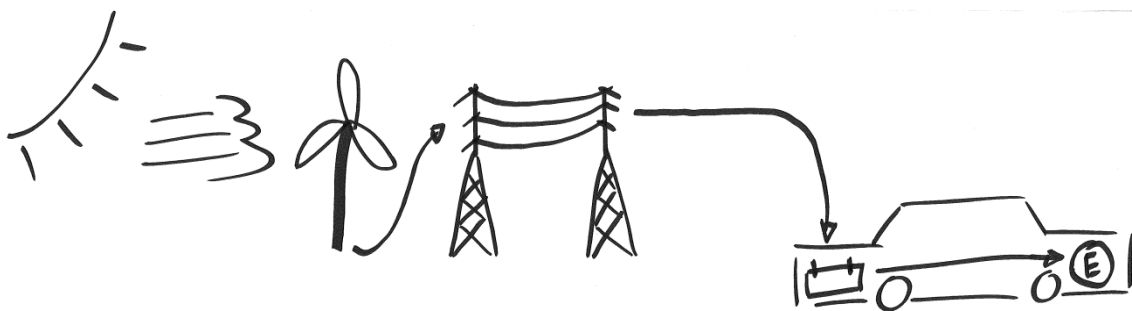


Figure 2 - An electric route: Sun → wind → grid → battery → electric motor

The electric route is simple and efficient but there is currently no way of storing large amounts of energy to be used for periods of no wind. The energy density of a vehicle battery is low and battery cost and lifetime are problematic issues.



Figure 3 – A hydrogen route: Sun → wind → electrolysis → hydrogen → fuel-cell → electric motor

The hydrogen route is more complex and less efficient compared to the electric route. Storage of energy is possible but not trivial, especially not in the vehicle. Both the fuel cell and the storage facility for hydrogen in the vehicle are costly at the current state of development.

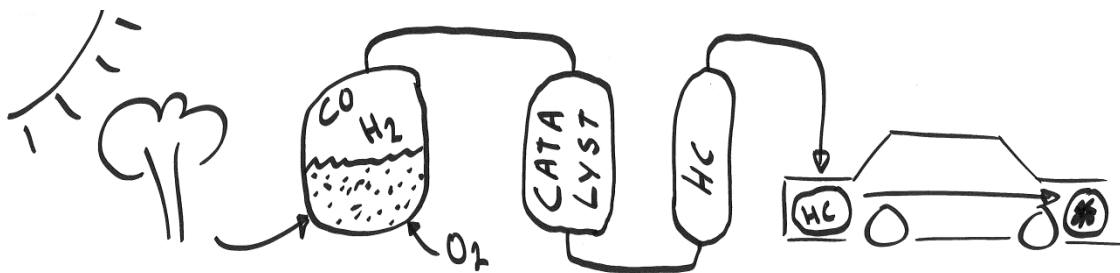


Figure 4 – A hydrocarbon route: Sun → biomass → gasification → hydrocarbons → combustion engine

The hydrocarbon route is also less efficient than the electric route but the storage of energy is trivial and the installations in the vehicle are proven and cheap technologies.

There are many other ways of producing energy for vehicles in a CO₂-neutral way than those illustrated above but the intent is just to show that hydrocarbons are merely energy carriers just like electricity and hydrogen. The major benefits of hydrocarbons are how easy they can be transported and stored.

Although DME needs to be under a moderate pressure in order to be in its liquid state it is still much easier and cheaper to handle than liquid hydrogen and the existing infrastructure for liquefied petroleum gas (LPG) can be used for DME with minor modifications.

Figure 4 shows one possible CO₂-neutral hydrocarbon route: Gasification and conversion of biomass to hydrocarbon fuel. There are a number of other possible hydrocarbon routes.

The following section will describe why the author considers DME to be especially interesting amongst the hydrocarbon energy carriers.

1.3.2 Well-to-wheel efficiency

If an alternative fuel is to have anything more than academic interest it is necessary to understand and evaluate a number of issues related to its use.

- Compatibility with engineering materials
- Customer perception
- Economy
- Energy density
- Harmful emissions during production and use
- Infrastructure
- Safety and health
- Sustainable availability

The list is alphabetically ordered. The political environment will to some extent determine the ranking of some of the issues so it is difficult once and for all to determine the merits of a new fuel. Some of the hard numbers that quantify the technical performance of DME will be defined and discussed in the following section.

DME must be viewed as an energy carrier and not an energy source since it cannot be mined or drilled. The earth's crust or atmosphere does not contain significant quantities of DME.

DME is a synthetic fuel that can be produced in different ways. Energy, carbon, hydrogen and oxygen must be available for this to be possible. This is the case for all synthetic fuels, but DME has a number of advantages over the other synthetic fuels. These will be described here by comparing them to some other alternative fuels.

At first a distinction is made between production of fuel (Well-to-Tank) and consumption of fuel (Tank-to-Wheel). This way of distinguishing between production and consumption is illustrated in Figure 5.

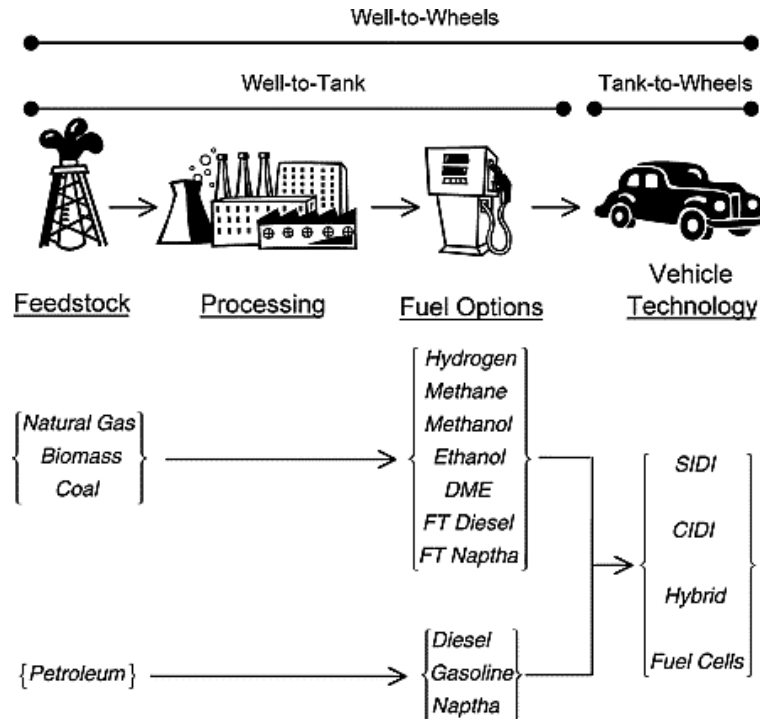


Figure 5 - Well-to-tank-to-wheel [4]

1.3.3 Well-to-tank efficiency

To evaluate the efficiency of the production the so-called well-to-tank efficiency can be used. It is defined as:

$$\eta_{\text{WTT}} = \frac{\text{energy}_{\text{fuel}}}{\sum \text{energy}_i} \quad (1)$$

i = energy in feedstock, feedstock recovery, fuel manufacturing, fuel distribution etc.

Figure 6 shows a comparison of well-to-tank efficiencies. DME ranks highest among the energy carriers.

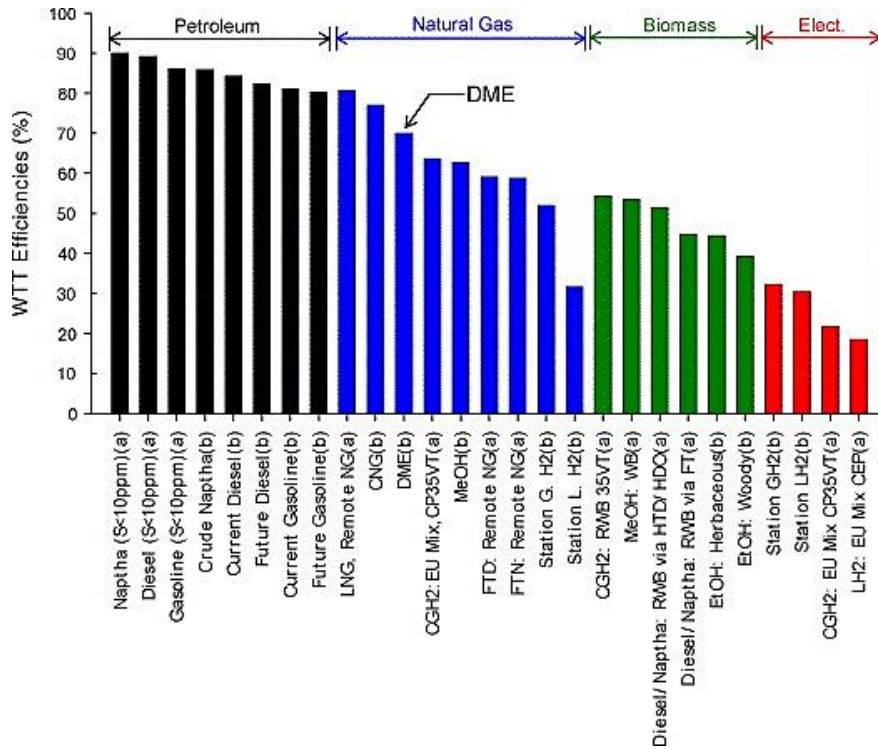


Figure 6 - Well-to-tank efficiencies for different fuels [4].

Of the fuels derived from natural gas (DME, methanol, naphta, hydrogen, diesel, etc.), biomass or electrolysis, the production of DME is the most energy efficient process [4]. Unconverted natural gas has to be in a cryonic state or pressurized to very high levels to have a high enough energy density to make transportation over large distances feasible. The infrastructure for DME is simpler and cheaper due to low vapor pressure.

The process that leads to the high WTT efficiency for DME shown in Figure 6 can be different types of partial combustion of the feedstock into synthesis gas (CO and H₂). Auto thermal reforming is used in the case of natural gas as feedstock. Gasification is used in the case of biomass as the feedstock. The synthesis gas contains the building blocks needed to produce DME (carbon, hydrogen and oxygen) in the following catalytic reactor.

In addition to being more efficient this thermal process used for DME is quicker and requires lower production plant investments than for example the fermentation process used for ethanol production [5][6].

1.3.4 Tank-to-wheel efficiency

On the consumption side a tank-to-wheel efficiency for a vehicle can be defined as:

$$\eta_{\text{TTW}} = \frac{\text{energy}_{\text{at wheels}}}{\text{energy}_{\text{fuel}}} \quad (2)$$

This efficiency will be dependent on the vehicle technology used and it is listed as such in Figure 7.

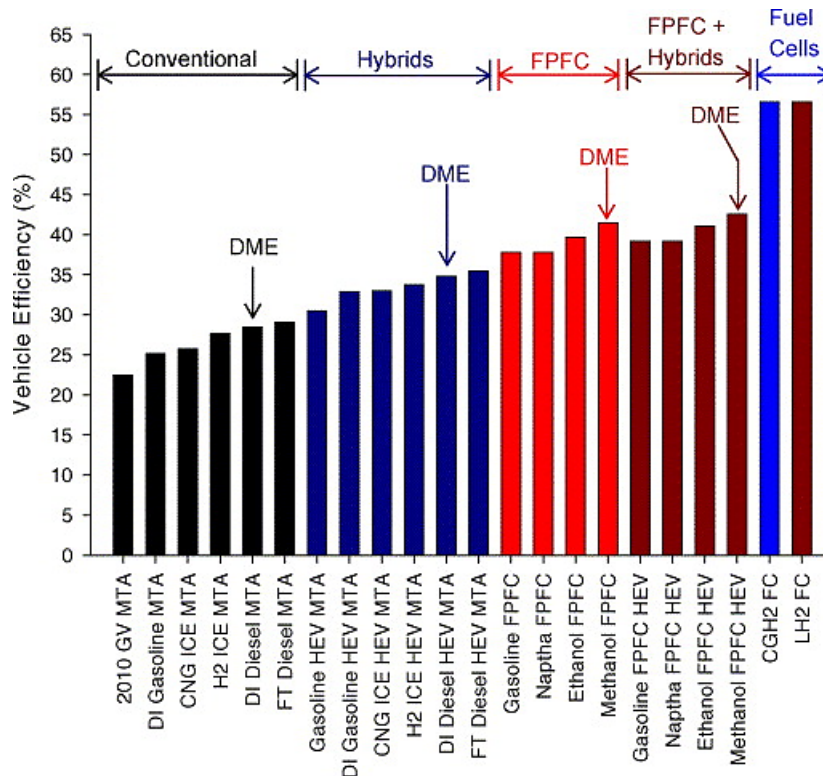


Figure 7 - Tank-to-wheel efficiencies for different fuels [4]

DME ranges among the best tank-to-wheel efficiencies almost independently of the vehicle technology used. Since both the well-to-tank and the tank-to-wheel efficiency is good the result is an efficient energy carrier. No matter where the energy comes from in the first place, a high well-to-wheel efficiency is a key factor in reducing well-to-wheel greenhouse gas emissions from transportation. The high well-to-wheel efficiency, the clean burning properties and the possibility of producing DME from remote energy sources like stranded natural gas are motivating the use of DME as a fuel [7][3][8].

A recent study performed in collaboration by the four main universities in Denmark considered the best way to meet the government's target of a fossil free Denmark by 2050. The study was called CEESA (Coherent Energy and Environmental System Analysis) [9]. The recommended scenario for the transport sector is shown in Table 1.

Table 1 - CEESA recommendation

| Transport | <i>CEESA-2050</i> |
|--------------------|-------------------|
| Direct electricity | 22% |
| Bio-DME/Methanol | 44% |
| Syn-DME/Methanol | 34% |

The majority of the energy to the transport sector is to come from biomass gasification (bio-DME/Methanol) and synthetic fuel (syn-DME/methanol) produced by reverse operation of solid oxide fuel cells that produce synthesis gas from sequestered CO₂ and steam.

The syn-DME/methanol route is illustrated in Figure 8.

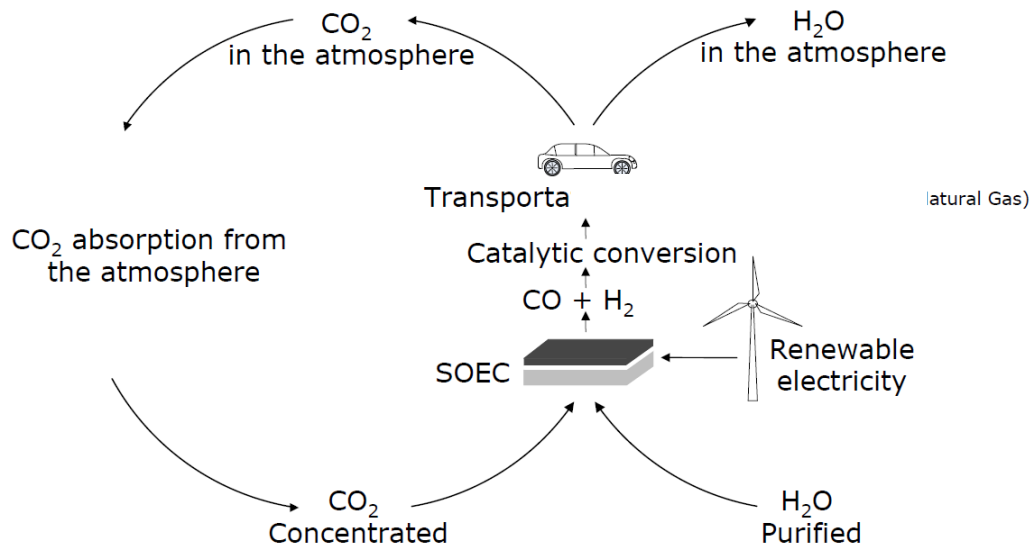


Figure 8 - Synthetic fuel from CO₂, steam and renewable electricity (Source: Søren Højgaard Jensen, RISØ DTU)

This emphasizes the importance of continued work to find the best ways to apply DME in internal combustion engines.

1.4 Commercialization of DME

When it comes to the wide spread use of alternative fuels there is always a chicken-and-egg situation: as long as there are no vehicles to consume the new fuel the oil companies will not produce it, and as long as the fuel is not available at the pump the car manufacturers will not dare to spend money on developing a car for it.

This is probably the major reason why ethanol so far has been the most successful among the alternative fuels. It is possible to cost effectively produce flexi-fuel vehicles that are able to run on both ordinary gasoline and ethanol. Such vehicles are produced in great numbers in Brazil due to the country's high volume production of ethanol from sugar cane.

This leads to the conclusion that if you want to design a new engine type then make sure it can run on traditional fuels. Vice versa, if you are developing a new fuel make sure that it can be used in existing engines.

This thesis deals with the development of a new engine for a new fuel. For the reasons stated above it is therefore not a thesis that is likely to be of commercial interest in the short term. But in the long term it will be increasingly difficult to satisfy political and consumer requirements with existing engines and fuels and it will be necessary to go beyond business-as-usual thinking to provide sustainable solutions. Eventually we will also simply run dry of fossil fuels. It is therefore of interest to society to explore what can be achieved with DME given its merits described in this chapter.

Despite the difficulties in introducing a new fuel a consortium of industrial partners in Sweden has made an effort to get started with DME. A significant step forward with respect to sustainable production of DME has been the consortiums opening of a biomass based DME production plant in Piteå, Sweden in 2010.

1.4.1 BioDME

The purpose of the BioDME plant in Piteå, Sweden is the production of DME from lignocellulosic biomass at an industrial scale, and its use as a vehicle fuel as well as for industrial processes.

The project started in 2008 as a demonstration of an environmentally optimized biofuel for road transport, covering the full chain from biofuel production from biomass to the use and testing in vehicles. A fleet of Volvo trucks is testing the DME in order to check engine compatibility, technical standards and commercial possibilities.

The partners involved in the project are:

- CHEMREC - has experience in the field of black liquor gasification technology
- Delphi - is a leading supplier of diesel injection equipment
- ETC - a research and development center with focus on combustion, gasification and biorefining processes

- Haldor Topsøe - supplier of catalysts and technology for the refining industry
- PREEM - the largest oil company in Sweden
- Total - one of the major oil and gas groups in the world
- Volvo - one of the world's leading manufacturers of trucks, buses, construction equipment etc.



Figure 9 - BioDME pilot plant in Piteå, Sweden

In 2010 the pilot plant was inaugurated, it has a capacity of about 4 ton DME per day using forest residues as feedstock. During the project four filling stations were built in different locations in Sweden. Moreover, the DME produced will be evaluated for compatibility with materials (rubber, plastic, metals) and to determine the minimum quality to ensure engine durability (DME composition, properties, engine oil requirements etc.). Field tests are taking place during 2010 – 2013 with a planned yearly average distance of 100,000 km per truck. In November 2011 213,000 km's had been accumulated by the test fleet.

The DME is produced from black liquor through the production of clean synthesis gas and a final fuel synthesis step. Black liquor is an aqueous solution of lignin residues, hemicellulose and inorganic chemicals, obtained as a waste from the Kraft process when digesting pulpwood into paper pulp.

The combustion engine group at DTU was invited to the inauguration in Sweden in September 2010. The 4th International DME Conference was held in Stockholm just prior to the inauguration of the bio DME plant in Piteå. The Technical Review Committee of the conference chose the authors contribution about DME engine technology as the key technical presentation at the conference [10].

1.5 State of the Art - DME as an Engine Fuel

1.5.1 CI applications

The first experiments with DME as a compression ignition engine fuel were done by Spencer C. Sorenson and Svend-Erik Mikkelsen [2]. It was quickly realized that once the fuel has been delivered to the combustion chamber it works well. It mixes and ignites easily and produces power outputs at least as high as for diesel operation and at similar efficiencies. The emissions of harmful substances are also substantially lower for DME. Especially the emission of soot is near-zero [11][12]. The problems lie in the fuel injection system. The low lubricity of DME and its incompatibility with a range of elastomers commonly applied in fuel injection system for sealing purposes posed problems for the design of reliable fuel delivery systems. The modulus of elasticity of DME is five times lower than diesel which also increases the pumping work required for compression to a certain injection pressure. Because the injection pressure necessary for satisfactory performance is It also changes the oscillations

Ion M. Sivebaek developed and validated a test method suitable for investigations into the lubricity of DME and other very thin fluids. This method was used to compared DME to diesel in order to quantify the severity of the lubricity problems. The viscosity and lubricity of DME was indeed found to be lower than for diesel [13]. The test method and the validation of it was improved over a number of years and the result is the Volatile Fuel ViscoMeter (VFVM) [14]. Ions most recent value for the viscosity of DME and other selected data for DME and diesel are given in Table 2.

Table 2 – Comparison of DME and diesel

| | Unit | DME | Diesel |
|--------------------------|----------------------|---------------------------|-----------------------------|
| Chemical formula | | CH_3OCH_3 | $\text{C}_n\text{H}_{1.8n}$ |
| Molecular weight | [g/mol] | 46 | >100 |
| Lower heating value | [MJ/kg] | 28.8 | 42.5 |
| Saturated liquid density | [kg/m ³] | 668 | 840 |
| Boiling point | [°C] | -24.9 | 180-350 |
| Viscosity at 25°C | [kg/m s] | 0.184 | 2-4 |
| Vapor pressure at 25°C | [bar] | 5.1 | <0.01 |
| Critical pressure | [atm] | 52 | - |
| Critical temperature | [°C] | 127 | - |

At the time of writing DME as an engine fuel is being most actively researched in Scandinavia, Japan, South Korea and China. As mentioned in chapter 1.4 about commercialization of DME Volvo Trucks in Sweden is providing trucks for a fleet test operating on bio DME produced by gasification of waste from paper production. Volvo's efforts to demonstrate the application of DME in heavy duty diesel engines started before 2000 [15] and

have continued since. Both experimental [16][17][18] and numerical studies [19][20] have been performed.

Coordinator of the Bio DME project Per Salomonsson presented the technology Volvo has developed at the 7th Asian DME Conference held in November of 2011. Figure 10 shows the Volvo system.

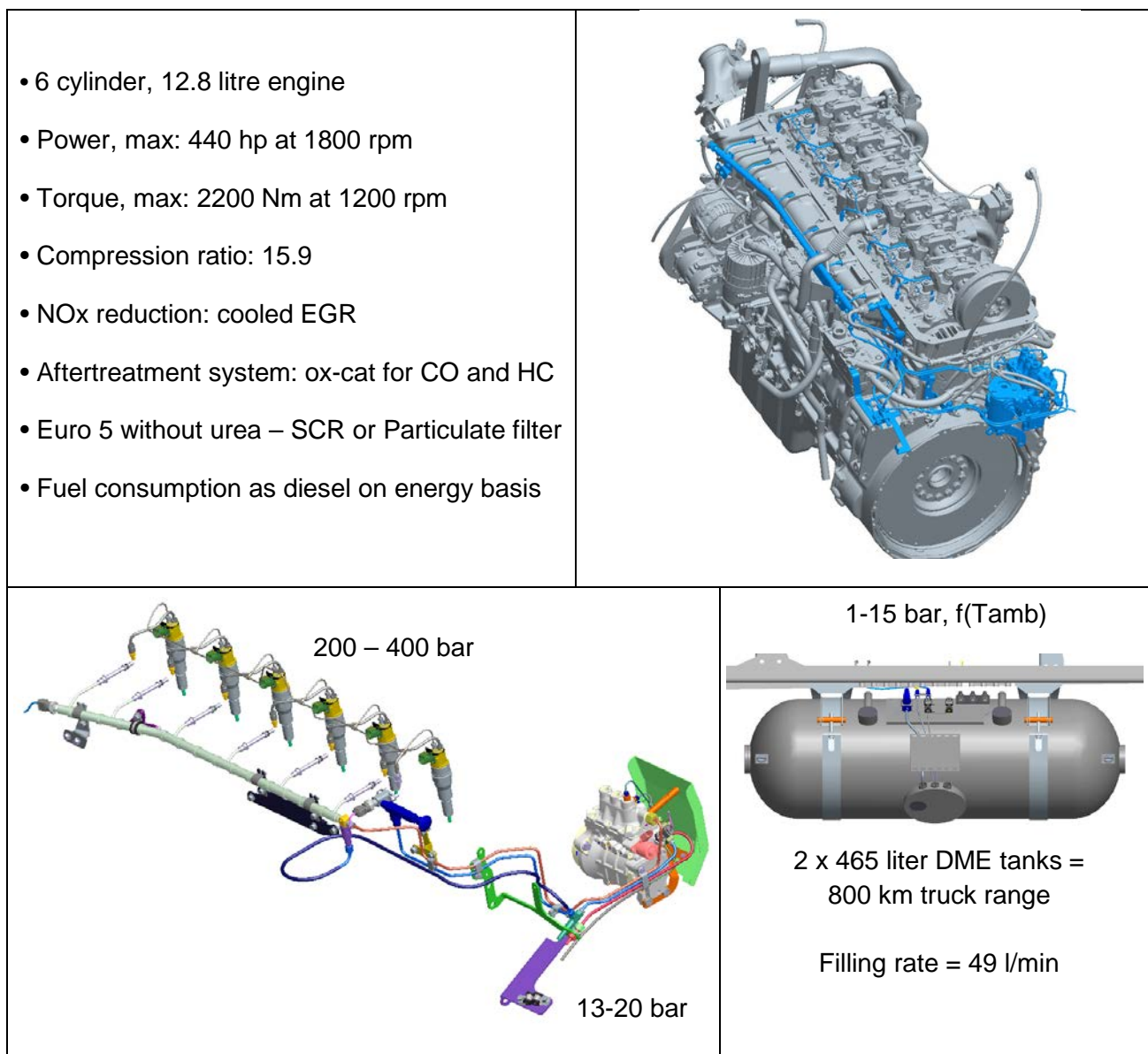


Figure 10 - Volvo Heavy Duty DME engine with common rail fuel system
(source: biodme.eu)

Power and efficiency is comparable to the un-modified diesel engine and Euro 5 is met without SCR or particulate filter. The fuel pump is a plunger and barrel type and a lubricating additive is necessary for reliable operation.

Professor Kajitani at Ibaraki University in Japan and co-workers did studies on a broad range of subjects related to the use of DME. Their early work concluded that soot and hydrocarbon emissions are very low for DME combustion in a CI engine. The emission of NO_x did not deviate much from the emission level when operating the same engine on diesel. They did however note that the lack of soot when operating on DME enabled the use of retarded injection timing that resulted in significant reductions of NO_x emission. This is an important point and is an interesting feature of DME. The lack of soot gives the engine designer an extra degree of freedom because the soot- NO_x trade-off known from diesel engines is not a problem in the same way [21].

Other of their studies found that the unburned hydrocarbons from DME combustion in a CI engine was mainly unreacted DME and other C_2 substances such as C_2H_2 , C_2H_4 and C_2H_6 [22][23].

An experimental study made in 2003 investigated the DME fuel spray in a constant volume vessel and in a diesel engine [24]. Diesel and DME injection was compared. The DME injector had injection holes 1.8 times larger to accommodate for the same calorific value of the fuel injection in both cases. The injection pressure was 250 bar. The DME spray was wider and that resulted in a shorter spray penetration length. The spray penetration for DME was 80% of that for diesel. The DME spray behaviour was found to follow the momentum theory for jets. Momentum theory also predicted that the average fuel-air ratio should be approx. 20% leaner for the DME spray. Due to the lower stoichiometric fuel air ratio for DME the resulting fuel-air equivalence ratio in the spray is about half that of diesel oil. These findings point to the need for combustion systems specifically developed for DME if the full potential of DME in terms of engine efficiency and emissions should be achieved.

Injector wear was also part of the studies made together with Mitsubishi Heavy Industries and Japan National Oil Corporation. It was found that although the lubricating additive HITEC4140 was used in a concentration of 1000 ppm there was significant wear on the plunger surfaces in the fuel pump after 107 hours of operation.

Recently Kajitani and his group has been involved in a DME engine concept at lower compression ratios [25].

The National Traffic Safety and Environmental Laboratory (NTSEL) in Japan has managed the national EFV 21 project that started in 2002 in which technical standards for the production and use of DME have been drafted [26][27][28]. Like Volvo, they focused on the use of DME in modified diesel engines in trucks. The engine and fuel system is similar in design and similar performance and emissions have been reported [29] [30][31][32][33]. They also used an additive to overcome the poor lubricity of DME.

The common denominators for the first ten years after the discovery of DME as an engine fuel have been to:

1. Apply DME to heavy duty engines at approximately 300 bar.
2. Control NO_x emissions with a combination of large amounts of EGR and retarded injection timing both of which can be applied without soot penalties due to the properties of DME.
3. Focus on the development of fuel handling and fuel injection equipment.

1.6 Motivation and Objectives

The original idea with the two-stroke DME engine for the DTU eco-car was to achieve diesel operation, and thereby high indicated efficiency, with low engine friction. Due to the fact that fuel injectors with low enough fuel flow rates weren't available the process ended up being late-injection HCCI or at least late-injection. How homogeneous the mixture was before ignition was not known. A number of questions therefore defined the objectives of this study: Is the fuel and air premixed before combustion? What are the harmful emissions as a function of load and speed? Are they low enough engine-out or can catalyst technology be applied to bring levels down to acceptable levels? Can any other measures be adapted in order to reduce emission levels?

Another motivating factor was that it may be a good idea to use a clean synthetic fuel such as DME for small engines. Although most studies concerning the use of DME in engines have so far focused on heavy duty engines it may make sense to solve small engine emission challenges by using cleaner fuel instead of expensive after treatment systems. The cost of such after treatment systems are high relative to the economy related to the applications that small engines are used in. Also, since cars and larger vehicles are put under strict regulation in terms of emissions, the emissions from small engines and vehicles constitute an increasing share of the total amount of harmful emissions from combustion engines [34][35][36][37][38][39][40].

1.7 Methods

Cycle simulation and engine experiments were used in combination to determine the combustion mode of the test engine. An optical cylinder head was designed and used to take pictures of the combustion for qualitative assessment of the premixing of fuel and air. A commercial fluid dynamics code was used to investigate the effect on heat transfer of using a very small engine. The effect on heat transfer of combustion chamber shape and the importance of blowby was also investigated using computational fluid dynamics.

2. Combustion Regime

There are basically three ways to burn fuel in an internal combustion engine. Homogeneous charge spark ignition (SI), direct injection compression ignition (CI) and homogeneous charge compression ignition (HCCI). Several variants of the latter can be categorized by the timing of fuel injection relative to the engine cycle giving rise to names like PCI (Premixed Compression Ignition) and PPCI (Partially Premixed Compression Ignition). In the following these combustion principles will be illustrated and discussed briefly in order to motivate this study. The illustrations are images taken from a number of excellent videos that the Combustion Research Facility at Sandia makes available at their web page [41]. The camera looks up through the piston which is transparent.

2.1.1 SI combustion

Nikolaus Otto invented the premixed combustion process where a homogeneous charge of fuel and air is ignited at the appropriate time by an external energy source. In Otto's original engine the external energy source was a flame. When technology permitted the flame was replaced by an electric spark, hence the name spark ignition engine. From the external ignition source a thermally driven flame front spreads out across the combustion chamber until it eventually is quenched near the combustion chamber wall. Figure 11 shows the combustion chamber of a spark ignited gasoline engine at the maximum heat release rate.

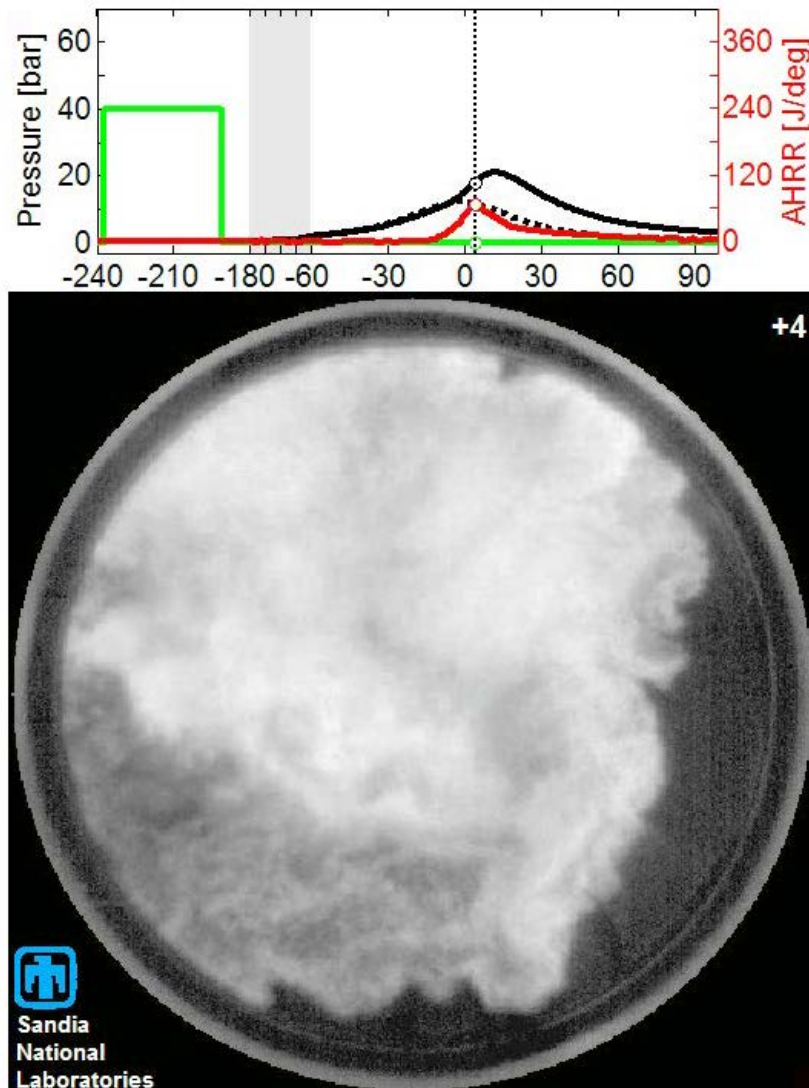


Figure 11 – SI combustion

Fuel and air is premixed so it is possible to operate at a fuel-air equivalence ratio of unity. This means that high power output without turbocharging is possible. Also, there are no fuel rich zones and therefore low engine-out soot. The heat release rate is limited by the speed of the thermally driven flame front. A fast heat release rate is desirable in order to extract as much work as possible from the hot products but a too fast heat release will result in peak pressure rise rates (PPRR) that are damaging for the engines mechanical parts. By correct design it is possible to achieve suitable heat release rates in an SI engine. CO, HC and NO_x emissions can be dealt with using a three-way catalyst. As long as operation is truly premixed soot emissions are low but modern designs that use in-cylinder fuel injection emit soot at levels that are not insignificant and may in the future need after treatment systems to cope with soot emissions.

The SI engine requires fuel with a high octane rating in order to operate with a compression ratio high enough to achieve acceptable efficiencies. If high compression ratios are employed along with a low octane fuel premature ignition may occur ahead of the thermal-

ly driven flame front due to the compression of the unburned charge. This produces strong noise, lower engine efficiency and may destroy the engine. The SI engine also needs to throttle the intake air flow to maintain a fuel-air equivalence ratio of unity at part load. The throttling results in pumping losses that reduce engine efficiency. The fact that the fuel and air is premixed before or during the initial phases of the compression stroke results in significant amounts of fuel being caught in cold regions of the combustion chamber. The flame front will quench before it reaches these regions and thus a part of the fuel is wasted. It must also be noted that the operation at stoichiometric fuel-air ratio, that is an advantage in terms of power output and thereby mechanical efficiency, is limiting the indicated efficiency. The high heat capacity of the stoichiometric combustion products reduces the temperatures and thereby pressures reached compared to an equivalent heat release in air. The diesel engine is less restricted in terms of reaching high energy conversion efficiencies and is described in the following.

2.1.2 CI combustion

Rudolf Diesel's idea was to remove the limit on compression ratio by not introducing the fuel before it should burn. This would enable the use of low octane rating fuels at high engine efficiency. In fact, the diesel engine operates best with low octane fuels. The ability of the fuel to ignite easily is of primary concern when producing diesel engine fuels. The Cetane number is used to quantify this ability. If the fuel Cetane number is too low a large amount of fuel will mix with air to within combustible limits before the onset of combustion. The ensuing premixed combustion will be fast since it is limited only by the chemical reaction rate and may result in engine damage if the premixed portion of the heat release is too rapid.

Figure 12 shows the combustion chamber at the peak of the mixing controlled heat release that is characteristic combustion mode for diesel operation.

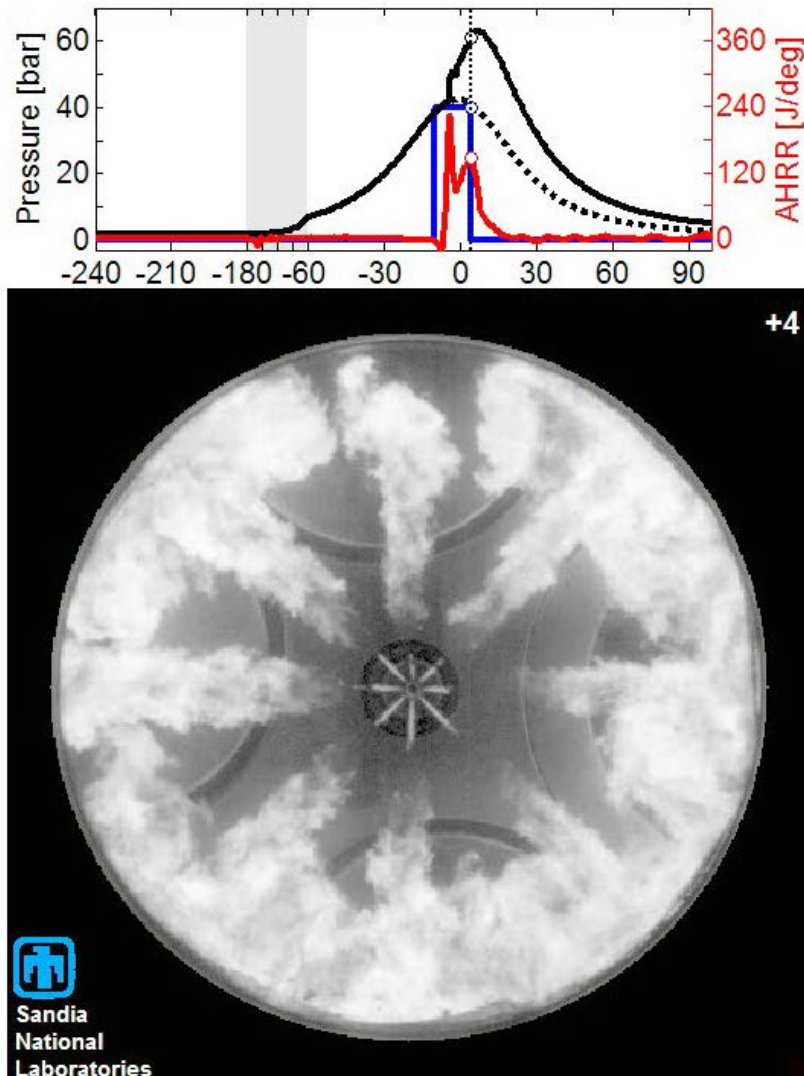


Figure 12 – DI combustion

The heterogeneity of the process is clear visible. The injector is placed at the centre of the combustion chamber and eight sprays of fuel are exiting radially outwards from that point. The liquid core of the spray is visible in the immediate vicinity of the injector tip. Strong luminosity from hot soot particles dominate the picture and are visible just downstream of the liquid core. The burning spray impinges with the piston bowl wall along the periphery of the picture. Although this increases heat losses to the walls it spreads out the spray further and enables effective utilization of the large amounts of air available at the largest diameter of the combustion zone. That complete utilization of the air in the cylinder cannot be achieved with a mixing controlled combustion process is one of the major drawbacks of diesel combustion. The limit on fuel-air equivalence ratio is approximately 0.7. Developments in turbocharger technology have made this less of a drawback though. The non-existence of premature ignition makes it possible to apply high charge air pressures and thereby develop high specific output.

The diesel engine can be operated at high compression ratios, it does not require throttling, it does not have fuel in crevices that is not burnt and the overall lean operation enables high indicated efficiencies.

2.1.3 HCCI combustion

True HCCI operation compresses a homogeneous mixture of fuel and air to the point of spontaneous ignition. Once ignition has occurred combustion will proceed quickly since it is not limited by transport processes but only the chemical reaction rate. If spontaneous ignition occurs at TDC the resulting process is actually what Nikolaus Otto had in mind when he designed the SI engine, a constant volume combustion process. Figure 13 shows HCCI combustion at peak heat release.

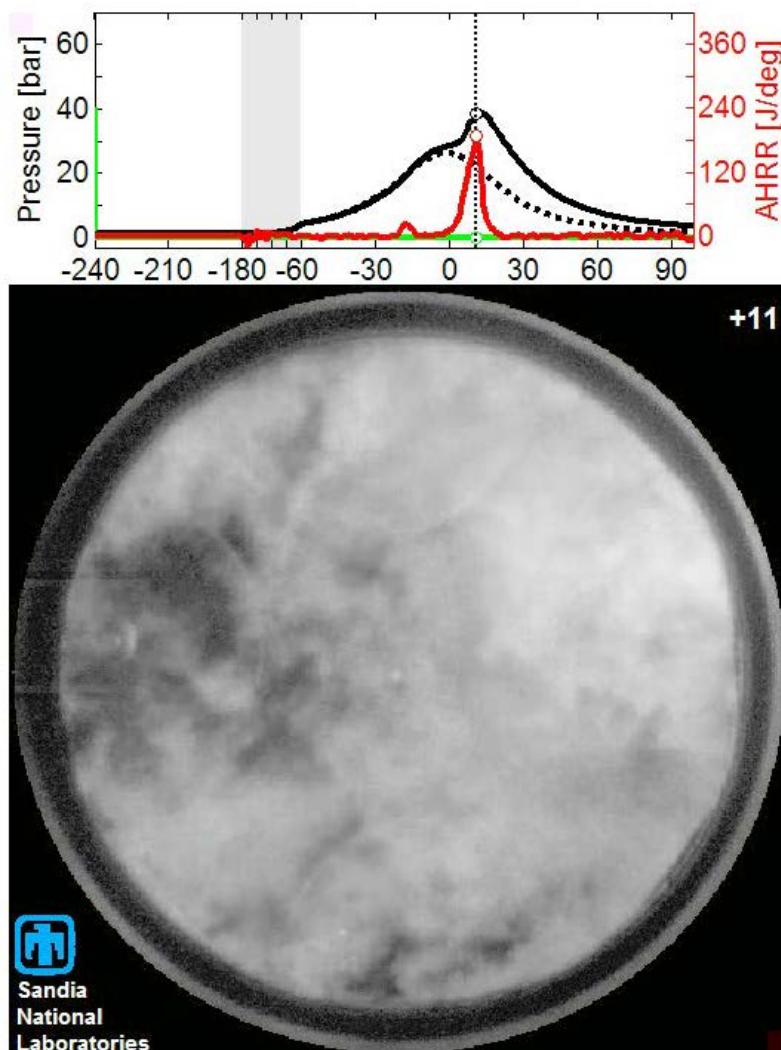


Figure 13 – HCCI combustion

Fortunately for Otto the engine he built had a slower combustion process and did not completed combustion at constant volume. For that reason the engine was reliable and was eventually very successful. It has been found that although HCCI combustion is the theo-

retical optimum the rapid heat release produces strong noise and the high pressure rise rate is capable of destroying the HCCI engine. Also, making sure the spontaneous ignition happens at the desired time is difficult in praxis especially at transient operating conditions. Negotiating these problems has spawned numerous studies in the past twenty years. The basic conclusion has been that HCCI operation at higher fuel-air equivalence ratios than 0.5 does not make a lot of sense. The formation of thermal NO starts beyond that point and the problems with noise and pressure rise rate are significant already at leaner conditions than that [42, 43].

2.1.4 Derived HCCI concepts

The numerous studies performed to find ways to deal with the challenges of HCCI engine operation have produced some derived concepts: PCCI (Premixed Charge Compression Ignition), PPC (Partially Premixed Combustion), PCI (Premixed Compression Ignition), PFS (Partial Fuel Stratification) and RCCI (Reactivity Controlled Compression Ignition) to name but a few.

Recent studies have attempted to reduce the reaction rate by introducing charge inhomogeneity and using fuels that have an ignition delays that are sensitive to fuel-air equivalence ratio (PFS) [44]. In this way the conversion of fuel happens more gradually resulting in acceptable pressure rise rates at higher fuel air ratio than with a completely homogeneous mixture. A similar concept that inducts the majority of the fuel premixed with air from the manifold and then adds a direct injection of a different fuel to create inhomogeneity and reactivity differences has been named RCCI (Reaction Controlled Compression Ignition) [45].

Most of the derived HCCI concepts are based on the idea of re-introducing inhomogeneity to reduce reaction rate and they typically introduce some level of late-injection HCCI.

Also, adding fuel late on the compression stroke by electronically controlled direct injection in itself makes it easier to time the combustion event. Figure 14 illustrates the process when all of the fuel is injected late on the compression stroke.

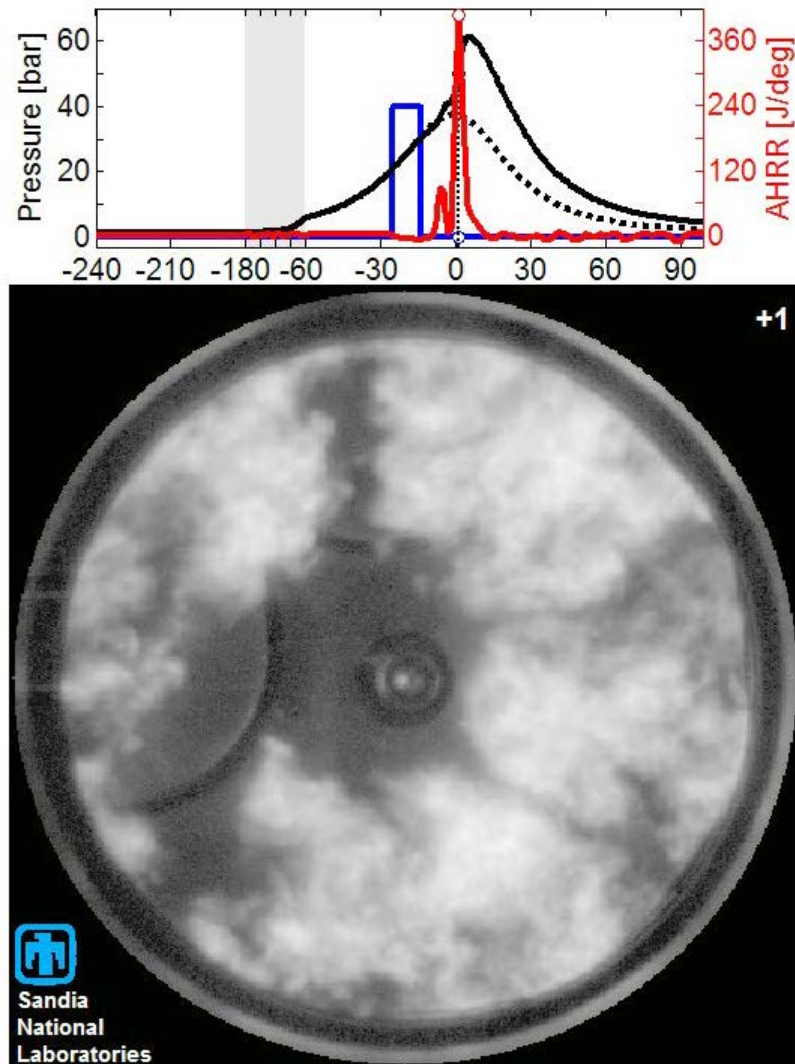


Figure 14 – Late-injection HCCI

This process is similar to the one in the test engine of this study. All of the fuel is injected near TDC on the compression stroke and fuel injection is completed before combustion starts. This method makes it easier to control ignition timing but pressure rise rates can still be a problem.

The present study aims to describe the behavior of a small late-injection HCCI engine in terms of combustion mode and emissions. It also aims to test possible ways of improving performance and emissions and the effect of after treatment.

3. Experimental Setup

At this point the reader is directed to the papers written by the author that describe the engine concept and test setup used. The papers are attached as appendices to this thesis. Paper I is: "A 50cc Two-Stroke DI Compression Ignition Engine Fuelled by DME". Paper II is: "Optimizing the Performance of a 50cc Compression Ignition Two-Stroke Engine Operating on Dimethyl Ether".

A few pictures are shown here as appetizers.

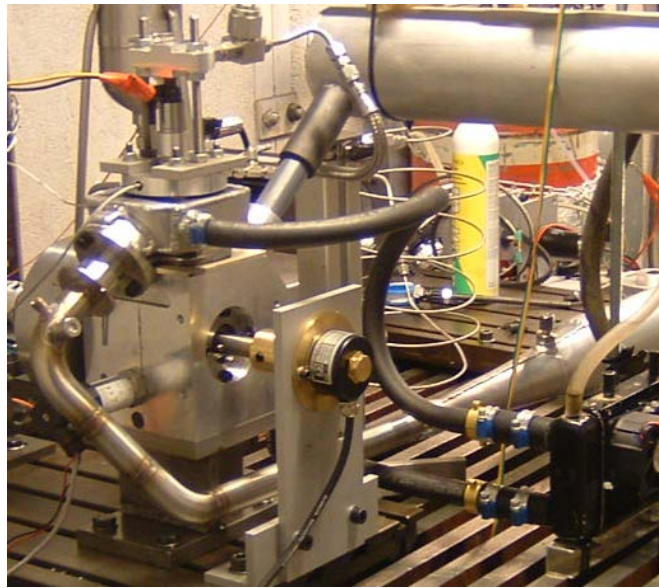
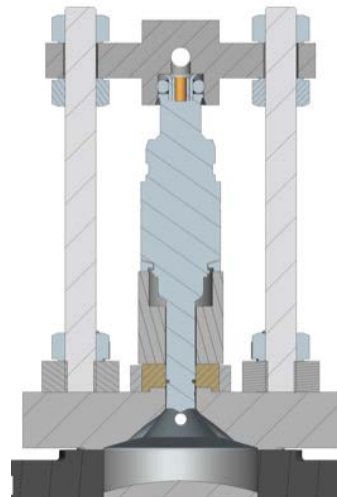


Figure 15 - Engine test setup for (2nd prototype)



Cylinder head and injector



Cut-away view

Figure 16 – Cylinder head and surrounding parts (2nd prototype)

4. Flame temperatures

The effect of using a special fuel is evaluated by determining the adiabatic flame temperatures. The flame temperatures of the primary reference fuels iso-octane and n-heptane along with Jet-A is compared to DME in Table 3. Jet-A acts here as a substitute for diesel since it is the substance available in the JANAF tables published by NASA that has properties most similar to ordinary pump diesel. The JANAF tables have been used exclusively for evaluation of properties throughout this study. A Matlab program was written that iterates to find the temperature at which the equilibrium products have the same enthalpy as the unburned fuel-air mixture (constant pressure combustion). The resulting flame temperatures are given in Table 3. The reactants are initially at standard conditions of 101325 Pa and 298.15 K.

Table 3 - Adiabatic flame temperatures at standard conditions and $\phi = 1$

| | | iso-octane | n-heptane | Jet-A | DME |
|------------------------------|----------|------------|-----------|--------|--------|
| Fuel/air – ratio | [kg/kg] | 0.0661 | 0.0659 | 0.0682 | 0.111 |
| Burned temperature (const p) | [K] | 2272 | 2275 | 2280 | 2284 |
| LHV | [kJ/kg] | 44,651 | 44,922 | 43,352 | 28,835 |

The variation in burned temperature between the fuels is small. For combustion in an engine the initial state of the reactants will be a significantly higher pressure and temperature due to the compression before ignition. For a naturally aspirated compression ignition engine, like the test engine of this study, approximate values of pressure and temperature of the charge just prior to combustion can be found by applying a polytropic state change from atmospheric conditions with a suitable compression ratio and polytropic coefficient. The compression ratio and polytropic coefficient used here are 15 and 1.35 respectively.

$$p_2 = p_1 \left(\frac{V_1}{V_2} \right)^\gamma = 1.01325 \cdot \left(\frac{15}{1} \right)^{1.35} = 39.2 \text{ bar} \quad (3)$$

$$T_2 = T_1 \left(\frac{p_2}{p_1} \right)^{\frac{\gamma-1}{\gamma}} = 298.15 \cdot \left(\frac{39.21}{1.01325} \right)^{\frac{1.35-1}{1.35}} = 769 \text{ K} \quad (4)$$

Both the constant pressure and constant volume burned temperatures at end of compression conditions are shown in Table 4.

Table 4 - Adiabatic flame temperatures for initial conditions 39.2 bar and 769 K

| | | iso-octane | n-heptane | Jet-A | DME |
|------------------------------|----------|------------|-----------|--------|-------|
| Fuel/air – ratio | [kg/kg] | 0.0661 | 0.0659 | 0.0682 | 0.111 |
| Burned temperature (const p) | [K] | 2621 | 2623 | 2632 | 2627 |
| Burned temperature (const v) | [K] | 2970 | 2972 | 2981 | 2970 |

Also for this starting condition the difference in flame temperatures is small between the fuels. This indicates that NO emission from an engine operating on DME should be similar to the other fuels listed provided that the mode of combustion and the operating conditions are the same. Due to the non-sooting properties of DME it is possible though to retard combustion phasing of an engine operating on DME so that peak combustion temperatures are lowered without getting an increase in soot which would otherwise be the case for e.g. diesel operation. This is one of the primary benefits of using DME in an ordinary diesel engine. The absence of soot gives an extra degree of freedom when optimizing for low engine out NO.

Table 5 and Table 6 give additional data for the combustion of DME in air. Although DME contains oxygen the fuel-air equivalence ratios given here are defined as normally.

$$\varphi = \frac{FA}{FA_{stoich}} \quad [kg/kg] \quad (5)$$

A more ideal way of quantifying the mixture stoichiometry for oxygenated fuels is not applied but described in this reference [46].

Table 5 - DME, $\varphi = 1$, const p

| | | | | |
|-------------------|---------|--------|--------|--------|
| Start temperature | [K] | 300 | 600 | 900 |
| Flame temp. | [K] | 2285 | 2413 | 2535 |
| Heat of comb. | [kJ/kg] | 26,675 | 25,269 | 23,392 |
| CO | [%] | 1.38 | 2.19 | 3.16 |
| H ₂ | [%] | 0.41 | 0.65 | 0.95 |

Table 6 - DME, $\varphi = 0.5$, const p

| | | | | |
|-------------------|---------|--------|--------|--------|
| Start temperature | [K] | 300 | 600 | 900 |
| Flame temp. | [K] | 1561 | 1794 | 2034 |
| Heat of comb. | [kJ/kg] | 28,752 | 28,590 | 28,148 |
| CO | [ppm] | 2.4 | 40 | 363 |
| H ₂ | [ppm] | 1.3 | 16 | 117 |

5. Cycle Simulation

Cycle simulation is a means to predict performance and emissions of an engine process. Cycle simulation of something as complex as a combustion engine is not trivial though. While there are sound methods that can be applied for well-defined state changes and chemical activity there are a lot of processes that are difficult to model accurately, the scavenging of a two-stroke engine and the details of combustion to name two. On the other hand, to make experiments without a theoretical tool to guide the experiments is all but stupid and the modeling work in itself is a way to work through the different steps of the engine process in a detailed way that gives the modeler valuable insights.

The possibility of high engine efficiency and low emissions levels with HCCI combustion has been investigated extensively. Both theory and experiment has shown that it is possible. The limitation is the load limit imposed by the very rapid combustion that produces very high pressure rise rates within the engine cylinder. This puts excessive stresses on the mechanical parts of the engine and also produces high noise levels. From a modeling point of view HCCI combustion is simpler than spark ignition combustion and traditional diffusion flame compression ignition combustion. Ideally the cylinder content is homogeneous and a chemical kinetics mechanism can be set up that responds to the heating of the charge that occurs during compression eventually leading to hot ignition. Depending on the level of sophistication of the mechanism a more or less accurate description of the progress of reactions and resulting species concentrations can be found [47]. What is typically seen for HCCI combustion is that the reactions are very fast once hot ignition takes place.

In practical experiments with HCCI engines the actual timing of combustion is very sensitive to deviations from the modeled system. Even small variations in local fuel air equivalence ratio have an influence on ignition timing. Also, since temperature is of utmost importance to chemical reaction rates the modeled cylinder wall temperature and heat transfer rates will have to be very accurate in order to predict the ignition timing of the actual engine. Due to issues such as these, ignition timing is not modeled but chosen by the modeler in the cycle simulation used in this study. If the fuel and air are actually premixed prior to ignition, the reactions are very fast once ignition has occurred and chemical equilibrium is therefore a meaningful estimate of the composition after ignition. This is true for all important species except nitrogen oxide. Formation of nitrogen oxide is predicted by applying the extended Zeldovich mechanism for NO formation.



The following bullets provide a summary of how the model operates:

- Zero-dimensional
- Gas properties are a function of temperature and composition evaluated using the JANAF 9-coefficient polynomials
- Constant volume combustion, but reactions updated during expansion
- Blair's two-stroke scavenging model [48]
- Mixing with scavenge air both for the exhaust stream and the cylinder content is done at exhaust pressure which is considered constant.
- Woschni or Annand heat transfer
- Chemical equilibrium for 11 species using Wein's method [49] above 1750 K
- Zeldovich mechanism for NO
- Fuel can be added by mass or alternatively such that a certain trapped equivalence ratio is reached

Port flow is not calculated but isentropic expansion of the products to exhaust pressure and mixing with short-circuiting scavenge air happens immediately after the exhaust port starts to open. Scavenging of the cylinder and the resulting mixing of residuals and scavenge air happens at BDC. Port closure prior to compression is also instantaneous.

To give the reader a level of confidence in the predictions of the model, results of gradually increasing complexity will be given here starting with a simulation of a simple air cycle and progressing with operation on diesel fuel. The model is not designed for the diesel process but is capable of giving indications of the highest possible efficiency and power output for the diesel cycle. These are then compared to simulation results with DME. A naturally aspirated engine cylinder of 500 cc running at 3000 rpm is simulated for these comparisons. A scavenging process of a two-stroke engine is implemented in the model so in order to estimate four-stroke engine performance the delivery ratio is set so high that the residual mass fraction is near zero.

The results of the simulations for three different compression ratios are shown in Table 7. In grey is the simple air cycle with a gamma of 1.4. Next is the result with temperature and composition dependent properties with a very low fuel-air equivalence ratio ($\phi = 0.01$). Then the fueling is increased to $\phi = 0.7$ to show the effect of changed composition. In row four the results when typical intake valve closing and exhaust valve opening angles are introduced. Row five introduces Woschni heat transfer. Row seven moves the combustion event to 10 degrees after TDC to match the typical peak pressure position of an actual engine.

Table 7 - Cycle simulation results for a 500 cc cylinder @ 3000 rpm operating on diesel:

| | | | | |
|---|-----------------------------------|------|------|------|
| 1 | CR | 15 | 20 | 25 |
| 2 | Air Cycle, $\gamma = 1.4$ | 66.2 | 69.8 | 72.4 |
| 3 | $\gamma(t,x)$, ($\phi = 0.01$) | 65.0 | 68.5 | 70.8 |
| 4 | $\phi = 0.7$ | 55.7 | 59.5 | 62.2 |
| 5 | IC/EO = -125/125 | 53.3 | 57.2 | 60.0 |
| 6 | Woschni HT | 50.3 | 53.6 | 55.8 |
| 7 | Tcomb = 10° ATDC | 49.2 | 52.4 | 54.4 |

The result of a cycle simulation is shown in Figure 17.

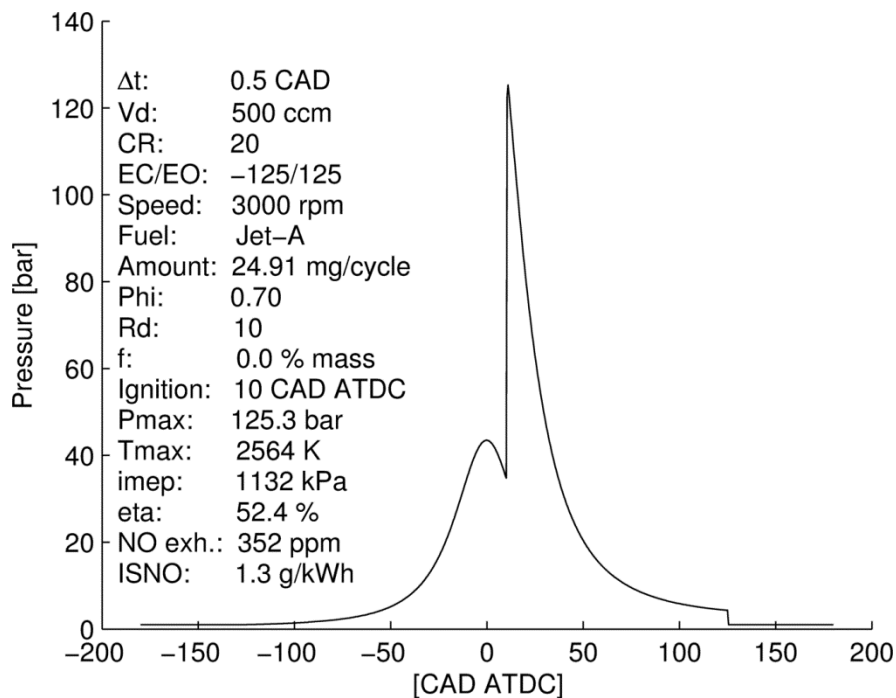


Figure 17 – Cylinder pressure for simulation in bottom row of Table 7 for CR = 20.

$\Phi = 0.7$ has been used since the smoke limit of diesel engines has approximately that value. Measured values of indicated efficiency in an automotive diesel engine will be slightly lower than those given in the bottom row of Table 7. This is primarily due to the finite rate of combustion that is a result of the diesel combustion process. The classical diesel process is actually a constant pressure process which is in contrast to the constant volume process simulated here. Despite of this the large low speed engines, like those used for marine propulsion, complete combustion quickly in terms of crank angle degrees and produce efficiencies very close to those shown in the bottom row of Table 7. In Table 8 the equivalent results for DME operation are presented.

Table 8 - Cycle simulation results for a 500 cc cylinder @ 3000 rpm operating in DME

| | | | |
|-----------------------------------|------|------|------|
| CR | 15 | 20 | 25 |
| Air Cycle, $\gamma = 1.4$ | 66.2 | 69.8 | 72.4 |
| $\gamma(t,x)$, ($\phi = 0.01$) | 65.0 | 68.5 | 70.8 |
| $\phi = 0.7$ | 55.2 | 58.9 | 61.6 |
| EC/EO = -125/125 | 52.8 | 56.7 | 59.5 |
| Woschni HT | 49.8 | 53.1 | 55.4 |
| Tcomb = 10° ATDC | 48.8 | 51.9 | 54.0 |

It is clear from Table 7 and Table 8 that there is hardly any difference in engine efficiency between DME operation and diesel operation. For similar engines the efficiency using DME can be expected to be similar to diesel. Using simulation settings equal to those used to find the engine efficiencies given at the bottom of Table 7 and Table 8, and varying one of those settings at a time, a number of plots are created to illustrate the difference between diesel and DME operation. The basic settings are given in Table 9.

Table 9 – Default simulation settings for DME and Diesel comparisons

| | | |
|------------------------------------|------------|------------|
| Cylinder size | [ccm] | 500 |
| Compression ratio | [] | 20 |
| Intake & exhaust pressure | [kPa] | 101.325 |
| Engine speed | [rpm] | 3000 |
| Trapped fuel-air equivalence ratio | [] | 0.7 |
| IC / EO | [CAD ATDC] | -125 / 125 |
| Combustion timing | [CAD ATDC] | 10 |
| Delivery ratio ¹ | [] | 10 |
| Heat transfer | | Woschni |

¹ A high delivery ratio is applied so that there is only an insignificant amount of residual gas.

The settings were chosen so that they approximate an automotive design at full load except for the lack of turbocharging. The indicated efficiency as a function of fuelling level is given in Figure 18.

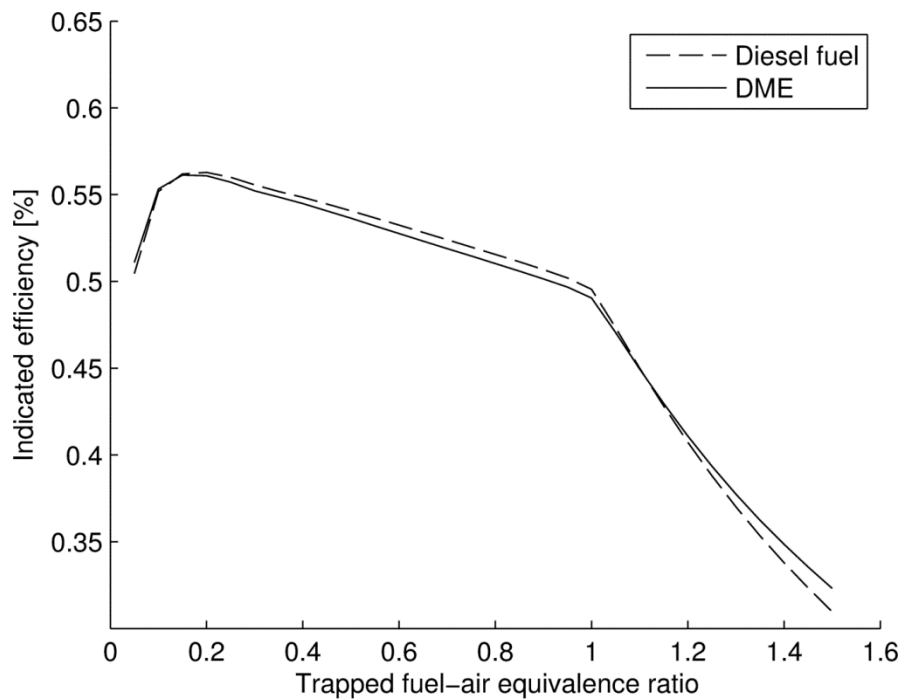


Figure 18 - Engine efficiency for diesel fuel and DME

Diesel fuel has a slight advantage in terms of efficiency in the usable fuel-air equivalence range. The dip in efficiency below a fuel-air equivalence ratio of 0.2 is because the simulation is not adiabatic but applies the heat losses predicted by Woschni.

The power level simulated with DME and diesel is illustrated in Figure 19.

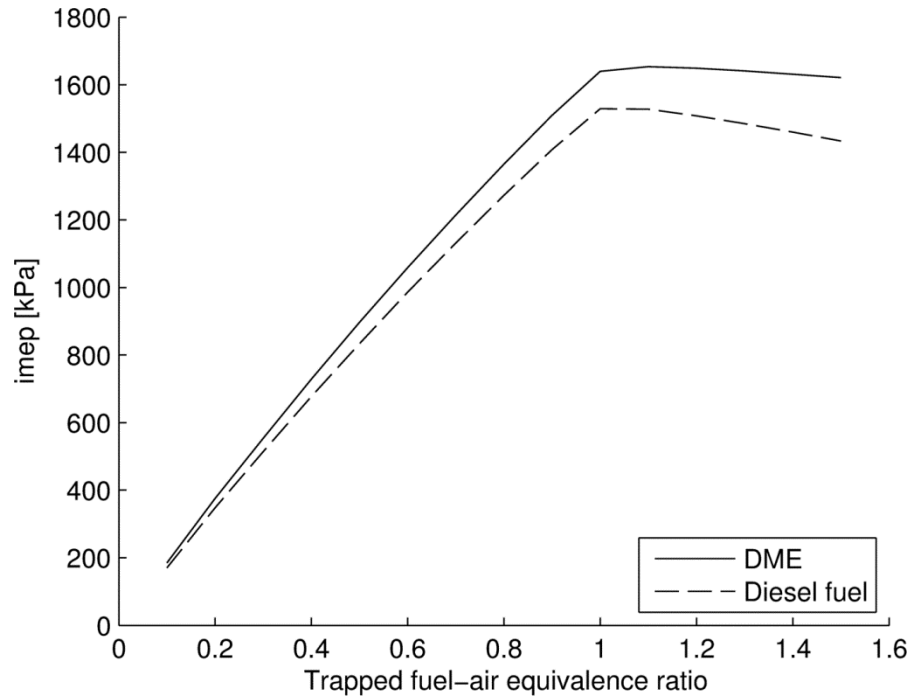


Figure 19 - Indicated mean effective pressure for DME and diesel fuel

Figure 19 shows that the power output is higher for DME than diesel. This is a direct result of the fact that the heating value per kg air for a given fuel-air equivalence ratio is higher for DME than for diesel. The difference is illustrated in Table 10.

Table 10 - Lower heating value per kg air of mixture

| | | Diesel | DME |
|-------------------|---------------|--------|--------|
| AF_s | $[kg_f/kg_a]$ | 0.0682 | 0.111 |
| LHV | $[kJ/kg_f]$ | 43,352 | 28,835 |
| $AF_s \times LHV$ | $[kJ/kg_a]$ | 2,956 | 3,203 |

The difference in the heating value per kg air in the mixture is:

$$\frac{3203 - 2956}{2956} \cdot 100\% = 8.4\% \quad (9)$$

The simulated imep values for $\phi = 1$ in Figure 19 are 1640 and 1529 kPa for DME and diesel respectively. This is a difference of:

$$\frac{1640 - 1529}{1529} \cdot 100\% = 7.3\% \quad (10)$$

The slightly smaller simulated performance increase when using DME instead of diesel can be explained by increased heat losses due to the higher cycle temperatures.

DME is capable of producing higher outputs than diesel. This difference may be even larger in a real engine since the soot less combustion of DME enables higher fuel-air equivalence ratios without reaching a soot limit. This also enables better transient response for turbocharged engines since a higher fuel-air ratio can be tolerated during periods of turbo lag. This has been experienced with vehicle tests in Japan [28, 29].

The simulated NO emission is given in Figure 20.

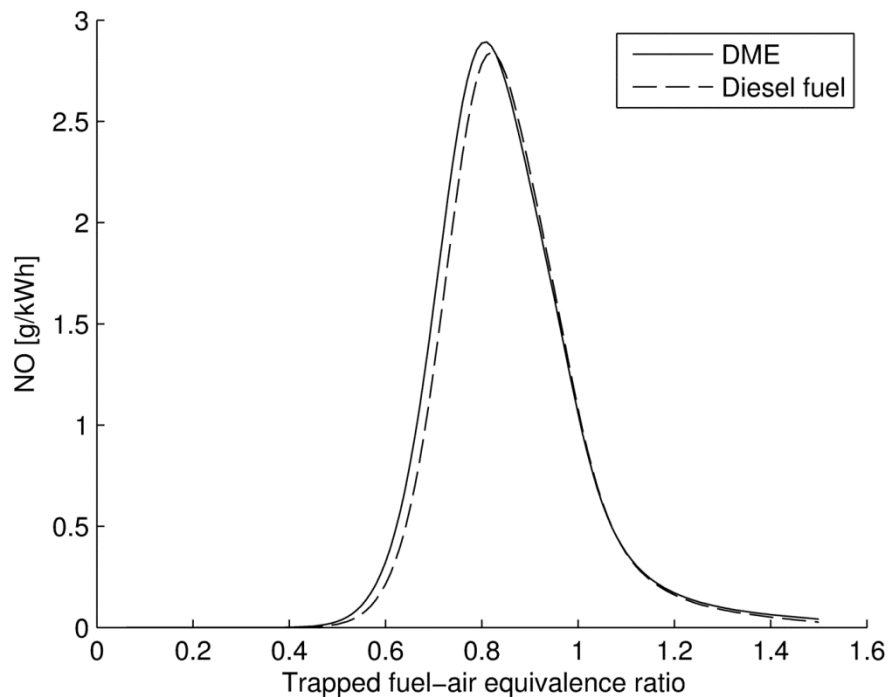


Figure 20 - Zeldovich NO emission for DME and diesel

As expected the maximum NO values are at slightly lean conditions where both temperature is high enough and oxygen is available to form thermal NO. At slightly lean conditions free oxygen atoms and OH radicals are also present. Both of these contribute to NO formation via the Zeldovich mechanism. DME shows a higher NO emission than diesel. This is to be expected for the same reason that the power output is higher. There is more energy released per kg air when operating on DME than diesel which results in higher maximum cycle temperatures. Relative to the engine simulated in

Table 7 and Table 8 there are a number of differences to the engine used in the experiments in this study. The main differences are listed in Table 11.

Table 11 - Deviations from automotive design

| Parameter | [unit] | Automotive diesel | Test engine |
|---------------|------------|-------------------|-------------|
| Cycle | [] | 4-stroke | 2-stroke |
| Port timing | [CAD ATDC] | -125/125 | -109/109 |
| Cylinder size | [ccm] | 500 | 50 |

The effects of these deviations from are investigated using the model and presented in Table 12. Rows 3, 4 and 5 show the gross indicated efficiencies when introducing changed port timing, the smaller cylinder size and the two-stroke scavenging model. The range of compression ratios used earlier is also used here.

Table 12 - Results of deviations from automotive design

| 1 | CR | 15 | 20 | 25 |
|---|---------------------|------|------|------|
| 2 | Automotive DME | 48.8 | 51.9 | 54.0 |
| 3 | EC/EO = -109/109 | 47.0 | 50.2 | 52.4 |
| 4 | 50 cc cylinder | 46.3 | 49.3 | 51.4 |
| 5 | 2-stroke scavenging | 45.1 | 48.1 | 50.1 |

The two-stroke scavenging model is G. P. Blair's [48] with a delivery ratio of 1. A delivery ratio of 1 is a reasonable estimate for a well-designed air intake system.

A reduction in potential efficiency of approximately four percentage points, resulting from the change from an automotive size four-stroke to a 50cc two-stroke, is found for all compression ratios in Table 12. For reasons discovered during analysis of the pressure traces from the first prototype engine used in this study, the actual efficiency will be lower still.

Heat release analysis of motoring had shown that Woschni under predicted the losses [10]. It was found that the heat transfer correlation developed by Annand agreed better with experimental results. Using Annand's expression instead of Woschni's gives a significant reduction in potential efficiency. The difference between Woschni and Annand is shown in Table 13.

Table 13 - Effect on engine efficiency due to choice of heat transfer model

| CR | 15 | 20 | 25 |
|---------|------|------|------|
| Woschni | 45.1 | 48.1 | 50.1 |
| Annand | 40.2 | 42.7 | 44.3 |

Here, Annand's model is used without the radiation term. The experimental data that backs up the use of Annand's method was based on motoring which is certainly without radiation. Also, the absence of soot, and thereby radiation, when DME burns is a unique

feature of the fuel (ref) which also supports not using the radiation term. Annand's equation is equation (11). The radiation term, in grey, is not used.

$$Q_w = A \left[a \frac{k}{B} Re^b (T_{wall} - T) + c\sigma(T^4 - T_w^4) \right] \quad (11)$$

Where

$$Re = \frac{S_p B}{\nu} \quad (12)$$

And

$$a = 0.76, b = 0.64 \text{ and } c = 0.54 \quad (13)$$

The version of Woschni's heat transfer correlation that is used in this study is given in equation (14).

$$Q_w = 3.26 \cdot B^{0.2} p^{0.8} T^{0.55} w^{0.8} \quad (14)$$

Where

$$w = k_1 S_p + k_2 V_d \left[\frac{T_1}{V_1 p_1} \right] (p - p_{motoring}) \quad (15)$$

The index 1 refers to a point in the cycle, in this study chosen to be the start of compression. The coefficients are:

$$k_1 = 2.28 \text{ and } k_2 = 3.24 \cdot 10^{-3} \quad (16)$$

The coefficients in equation (16) are valid for compression and expansion. The effect of the extra heat transfer predicted by Annand's correlation is illustrated in Figure 21. The fuel used here is DME only. In the remaining figures in this chapter the default settings of the model are as given in Table 14. Changes are marked in grey.

Table 14 - Change in default simulation settings

| | | Comparison of DME and diesel | DME two-stroke operation |
|---------------------------|-------|------------------------------|--------------------------|
| Cylinder size | [ccm] | 500 | 50 |
| Compression ratio | [] | 20 | 20 |
| Intake & exhaust pressure | [kPa] | 101.325 | 101.325 |

| | | | |
|------------------------------------|------------|------------|------------|
| Engine speed | [rpm] | 3000 | 3000 |
| Trapped fuel-air equivalence ratio | [] | 0.7 | 0.7 |
| IC / EO | [CAD ATDC] | -125 / 125 | -109 / 109 |
| Combustion timing | [CAD ATDC] | 10 | 10 |
| Delivery ratio | [] | 10 | 1 |
| Heat transfer | | Woschni | Annand |

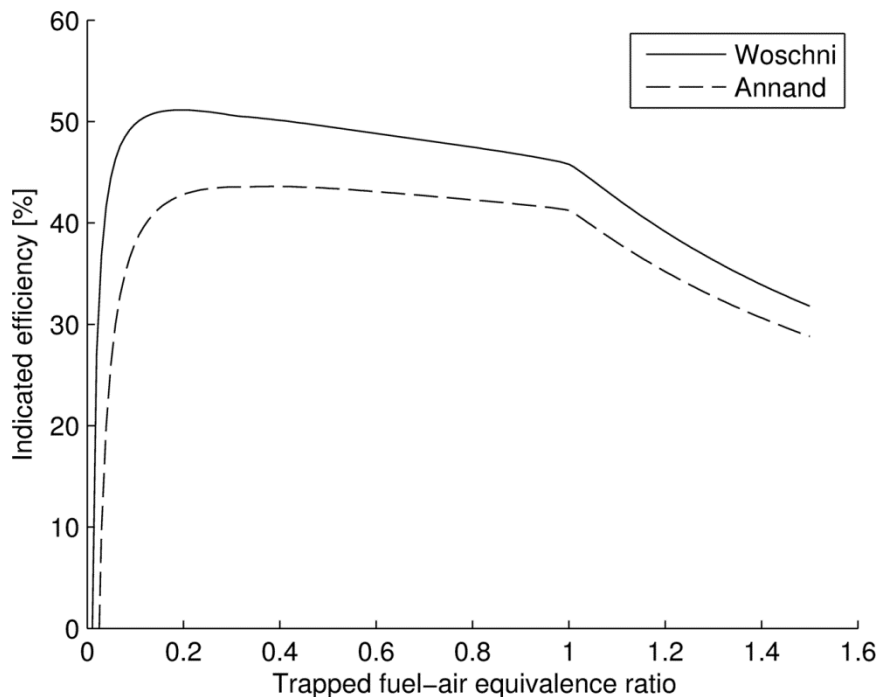


Figure 21 - Annand vs. Woschni heat transfer

The application of Annand's heat transfer correlation instead of Woschni's has a significant negative effect on the indicated efficiency. The positive effect of a lean mixture is nearly gone when Annand's heat transfer correlation is used. Still, the indicated efficiencies are above 40% for fuel-air equivalence ratios between 0.2 and 1.

Woschni correlates the heat transfer to the mean piston speed to the power 0.8. See equations (14) and (15). Annand also relates heat transfer to piston speed via the Reynolds number and in this case the exponent is 0.64. This means that for both heat transfer correlations the predicted heat loss per cycle should drop when the engine speed is in-

creased leading to improved efficiency. The simulations results with varying engine speed are shown in Figure 22.

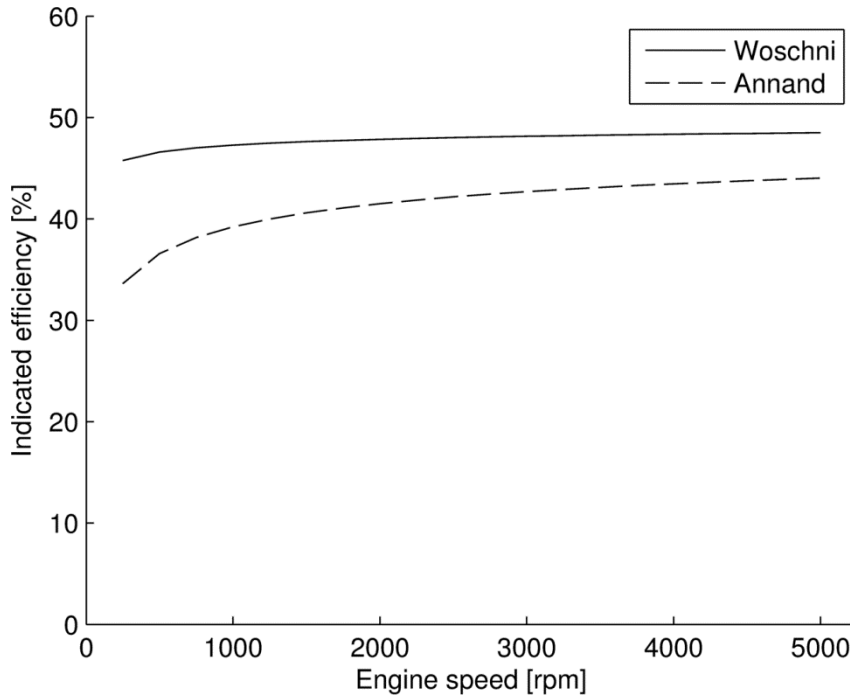


Figure 22 - Effect of engine speed on efficiency ($\phi = 0.7$)

The efficiency does increase with speed and most notably when using Annand's correlation. The monotonic increase shown in Figure 21 is also a result of the constant volume combustion which is simulated. If, as would be the case in praxis, combustion duration extends over an increasing crank angle interval at increasing engine speeds it would eventually lead to lower efficiencies due to the reduced effective expansion ratio of the combustion products that were formed at a later crank angle.

Figure 23 gives the indicated efficiency as a function of compression ratio for both heat transfer correlations.

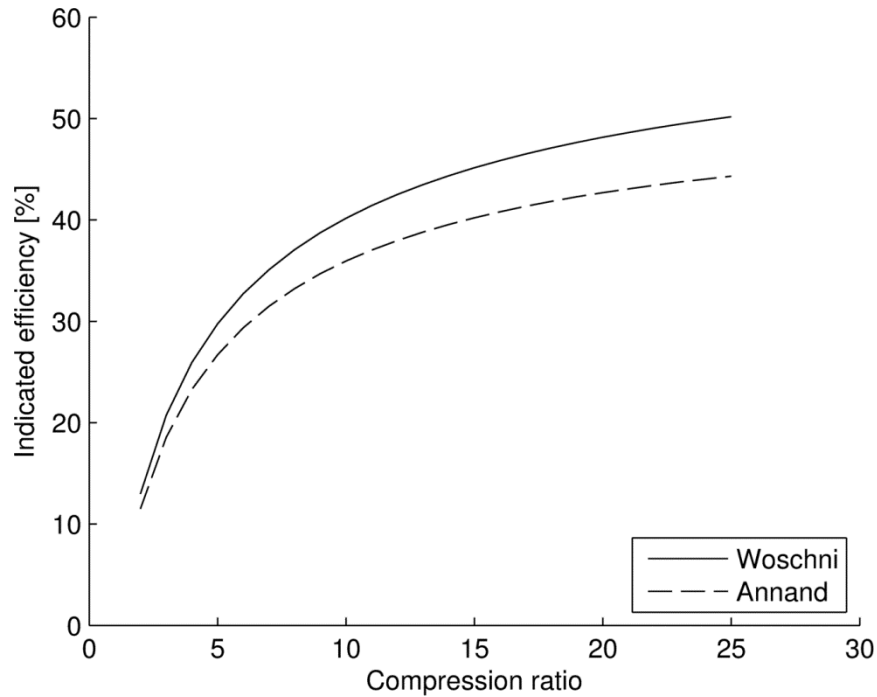


Figure 23 - Effect of compression ratio ($\phi = 0.7$, $N = 3000$)

Even at a compression ratio of 25 the curves indicate that further increases in compression ratio will improve efficiency. It is important to note here, that the model does not include mass losses past the piston and rings. Mass losses would reduce the slope of the curves in Figure 23. Also, the high pressure levels that are a result of applying very high compression ratios will induce larger forces on the piston and crank mechanism which will increase friction and thereby reduce brake efficiency. Temperature levels at high compression ratios will also be high. Figure 24 shows the effect of compression ratio on specific NO emission.

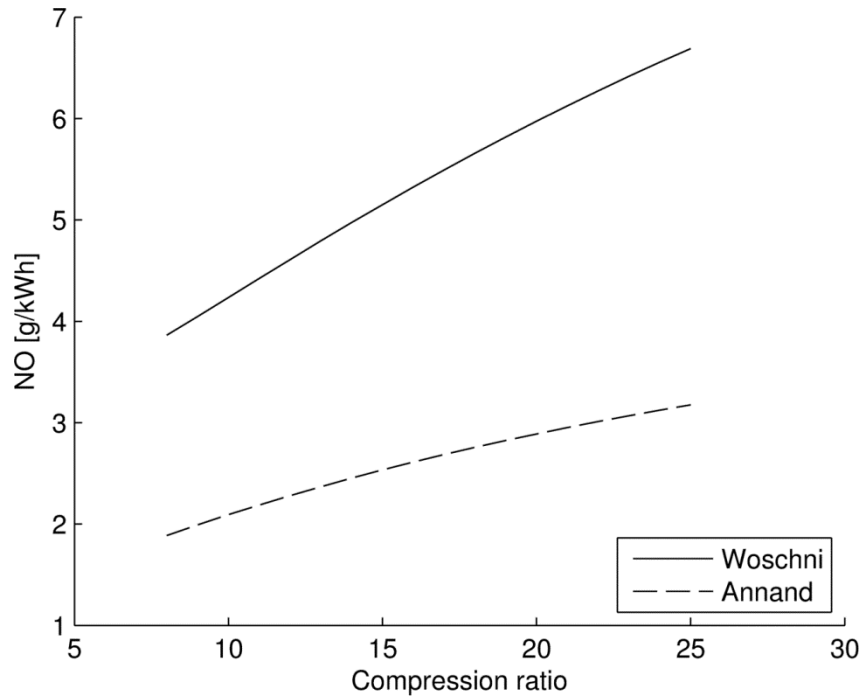


Figure 24 - Indicated specific NO emission ($\phi = 0.7$, $N = 3000$)

For the reasons summarized above compression ratios higher than 25 are rarely encountered in actual engine designs.

The effect of combustion phasing is illustrated in Figure 25.

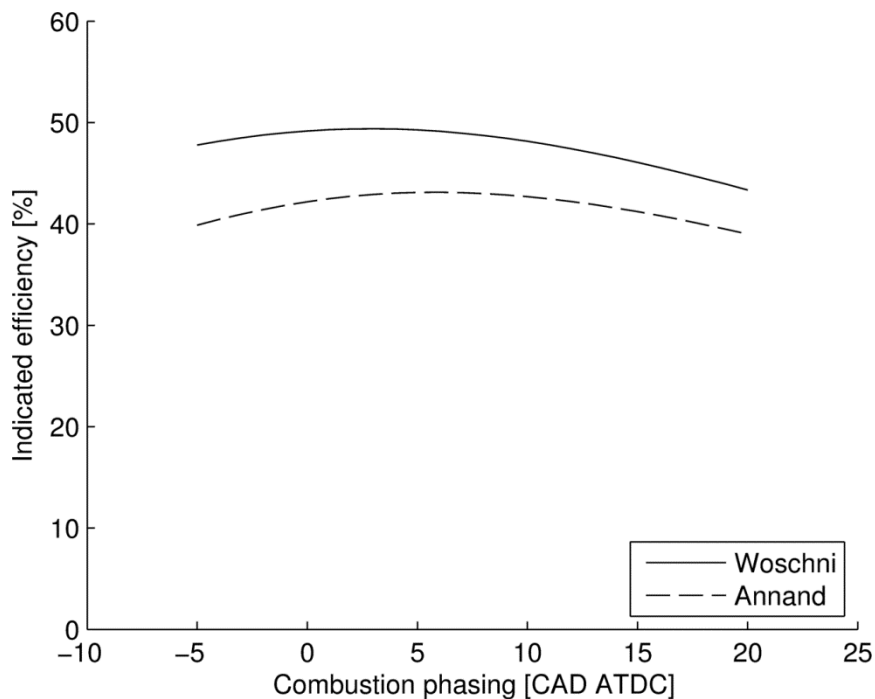


Figure 25 - Effect of combustion phasing on efficiency ($\phi = 0.7$, $N = 3000$)

The model predicts optimum combustion phasing at 3 crank angle degrees after TDC when using Woschni. For Annand, the optimum combustion phasing is at 6 crank angle

degrees, due to the increased heat losses. The previous model runs were done with a combustion phasing of 10 degrees after TDC. This is because experience has shown that combustion phasing earlier than that produces unacceptable pressure rise rates and noise. These issues are dealt with in more detail in chapter 12. Also NO emission increases when combustion phasing is advanced. The simulation results are given in Figure 26.

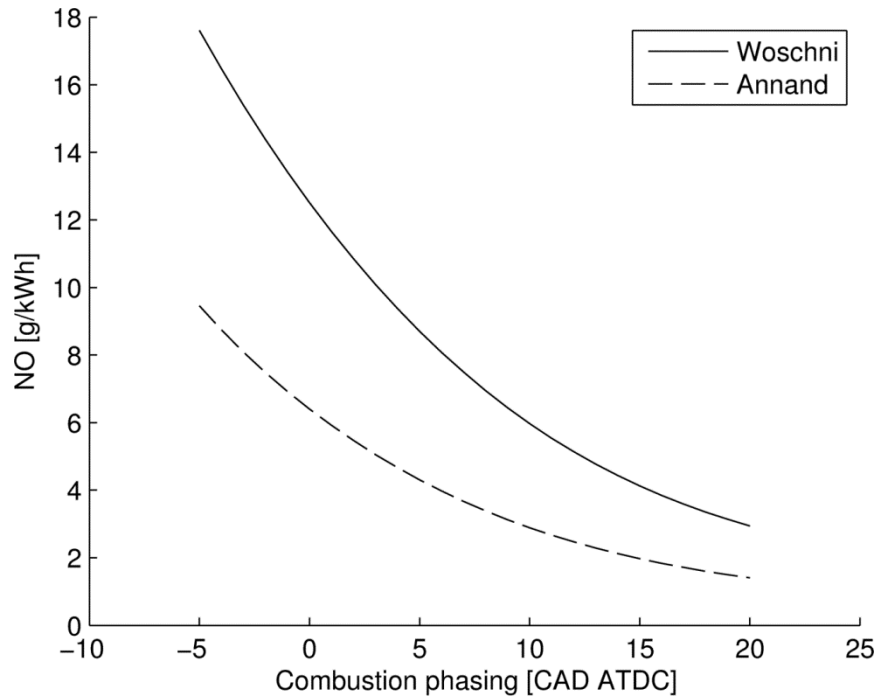


Figure 26 - Effect of combustion phasing on indicated specific NO emission
($\phi = 0.7$, $N = 3000$)

Although predictions of the possible efficiencies of a traditional compression ignition engine can be done using this model it is not able to predict emissions from such an engine. In a diesel engine where fuel injection and combustion occurs simultaneously the fuel air mixture is heterogeneous. The fuel-air equivalence ratio for the combusting zones varies between 4 and 1 depending on time and position relative to the fuel injector [50]. It is the aim of this study to test and further develop a two-stroke engine that uses late-injection HCCI. If the combustion in the test engine does turn out to be predominantly premixed the model should be able to show trends in power, efficiency and emissions that we should expect to see in experiments with such an engine. Due to the importance of the heat transfer correlation employed in the simulations the heat transfer characteristics were studied numerically using CFD and compared to experiments in chapter 11.

6. Performance and Emissions

In this chapter the performance and emissions are compared to the simulated values found in chapter 5. If the combustion realized in the test engine is predominantly premixed there should be agreement between the trends. First, the indicated efficiency as a function of fuel-air equivalence ratio is presented in Figure 27.

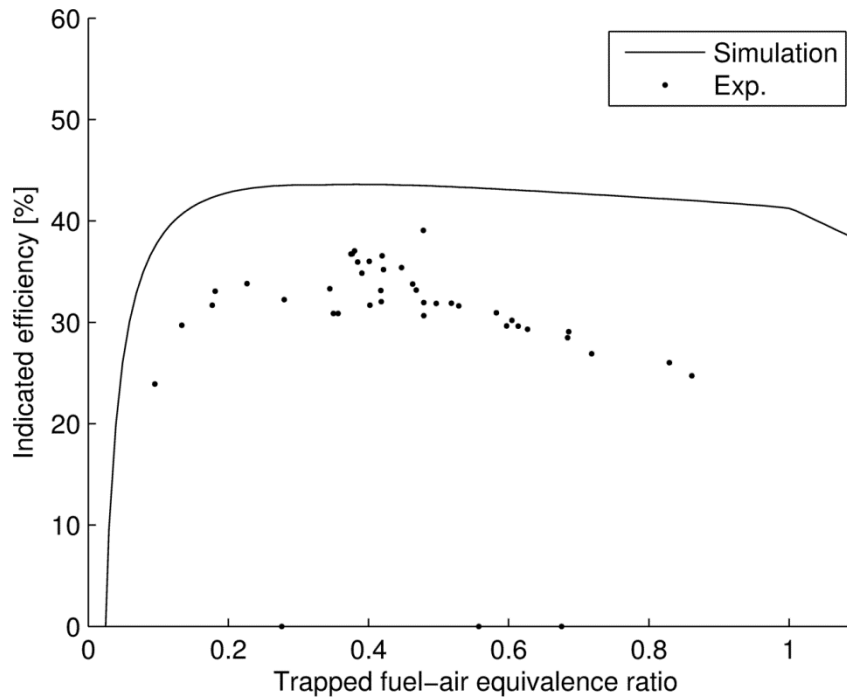


Figure 27 - Effect of fuel-air equivalence ratio on indicated efficiency

All measured indicated efficiencies are lower than the simulated. This is expected since the simulation operates with constant volume combustion and the combustion in the test engine will have a finite rate. The general trends agree though. At low loads the measured efficiency drops off due to heat losses being high relative to heat release from combustion. At high loads the measured efficiency drops off with a steeper slope than the simulation results. The primary reasons are increased combustion duration and reduced combustion efficiency, both due to insufficient fuel-air mixing which is a result of the increased mass of injected fuel. As the fueling level is increased the injection timing also has to be retarded to avoid excessive knocking. Together, these effects produce a steeper negative slope than the simulated.

The accumulated apparent heat releases for half and full load are plotted in Figure 28 to show these effects. In order to better be able to compare the traces after start of combustion the negative apparent heat release before combustion which is due to heat losses has been removed and the curves start at the first non-negative heat release. This is particularly useful when the normalized heat release is plotted.

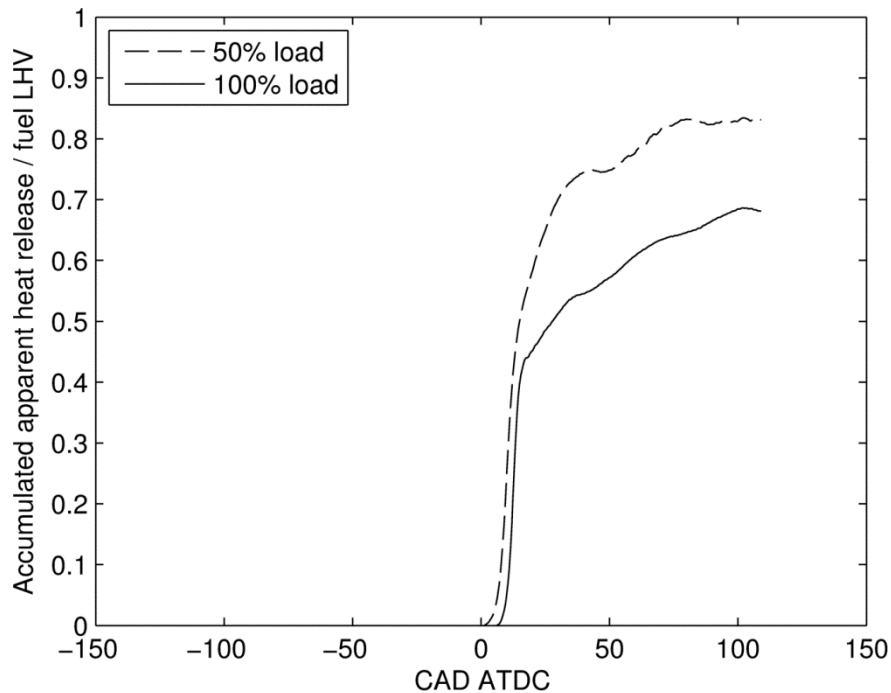


Figure 28 - Effect of fuelling level on apparent heat release

The first part of the heat release is quite similar for 50% and 100% load. After that, it is clear from Figure 28 that it is significantly easier for the 50% load case to find sufficient oxygen to continue combustion than it is for the 100% load case. The combustion proceeds quicker and the combustion efficiency is higher for the 50% load case. No heat transfer correlation has been applied so the actual combustion efficiency is higher than the end values in Figure 28. Both curves are measured with the combustion timing set for optimum engine efficiency.

Figure 28 also shows that the engine is not able to mix fuel and air sufficiently before the onset of combustion to operate completely in PCI mode. To improve fuel-air mixing the injection timing could either be advanced or retarded a sufficient distance away from TDC such that the gas temperature is lower when the fuel is injected and ignition delay then would be longer. It turns out that it is not possible to move the injection timing much in any direction. Advancing the fuel injection leads to strong knock except at low loads. Retarding the fuel injection eventually results in misfires. Figure 29 shows accumulated heat release for the earliest and latest injection timings possible at 70% load.

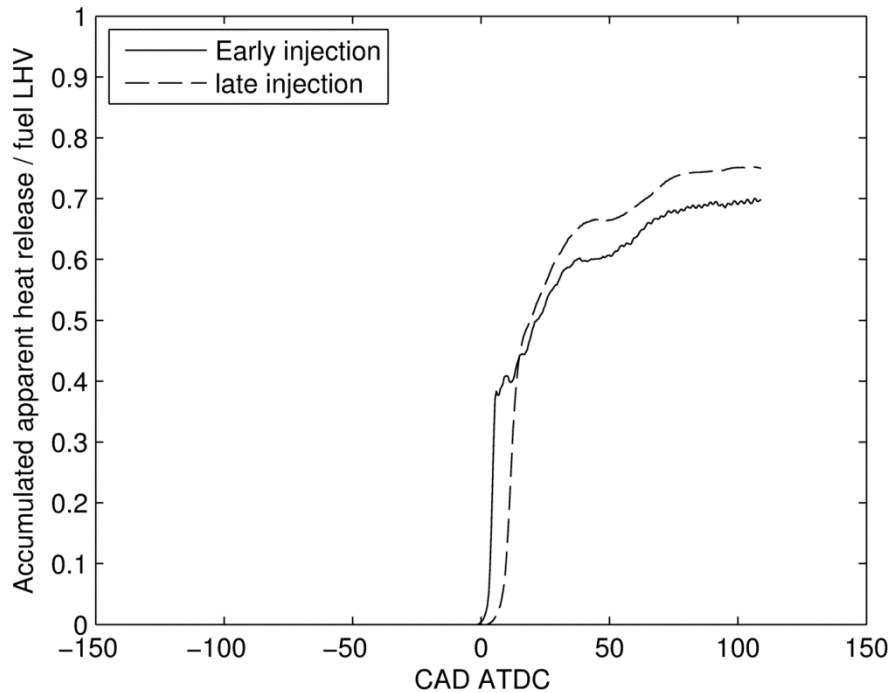


Figure 29 - Effect of combustion phasing on apparent heat release

Early injection is 21° BTDC and late injection is 17° BTDC. The resulting ignition delays are given in Table 15.

Table 15 - Ignition delay for early and late injection

| | SOI | CA10 | Ignition delay |
|-----------------|----------|-----------|----------------|
| Early injection | 21° BTDC | 3.5° ATDC | 24.5 |
| Late injection | 17° BTDC | 9.5° ATDC | 26.5 |

Table 15 shows that the ignition delay is hardly affected by the small changes in injection timing that are possible.

The injected fuel mass is kept constant for both injection timings so the reduced heat release for the early injection curve relative to the late injection curve seen in Figure 29 is either a result of increased heat losses or incomplete combustion. Table 16 shows that the combustion completeness is comparable for the two cases so there must be significantly

increased heat losses associated with early injection timing and thereby combustion timing. This seems reasonable since the combustion temperatures will be higher for early combustion.

Table 16 - CO and HC emissions for early and late injection timing

| | CO [%] | HC [ppm] |
|-----------------|--------|----------|
| Early injection | 0.58 | 395 |
| Late injection | 0.60 | 406 |

It is clear that the premixing before combustion is not complete. A significant part of the heat release happens in a mixing controlled mode. A range of different cylinder head designs and injector positions were tested during a master thesis project supervised by the author [51]. Although there were differences in the performance the general picture remained the same: 50 to 65% of the heat release happened quickly in a premixed fashion and the remaining heat release was a slow mixing controlled process.

The result in terms of NO_x emissions as a function of load is shown and compared to the simulation results in Figure 30.

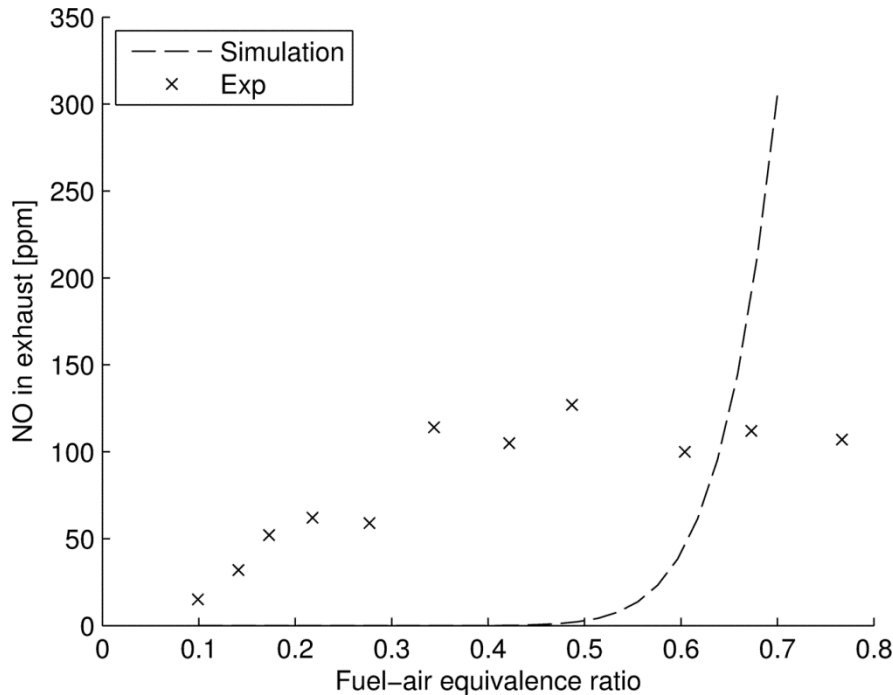


Figure 30 - NO_x emission as a function of load - simulation and exp.

Even at the lowest loads measurable quantities of NO_x are formed in rich zones that are a result of the incomplete mixing. As the load is increased NO_x emissions increase up to the point of maximum engine efficiency. At even higher loads the NO_x emissions are not increasing further. This is due to the slower heat release in the mixing controlled combustion

phase which, combined with the continuing expansion of the cylinder volume, puts a limit on the temperature increase due to increased fuelling. The simulation does not show that same limit on NO formation since it has constant volume combustion.

The effect on NO_x emission as a function of combustion phasing is shown in Figure 31.

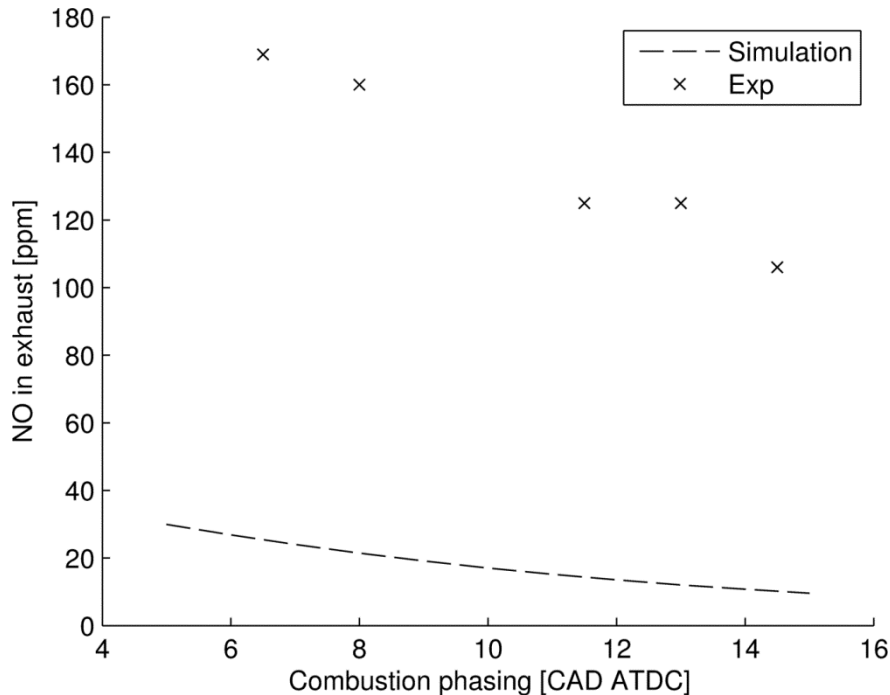


Figure 31 - Effect of combustion phasing on NO

The measured NO_x emissions are significantly higher than the values calculated using the single zone simulation. The global fuel-air equivalence ratio is approximately 0.5 and the single-zone simulation returns a quite low flame temperature because the excess air acts as an inert component that must also be heated by the combustion. The low flame temperature is the reason for the low simulated NO emission. In fact, this is the basic idea behind the HCCI engine concept: Using lean combustion to achieve low combustion temperatures and thereby NO_x emissions. Since the latter part of the heat release is mixing controlled it is likely to happen at an equivalence ratio close to one which would create the temperatures needed to produce the NO levels measured in the exhaust.

At this point the only knowledge about the degree of premixing comes from the heat release curves. Further insights could be gained from images of the combustion process. Chapter 7 describes the design of an optical access cylinder head and the images captured with it.

7. Optical Access Cylinder Head

Due to the small dimensions of the engine it was considered possible to use borosilica instead of quartz as the transparent part of the cylinder head. Borosilica is probably better known by its trade name Pyrex. It is used for everything from laboratory glassware to cooking. Its main advantage over normal glass is its lower thermal expansion coefficient which makes it more resistant to thermal shocks than ordinary glass. It is also easy to shape so that the desired dimensions for this application could be achieved by melting and forming the glass.

Figure 32 shows an exploded view of the optical cylinder head and surrounding parts. The discs above and below the optical window are made of PTFE (Teflon). The bottom one seals between the cylinder head and the optical window. Both the bottom and the top disc also act as a means to distribute the clamping force from the bolts onto the window in a distributed manner.

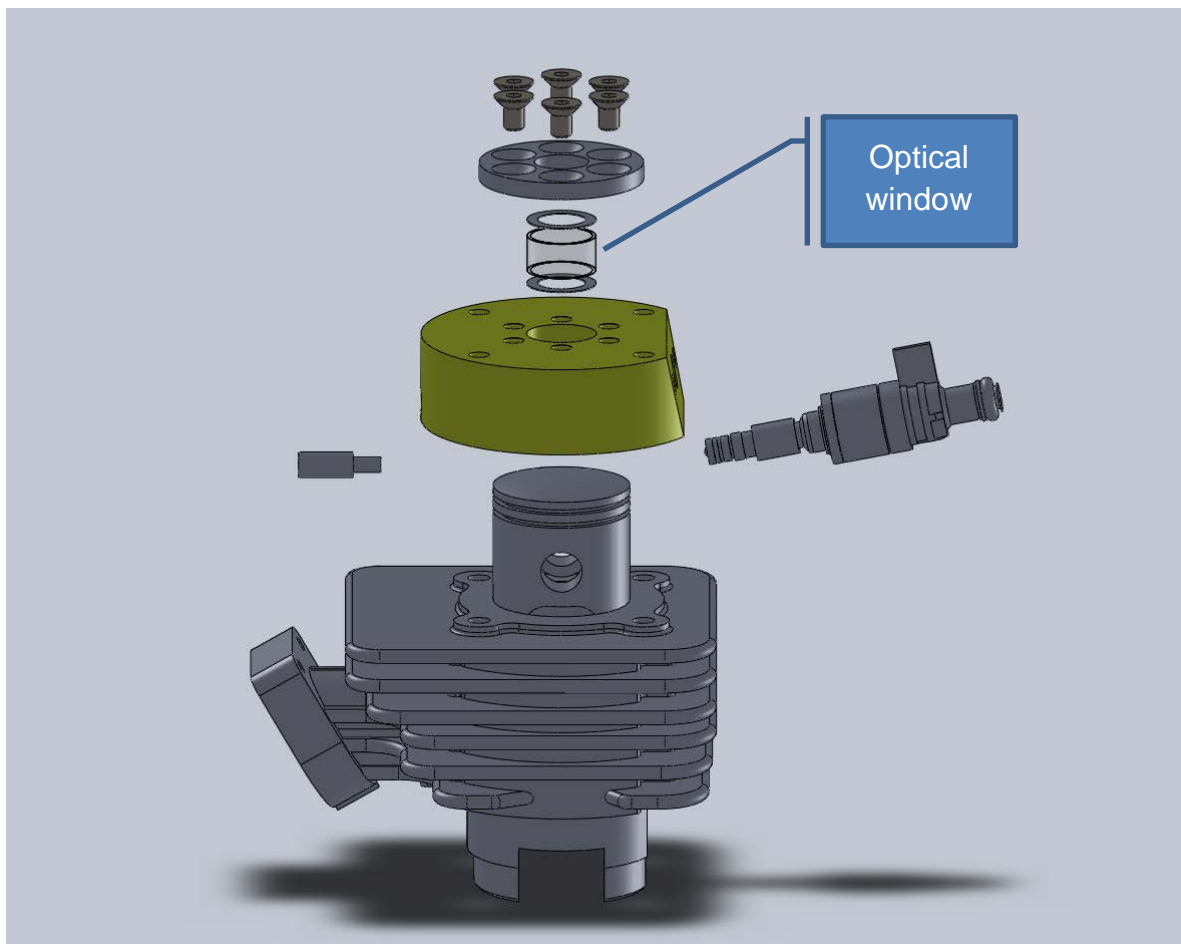


Figure 32 - Exploded view of optical cylinder head (green) and surrounding parts

In order for the setup to be accessible by the camera it was decided to move the injector down onto the side of the cylinder head. In this way the camera could hang above the cylinder head and have an unobstructed view of the entire combustion chamber within the squish zone. The cylinder head shape was axisymmetric like most of the other tested cylinder head designs but the conical shape of the combustion chamber was dispensed with in favour of a cylindrical combustion chamber. This would make it possible for the camera to see the entire combustion zone inside of the squish areas. The squish area ratio was increased from 60 to 85% in order to have sufficient height to fit the injector from the side.

Figure 33 shows a cut-away view of the solution. The injector is on the right, the cylinder pressure sensor on the left side of the cylinder head shown in green. The mounting arrangement for the injector is not shown.

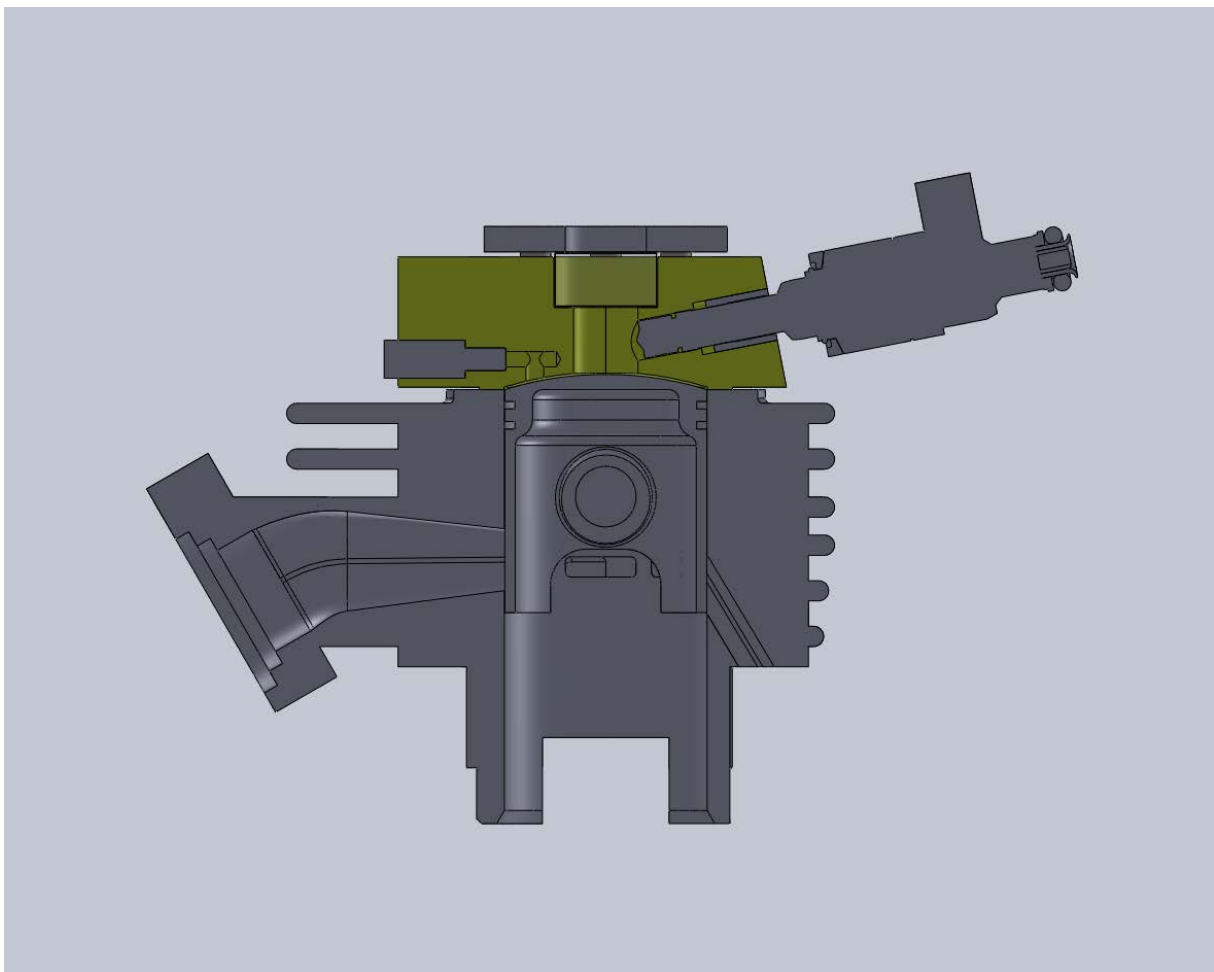


Figure 33 - Cut-away showing the optical cylinder head and adjacent parts

The injector is designed such that the spray is tilted 11° away from the injector axis. The injector bore is tilted the same amount such that the spray centre is entering the chamber horizontally. This is shown in Figure 34 and Figure 35.

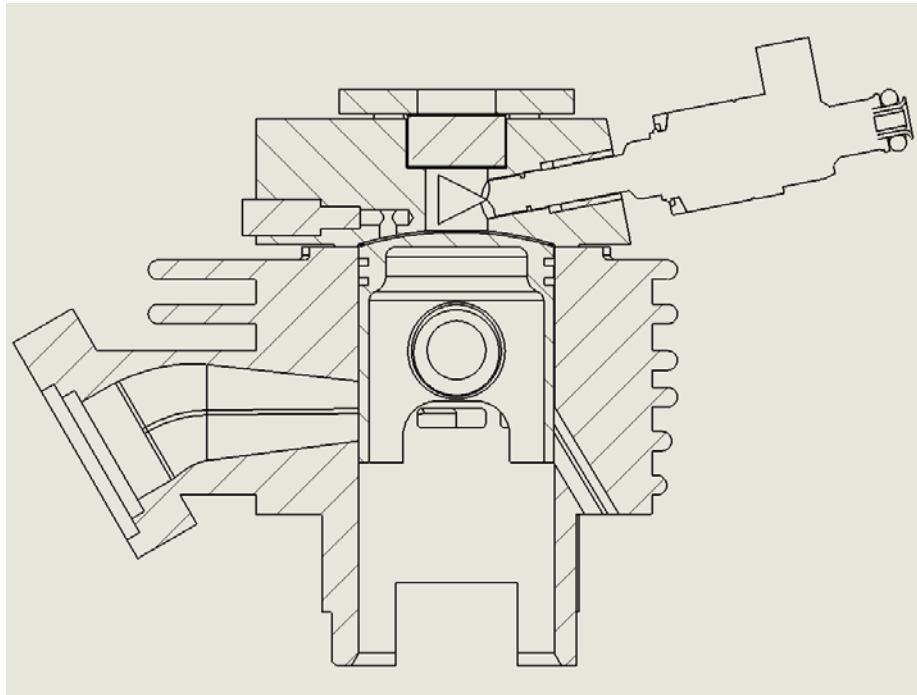


Figure 34 - Section view of optical access solution

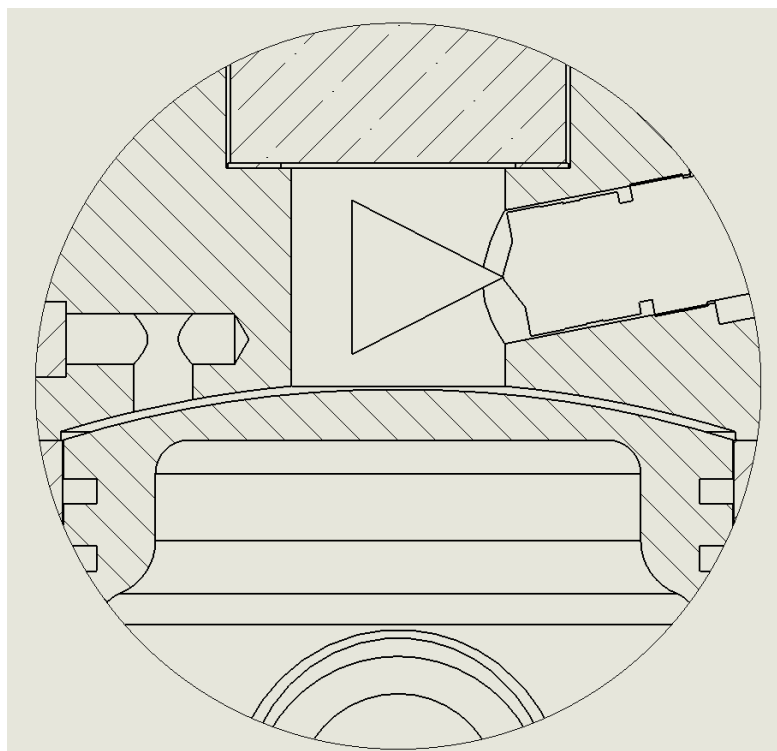
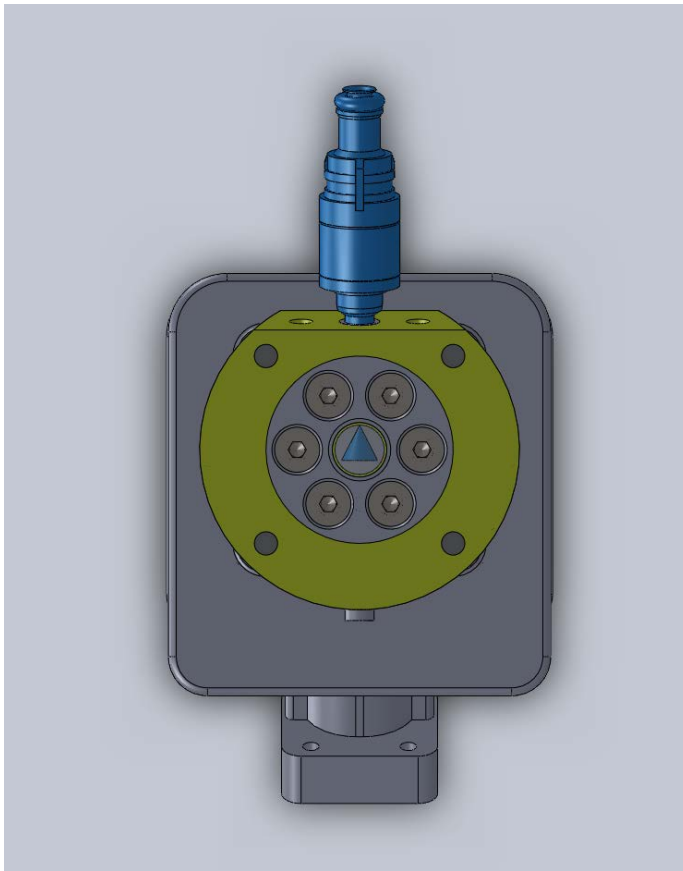
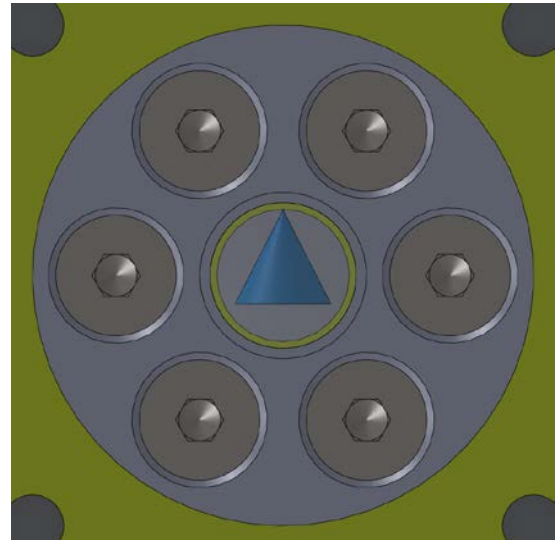


Figure 35 - Detail of combustion chamber for optical access solution

Figure 36 shows the arrangement from the point of view of the camera.



(a)



(b)

Figure 36 - (a) Injector, cylinder and optical cylinder head as seen from the camera. (b) Detail of the window into the combustion chamber. Injector and spray cone angle displayed in blue.

In order to make sure that the combustion mode of the optical cylinder head is not too different from the all-metal design some performance numbers and a heat release analysis is compared with the all-metal design.

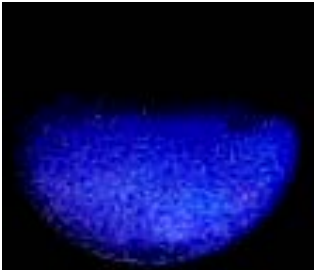
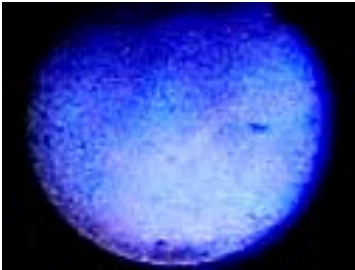
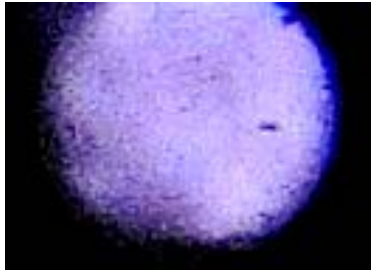
| | | |
|---|---|---|
|  |  |  |
| Cold flame spreading | Peak luminosity from cold flame | Hot ignition and main heat release |

Figure 37 – Images of the combustion stages

Previous studies of the phases of HCCI auto-ignition have revealed similar patterns as Figure 37 illustrates for this engine [52]. DME is a two-stage ignitino fuel. At first, a low temperature heat release (LTHR) occurs which is called the “cold flame”. The luminosity in this phase is in the blue spectrum. Then, the high temperature heat release (HTHR) is triggered. The majority of the heat is released in the HTHR. A shift in the colour towards red happens once the HTHR starts due to the emission from water at longer wave lengths.

Table 17 - Burning lube oil droplet

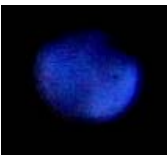
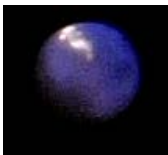



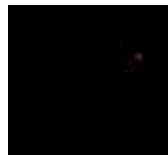
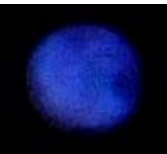


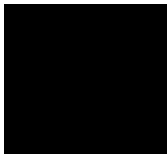
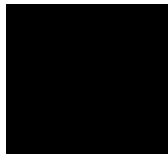
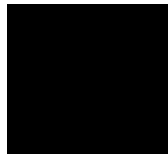
| | | | | | |
|---|---|---|---|---|---|
|  |  |  |  |  |  |
|  |  |  |  |  |  |
| X CAD | +10° | +20° | +30° | +40° | +50° |

Table 17 shows a series of pictures of normal combustion and a series with abnormal combustion. The top row is the abnormal combustion. What appears to be lube oil droplet is ignited during the later stages of DME combustion an can be seen traveling across the

combustion chamber for a period of 40 CAD. The picture series' are interesting because they show the very different nature of DME and oil combustion. The yellow sooting flame that the oil droplet has is not seen with DME.

8. Indirect injection

Investigation of charge preparation strategies for controlled premixed charge compression ignition combustion using a variable pressure injection system [53]

In an attempt to improve premixing an indirect injection cylinder head was designed. The match between fuel injector and cylinder head for the direct injected engine was based on the spray pattern of the injector and not much else. An indirect injection cylinder head would not be so reliant on the matching since the air motion is much stronger and it was thought that it would be worthwhile to design and test such a cylinder head.

The cylinder head was manufactured such that the normal squish height of 0.5mm was retained. The opening, or throat, into the prechamber was kept rather large compared to traditional indirect engines. The throat area was 4.5% of the bore where 1.5% is more typical. This was done to reduce pressure and heat losses associated with the in- and outflow of air. It was felt that given the properties of DME it would not be necessary to create as strong an air flow as that typically used in diesel indirect injection engines.

Despite the use of a compression ratio of 22 starting was more difficult. Preheating the engine to approx. 60°C was necessary.

A comparison of the pressure traces at peak efficiency is given in Figure 38.

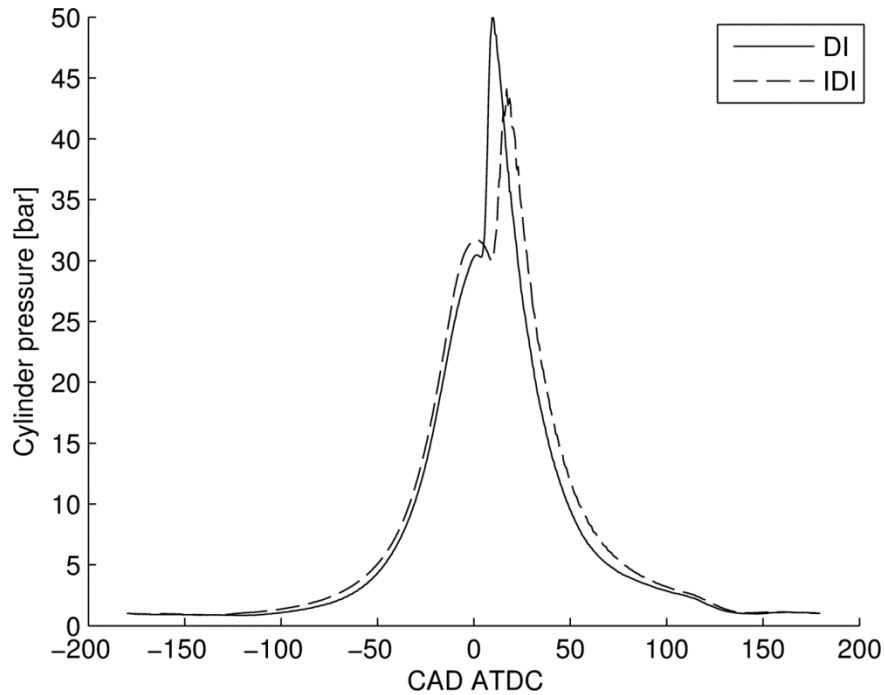


Figure 38 – Comparison of DI and IDI pressure traces. Bmep 350 kPa.

The higher compression ratio can be seen on the compression stroke but the injection timing is delayed from 29 CAD BTDC to 21 CAD BTDC in order to achieve best efficiency for the IDI cylinder head. This results in a lower maximum pressure. The heat release traces are given in Figure 39.

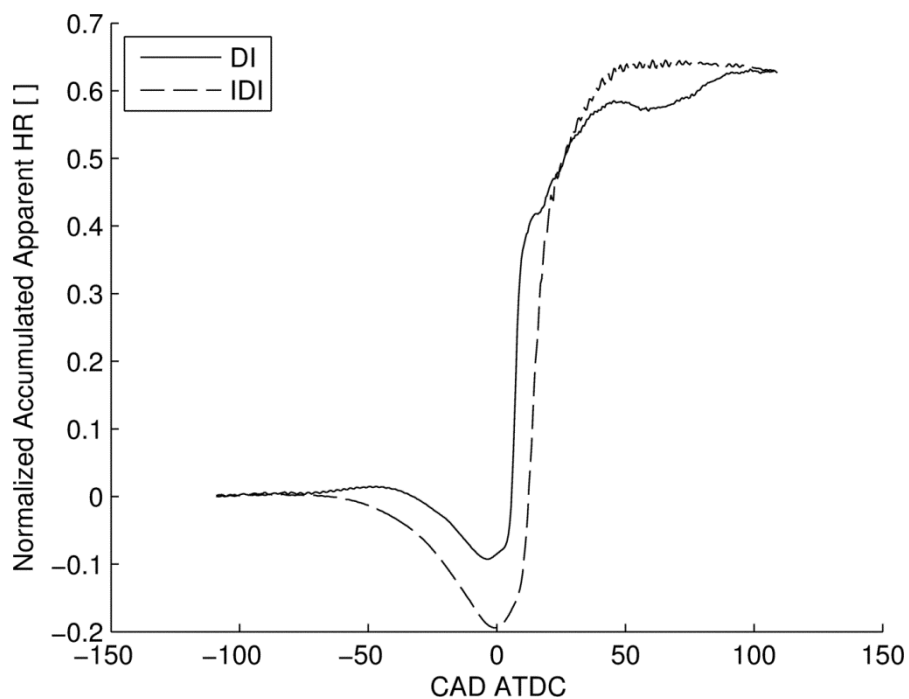


Figure 39 – Comparison of DI and IDI heat release. Bmep 350 kPa.

The increase in heat losses due to the narrow passage to the prechamber is clearly seen. As could be seen on the cylinder pressure plot the heat release is also retarded for the IDI

cylinder head. Although a lot of heat loss occurs on the compression stroke the peak in accumulated heat release is higher for the IDI case. This indicates that combustion is more complete. To see this more clearly the same curves are drawn in Figure 40 but starting from zero at the time of the first heat release from combustion.

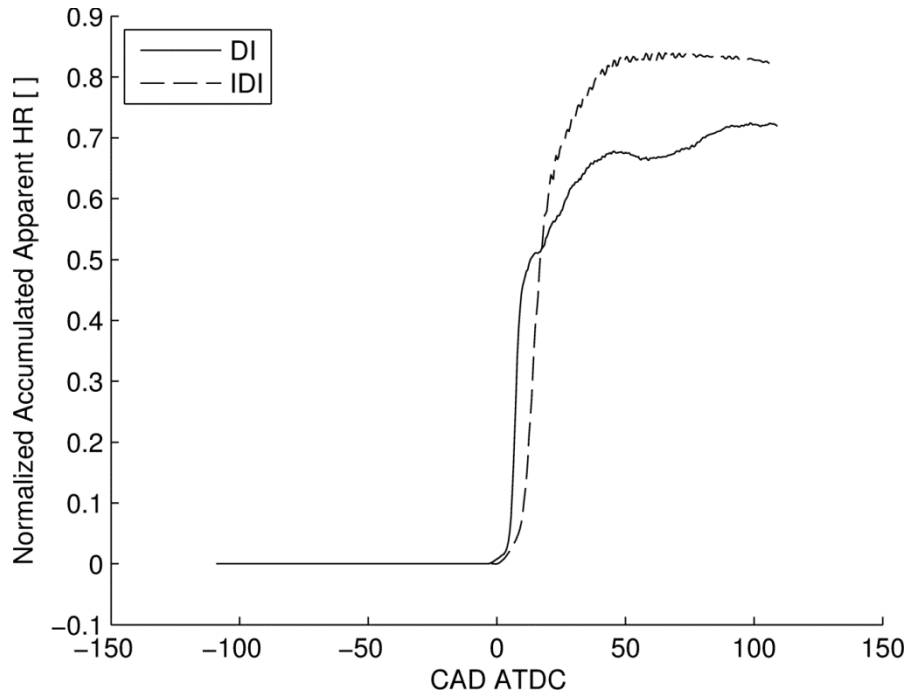


Figure 40 - Comparison of DI and IDI heat release after start of combustion

Figure 40 shows that combustion is completed faster for the IDI cylinder head. Although it gets going later it is completed at around 50 CAD ATDC. The direct injected cylinder head runs out of premixed fuel and air after when approx. 50% of the heat release has occurred and mixing controlled combustion takes place all the way to 90 CAD ATDC. Clearly the IDI cylinder head provides better premixing than the DI.

The resulting brake efficiencies are plotted in Figure 41.

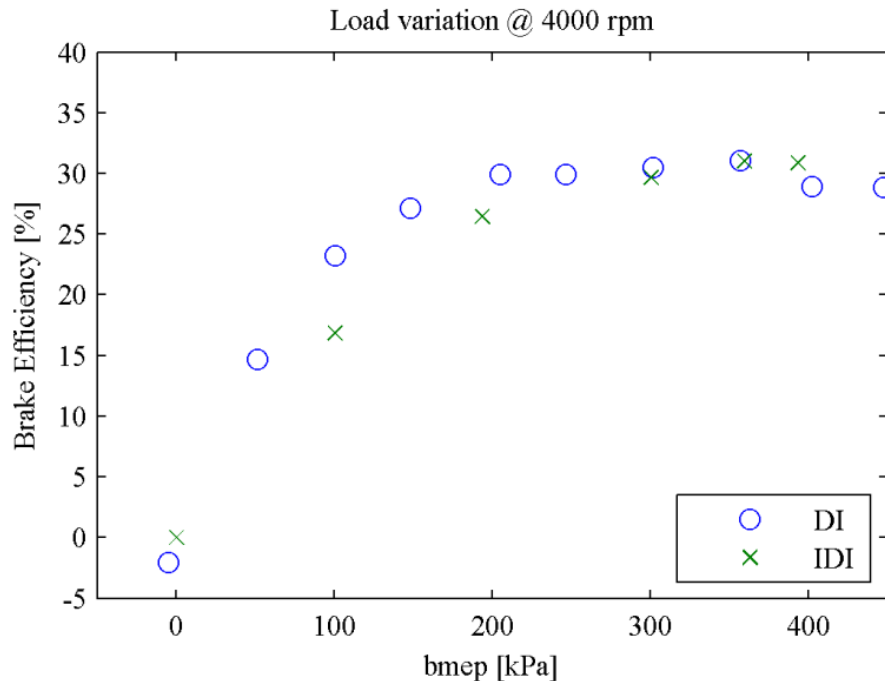


Figure 41 - Brake efficiency for DI and IDI operation

Due to the increased pressure and heat transfer losses the efficiency of the IDI is not better than the DI. That it is just as good at high loads is a result of more complete combustion. The 450 kPa bmep point could not be held for the IDI cylinder head for the duration of a complete efficiency test. So despite the better mixing the maximum load is slightly reduced for the IDI cylinder head. At lower loads the efficiency is lower in the IDI case. Pressure and heat losses are suspected to grow relative to the heat release when the load is decreased.

The more complete combustion at high loads can be seen in Figure 42 and Figure 43 showing the CO and HC emissions.

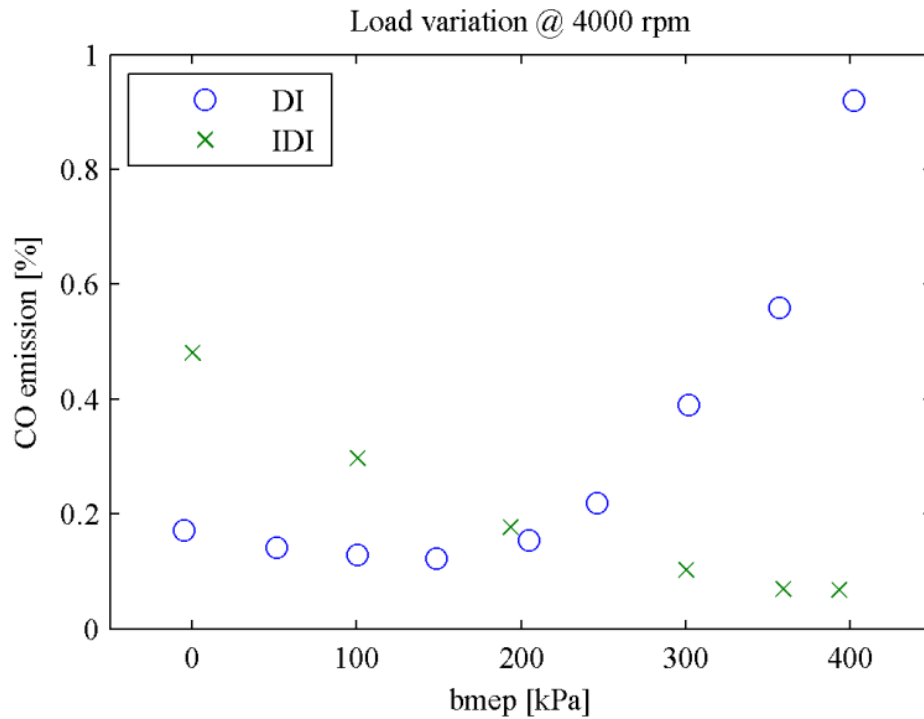


Figure 42 - CO emissions for DI and IDI operation

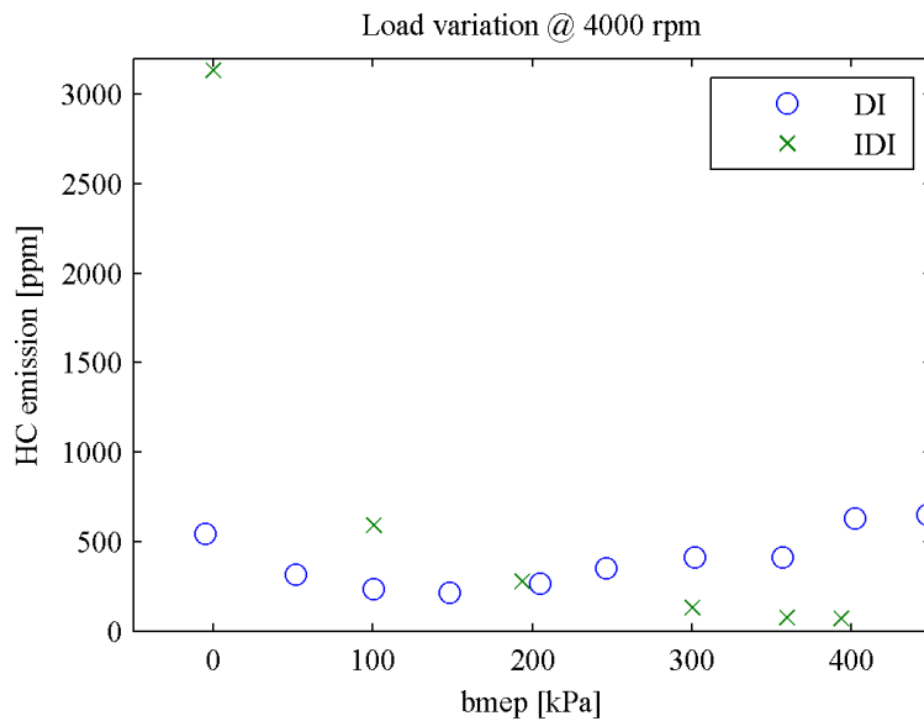


Figure 43 - HC emissions for DI and IDI operation

It is interesting that the curves for DI and IDI are basically opposite in trend. When the load is increased the CO emission from DI operation increases dramatically. Mixing rates are

insufficient to complete CO oxidation before reactions quench in the expansion stroke. HC emissions also increase with increasing load. IDI operation shows monotonically falling values of CO and HC with increasing load. The charge in the prechamber is well premixed and increasing fuel-air equivalence ratio with increasing load increases the combustion temperature and therefore the combustion completeness. The charge remains leaner than stoichiometric also at full load so CO emission does not start to increase due to dissociation.

When reducing the load the IDI case shows increasing emissions of CO and HC. The mixture in the prechamber is so lean that although it is well mixed combustion is not complete. This is a typical feature of lean low-temperature combustion [42].

The NO_x emissions verify the lower temperature of combustion at low load for the IDI case. This is shown in Figure 44. As the load is increased the NO_x emissions increase to the level of DI op.

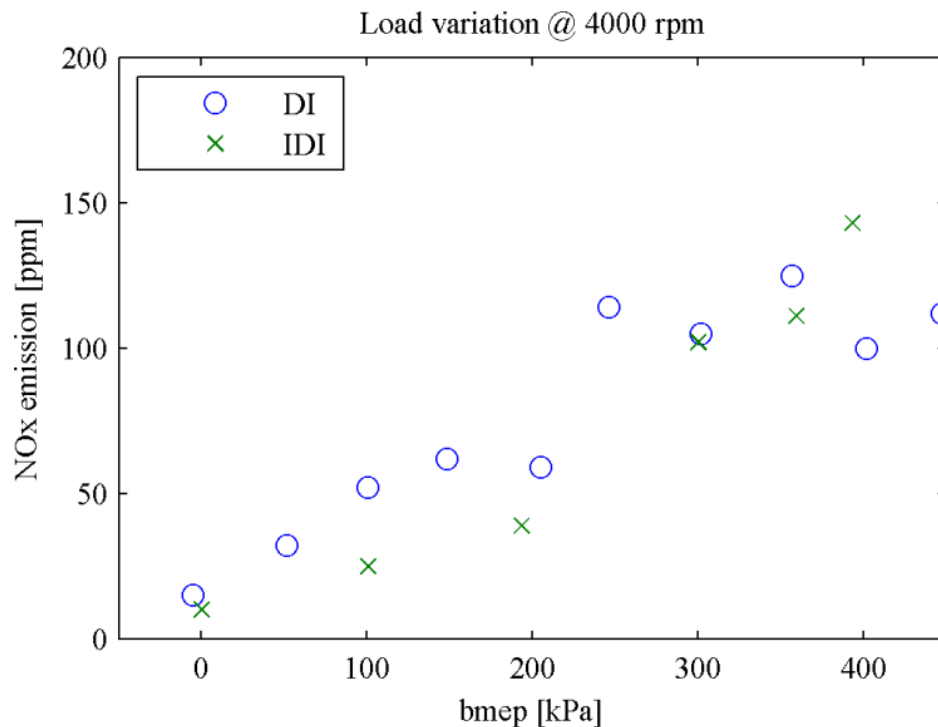


Figure 44 - NO_x emissions for DI and IDI operation

The experiments with an IDI cylinder head have shown that premixing can be improved compared to the DI case. At high loads this results in more complete combustion and reduced emissions of CO and HC but NO_x emission levels are approx. the same. At low loads NO_x emissions are significantly lower but the reason is lower combustion temperatures and that increases the CO and HC emissions.

9. EGR

9.1 Theory

In the early stages of the development of exhaust gas recirculation (EGR) as a NO_x emission control method it was thought that the primary reason for EGR's effectiveness in reducing engine out NO_x was the higher heat capacity of CO_2 relative to N_2 . The higher heat capacity of CO_2 would reduce the flame temperature and thereby NO_x emissions. It is now clear that the heat capacity of CO_2 is not the primary reason for the effectiveness of EGR. In the following the actual effect of EGR on flame temperatures will be investigated in order to evaluate the potential of internal EGR for NO_x suppression in a two-stroke engine.

The plots presented are created by a range of Matlab programs written or modified by the author. The calculated flame temperatures are the adiabatic flame temperatures for equilibrium compositions with properties based on the latest 9-coefficient NASA polynomials.

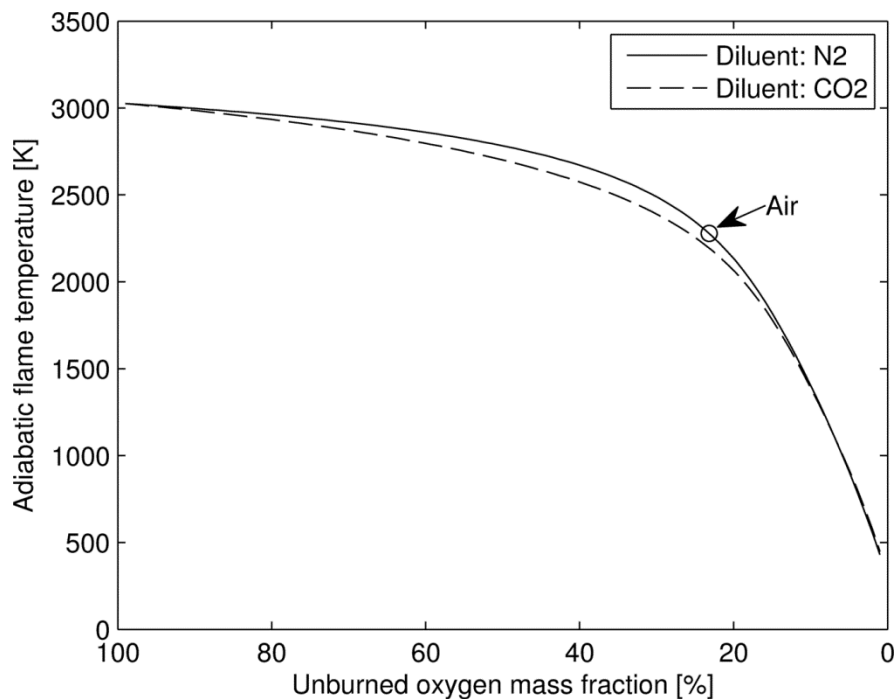


Figure 45 - Flame temperatures for stoichiometric combustion of DME in atmospheres consisting of oxygen and nitrogen (Air) and oxygen and CO_2 (equilibrium products).

Figure 45 illustrates the effect of completely replacing N_2 with CO_2 in the combustion air. This is an extreme situation and serves only to show that the higher heat capacity of CO_2 relative to N_2 does reduce the flame temperature somewhat. A more realistic case is to

consider stoichiometric flame temperatures based on dilution of atmospheric air with either N_2 or CO_2 . This is shown in Figure 46.

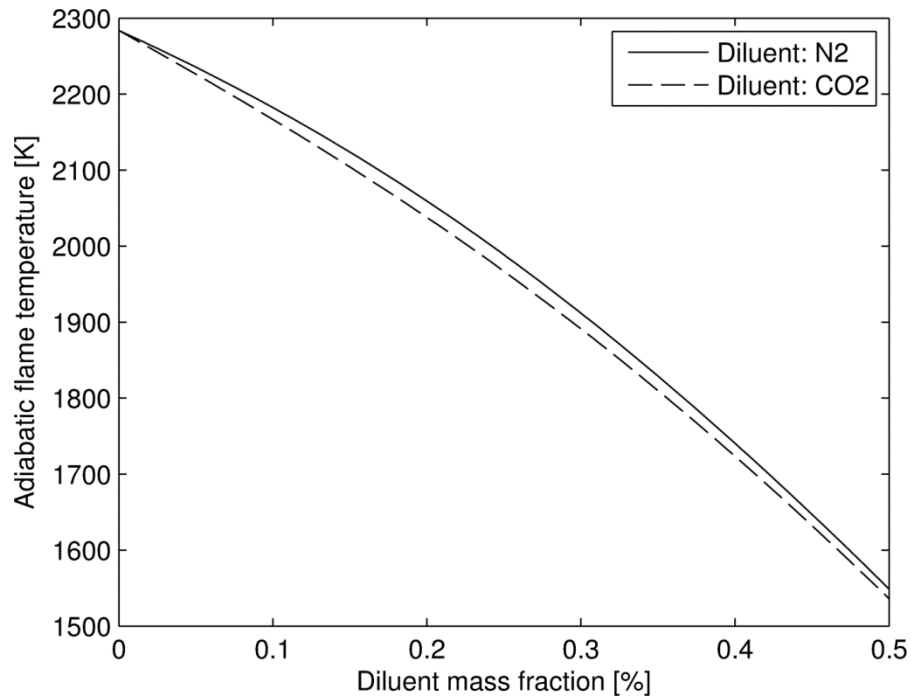


Figure 46 Flame temperature as a function of dilution of atmospheric air with N_2 and CO_2 respectively.

Figure 46 shows the case where N_2 is not completely replaced by CO_2 but the atmospheric combustion air is diluted by N_2 and CO_2 respectively. Since in this case N_2 is not completely replaced by CO_2 the difference is significantly smaller. Figure 46 has diluent mass fraction on the x-axis. Figure 47 shows the same results but with oxygen mass fraction on the x-axis.

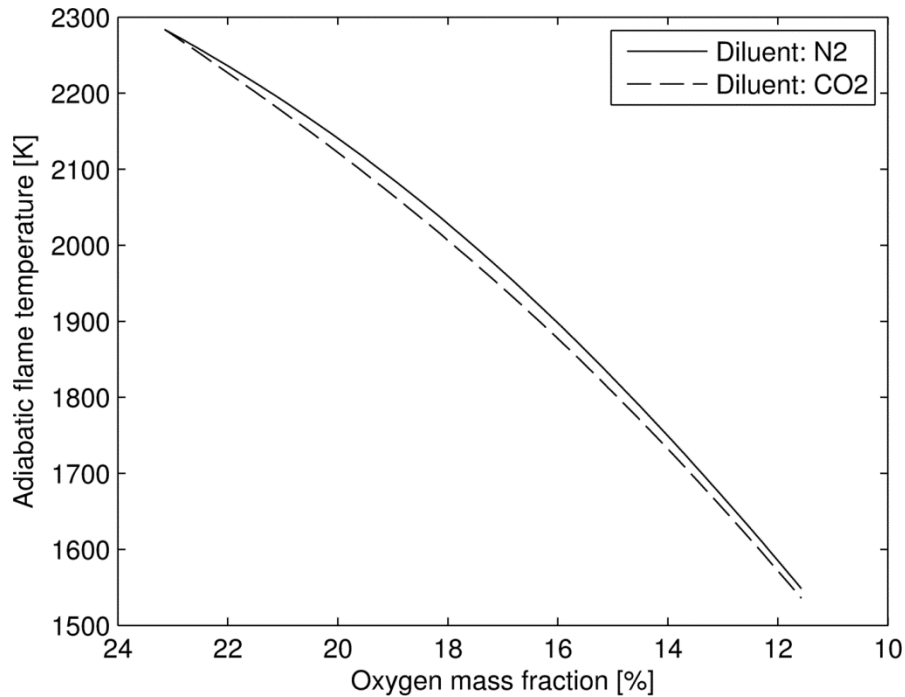


Figure 47 - Flame temperature as a function of oxygen mass fraction for atmospheric air diluted by N₂ and CO₂ respectively.

It is clear from Figure 47 that the oxygen content of the combustion air is more important to the flame temperature than the higher heat capacity of CO₂ relative to N₂.

The results shown up to this point has been for reactants at standard conditions and for dilution with pure N₂ or CO₂. In an engine the diluent would be recycled exhaust gas (EGR) and the reactants would be compressed to a temperature and pressure level significantly higher than standard conditions (1 atm & 298 K).

In order to study the effect of EGR on flame temperatures in an engine it is necessary to determine the composition of the reactants and to compress those reactants to a similar level as that reached in an engine. This is done by the cycle simulation.

9.2 Experiments

The effect of throttling the engine on NO_x emissions are illustrated in Figure 48.

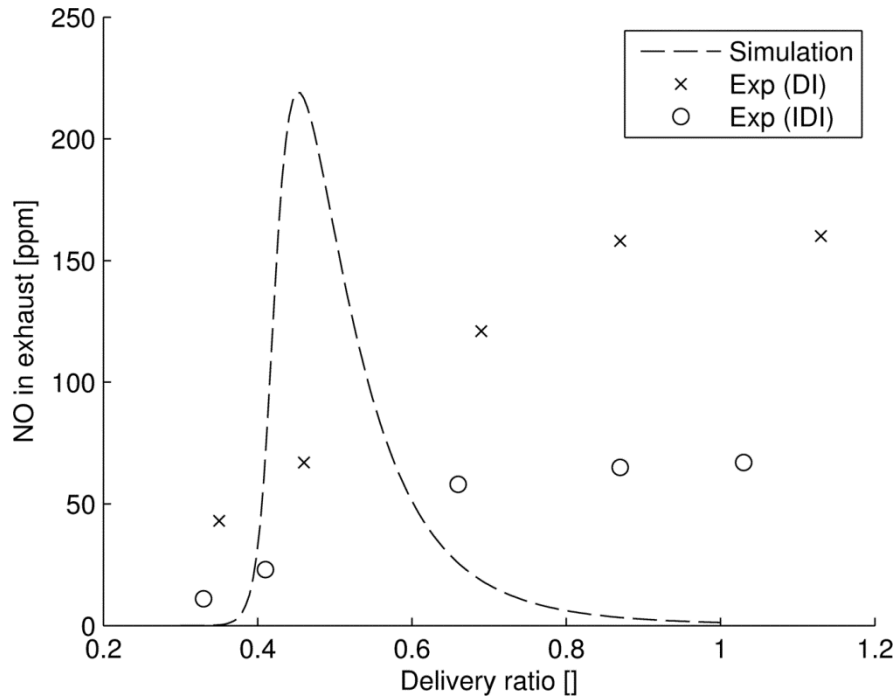


Figure 48 - NO_x emissions as a function of throttling

If the entire fuel-air mixture was completely premixed, such as the simulation assumes, there would be a peak in NO formation just lean of stoichiometric conditions. This is the peak shown by the simulation result in Figure 48. The results indicate that the charge is not completely premixed in neither the DI nor the IDI engine and the combustion zone can therefore be regarded as a large number of small flames that burn at different local fuel-air ratios. Only a fraction of them will be burning at the slightly lean fuel-air ratio that produces the high NO formation rates. For that reason the peak is not visible in the experimental data. Once the engine is throttled so much that the global fuel air ratio approaches rich conditions the experimental NO_x values tend toward zero. This is especially true for the IDI engine that mixes fuel and air best.

10. Aftertreatment

10.1 Performance of an Oxidation Catalysts

In the second paper by the author [54] the effect of adding an oxidation catalyst was calculated based on catalytic conversion efficiencies given in the literature [55]. These efficiencies were obtained with gasoline direct injected two-stroke engines. Since there might be differences in catalyst performance when changing to a different fuel and a different combustion concept it was decided to test the performance of an oxidation catalyst on the engine of this study.

10.2 Experimental setup

The catalyst used was based on a metal substrate. A normal size of the catalyst relative to the engine was chosen based on the so-called space velocity:

$$SV = \frac{\text{Volumetric flow rate of gas}}{\text{Volume of catalyst}} \quad (17)$$

Other parameters of the oxidation catalyst are listed in Table 18.

Table 18 - Specifications for oxidation catalyst

| | | |
|------------------------|-----------------------|---------|
| Length | [mm] | 79 |
| Diameter | [mm] | 39 |
| Washcoat powder size | [μm] | 0.4 |
| Precious metal loading | [gr/ft ³] | 40 |
| Palladium/platinum | [] | 2/1 |
| Channels | [ch/in ²] | 300 |
| Space velocity | [1/h] | 275,000 |

The mounting of the catalyst in the exhaust system of the two-stroke engine is illustrated in Figure 49 and Figure 50.

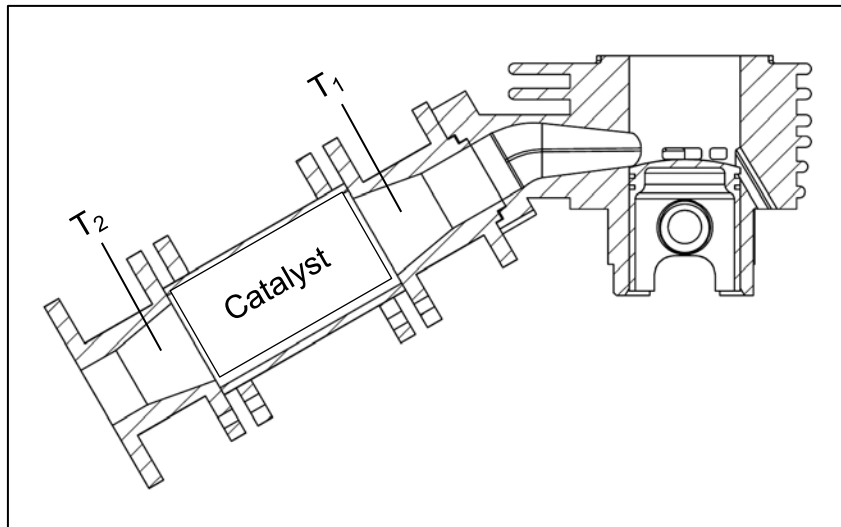


Figure 49 - Cut-away showing mounting of oxidation catalyst

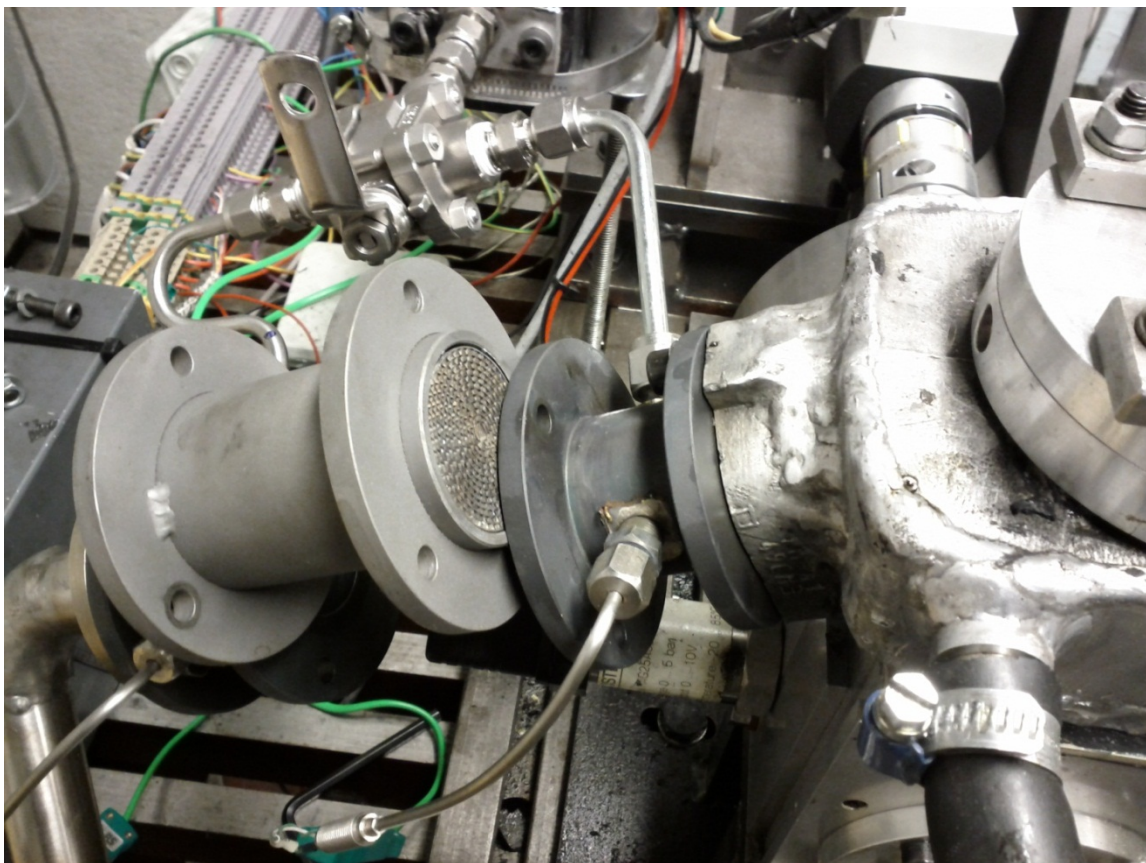


Figure 50 - Oxidation catalyst being fitted in test setup (cat. element is Ø39mm)

10.3 Results

The in-direct injection cylinder head and a high efficiency operating point was chosen for catalyst test: 3000 rpm and 350 kPa. No unusual things were noted during start-up and

warm-up although the exhaust system had been changed. The intake air flow rate had dropped slightly compared to the case without a catalyst in the exhaust. The delivery ratio was 1.10 where it was normally 1.15 for this operating point. The engine brake efficiency was not reduced though and remained at 29%.

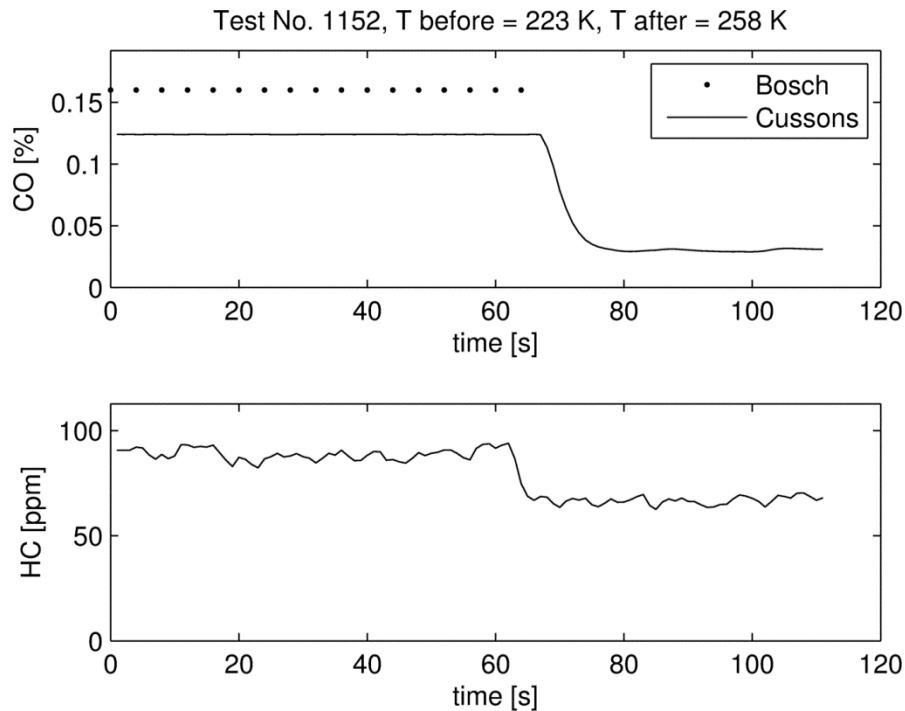


Figure 51 - CO and HC emissions before and after oxidation catalyst

Table 19 - Oxidation catalyst performance at normal operating point

| | | Before catalyst | After catalyst | Conversion |
|---------------------|-------|-----------------|----------------|------------|
| Exhaust temperature | [°C] | 223 | 258 | |
| CO | [%] | 0.16 | 0.03 | 81% |
| HC | [ppm] | 95 | 65 | 32% |

Table 19 shows that conversion of CO is quite good even at the low temperatures. This is in accordance with modelling results that predict that CO conversion increases rapidly over 150°C [56]. HC oxidation is not very effective though.

Throttling the engine intake while maintaining the same fuelling level was tried in an effort to both increase exhaust temperature and CO emissions so that the catalyst would experience higher temperatures. The intake was closed until the fuel-air equivalence ratio at the entrance to the oxidations catalyst was stoichiometric. This required running the engine combustion rich to compensate for the air short-circuiting directly to the catalyst during the two-stroke scavenging process. The increase in exhaust temperature was therefore minor. The effect on conversion rates is shown in Table 20.

Table 20 - Oxidation catalyst performance at near stoichiometric conditions

| | | Before catalyst | After catalyst | Conversion |
|---------------------|-------|-----------------|----------------|------------|
| Exhaust temperature | [°C] | 237 | 607 | |
| CO | [%] | 6.39 | 0.15 | 98% |
| HC | [ppm] | 576 | 150 | 74% |

CO conversion is almost complete and HC conversion is much better but still not complete. Considering the special conditions required to reach 74% conversion of HC it is concluded that an oxidation catalyst is effective for CO but has low conversion efficiency for HC which has also been the conclusion for two-stroke gasoline engines [55].

11. Heat Transfer

11.1 Experimental results for motoring

The measured cylinder pressure deviates significantly from simulated values. Figure 52 shows the results for the conditions given in Table 21.

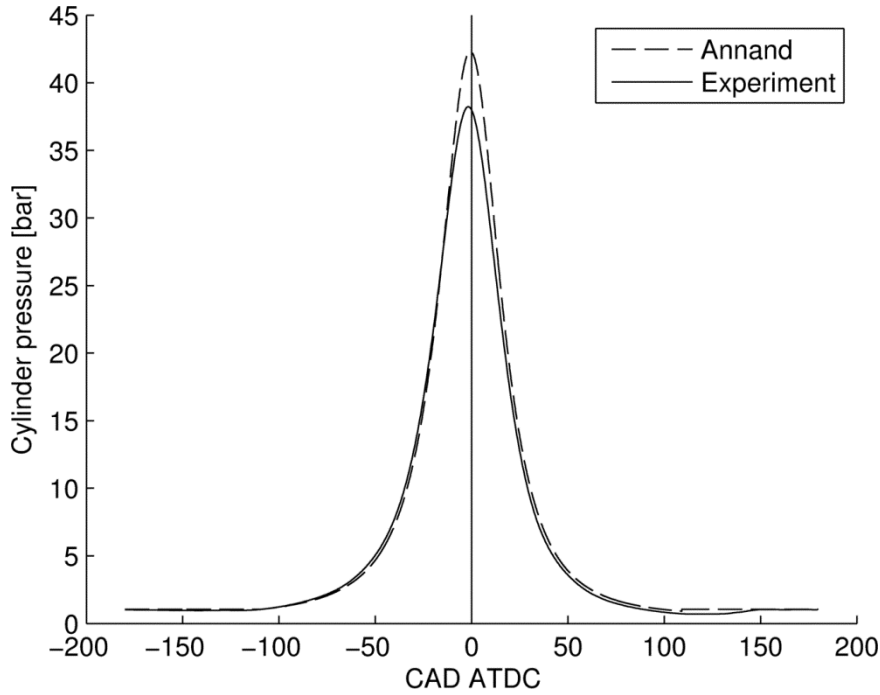


Figure 52 - Motoring cylinder pressure

To investigate this difference further the first law for a closed system was applied to the cylinder content during the closed cycle. Assuming also ideal gas behavior the apparent heat release formula (18) is the result.

$$\dot{Q}_{AHR} = \dot{Q}_{HR} + \dot{Q}_w = \frac{\gamma(T)}{\gamma(T) - 1} p \frac{dV}{d\theta} + \frac{1}{\gamma(T) - 1} V \frac{dp}{d\theta} \quad (18)$$

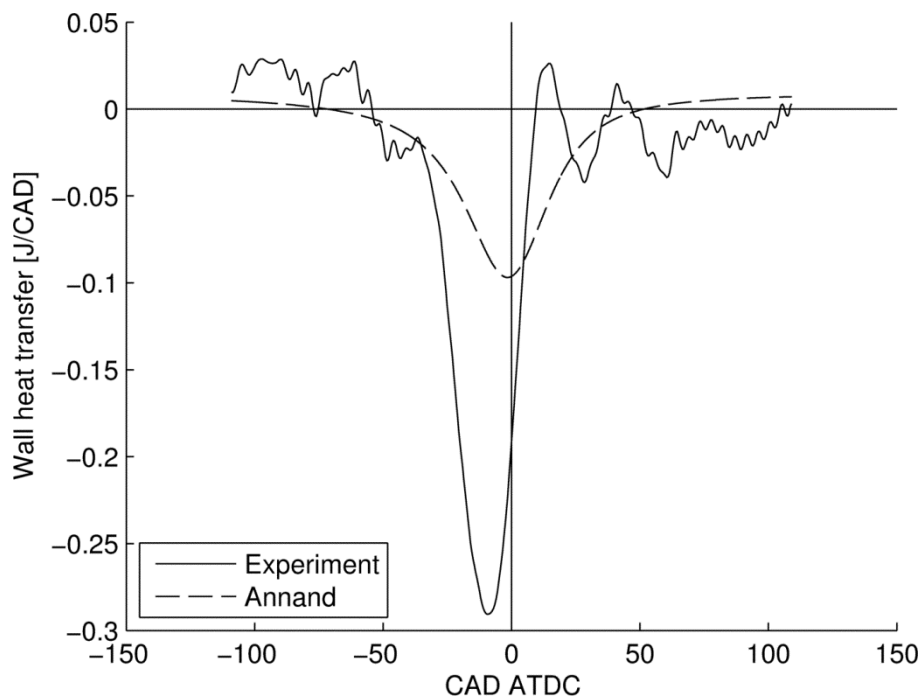
For the case of motoring the heat release is zero and (18) simplifies to (19).

$$\dot{Q}_w = \frac{\gamma(T)}{\gamma(T) - 1} p \frac{dV}{d\theta} + \frac{1}{\gamma(T) - 1} V \frac{dp}{d\theta} \quad (19)$$

The wall heat transfer determined in this way is, in Figure 53, compared to the results of an engine simulation using Annand's heat transfer correlation for the same conditions. The conditions are given in Table 21.

Table 21 - Motoring conditions

| | | Test | Simulation |
|---------------------------|------------|------------|------------|
| Cylinder size | [ccm] | 50 | 50 |
| Compression ratio | [] | 21.1 | 21.1 |
| Engine speed | [rpm] | 3000 | 3000 |
| IC / EO | [CAD ATDC] | -109 / 109 | -109 / 109 |
| Cooling water temperature | [°C] | 85 | - |
| Cylinder wall temperature | [°C] | - | 100 |

**Figure 53 - Comparison of experimental and Annand heat transfer in motoring**

A surprising feature of Figure 53 is the positive heat transfer just after TDC for the experimental trace. At this time which is between 10 and 20 CAD's ATDC the bulk gas temperature is still significantly higher than the wall. The engine is converted so that the compression ratio is approximately twice as high as the original design. The resulting higher pressure levels put additional strain on the components and the volume function may be affected. A bachelor student that the author supervised did a number of finite element stud-

ies of the engine components in order to establish the deviation from the ideal undeformed volume function caused by the cylinder pressure [57]. The results showed that deformation was significant and that the crankshaft and connecting rod were the primary sources of deformation. It was also determined that a simple correction of the volume function was sufficient to capture the deformation due to cylinder pressure.

$$V = V_{undeformed} + k_p(p_{cylinder} - p_{crankcase}) \quad (20)$$

The value of the constant was found to be:

$$k_p = 4.77e^{-14} \left[\frac{m^3}{Pa} \right] \quad (21)$$

The value is only valid for this particular engine design.

Others have reported the use corrections to the undeformed volume function and included deformation due to inertial forces [58]. In this study, deformation due to inertial forces was found to be insignificant for the engine speeds under consideration and equation (20) was used as it is shown here.

Using equation (20) in the apparent heat release analysis Figure 53 changes to Figure 54. The correction has only applied for the motoring analyses in this study. For analysis of the firing cycle these small volume deviations are less of importance.

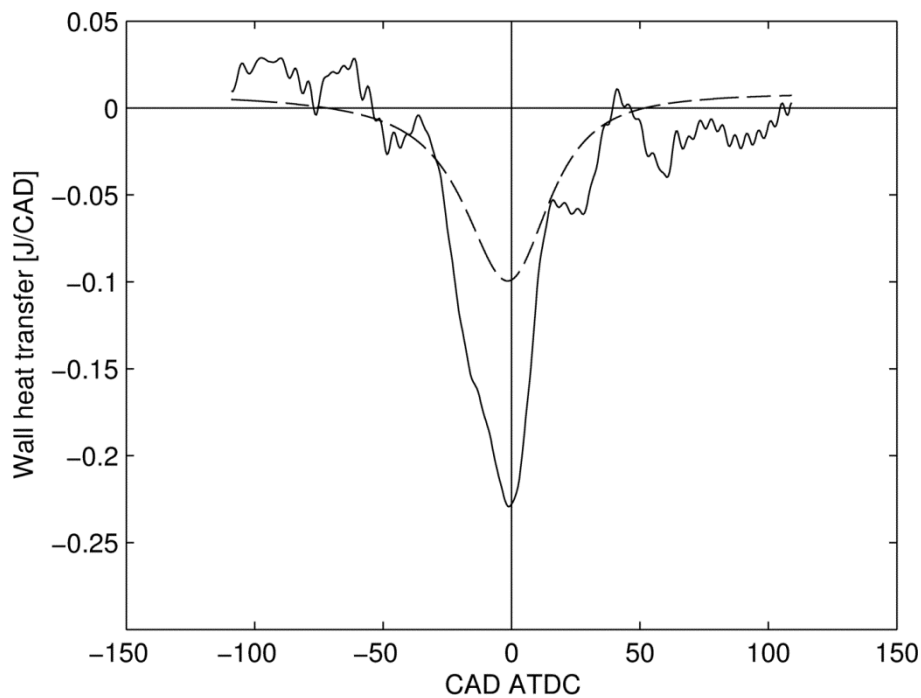


Figure 54 – Comparison of experimental and Annand heat transfer when equation (20) is applied

The strong positive peak after TDC is gone and the general picture is also more symmetrical. The maximum negative value is still more than twice as large as predicted by Annand. An explanation for this could be the strong forced air motion created by the low clearance height in the squish zone. The fact that squish motion does increase the heat loss was verified in the first paper by the author [59]. Another reason could be that the expression by Annand was not validated on engines as small as the test engine of this study. In order to study the effect of engine size and squish motion a CFD model for motoring was set up.

11.2 CFD

The heat losses inferred from motoring experiments show large peak values that correlations like Woschni's and Annand's do not predict. There are a number of possible reasons for the deviation.

- 1) The correlations are not valid for the small displacement volume of the test engine.
- 2) The test engine may have stronger squish motion than the engines used for validation of the heat transfer correlations.
- 3) The heat transfer correlations only predict heat transfer. Heat release analysis of motoring pressure traces cannot distinguish heat and mass transfer. Mass transfer out of the cylinder due to blow by may therefore be the cause of the deviation.

It was decided to investigate these effects using CFD analysis of the motoring cycle. The commercial code StarCD (v. 4.14) was used to run a Reynolds Averaged Navier Stokes (RANS) simulation. The effect of size and squish was investigated first and then blowby was included in the CFD analysis. The geometry, mesh, boundary conditions and initial conditions for the CFD model will be discussed in the following.

In order to be able to quantify and compare the wall heat transfer for a complete cycle a heat transfer mean effective pressure is defined.

$$qmep = \frac{Q_w}{V_d} \quad (22)$$

Where Q_w is the wall heat transfer per cycle. The units of $qmep$ are kPa.

11.2.1 Geometry

Table 22 shows a 2x2 matrix that illustrates the general idea behind the investigation. The four possible combinations of two different cylinder sizes and two different cylinder head designs are simulated in order to see the effect on heat transfer as calculated by the CFD code.

Table 22 - CFD simulation matrix for size and squish effects

| | 500cc cylinder | 50cc cylinder |
|-----------|----------------|---------------|
| No squish | Type 1 | Type 2 |
| Squish | Type 3 | Type 4 |

A 500cc cylinder was chosen as the large cylinder since this is a typical automotive cylinder size for which Woschni's correlation has been applied with success.

To be able to use a structured mesh and provide results of a more general nature a number of decisions were made that depart from the design of the test engine. These deviations are listed in Table 23.

Table 23 – Differences between CFD model and test engine (type 4 as example)

| | Test engine | CFD model |
|----------------------|--------------|---------------|
| Bore & stroke | 40 x 39.1 mm | Bore = Stroke |
| Connecting rod ratio | 4.09 | 4 |

| | | |
|-------------------|--------------------|---------------------------|
| Compression ratio | 13 - 22 | 20 |
| Piston top | Dome | Flat |
| Cylinder head | Cone + squish zone | Cylindrical + squish zone |
| Ports | Cylinder ports | None |
| Crevice | Yes | No |
| Blowby | Yes | No |

The differences in bore, stroke and connecting rod length are considered minor. A range of compression ratios were used during the experimental work. A value of 20 is used at first here since it is the lowest compression ratio for which the test engine can start cold and it is also a typical compression ratio for diesel engines in general. The differences in piston top and cylinder head geometries do introduce differences between the modelled and the real flow. But the main focus was to use CFD to investigate the effects of engine size and squish versus no-squish and modelling the detailed geometry correct is therefore considered less important. A structured grid that can be refined systematically was prioritized.

Since no transfer or exhaust ports were modelled a full compression and a full expansion stroke for motoring was simulated. The results are therefore equally valid for two-stroke engines and four-stroke engines.

11.2.2 Mesh

The geometries and therefore also the meshes used in the following are axisymmetric and the meshing is therefore performed in cylindrical coordinates. To reduce the computational effort only a section of the cylinder is modelled. In Figure 55 the entire cylinder for the simplest mesh is displayed alongside the sector used during the computations.

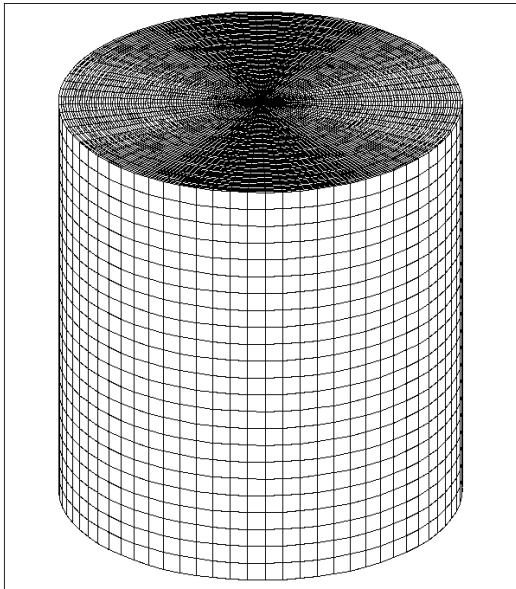
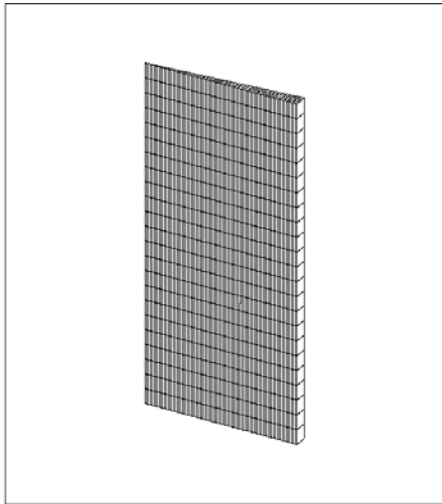
| | |
|---|--|
|  |  |
| <p>Entire cylinder – 142,416 cells</p> | <p>One 5° sector – 1978 cells</p> |

Figure 55 – 5° cylinder sector used for computations (500cc shown)

Although 142,416 cells would not result in excessively long computing times it is unnecessary to run the simulations for the entire cylinder when it is axis-symmetric. Later, when crevice volumes and blowby are introduced, it will also turn out to be a significant advantage that only a sector is modelled.

The sector is only one cell wide. Cyclic boundary conditions are applied to the sides of the sector such that flow out of the side of a cell enters into the same cell on the other side. This method makes it possible to introduce swirl if desired.

For internal combustion engines the mesh generation is complicated by the movement of the piston and sometimes also valve motion and sliding interfaces with cylinder ports. A number of the most recent commercial CFD packages offer solutions tailored to deal with these specific challenges. The basic StarCD package used in this study does not have these options instead it offers the possibility to define mesh vertex movement by updating the grid during the simulation using a Fortran user subroutine called “newxyz.f”. This function was therefore set up to move all vertices below the cylinder head. The movement is done in a linearly decreasing fashion such that the vertices on the piston surface follow the

piston, the vertices midway between piston and cylinder head move at half the piston speed and the vertices on the cylinder head do not move.

In this way the number of cells that define the fluid domain is constant throughout a simulation but in the axial direction they are compressed on the compression stroke and expanded on the expansion stroke. The method requires the cells to be long in the axial direction at BDC. This is necessary to avoid excessive cell aspect ratios near TDC. Figure 56 shows the mesh deformation for the simplest geometry (no squish).

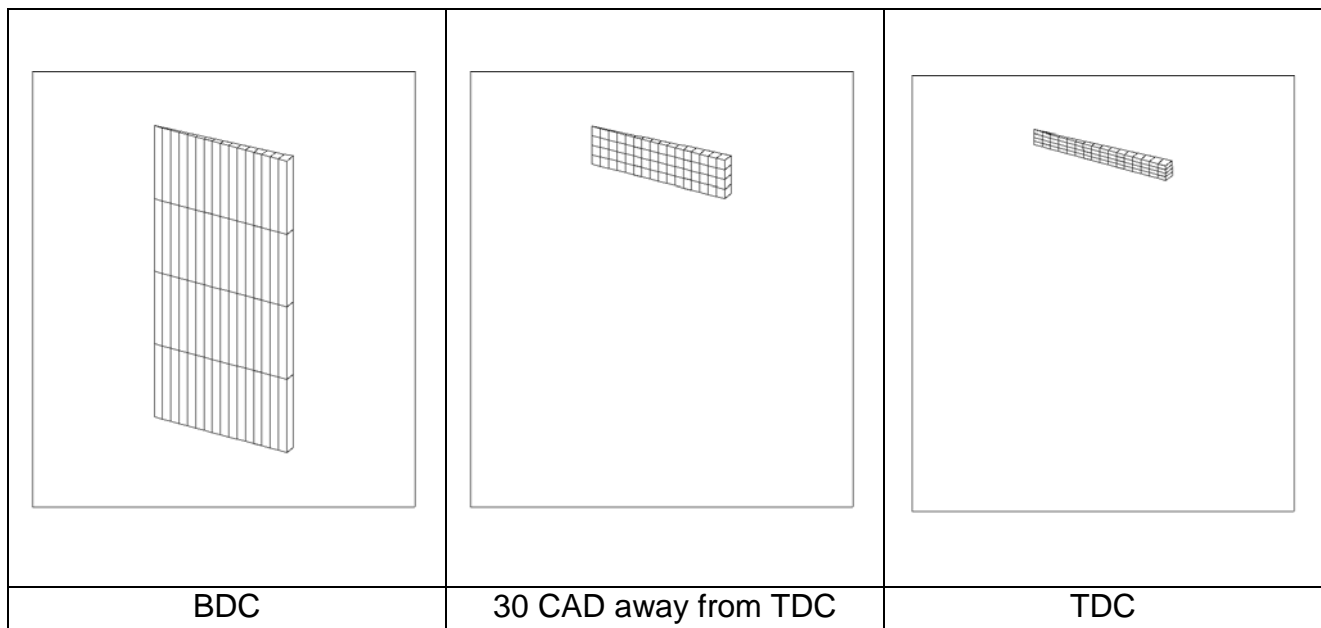


Figure 56 - Mesh deformation during simulation

To be able to see the individual cells the mesh shown in Figure 56 is very coarse. At BDC the cells are eight times as long in the axial direction as in the radial direction. At TDC the aspect ratio is approximately reversed. In this way, cells with a very high aspect ratio are avoided throughout the simulation although the number of cells is unchanged. The STAR-CD manual defines 10 to be the limit on aspect ratio [60].

The mesh used during simulations is designed according to the modelling method used. To avoid high cell counts and the accompanying requirements on computational resources a high Reynolds number model is used. This means that the physical wall boundary layer is not resolved but a wall function is applied that requires the near-wall cell to be placed in the so-called log-layer. The log-layer is the layer near the wall in which both turbulent and viscous effects are important and where it has been shown that the dimensionless velocity and wall distance are related in a logarithmic fashion. This is illustrated in Figure 57.

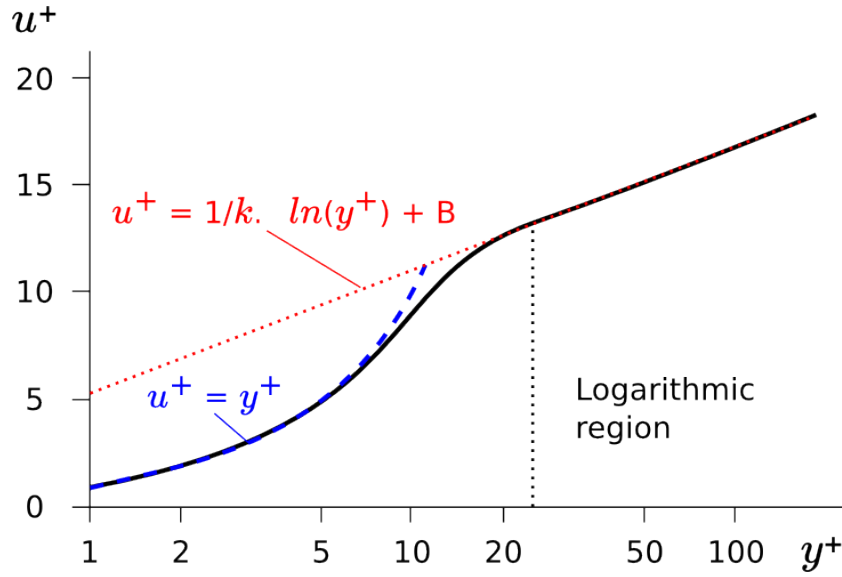


Figure 57 - Boundary layer profile [61]

High Reynolds number modelling therefore requires the y^+ values of the near wall cell centroid (p) to be within certain limits.

$$30 < y_p^+ < 100 \quad (23)$$

The y^+ number is defined as.

$$y^+ = \frac{\rho u_\tau y}{\mu} \quad (24)$$

Where

$$u_\tau = \sqrt{\frac{\tau_w}{\rho}} \quad (25)$$

And y is the normal distance from the wall, τ_w is the shear stress at the wall, ρ the fluid density and μ the molecular dynamic viscosity.

Since the flow is not known before the simulations are run finding an appropriate mesh is an iterative procedure. After a simulation run the y^+ values of the near-wall cells are plotted and compared to equation (23). Figure 58 shows the minimum and maximum y^+ values per crank angle degree of the simulation with a radial cell size of 1 mm. It also shows the range within which 80% of the cell y^+ values lie. This range is between the dotted lines. Figure 58 shows that more than 80% of the y^+ values are within the limits for the important range ± 90 degrees around TDC.

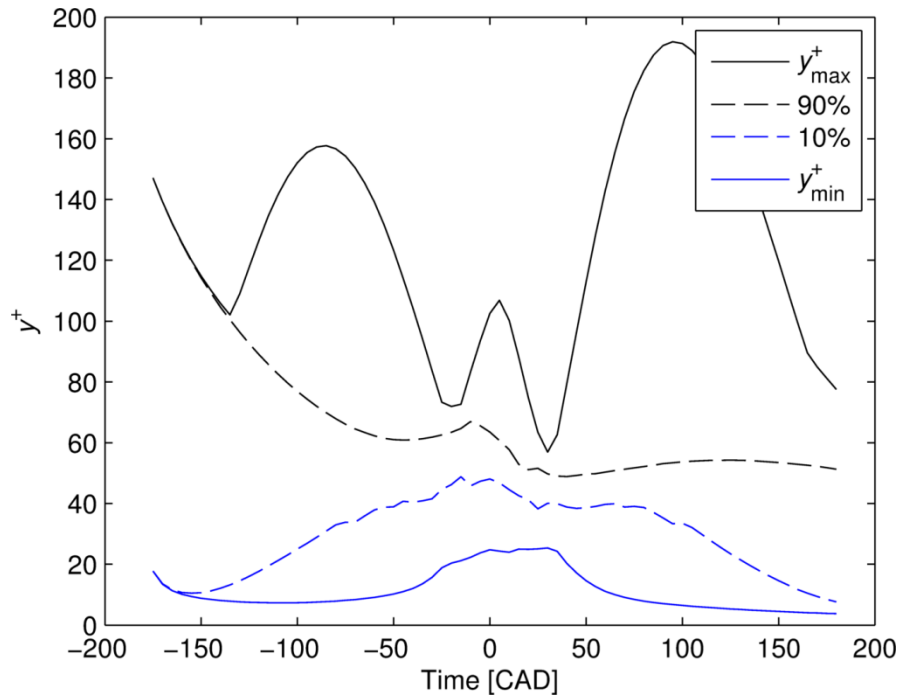


Figure 58 – Min, max and percentile lines of y^+ values of near wall cells

The wall function employed has specifically been developed for engines where the flow is highly compressible [62].

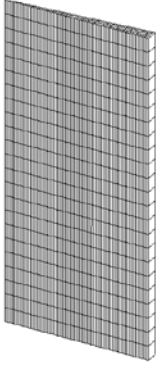
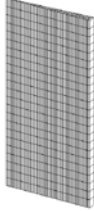
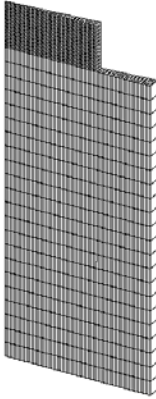
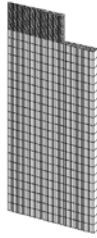
A summary of the geometries defined is given in Table 24.

Table 24 - Basic settings for the type 4 simulation

| Type | | 1 | 2 | 3 | 4 |
|-------------------------|-------|------------------------|------------------------|------------------------|------------------------|
| Displacement | [ccm] | 500 | 50 | 500 | 50 |
| Bore | [mm] | 86 | 39.93 | 86 | 39.93 |
| Stroke | [mm] | 86 | 39.93 | 86 | 39.93 |
| CR | [] | 20 | 20 | 20 | 20 |
| Wall temp. | [K] | 373 | 373 | 373 | 373 |
| Squish | [] | 0.0 | 0.0 | 0.6 | 0.6 |
| Deck clearance | [mm] | 0.92 | 0.5 | 0.92 | 0.5 |
| Moving mesh method | - | Axial cell deformation | Axial cell deformation | Axial cell deformation | Axial cell deformation |
| Cell aspect ratio @ BDC | [] | 8 | 8 | 8 | 8 |

The geometries used are shown Table 25..

Table 25 – CFD geometries

| | 500cc cylinder | 50cc cylinder |
|-----------|--|---|
| No squish |  |  |
| Squish |  |  |

11.2.3 Boundary conditions

All the wall boundaries surrounding the fluid domain are set to a fixed temperature of 100°C. Conjugate heat transfer where the temperature distribution in the wall is also calculated is therefore not simulated. The fixed temperature was chosen based on the cooling water temperature of the experiments which was 85°. The simulations will subsequently be compared to those experiments. The thermal resistance of the walls is set to zero because the thermal resistance of the fluid boundary layer is orders of magnitude higher than the thermal resistance of the metallic walls of an engine [63].

Table 26 shows the remaining boundary conditions.

Table 26 - CFD boundary conditions

| | |
|--------------|-------------------------------------|
| Piston | No slip wall moving at piston speed |
| Liner | No slip wall |
| Head | No slip wall |
| Sector sides | Cyclic |

11.2.4 Initial conditions

Because the simulated geometry did not include ports it was not possible to run several cycles to establish the flow field before the simulation of the closed cycle of interest.

Setting up a flow field that resembles the tumbling flow that is the likely result of the scavenging process would either require modelling the ports and associated ducts and running consecutive cycles to establish the initial flow or having detailed measurements of the actual flow field. Since ports and ducts were not included in the model and measurements were not available a reasonable starting point for the analysis had to be defined. It was decided to start most of the simulations with all mean flow velocities set to zero but with the boundary conditions set up so that it was possible to introduce an swirling initial field that is defined by solid disk rotation about the cylinder axis. Setting the initial turbulence quantities to zero is neither realistic nor possible. The turbulence models need a valid starting point. The required initial turbulence quantities are the turbulent kinetic energy k and the dissipation rate ϵ . The turbulent kinetic energy is defined as:

$$k = \frac{1}{2} (\overline{u'^2} + \overline{v'^2} + \overline{w'^2}) \quad (26)$$

If the turbulence is assumed isotropic this is equal to:

$$k = \frac{1}{2} (3 \cdot \overline{u'^2}) = \frac{3}{2} \cdot \overline{u'^2}$$

Now, since turbulence intensity is defined as:

$$TI \stackrel{\text{def}}{=} \frac{u'}{U} \quad (27)$$

Where U is a reference mean flow velocity that we choose to set equal to the mean piston speed S_p since the flow speed must at least scale with the piston speed, we have that:

$$U = S_p \quad (28)$$

And,

$$k = \frac{3}{2} (S_p \cdot TI)^2 \quad (29)$$

Which is the initial value of the turbulent kinetic energy k .

The initial value of the dissipation rate is based on the turbulent kinetic energy k and an estimate of the mixing length ML through equation (30).

$$\varepsilon = C_\mu^{3/4} \left(\frac{k^{3/2}}{ML} \right) \quad (30)$$

The estimate of the mixing length is taken from [64] to be 0.1 times the cylinder bore.

11.2.5 Discretization

Temporal discretization is done by the fully implicit Euler Scheme. The time steps were chosen such that all residuals got below 10^{-4} within 15 outer iterations at each time step.

The spatial discretization scheme employed is the MARS scheme: Monotone Advection and Reconstruction Scheme. The MARS scheme is an advanced scheme that is second-order accurate. According to the STAR-CD manual the MARS scheme possesses the least sensitivity of solution accuracy to mesh structure and skewness. The compression level used is the STAR-CD default of 0.5.

11.2.6 Grid independence

A coarse grid with a low cell count is faster to compute but it may not describe the actual flow well. In the following the same case is calculated on increasingly fine grids to see how fine the grids have to be before the solution, in terms of heat transfer, does not change any longer. The fineness of a grid is stated by giving its radial cell size. As described in chapter 11.2.2 (Mesh) the cell size in the axial direction is 8 times larger and the sector is 1 cell wide. Therefore, giving the radial cell size (dx) is enough to describe the grid completely.

For the reasons described in chapter 11.2.2 (Mesh) it is important that the near-wall cells are not refined in the grid independence study. Only the cells internally in the fluid domain can be freely refined. Otherwise the y^+ values become smaller than acceptable. The result of the grid independence study is given in Figure 59.

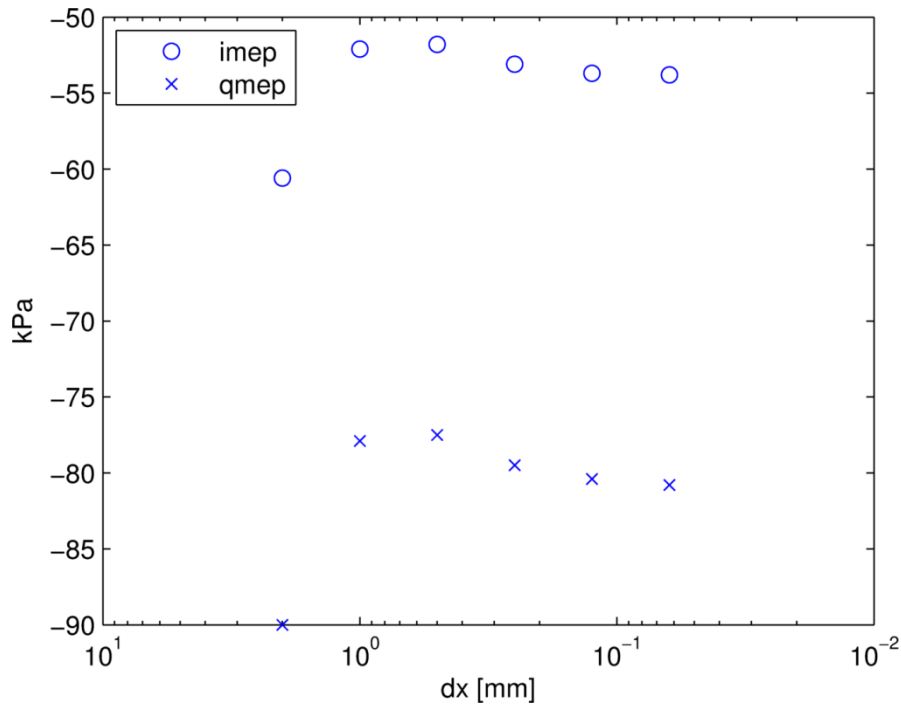


Figure 59 - Grid independence study

Below a radial cell size of 0.125 mm's the solution does not change by further refinement and 0.125 mm's is therefore chosen as the cell size in the central fluid domain away from the walls.

11.2.7 Time step independence

The larger the time steps that are possible while retaining simulation accuracy the faster the computation times. In order to check what time step size was required for satisfactory results a number of simulations were run with different time step sizes. The result is shown in Figure 60.

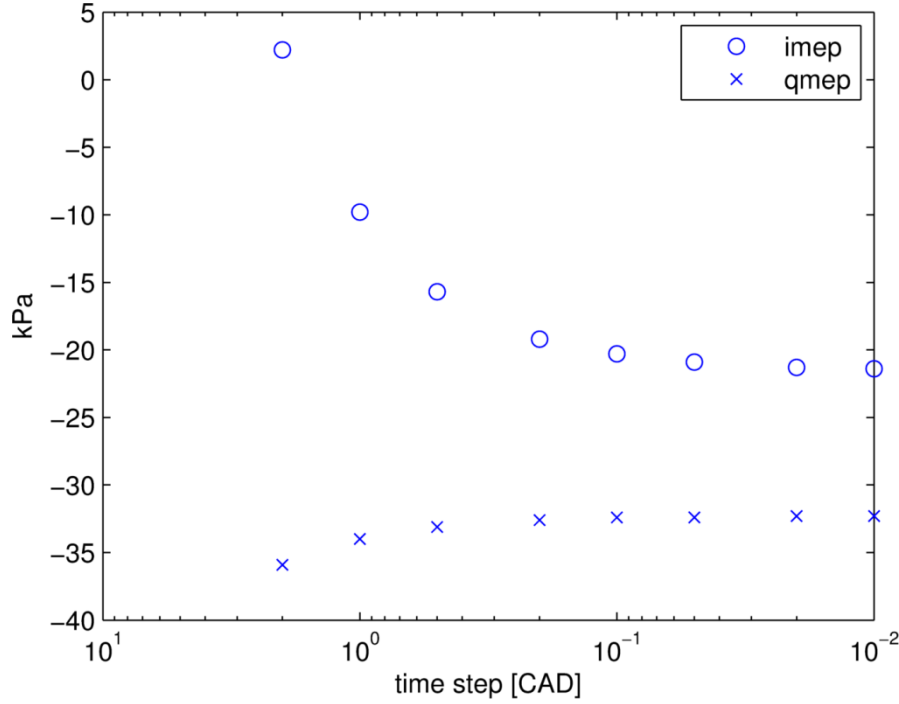


Figure 60 - Effect of time step size in CFD computation

The imep calculated at a time step size of 2 CAD is clearly in error with the physics of the problem. The value is positive which indicates that if the engine had no friction it would be able to run without combustion. As the time step size is decreased the solution converges to imep = -21 and qmep = 32. These values are reached for time steps shorter than 10^{-1} CAD. Time steps of 10^{-2} CAD are used for the following computations. This will also ensure, and that has been checked after each run, that the Courant-Friedrichs-Lewy (CFL) criterion is also satisfied during the simulations.

$$C = \frac{u\Delta t}{\Delta x} \leq 1 \quad (31)$$

Where u is the local velocity, Δt is the simulation time step, Δx is the cell size and C is the Courant number. The Courant number describes how far the fluid has moved relative to the cell size during a time step of the simulation. It can be shown, and it also seems intuitively correct, that if the fluid moves through many cells during a single time step then the results may not be accurate [64].

At first, engine size and squish effects were considered. After that, the effect of blowby was included.

11.2.8 Engine size and squish effects

Although time step size and grid independence has been checked the solutions for the four geometries in Table 25 are still the result of specific settings in the CFD model some

of which are uncertain. In order to check the sensitivity of the CFD model to parameter variations a number of the parameters have been varied in a systematic way.

The parameters chosen for the parameter study are the initial turbulence level in the cylinder, the in-cylinder swirl and the turbulence model used. The initial turbulence level is not known from measurements. Two levels has been used the CFD simulations, a low and a high level, 5 and 10 % respectively. Also, the in-cylinder swirl is not known from measurements. Actually, it is unlikely that orderly swirl around the cylinder axis is the result of a loop scavenged two-stroke engines scavenging process. On the other hand, no mean flow motion at the start of the closed cycle is also unlikely. The geometry simulated is a sector of the cylinder, to keep computational time down, so it is easy to apply cyclic boundaries on the side of the sector and then impose a swirling flow. Although the swirling flow imposed in this way is probably in error with the actual flow it presents an opportunity to see the effect of an initial mean flow field that is not zero. A swirl number of zero and unity were tried in the simulations. The swirl number is defined in eq. (32).

$$SN = \frac{\omega_{swirl}}{\omega_{engine}} \quad (32)$$

Finally the turbulence model was varied. Turbulence modelling is not a mature science but it is necessary to use turbulence modelling due to the computational resources required for direct numerical simulation (DNS). DNS resolves the turbulence in both space and time and therefore does not need a turbulence model. The turbulence models applied here are the k- ω model and the RNG model. The k- ω model is used because it is the industry standard and the RNG model is used because it is often used by engine researchers [65][66].

These parameter variations are run for both the small and the large geometry (50 and 500 cc) with and without a squish zone. The effect of cylinder size can then be estimated based on the average of CFD calculations with different parameter settings instead of just stating the difference between the four geometries with the same settings that are chosen more or less randomly due to the limited knowledge of the actual conditions in the cylinder. The parameters are summarized in Table 27.

Table 27 - CFD parameter settings

| | | |
|--------------------|-------------|--------|
| Engine size | 500 cc | 50 cc |
| Squish | 0 % | 60 % |
| Initial turbulence | 5 % | 10 % |
| Swirl | SN = 0 | SN = 1 |
| Turbulence model | k- ω | RNG |

In total $2^5 = 32$ simulations were run to complete the parameter study. The combinations are written out in Table 28.

Table 28 – Combinations of settings in parameter study. Settings for result 1 are shown in green.

| Engine size | Squish | Initial turbulence | Swirl | Turb. model | CFD / Woschni |
|-------------|-----------|--------------------|----------|-------------|---------------|
| 50cc | No squish | low turb. | No swirl | k-eps | Result 1 |
| 50cc | No squish | low turb. | No swirl | RNG | Result 2 |
| 50cc | No squish | low turb. | Swirl | k-eps | Result 3 |
| 50cc | No squish | low turb. | Swirl | RNG | Result 4 |
| 50cc | No squish | high turb. | No swirl | k-eps | Result 5 |
| 50cc | No squish | high turb. | No swirl | RNG | Result 6 |
| 50cc | No squish | high turb. | Swirl | k-eps | Result 7 |
| 50cc | No squish | high turb. | Swirl | RNG | Result 8 |
| 50cc | Squish | low turb. | No swirl | k-eps | Result 9 |
| 50cc | Squish | low turb. | No swirl | RNG | Result 10 |
| 50cc | Squish | low turb. | Swirl | k-eps | Result 11 |
| 50cc | Squish | low turb. | Swirl | RNG | Result 12 |
| 50cc | Squish | high turb. | No swirl | k-eps | Result 13 |
| 50cc | Squish | high turb. | No swirl | RNG | Result 14 |
| 50cc | Squish | high turb. | Swirl | k-eps | Result 15 |
| 50cc | Squish | high turb. | Swirl | RNG | Result 16 |
| 500cc | No squish | low turb. | No swirl | k-eps | Result 17 |
| 500cc | No squish | low turb. | No swirl | RNG | Result 18 |
| 500cc | No squish | low turb. | Swirl | k-eps | Result 19 |
| 500cc | No squish | low turb. | Swirl | RNG | Result 20 |
| 500cc | No squish | high turb. | No swirl | k-eps | Result 21 |
| 500cc | No squish | high turb. | No swirl | RNG | Result 22 |
| 500cc | No squish | high turb. | Swirl | k-eps | Result 23 |
| 500cc | No squish | high turb. | Swirl | RNG | Result 24 |
| 500cc | Squish | low turb. | No swirl | k-eps | Result 25 |
| 500cc | Squish | low turb. | No swirl | RNG | Result 26 |
| 500cc | Squish | low turb. | Swirl | k-eps | Result 27 |
| 500cc | Squish | low turb. | Swirl | RNG | Result 28 |
| 500cc | Squish | high turb. | No swirl | k-eps | Result 29 |
| 500cc | Squish | high turb. | No swirl | RNG | Result 30 |
| 500cc | Squish | high turb. | Swirl | k-eps | Result 31 |
| 500cc | Squish | high turb. | Swirl | RNG | Result 32 |

The first two columns show the parameters of primary interest. These are the engine size and whether the combustion chamber has a 60% squish zone or not. The results of the simulations are then compared with the predictions of Woschni's heat transfer correlation used in combination with a single-zone cycle simulation set up to match the CFD simulations. Woschni's heat transfer correlation is given by equations (14), (15) and (16).

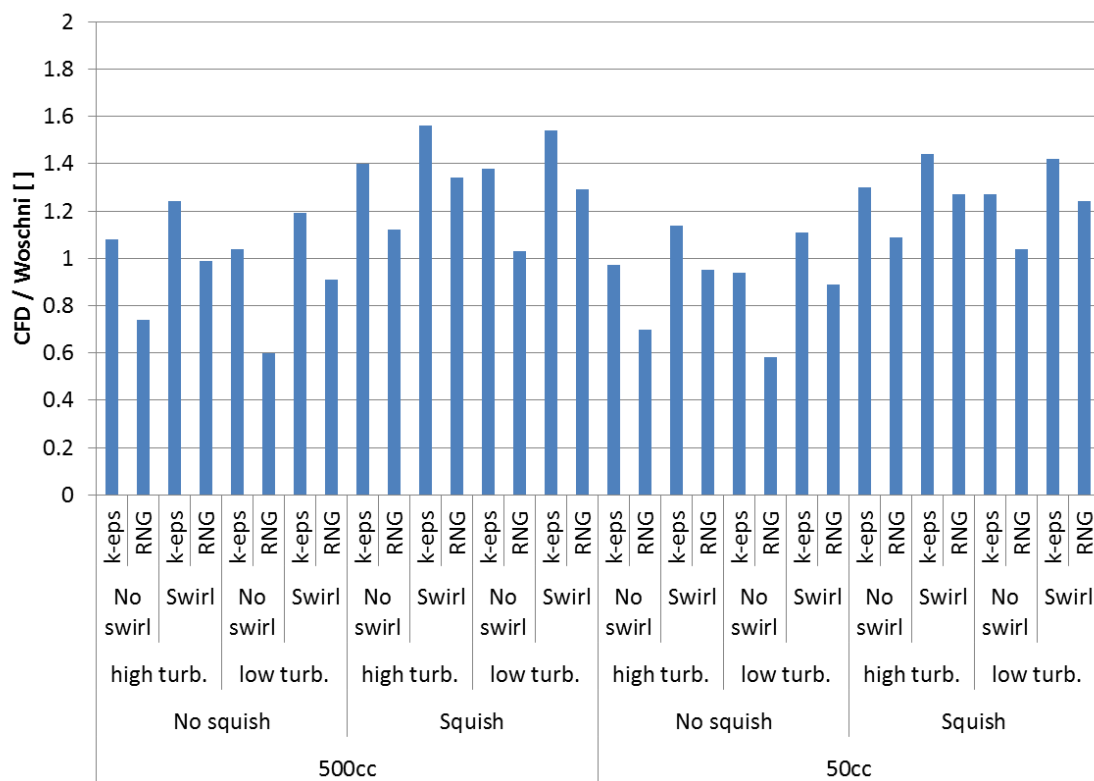


Figure 61 - CFD results relative to Woschni heat transfer during a closed cycle - all simulations

Although Figure 61 shows all results it is difficult to interpret. Averaging all 16 columns for the 500 cc cylinder and then all the 16 columns for the 50 cc cylinder gives Figure 62.

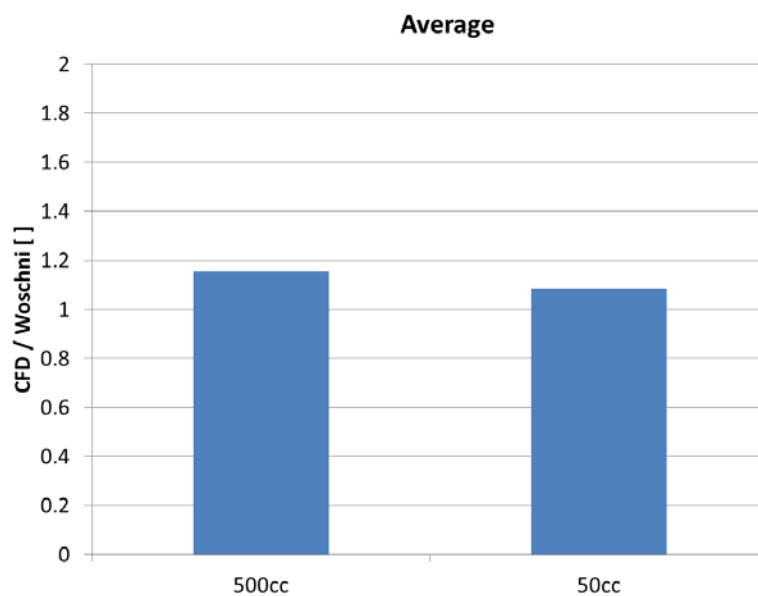


Figure 62 - Effect of cylinder size on CFD heat transfer relative to Woschni's prediction

Figure 62 shows that CFD does not predict a higher closed cycle heat transfer than Woshni's correlation. Actually the heat transfer is slightly lower for the 50cc cylinder.

Performing the same type of averaging for squish versus no-squish the result is Figure 63.

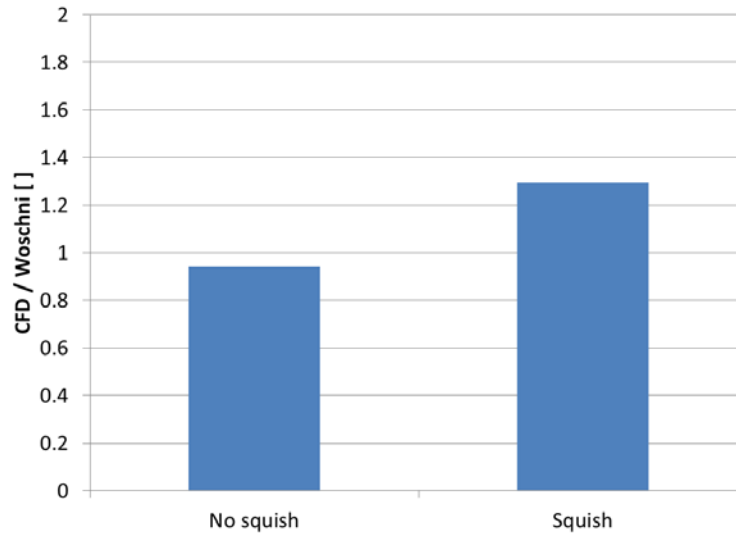


Figure 63 - Effect of squish on CFD heat transfer relative to Woschni's prediction

Figure 63 shows that adding a squish zone significantly increases the heat transfer in the CFD simulations relative to Woschni's prediction. This is to be expected since the only change experienced by Woschni's correlation is the added heat transfer area due to the addition of the sides of the combustion chamber in the cylinder head whereas the CFD also models the strong forced convection in and out of the squish zone between the piston and the cylinder head.

The remaining three parameters have been averaged in a similar way and the results are summarized in Table 29.

Table 29 – Average effect of parameter settings on CFD heat transfer result

| | Level 1 | Level 2 | Level 1 average | Level 2 average | Change |
|--------------------|-------------|---------|-----------------|-----------------|--------|
| Engine size | 500 cc | 50 cc | 1.15 | 1.08 | -6% |
| Squish | 0 % | 60 % | 0.94 | 1.30 | +38% |
| Initial turbulence | 5 % | 10 % | 1.09 | 1.15 | +5% |
| Swirl | SN = 0 | SN = 1 | 1.02 | 1.22 | +20% |
| Turbulence model | k- ω | RNG | 1.25 | 0.99 | -21% |

The original simulation matrix, Table 22, can now also be completed. The values shown in Table 30 are the averages of $2^3 = 8$ simulation results where initial turbulence, swirl and turbulence model have been varied.

Table 30 - Effect of engine size and squish (values are relative to Woschni)

| | 500cc cylinder | 50cc cylinder |
|-----------|----------------|---------------|
| No squish | 0.97 | 0.91 |
| Squish | 1.33 | 1.26 |

The CFD calculations generally agree well with Woschni's predictions. The effect of decreasing the engine size is a small reduction in heat transfer compared to Woschni's prediction. One of reasons why the CFD analysis was made was to see if CFD could predict an increase in heat transfer due to a reduction in engine size that would be larger than Woschni's prediction and thereby explain the results of motoring analysis. This is clearly not the case. The CFD heat transfer for the small engine actually falls 6% relative to Woschni's prediction.

A second reason for the CFD analysis was to see if the addition of squish could have such an effect. CFD heat transfer results for simple pancake combustion chamber geometries without any squish result in heat transfer 6% lower than Woschni. CFD results for geometries with sharp edged 60% squish zones result in heat transfer 30% higher than Woschni. The actual engine geometries that Woschni has been applied to successfully probably fall between the two categories simulated in CFD and it therefore makes sense that the CFD results are placed above and below Woschni's prediction. But even though the effect of squish is pronounced in CFD it is not strong enough to explain the results from motoring analysis.

The effect of doubling the initial turbulence level is a 5% increase in heat transfer so the calculations are not very sensitive to initial turbulence.

Increasing the initial swirl from a swirl number of 0 to 1 increases the heat transfer by 20% and is therefore quite significant.

The effect of changing the turbulence model is of the same size as adding swirl. This is a drawback of CFD modelling using turbulence models. The choice of turbulence model changes the results significantly. The heat transfer is reduced by 21 percent by changing from k- ω to RNG. The average result of calculation with RNG is 0.99 times the heat transfer predicted by Woschni whereas for the k- ω model the factor is 1.25 and the RNG model is therefore considered best.

The instantaneous spatially averaged heat transfer rates as a function of crank angle for the 50cc cylinder without and with squish are shown in Figure 64 and Figure 65. Initial turbulence is 10%, there is no swirl and the turbulence model is the RNG-model.

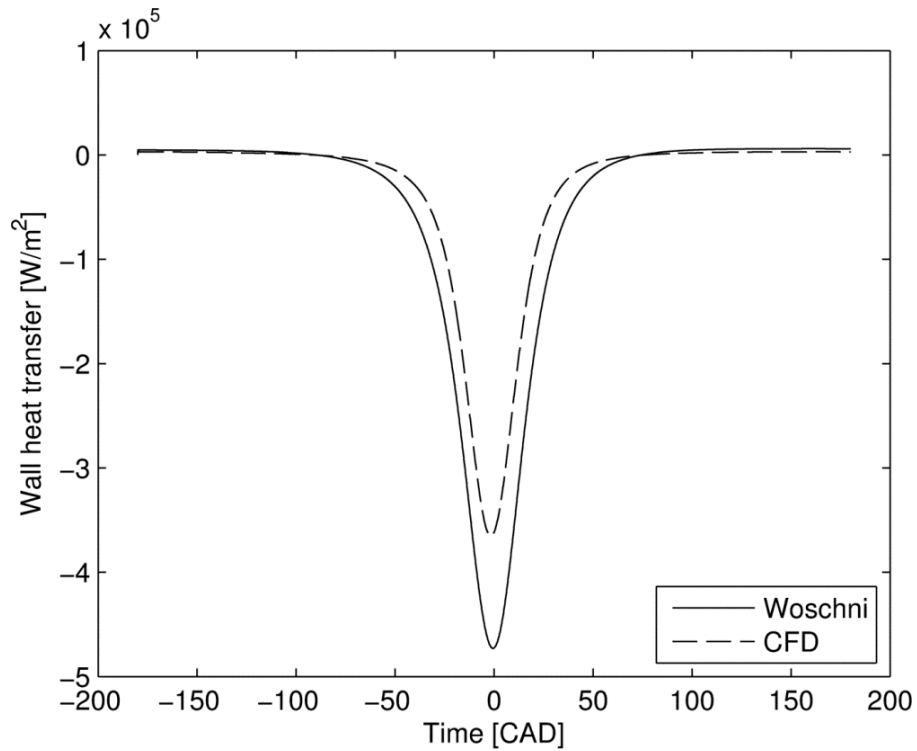


Figure 64 - Heat transfer for the 50cc cylinder without squish

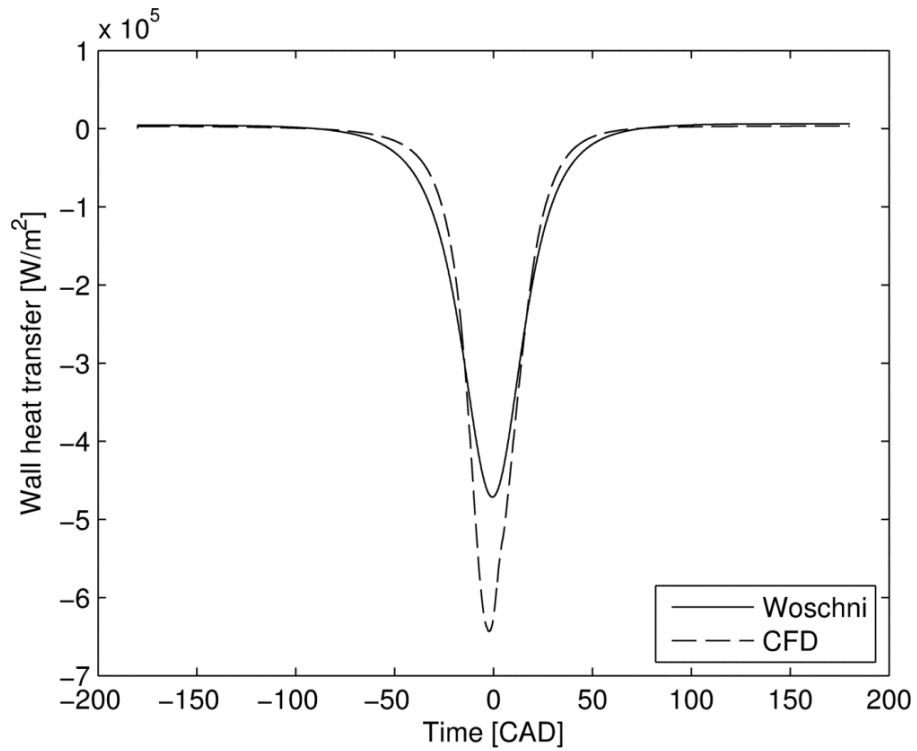


Figure 65 - Heat transfer for the 50cc cylinder with 60% squish zone

The temperature distribution at TDC with and without squish is shown in Figure 66.

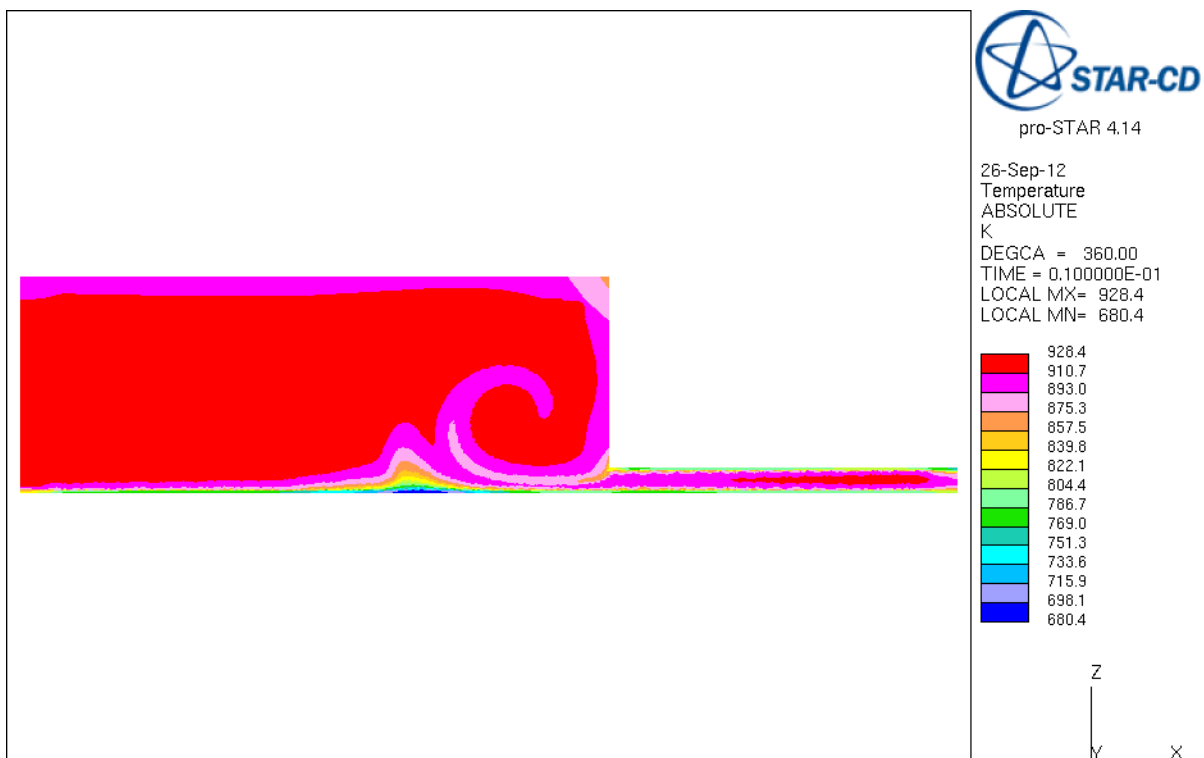


Figure 66 - Temperature field at TDC for geometry with squish

The tongue of cold air flowing in from the squish on the right stands out. The maximum temperature in the domain is 928 K. This is significantly above the value of 900 K predicted by the single-zone cycle simulation using Woschni's expression although the total heat transfer during the cycle predicted by CFD is 1.12 times the cycle simulation result. The concept of an adiabatic core is evident here.

The associated flow field is illustrated in Figure 67 by plotting the velocity magnitude.

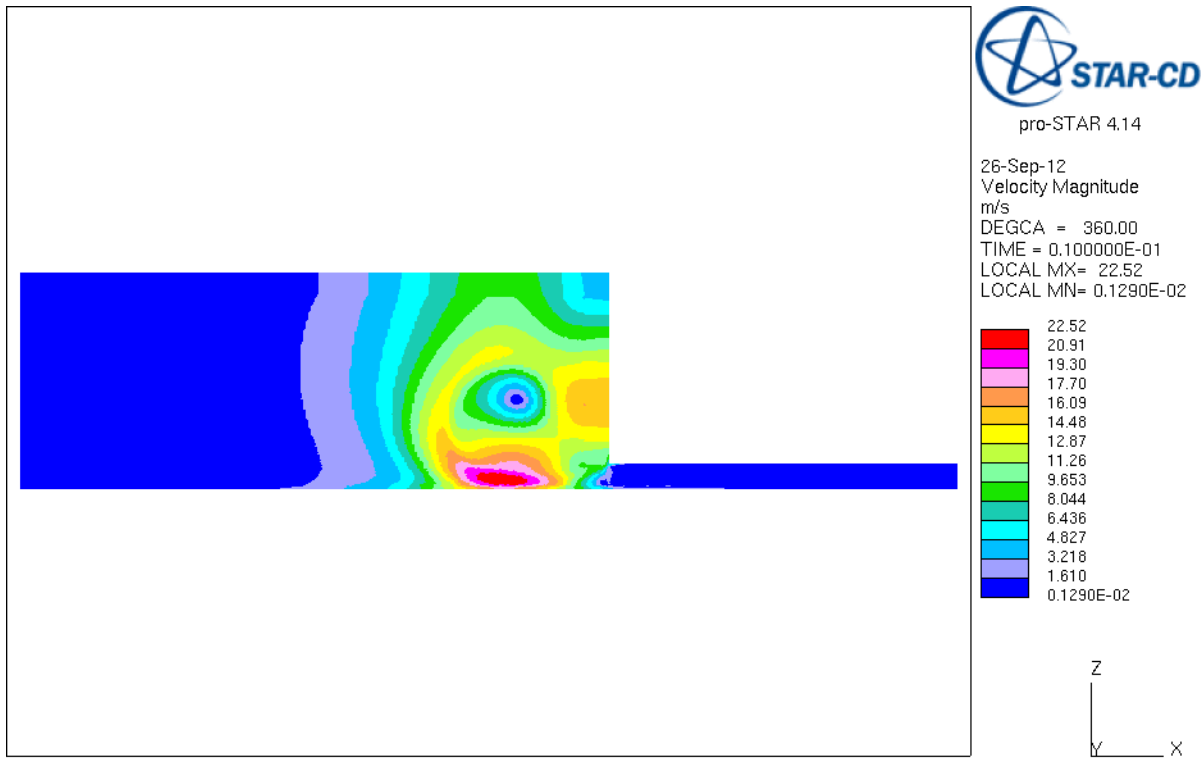


Figure 67 - Velocity magnitude field at TDC for geometry with squish

At TDC the piston speed is zero and the driving force behind the flow of air from the squish zone and inwards is gone. That is why the velocity is near zero in the squish zone. The air ejected from the squish zone is still moving fast though and is visible as the red area just inwards of the squish zone. The maximum velocity is 22.5 m/s. The vortex in the main chamber formed by the squish flow is centered around the vortex core visible by the low-velocity blue zone just above the fast moving squish flow in red.

To illustrate the flow in the squish zone before it stops the velocity magnitude is plotted also for the situation 10 CAD before TDC. See Figure 68.

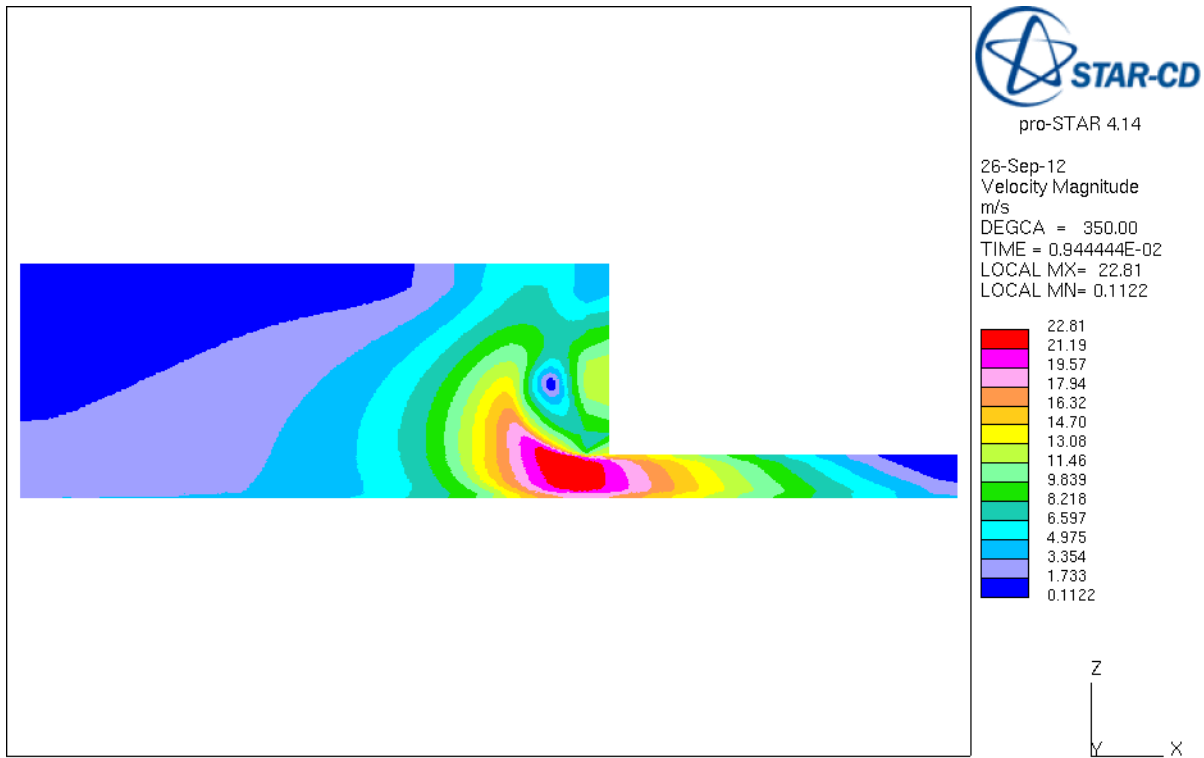


Figure 68 - Velocity magnitude field 10 CAD BTDC for geometry with squish

In Figure 68 the gradual increase in squish velocity towards the inner edge of the squish zone can easily be seen.

After TDC the squish flow is reversed. A CFD result for 10 CAD after TDC is shown in Figure 69.

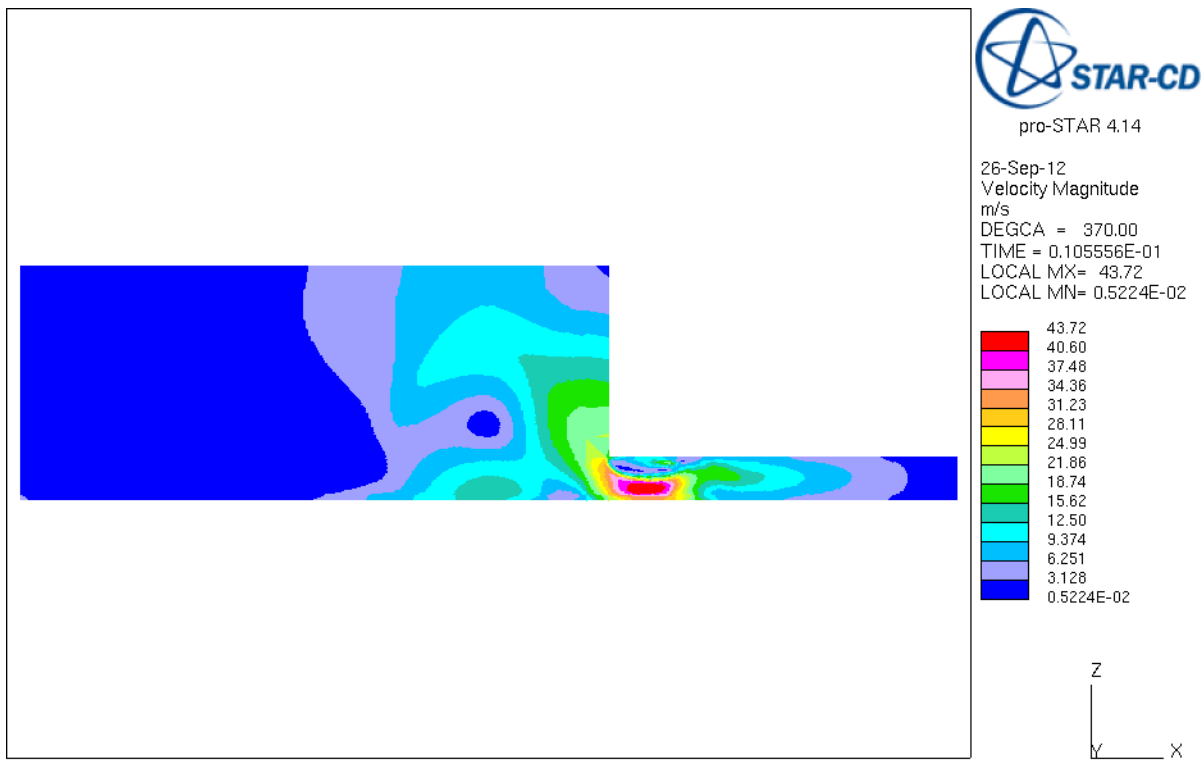


Figure 69 - Velocity magnitude field 10 CAD ATDC for geometry with squish

It is interesting to note that the recirculation zone just above the red high speed area is increasing the maximum squish flow speed after TDC. The maximum speed is 43.7 m/s 10 CAD after TDC where it was only 22.8 m/s 10 CAD before TDC. This corresponds with the effective flow area being approximately reduced 50% as seen in Figure 69.

11.2.9 Effect of blowby

If the CFD calculations are correct they verify Woschni's heat transfer correlation. The significant differences between simulated and measured motoring cycles must then be due to a mass loss out of the cylinder. Modeling the actual blowby process is very complicated if at all possible. Another way to evaluate mass losses is to more or less arbitrarily choose the size of a blowby passage and introduce that into the CFD model. Then adjust the size of the passage until the measured and the modeled motoring cycles are close to each other and then compare with measure values of blowby. This has been done and the resulting mass loss relative to the trapped air in the engine cylinder is 6.8% at 3000 rpm. This compares well with measured values from the literature [67].

The test setup used in the literature reference is shown in Figure 70.

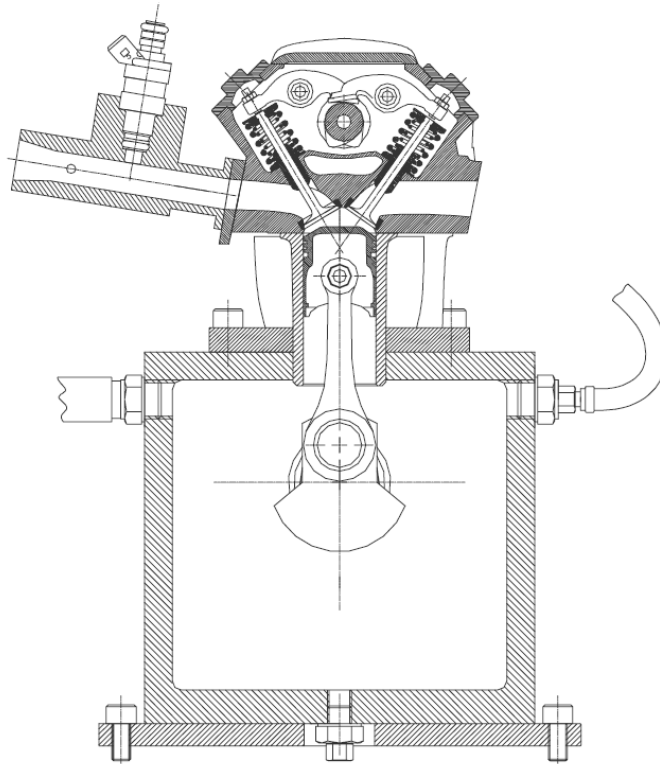


Figure 70 - Blowby experimental setup [67]

The measured levels of blowby as a function of engine speed is shown in Figure 71.

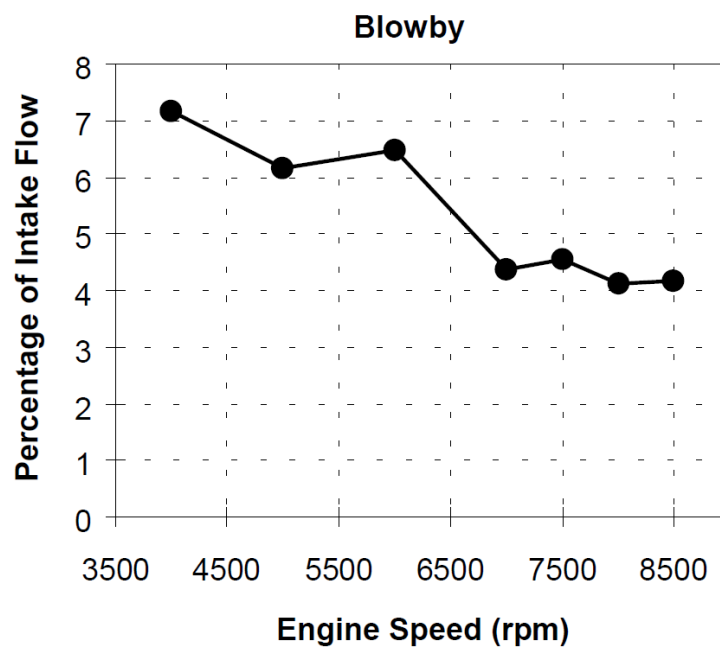


Figure 71 – Measured blowby from 50cc four-stroke engine [67]

It is concluded that blowby and not increased heat transfer is the cause of the low maximum pressures during motoring with the test engine.

12. Combustion Noise

12.1 Peak Pressure Rise Rate (PPRR)

The peak pressure rise rate is often used to describe the harshness of operation of an engine. It is especially relevant to consider for HCCI engines. For engines operating in true HCCI mode the peak pressure rise rate essentially establishes the load limit. If a value of 10 bar/CAD is exceeded the engine will typically start to knock and engine damage may also occur. A measure that also takes into account the effect of the absolute pressure level has also been developed [68]. This is important for boosted engines. The ringing intensity is estimated by applying eq. (33).

$$Ringing\ Intensity \approx \frac{1}{2\gamma} \frac{\left(\beta \frac{dP}{dt_{max}}\right)^2}{P_{max}} \sqrt{\gamma R T_{max}} \quad (33)$$

Where β is the ratio between the amplitude of the pressure waves and the maximum rate of cylinder pressure rise.

Since the engine of this study was not boosted the measure used to quantify and judge the combustion harshness was the peak pressure rise rate directly.

The peak pressure rise rates given in the following are calculated according to [42]:

$$\frac{dp}{d\theta} \sim \frac{\Delta p}{\Delta \theta} = \frac{p_{i+1} - p_i}{\theta_{i+1} - \theta_i} \quad [bar/CAD] \quad (34)$$

Figure 72 shows the result of plotting all pressure rise rates in one plot as a function of load.

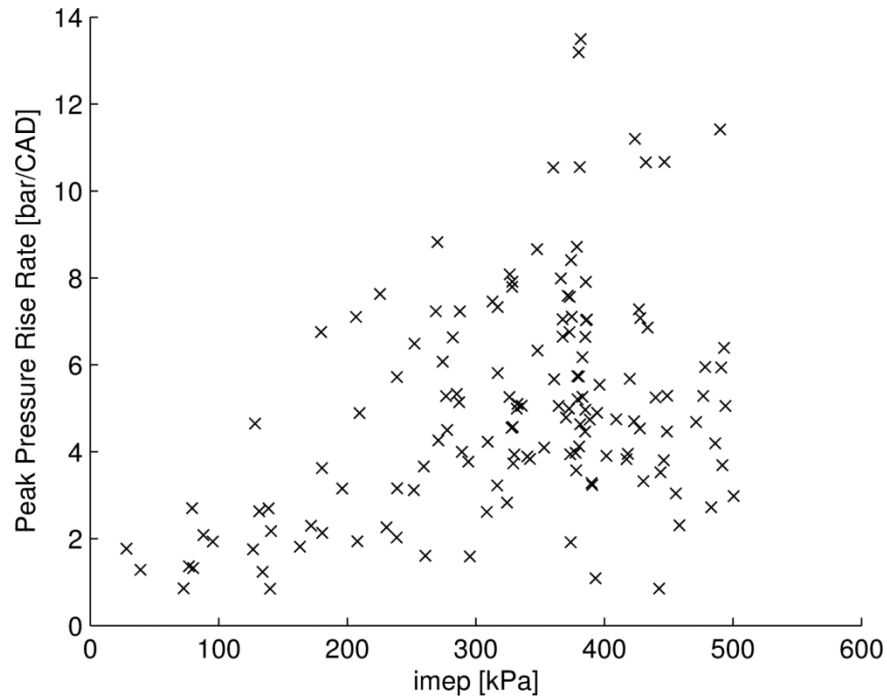


Figure 72 - Pressure rise rate as a function of load

Figure 72 shows that there is a large spread of the values but at low loads the peak pressure rise rate is well below the critical 10 bar/CAD. The peak pressure rise rate increases with increasing load as expected. The two highest values in Figure 72, that seem to be outliers, are indeed that. They represent the two earliest injection timings of an injection timing sweep.

Figure 73 shows the peak pressure rise rate as a function of combustion phasing given as the crank angle degree for maximum cylinder pressure.

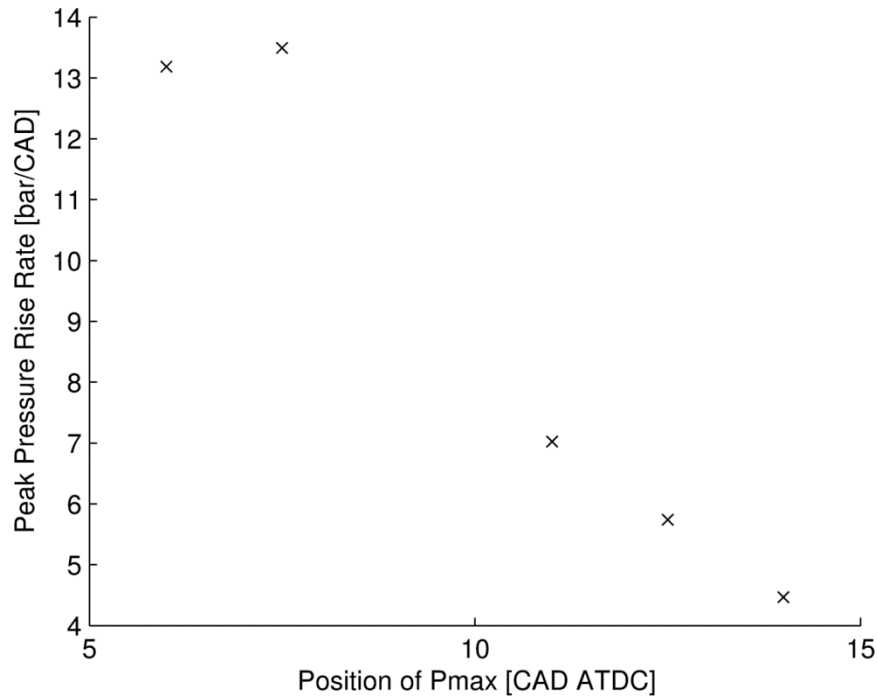


Figure 73 - Peak pressure rise rate as a function of Pmax position

It seems as if a test point at around 9 CAD is missing but making an even spread of these values are difficult in praxis. Combustion phasing is strongly linked to injection timing and even the most minute change of injection timing results in a marked move of the main combustion event. Figure 73 shows what could be achieved within reasonable time. The two operating points having a peak pressure rise rate between 13 and 14 bar/CAD clearly distinguished themselves as being very noisy. Maximum pressures falling between 10 and 15 CAD ATDC always give the best efficiencies for the test engine and the engine is much quieter at those conditions.

13. Estimation of passenger car performance

In order to investigate the “real world” performance the HCCI two-stroke engine a mathematical model has been developed for that purpose during the project period. It is based on the classical mechanics of a moving vehicle as it is described for example in [63].

13.1 NEDC cycle simulations

The model is capable of simulating driving cycles such as the New European Driving Cycle (NEDC) which is the driving cycle used by EU to define the requirements for vehicle emissions and fuel economy.

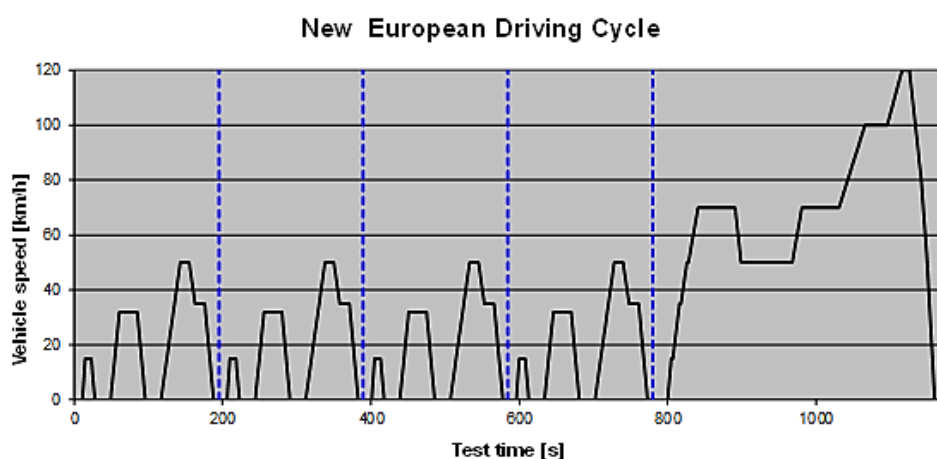


Figure 74 - NEDC cycle

The model has been run for some existing commercial cars and the fuel economy results are compared with the official numbers in Table 31 in order to evaluate the accuracy of the model.

Table 31 – Comparison of official fuel economy numbers and simulation results:

| Car | Test | Simulation | Deviation |
|-----------------------------------|--------|------------|-----------|
| | [km/l] | [km/l] | [%] |
| 1998 Citro  n Saxo 1.5 diesel | 18.9 | 19.9 | + 5.3 |
| 2000 VW Lupo 1.2 turbo diesel | 31.3 | 28.5 | - 8.9 |
| 2007 Ford Mondeo 1.8 turbo diesel | 16.9 | 17.3 | + 2.4 |

Without resorting to an actual statistical calculation Table 31 shows that the model is accurate to within approximately $\pm 10\%$. Considering how different the three vehicles are this is a quite good accuracy. It seems that the model includes the most relevant parameters.

The reason why the simulation of the VW Lupo has the largest deviation is probably because it is the most advanced vehicle in terms of energy efficiency. The internal friction in the Lupo engine has been optimized and it is likely that this is one of the most significant reasons for the deviation since the model uses a traditional friction model for all vehicles.

The model is slightly optimistic with respect to the two more traditional vehicles: The Citroen Saxo and the Ford Mondeo. The reason for this is probably that the model does not take into consideration the detrimental effects on engine efficiency when an engine is started from cold which is the case in the NEDC cycle.

In order to see the effects on fuel economy on the simulated vehicles by switching to an HCCI two-stroke engine a number of choices are made:

1. The two-stroke engine displacement is chosen so that the engine torque level is unchanged (the acceleration performance of the car is unchanged).
2. The two-stroke engine efficiency is set equal to the efficiency of the 50cc test engine.
3. For the turbocharged cars the two-stroke engine is simulated as getting the same relative torque increase as the four-stroke engines get by turbocharging.
4. The weight of the vehicles has not been changed. It is assumed that the lower mass of a smaller displacement two-stroke engine is balanced by a heavier DME fuel system.
5. The gearing of the car is unchanged.

Table 32 – Fuel efficiency improvement by fitting an HCCI two-stroke engine in a passenger car:

| Car | Std. | Two-Stroke | Change |
|-----------------------------------|-------------|-------------------|---------------|
| | [km/l] | [km/l] | [%] |
| 1998 Citroén Saxo 1.5 diesel | 19.9 | 23.2 | + 16.6 |
| 2000 VW Lupo 1.2 turbo diesel | 28.5 | 31.1 | + 9.1 |
| 2007 Ford Mondeo 1.8 turbo diesel | 17.3 | 18.5 | + 6.9 |

Based on the decisions above it is clear from Table 32 that there would be a fuel efficiency improvement for all three vehicles if they had an HCCI two-stroke engine installed. An interesting trend can also be observed. The improvement is the greatest for the non-turbocharged Citroen Saxo and among the two turbocharged cars it is the greatest for the oldest one. This is no coincidence. The progress in engine technology in recent years has enabled high specific power outputs from small four-stroke diesel engines. Brake mean effective pressures (bmep) in excess of 2000 kPa are now possible. This has a significant impact on four-stroke engine efficiency and thereby vehicle fuel efficiency.

It is difficult to achieve a higher brake mean effective pressure than 800 kPa with a non-turbocharged four-stroke diesel. Poor combustion efficiency and high smoke emissions establish this limit. The situation for the three cars under consideration is shown in Table 33.

Table 33 – Absolute and relative break mean effective pressures

| Car | bmep | bmep / (800 kPa) |
|-----------------------------------|-------------|-------------------------|
| | [kPa] | [] |
| 1998 Citroén Saxo 1.5 diesel | 782 | 0.98 |
| 2000 VW Lupo 1.2 turbo diesel | 1446 | 1.81 |
| 2007 Ford Mondeo 1.8 turbo diesel | 2234 | 2.79 |

The non-turbocharged Citroén Saxo is very close to 800 kPa as would be expected. The VW Lupo is turbocharged to almost twice the specific output. The Ford Mondeo is turbocharged to an even higher degree.

Since the internal friction in an engine is strongly dependent on engine speed but not on engine load this increase in specific output achieved by a torque increase at unchanged engine speeds results in higher mechanical engine efficiencies according to:

$$\eta_m = \frac{bmep}{bmep + fmep} \quad (35)$$

The friction mean effective pressure (fmep) is speed dependent but here a value of 200 kPa has been chosen in order to do a comparison. It is equivalent to the fmep of a four-stroke diesel at an engine speed of 2500 rpm according to [69]. Using this value the mechanical efficiency at full load can be approximated – see Table 34.

Table 34 – Approx. mechanical efficiency at full load.

| Car | bmep | bmep / (800 kPa) | η_m |
|-----------------------------------|-------|------------------|----------|
| | [kPa] | [] | [] |
| 1998 Citro  n Saxo 1.5 diesel | 782 | 0.98 | 0.80 |
| 2000 VW Lupo 1.2 turbo diesel | 1446 | 1.81 | 0.88 |
| 2007 Ford Mondeo 1.8 turbo diesel | 2234 | 2.79 | 0.92 |

The efficiency of the two-stroke engine can be calculated in a similar way.

Table 35 – Mechanical efficiencies for the two-stroke engine at full load.

| Car | bmep 2S | η_m 2S |
|-----------------------------------|---------|-------------|
| | [kPa] | [] |
| 1998 Citro  n Saxo 1.5 diesel | 450 | 0.87 |
| 2000 VW Lupo 1.2 turbo diesel | 813 | 0.92 |
| 2007 Ford Mondeo 1.8 turbo diesel | 1257 | 0.95 |

Going back and looking at the change in fuel efficiency (Table 32) it is clear that there is a relation between the change in mechanical efficiency and the change in fuel efficiency. This is the major benefit of the two-stroke engine. The lower internal friction enables good engine efficiencies even though the power output per engine cycle is significantly lower than for the four-stroke diesel engine.

Then why don't we all drive around in cars with two-stroke engines? The improvement in fuel consumption with a two-stroke engine that was computed above is not new knowledge. During the 1990's there was renewed interest in the gasoline two-stroke engine for passenger cars for this very reason [48]. The advent of direct injection systems for gasoline that were capable of quickly creating a homogenous fuel-air mixture made it possible to manufacture efficient direct injection two-stroke engines. But there were a number of issues to deal with that finally stopped further progress for the gasoline two-stroke engine:

1. Use of three-way catalyst
2. Engine durability

1. Due to the scavenging principle of a two-stroke engine it is impossible to avoid that some of the scavenge air continues directly out in the exhaust pipe. This excess air is not compatible with the operation of a three-way catalyst. Spark ignition combustion of gasoline produces significant amounts of NO_x and since a three-way catalyst could not be used it was not possible to get below emission limits.
2. The two-stroke engine concept with the lowest internal friction, and thereby the best fuel efficiency benefits, uses the crankcase as its scavenging pump. Figure 75 shows a spark ignited gasoline engine but the scavenging principle is the same for crankcase scavenged direct injection engines.

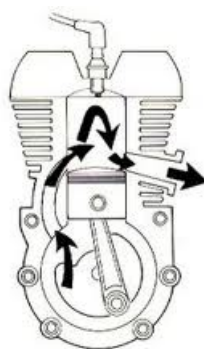


Figure 75 – Crankcase scavenged two-stroke engine

This means that the crankcase cannot be filled with oil as it is in a four-stroke engine. A system called wet sump lubrication. The wet sump crankcase with plain bearings, which is used almost exclusively in car engines of today, has been proven through more than a century to be very reliable. A crankcase scavenged two-stroke engine adds small amounts of lubricant continuously to the crankcase. This oil passes through the crankcase and is eventually burned during combustion and exits with the exhaust gas. The oil does not burn as cleanly as the fuel and oil addition to the crankcase is therefore kept to the absolute minimum required. This marginal lubrication level can give problems related to the durability of the engine and this is an additional reason why car manufacturers have been reluctant to use two-stroke engines.

How do these challenges for the gasoline two-stroke engine apply to the DME two-stroke engine?

1. Since an HCCI engine always operates under lean conditions there will be an excess of air in the exhaust whether the engine concept is two- or four-stroke. A three-way catalyst is therefore not an option in any case. NO_x formation during combustion has to be limited and that is the whole purpose of the HCCI concept.
2. The situation for the DME two-stroke is quite similar to the gasoline two-stroke engine. There is one benefit though. Due to the high vapor pressure of DME compared to gasoline

there is very little, if any, wetting of the cylinder wall with DME. This can be the case with gasoline and fuel wetting of the cylinder walls reduce the viscosity of the lubricant film on the walls.

The practical experience during the project has shown no reliability issues with the main components of the DME two-stroke engine.

The obstacles that remain for the HCCI two-stroke engine are wear issues in the fuel injection equipment and that the NO_x emissions are a little too high at the current state of development. The latter is illustrated in Figure 76. Comparison is made to heavy duty vehicles since those values are given in g/kWh and not g/km that is used for cars. The reason why this comparison is better is that the only vehicle that the two-stroke engine has been fitted to is the DTU ecocar. This vehicle has such low fuel consumption that the emission per km is very low.

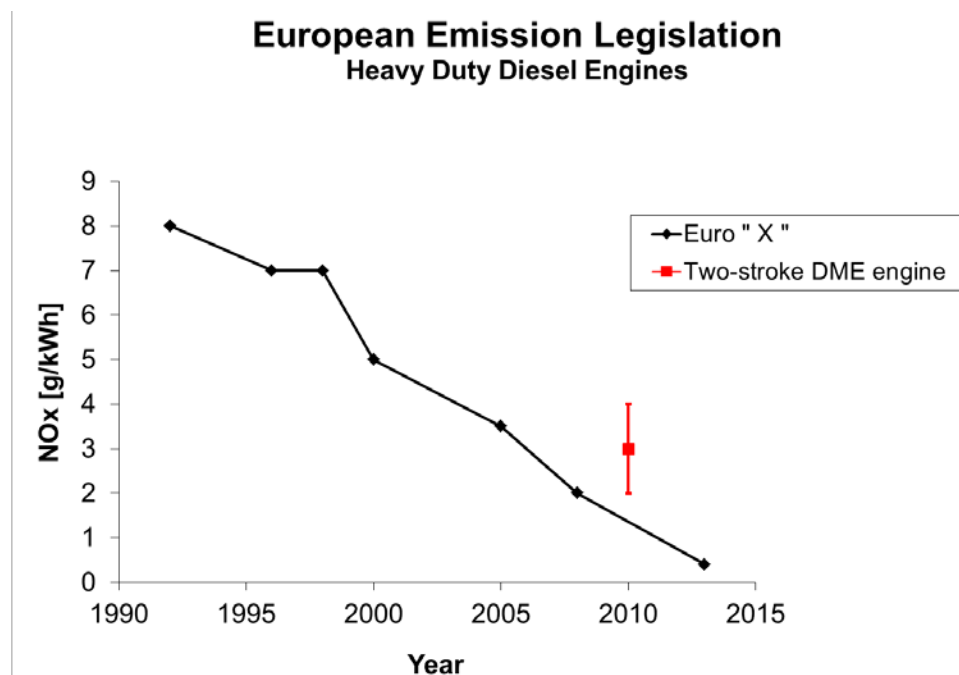


Figure 76 – Emission limits on a g/kWh basis

Figure 76 shows that the two-stroke engine complies with legislation up until 2005. Further work is needed to get below current legislation.

14. DME fuel pump

14.1 Concept

The first two-stroke engine prototype was tested with a DME fuel rail pressurized by helium to 100 bars. For the second prototype it was decided to also develop and build a DME pump that could supply the fuel rail. Due to the very low lubricity of DME the biggest challenge for engine researchers and manufacturers wanting to test DME has been to devise a reliable fuel injection pump [70]. Typically the solutions have been to modify an existing diesel pump using advanced metal coating techniques and add a lubricant additive to the DME. Typical levels of lubricant addition are 300-1000 ppm [7]. These modified diesel pumps have also had the plunger and barrel section isolated from the plunger actuation mechanism so that the actuation mechanism could be lubricated by ordinary lubrication oil. A different approach is presented in the following section. The basic idea was that it may be possible to use hydraulic type rod seals and avoid any direct contact between plunger and barrel since this engine does not benefit from injection pressures higher than 150 bars. In this way, solutions like advanced metal coatings would be unnecessary and the rod seals would serve, at the same time, to isolate the plunger and barrel section from the rest of the pump mechanism. The details of this design are outlined below.

14.2 Design

The pump is a single plunger jerk pump. Cam activated and spring return. Flow control is performed by inlet and outlet one-way valves. Avoidance of metal to metal contact between plunger and barrel is a central idea in the concept. This requires that the plunger is accurately guided relative to the barrel. No metal to metal contact is acceptable. This function is provided by a ball guide unit as shown in Figure 77. Sealing between plunger and barrel is achieved by means of a spring activated PTFE seals.

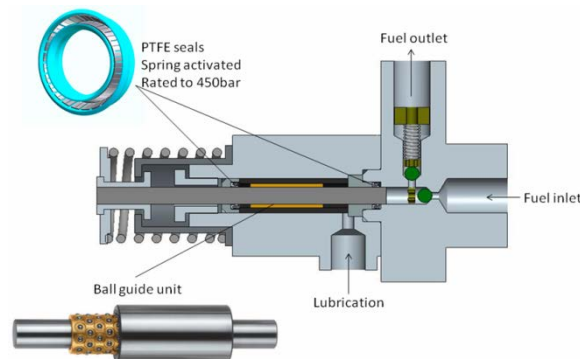


Figure 77 - Cross section of DME pump

Cavitation in the pump inlet and especially around the one-way inlet valve was a concern. If the temperatures of the fuel tank and the pump are the same then any pressure drop across the inlet valve would lead to cavitation. Cavitation would lower the volumetric effi-

ciency of the pump and could only be compensated for by higher feed pressures which would place higher demands on the feed pump. In order to get the lowest possible pressure drop across the inlet valve this is designed as a light plastic ball without spring return. The low pressure created in the barrel during the plunger down-stroke forces the ball away from its seat and inflow of DME commences. During the up-stroke of the plunger the pressure drop reverses direction and the ball moves back on the valve seat again. The outlet valve functions in the same way but has a return spring in order to achieve quick closing.

14.3 Performance

The pump was actuated in sinusoidal motion by an eccentric circular disc mounted on a servo motor. The inlet of the pump was connected to a one liter DME fuel tank on a scale. The DME fuel tank was pressurized with helium at a pressure of 3 bars higher than the DME vapor pressure. A relief valve kept the desired pressure level at the pump outlet. See Figure 78.

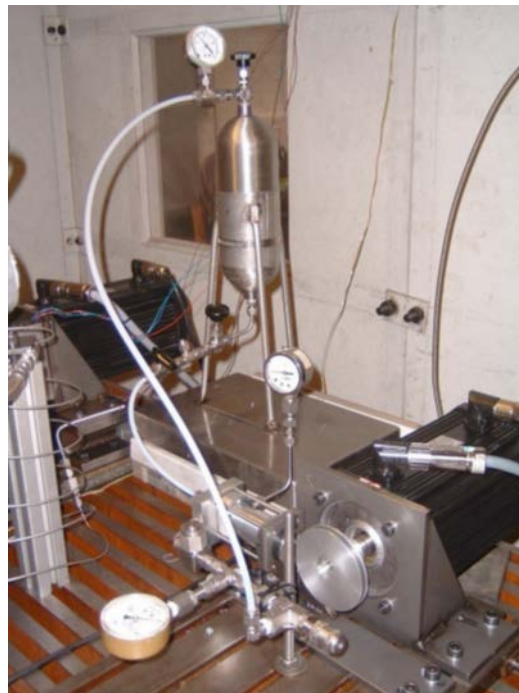


Figure 78 - DME pump test setup

The measured volumetric efficiencies are listed in Table 36.

Table 36 - Volumetric efficiency of DME pump

| Pump speed [rpm] | Volumetric efficiency [-] |
|-----------------------------|--------------------------------------|
| 500 | 0.88 |
| 750 | 0.89 |
| 1000 | 0.81 |

14.4 Durability

The rod seal between plunger and barrel facing DME at pressures varying from DME vapor pressure to full rail pressure determines the life of the pump. PTFE seals without fiber reinforcement had a lifetime of less than 5 hours. PTFE seals with carbon fiber reinforcement were tested and lasted longer but still showed signs of critical wear after 10 hours of operation. A measured leakage flow of 0.3 g/hour flows past the seal contact zone during operation. It was believed that this leakage flow washes away the lubricant in the seal contact zone and was the main reason for the high wear rates. In order to address this issue the front seal facing the DME was mounted oppositely so that the spring faced the lubricant side and the lubrication oil was pressurized to a level slightly higher than the DME pumping pressure. In this way there would continuously be a pressure gradient forcing lubricant into the DME and not vice versa, providing a lubricant film in the seal contact zone. With this concept there has been no critical wear on the seal for the remainder of the test period and the leakage of lubrication oil through to the DME side of the seal is negligible. The test period has included a mixture of dyno testing and testing with the engine in a small urban car used for fuel economy competitions, the latter accounting for the largest share of operational hours. The hours accumulated in the car have not been registered accurately but are approximately fifty hours. In conclusion it can therefore be said that a DME pump using rod seals between plunger and barrel could be a viable solution at the modest injection pressures tested in this study but the design proposed has not accumulated enough hours to draw any final conclusions.

15. Conclusion

The combustion mode and the emissions from a 50cc loop scavenged two-stroke engine operating on direct injected dimethyl ether were investigated. The engine was custom made to a vehicle that had been competing in the Shell Eco-Marathon fuel efficiency competition. In 2009 the vehicle equipped with this engine won the competition by driving 589 km/l gasoline equivalent. Focus had been entirely on fuel efficiency and the combustion mode that was the result of applying an automotive size injector to a 50cc engine was a result of necessity, not design choice. A study of combustion mode and emissions was desired.

During this study it was found that the late-injection of DME at high flow rates resulted in a high degree of premixing before combustion. This conclusion was based on colour images taken of the combustion zone. The images revealed that the luminosity from combustion was distributed throughout the chamber and only a few features could be traced back to the injector spray pattern. The initial heat release rates from combustion also indicated a quite high degree of premixing.

A cycle simulation employing a two-stroke scavenging model and running the extended Zeldovich mechanism for nitrogen oxide formation on top of a chemical equilibrium routine revealed that the premixing was not complete though. The reason for this was that the measured nitrogen oxide emissions were a factor of five higher than the calculated ones that assumed perfect premixing. Heat release analysis also verified that premixing could not be complete. It showed a slow mixing controlled combustion phase after the initial rapid heat release.

An attempt was made to improve the premixing by designing an in-direct injection cylinder head. As expected, the in-direct injection version of the engine had slightly lower efficiency due to pumping and heat transfer losses but the premixing was improved. This was verified by a higher fraction of rapid premixed heat release.

The improvements in premixing due to the indirect injection cylinder head dramatically reduced the emissions of carbon monoxide and unburned hydrocarbons at high load. At low load the situation was the opposite. The low combustion temperatures associated with highly premixed lean combustion resulted in high levels of carbon monoxide and unburned hydrocarbons compared to the direct injected version of the engine.

An oxidation catalyst was applied in order to test whether those emissions could be handled in aftertreatment. Oxidation of carbon monoxide was efficient but effective hydrocarbon oxidation was only possible if the engine was operated far from its best efficiency.

Finally, numerical studies of heat transfer showed that the high losses found when analysing the cylinder as a closed system should be contributed to blowby and not higher than normal heat transfer rates.

16. Nomenclature

| | |
|---------|-----------------------------------|
| A | Surface area |
| AF_s | Stoichiometric air-fuel ratio |
| ATDC | After top dead centre |
| B | Cylinder bore |
| BMEP | Brake mean effective pressure |
| BS | Brake specific |
| BDC | Bottom dead centre |
| BTDC | Before top dead centre |
| C | The Courant number |
| C_μ | A constant in the k-eps equations |
| CA | Crank angle |
| CA10 | Crank angle of 10% heat release |
| CA50 | Crank angle of 50% heat release |
| CAD | Crank angle degrees |
| CCS | Combined combustion system |
| CFD | Computational fluid dynamics |
| CGH2 | Compressed gaseous hydrogen |
| CI | Compression ignition |
| CNG | Compressed natural gas |
| CO | Carbon monoxide |
| CR | Compression ratio |

| | |
|------|---|
| CV | Control volume |
| DI | Direct Injection |
| DME | Dimethyl ether |
| DNS | Direct numerical simulation |
| DOC | Diesel oxidation catalyst |
| EGR | Exhaust gas recirculation |
| EO | Exhaust opening angle |
| EtOH | Ethanol |
| FC | Fuel cell |
| FMEP | Friction mean effective pressure |
| FPFC | Fuel processor fuel cell |
| FT | Fischer-Tropsch |
| FTD | Fischer-Tropsch diesel |
| FTN | Fischer-Tropsch naphtha |
| G | Gaseous |
| GDI | Gasoline direct injection |
| HC | Hydrocarbons |
| HCCI | Homogeneous charge compression ignition |
| HEV | Hybrid electric vehicle |
| HR | Heat release |
| HSDI | High-speed direct-injection |
| HTHR | High temperature heat release |
| HTR | High temperature reactions |

| | |
|-----------------|--|
| IC | Intake closing |
| ICE | Internal combustion engine |
| IDI | Indirect injection |
| IMEP | Indicated mean effective pressure |
| k-eps | Standard k-epsilon turbulence model |
| L | Liquid |
| LH2 | Liquefied hydrogen |
| LHV | Lower heating value |
| LNG | Liquefied natural gas |
| LPG | Liquefied petroleum gas |
| LTHR | Low temperature heat release |
| LTR | Low temperature reactions |
| MeOH | Methanol |
| ML | Mixing length |
| MTA | Manual transmission |
| N | Revolutions per minute |
| NEDC | New European driving cycle |
| NO | Nitrogen oxide |
| NO _x | Oxides of nitrogen |
| NTSEL | National Traffic Safety and Environmental Laboratory |
| p | Pressure |
| PCCI | Premixed charge compression ignition |
| PCI | Premixed compression ignition |

| | |
|-----------|--|
| PFS | Partial fuel stratification |
| PM | Particulate matter |
| PPC | Partially premixed combustion |
| PPCI | Partially premixed compression ignition |
| PPM | Parts per million |
| PPRR | Peak pressure rise rate |
| PTFE | Poly tetra flour ethylene |
| Q_{AHR} | Accumulated heat release |
| Q_{HR} | Heat release |
| Q_w | Heat transfer through wall |
| QMEP | Heat transfer mean effective pressure |
| RCCI | Reactivity controlled compression ignition |
| Re | Reynolds number |
| RNG | Renormalization group k-eps model |
| RPM | Revolutions per minute |
| RWB | Residual wood biomass |
| S_p | Mean piston speed |
| SCR | Selective catalyst reduction |
| SI | Spark ignition |
| SN | Swirl number |
| SOI | Start of injection |
| T | Temperature |
| T_w | Temperature of wall |

| | |
|-----------------------------|--|
| TDC | Top dead centre |
| THC | Total hydrocarbons |
| TI | Relative turbulent intensity |
| TTW | Tank-to-wheel |
| U | Reference velocity |
| u | Velocity along 1st coordinate direction |
| u' | Turbulent fluctuation velocity in the 1st coordinate direction |
| UHC | Unburned hydrocarbons |
| v' | Turbulent fluctuation velocity in the 2nd coordinate direction |
| V _d | Cylinder displacement volume |
| V _{undeformed} | Undeformed cylinder volume |
| w | Velocity along 3rd coordinate direction |
| w' | Turbulent fluctuation velocity in the 3rd coordinate direction |
| WB | Wood biomass |
| WTT | Well-to-tank |
| y _p ⁺ | Dimensionless wall distance at node point P |
| y ⁺ | Dimensionless wall distance |
| y | Cell centre distance from wall |
| η _m | Mechanical efficiency |
| θ | Crank angle |
| ν | Kinematic viscosity |
| σ | Stefan-Boltzmann's constant |
| φ | Fuel-air equivalence ratio |

| | |
|--------------------------|--|
| ω_{engine} | Angular rotational speed of engine |
| ω_{swirl} | Angular rotational speed of flow swirling around the cylinder axis |

References

1. Cassman, K. G. and Liska, A. J. "Food and fuel for all: realistic or foolish?", *JOHN WILEY & SONS LTD ,Biofuels Bioprod.Biorefining*. 1:18-23, 2007.
2. Sorenson , S. C. and Mikkelsen , S., "Performance and Emissions of a 0.273 Liter Direct Injection Diesel Engine Fuelled with Neat Dimethyl Ether", *Copyright 1995 Society of Automotive Engineers, Inc* ,1995.
3. Muradov, N. Z. and Veziroglu, T. N. ""Green" path from fossil-based to hydrogen economy: An overview of carbon-neutral technologies", *Pergamon-Elsevier Science Ltd ,Int J Hydrogen Energy*. 33:6804-6839, 2008.
4. Semelsberger, T. A., Borup, R. L., and Greene, H. L. "Dimethyl ether (DME) as an alternative fuel", *J. Power Sources*. 156:497-511, 2006.
5. Consonni, S., Katofsky, R. E., and Larson, E. D. "A gasification-based biorefinery for the pulp and paper industry", *Chemical Engineering Research & Design*. 87:1293-1317, 2009.
6. Zhang, W. N. "Automotive fuels from biomass via gasification", *Fuel Process Technol.* 91:866-876, 2010.
7. Arcoumanis, C., Bae, C., Crookes, R., and Kinoshita, E. "The potential of di-methyl ether (DME) as an alternative fuel for compression-ignition engines: A review", *Fuel*. 87:1014-1030, 2008.
8. Verbeek, R. and Weide, J. v. d., "Global assessment of dimethyl-ether: comparison with other fuels", *SAE International, Warrendale, Pennsylvania, USA*, Technical Paper 971607, 1997.
9. Lund, H., Hvelplund, F., and Mathiesen, B. V. "Coherent Energy and Environmental System Analysis", *Department of Development and Planning, Aalborg University, Fibigerstræde 13, 9220 Aalborg Ø, Denmark* ,2011.
10. Hansen, K. R., Nielsen, C. S., Sorenson, S. C., and Schramm, J., "Development of a Small Two-Stroke Diesel Engine Powered by DME", *International DME Association*,2010.
11. Sorenson , S. C., Mikkelsen , S. -, Hansen , J. B., and Sorenson , S. C., "Dimethyl Ether as An Alternative Fuel for Diesel Engines", *Institution of Mechanical Engineers (IMechE)* ,1996.
12. Mueller , C. J., Pitz , W. J., Pickett , L. M., Martin , G. C., Siebers , D. L., and Westbrook , C. K., "Effects of Oxygenates on Soot Processes in DI Diesel Engines: Experiments and Numerical Simulations", 2003.

13. Sivebaek, I. and Sorenson, S. "Dimethyl ether (DME) and other low boiling point fuels - Assessment of lubricity using the new Medium Frequency Pressurised Reciprocating Rig (MFPRR).", *Technical Research Centre Finland ,9th Nordic Symposium on Tribology Nordtrib 2000, Vol 2*. 201:604-616, 2000.
14. Sivebaek, I. M. and Jakobsen, J. "The viscosity of dimethyl ether", *Elsevier Science Ltd ,Tribology International*. 40:652-658, 2007.
15. Hansen , K. F., Nielsen , L., Hansen , J. B., Mikkelsen , S., Landælv , H., Ristola , T., and Vielwerth , K., "Demonstration of a DME (Dimethyl Ether) Fuelled City Bus", *SAE International ,2000-01-2005*, 2000.
16. Salsing, H. and Denbratt, I., "Performance of a Heavy-Duty DME Diesel Engine~An Experimental Study", *SAE International, Warrendale, Pennsylvania, USA*, Technical Paper 2007-01-4167, 2007.
17. Salsing , H. and Denbratt , I., "Performance of a Heavy Duty DME Engine - The Influence of Methanol and Water in the Fuel", *SAE International ,2012-01-0156*, 2008.
18. Salsing , H., Ochoterena , R., and Denbratt , I., "Performance of a Heavy Duty DME Engine - the Influence of Nozzle Parameters on Combustion and Spray Development", *SAE International ,2009-01-0841*, 2009.
19. Salsing , H., Rinaldini , C. A., Golovitchev , V. I., and Denbratt , I., "Performance and Emissions of a DME Diesel Engine Equipped With a Fuel-Specific, Common-Rail System", *Society of Automotive Engineers of Japan ,06A0501297*, 2006.
20. Salsing , H., Golovitchev , V., and Denbratt , I., "Numerical Analysis of Combustion and Emissions Formation in a Heavy Duty DME Engine", *SAE International ,2012-01-0156*, 2012.
21. Kajitani, S. and Nakayama, M. "Possibilities and problems of diesel engine operated with DME", *Society of Automotive Engineers of Japan ,52-7:49-55*, 1998.
22. Konno , M., Kajitani , S., and Suzuki , Y., "Unburned emissions from a DI diesel engine operated with dimethyl ether", *Society of Automotive Engineers of Japan,9935167*, 1999.
23. Chen, Z. L., Konno, M., and Kajitani, S. "Performance and emissions of DI compression ignition engines fueled with dimethyl ether (Performance and emissions in retrofitted engines)", *Jsmc International Journal Series B-Fluids and Thermal Engineering*. 43:82-88, 2000.

24. Oda, Y., Kajitani, S., and Suzuki, S., "Characteristics of spray formation and combustion in diesel engines operated with dimethyl ether", *SAE International, Warrendale, Pennsylvania, USA*, Technical Paper 2003-01-1925, 2003.
25. Kajitani, S. and Chen, Z. L. "Fundamental research on next generation fuel (dimethyl ether) engines", *Journal of Scientific & Industrial Research*. 62:133-144, 2003.
26. Narusawa, K., Goto, Y., Sato, Y., Ishi, H., and Odaka, M., "Research and Development Program of the Next-generation Environmentally Friendly Vehicles(EFVs) in Japan", *SAE International*, 2004.
27. Sato, Y. "Development and Popularization of Heavy-Duty Vehicles Fueled by Dimethyl Ether (DME) as New Clean Alternative Energy", *World Scientific and Engineering Academy and Society, Ps '09: Proceedings of the 9th Wseas International Conference on Power Systems*. 40-45, 2009.
28. Sato, Y., Nakamura, A., Takada, Y., and Nakamura, K., "Development of DME Vehicles and Strategy of Practical Use Penetration", *Society of Automotive Engineers of Japan, Inc., Tokyo, Japan*, Technical Paper 2008-08-0165, 2008.
29. Sato, Y., Nozaki, S., and Noda, T., "The performance of a diesel engine for light-duty truck using a jerk-type, in-line DME injection system", *SAE International, Warrendale, Pennsylvania, USA*, Technical Paper 2004-01-1862, 2004.
30. Nozaki, S., Noda, T., Ishikawa, T., Kasaya, M., Yanai, T., Kawamura, A., Sato, Y., and Oikawa, H., "Adaptation of Conventional Common Rail Type Diesel Injection System to DME Fuel", *Society of Automotive Engineers of Japan, Inc., Tokyo, Japan*, Technical Paper 2009-08-0271, 2009.
31. Yanai, T., Sato, Y., Kawamura, A., Oikawa, H., Nozaki, S., Noda, T., and Ishikawa, T., "Development and Engine Bench Testing of a Common Rail Type DME Injection System", *Society of Automotive Engineers of Japan, Inc., Tokyo, Japan*, Technical Paper Series 2008-5929, 2008.
32. Yanai, T., Sato, Y., Kawamura, A., Oikawa, H., Nozaki, S., and Ishikawa, T., "Development and Engine Bench Testing of a Common Rail Type DME Injection System (Second Report)~Required Injection Pressure on Full Load Condition", *Society of Automotive Engineers of Japan, Inc., Tokyo, Japan*, Technical Paper 2009-08-0272, 2009.
33. Tsuchiya, T. and Sato, Y., "Development of DME Engine for Heavy-duty Truck", *Copyright © 2006 SAE International*, Technical Paper Series 2006-01-0052, 2006.

34. Spezzano, P., Picini, P., Cataldi, D., Messale, F., and Manni, C. "Particle- and gas-phase emissions of polycyclic aromatic hydrocarbons from two-stroke, 50-cm(3) mopeds", *Atmospheric Environment*. 42:4332-4344, 2008.
35. Volckens, J., Olson, D. A., and Hays, M. D. "Carbonaceous species emitted from handheld two-stroke engines", *Atmospheric Environment*. 42:1239-1248, 2008.
36. Kirchberger, R. "Potential of High Technology 50 cm³ Two-Stroke and Four-Stroke Engines", *SAE Technical Paper 2007-32-0013*. 2007.
37. Alander, T., Antkaninen, E., Raunemaa, T., Elonen, E., Rautiola, A., and Torkkell, K. "Particle emissions from a small two-stroke engine: Effects of fuel, lubricating oil, and exhaust aftertreatment on particle characteristics", *Aerosol Science and Technology*. 39:151-161, 2005.
38. Rijkeboer, R., Bremmers, D., Samaras, Z., and Ntziachristos, L. "Particulate matter regulation for two-stroke two wheelers: Necessity or haphazard legislation?", *Pergamon Elsevier Science Ltd ,Atmospheric Environment*. 39:2483-2490, 2005.
39. Faiz, A., Gautam, S., and Gwilliam, K. M. "Technical and policy options for reducing emissions from 2-stroke engine vehicles in Asia", *International Journal of Vehicle Design*. 34:1-11, 2004.
40. Picini, P. "Particulate Polycyclic Aromatic Hydrocarbons and Particulate Matter Emissions From Two-Wheel Motor Vehicles", *SAE International ,Technical Paper*. 2005-24-020:2005.
41. Combustion Research Facility, "<http://crf.sandia.gov/>", *Sandia National Laboratories* ,2012.
42. Pedersen, T. D. and Schramm, J., "A study on the effects of compression ratio, engine speed and equivalence ratio on HCCI combustion of DME", *Copyright © 2007 Society of Automotive Engineers of Japan, Inc. and Copyright © 2007 SAE International* ,2007.
43. Pedersen, T. D. and Schramm, J., "Reduction of HCCI Combustion Noise Through Piston Crown Design", *Copyright © 2010 SAE International ,Technical Paper Series* 2010-01-1487, 2010.
44. Yang, Y., Dec, J., Dronniou, N., Sjöberg, M., and Cannella, W., "Partial Fuel Stratification to Control HCCI Heat Release Rates: Fuel Composition and Other Factors Affecting Pre-Ignition Reactions of Two-Stage Ignition Fuels", *Copyright © 2011 SAE International* ,2011-01-1359, 2011.

45. Splitter , D., Reitz , R., and Hanson , R. "High Efficiency, Low Emissions RCCI Combustion by Use of a Fuel Additive", *SAE International ,SAE Int.J.Fuels Lubr.* 3:742-756, 2010.
46. Mueller , C. J., "The Quantification of Mixture Stoichiometry When Fuel Molecules Contain Oxidizer Elements or Oxidizer Molecules Contain Fuel Elements", *SAE International*, Technical Paper Series 2005-01-3705, 2005.
47. Pedersen, T. D., "Homogeneous Charge Compression Ignition Combustion of Dimethyl Ether", PhD, *Technical University of Denmark*, 2010.
48. Blair, G. P., Design and Simulation of Two-Stroke Engines, *SAE*, 400 Commonwealth Drive, Warrendale, PA, ISBN 1-56091-685-0:623, 1996.
49. Weinberg, F. J. "Explicit Equations for the Calculation, by Successive Approximations, of Equilibrium Gas Compositions at High Temperatures - the Hydrogen+carbon+oxygen and the Hydrogen+carbon+oxygen+nitrogen Systems without Solid Carbon Formation", *Royal Society of London ,Proceedings of the Royal Society of London Series A-Mathematical and Physical Sciences.* 241:132-140, 1957.
50. Dec , J. E., "A Conceptual Model of DI Diesel Combustion Based on Laser-Sheet Imaging*", *SAE International*, Technical Paper Series 970873, 1997.
51. Hansson, C. and Dolriis, J. D., "Design and optimisation of DME two-stroke engine", Master thesis, *Technical University of Denmark*, MEK-FM-EP 2009-09, 2009.
52. Hwang, W., Dec, J., and Sjoberg, M. "Spectroscopic and chemical-kinetic analysis of the phases of HCCI autoignition and combustion for single- and two-stage ignition fuels", *ergamon Elsevier Science Ltd ,Combust.Flame.* 154:387-409, 2008.
53. Kokjohn, S. L. and Reitz, R. D. "Investigation of charge preparation strategies for controlled premixed charge compression ignition combustion using a variable pressure injection system", *Professional Engineering Publishing Ltd ,International Journal of Engine Research.* 11:257-282, 2010.
54. Hansen , K. R., Dolriis , J. D., Hansson , C., Nielsen , C. S., Sorenson , S. C., and Schramm , J., "Optimizing the Performance of a 50cc Compression Ignition Two-Stroke Engine Operating on Dimethyl Ether", *Copyright Â© 2011 SAE International* ,2011.
55. Nuti, M., Emissions from Two-Stroke Engines, *Society of Automotive Engineers*, ISBN 0-7680-0215-X:283, 1998.

56. McCullough, G., Douglas, R., Spence, S., and Cunningham, G. "Flowrate and heat transfer considerations for oxidation catalysts", *Professional Engineering Publishing Ltd ,Proc.Inst.Mech.Eng.Part D-J.Automob.Eng.* 218:229-241, 2004.
57. Jeppesen, J. B., "Deformation Analysis of Combustion Chamber", Bachelor Thesis, *Technical University of Denmark*, 2011.
58. Aronsson , U., Solaka , H., Chartier , C., Andersson , Å., and Johansson , B., "Impact of Mechanical Deformation due to Pressure, Mass, and Thermal Forces on the In-Cylinder Volume Trace in Optical Engines of Bowditch Design", *The Automotive Research Association of India* ,2011.
59. Hansen , K. R., Nielsen , C. S., Sorenson , S. C., and Schramm , J., "A 50cc Two-Stroke DI Compression Ignition Engine Fuelled by DME", *Copyright Â© 2008 SAE International* ,2008.
60. CD Adapco, CCM user guide - Star CD version 4.14, *CD Adapco* ,:504, 2010.
61. CFD Online, "Boundary layer profile", *CFD Online* ,2012.
62. Han, Z. Y. and Reitz, R. D. "A temperature wall function formulation for variable-density turbulent flows with application to engine convective heat transfer modeling", *Pergamon Elsevier Science Ltd ,Int.J.Heat Mass Transfer.* 40:613-625, 1997.
63. Sorenson , S. C., *Engine Principles and Vehicles*, *Spencer C. Sorenson*, Lyngby, Denmark, 2008.
64. Versteeg, H. K. and Malalasekera, W., *Computational Fluid Dynamics*, *Pearson Education Limited*, Edinburgh Gate, Harlow, Essex CM20 2JE, England, ISBN 978-0-13-127498-3:503, 2007.
65. Wang , B., Bergin , M. J., Petersen , B. R., Miles , P. C., Reitz , R. D., and Han , Z., "Validation of the Generalized RNG Turbulence Model and Its Application to Flow in a HSDI Diesel Engine", *SAE International* ,2012.
66. Kaario , O., Lendormy , E., Sarjovaara , T., Larmi , M., and Rantanen , P., "In-Cylinder Flow Field of a Diesel Engine", *Copyright © 2007 SAE International*,Technical Paper Series 2007-01-4046, 2007.
67. Callender , E., Douglas , R., and Thornhill , D., "The Potential of 50cc Four-Stroke Engines for Moped Applications", *SAE International* ,1998.
68. Eng, J. A., "Characterization of Pressure Waves in HCCI Combustion", *Copyright © 2002 Society of Automotive Engineers, Inc*,Technical Paper Series 2002-01-2859, 2002.

69. Heywood, J. B., *Internal Combustion Engine Fundamentals*, McGraw-Hill, Singapore, ISBN 0-07-100499-8:930, 1988.
70. McCandless, J. C., Teng, H., and Schneyer, J. B., "Development of a Variable-Displacement, Rail-Pressure Supply Pump for Dimethyl Ether", *Copyright © 2000 Society of Automotive Engineers, Inc*, Technical Paper Series 2000-01-0687, 2000.

**SAE TECHNICAL
PAPER SERIES**

2008-01-1535

A 50cc Two-Stroke DI Compression Ignition Engine Fuelled by DME

Kim R. Hansen, Claus S. Nielsen, Spencer C. Sorenson and Jesper Schramm
Technical University of Denmark

SAE *International*[™]

2008 SAE International Powertrains,
Fuels and Lubricants Congress
Shanghai, China
June 23-25, 2008

By mandate of the Engineering Meetings Board, this paper has been approved for SAE publication upon completion of a peer review process by a minimum of three (3) industry experts under the supervision of the session organizer.

All rights reserved. No part of this publication may be reproduced, stored in a retrieval system, or transmitted, in any form or by any means, electronic, mechanical, photocopying, recording, or otherwise, without the prior written permission of SAE.

For permission and licensing requests contact:

SAE Permissions
400 Commonwealth Drive
Warrendale, PA 15096-0001-USA
Email: permissions@sae.org
Tel: 724-772-4028
Fax: 724-776-3036



For multiple print copies contact:

SAE Customer Service
Tel: 877-606-7323 (inside USA and Canada)
Tel: 724-776-4970 (outside USA)
Fax: 724-776-0790
Email: CustomerService@sae.org

ISSN 0148-7191

Copyright © 2008 SAE International

Positions and opinions advanced in this paper are those of the author(s) and not necessarily those of SAE. The author is solely responsible for the content of the paper. A process is available by which discussions will be printed with the paper if it is published in SAE Transactions.

Persons wishing to submit papers to be considered for presentation or publication by SAE should send the manuscript or a 300 word abstract of a proposed manuscript to: Secretary, Engineering Meetings Board, SAE.

Printed in USA

2008-01-1535

A 50cc Two-Stroke DI Compression Ignition Engine Fuelled by DME

Kim R. Hansen, Claus S. Nielsen, Spencer C. Sorenson and Jesper Schramm
Technical University of Denmark

Copyright © 2008 SAE International

ABSTRACT

The low auto-ignition temperature, rapid evaporation and high cetane number of dimethyl ether (DME) enables the use of low-pressure direct injection in compression ignition engines, thus potentially bringing the cost of the injection system down. This in turn holds the promise of bringing CI efficiency to even the smallest engines.

A 50cc crankcase scavenged two-stroke CI engine was built based on moped parts. The major alterations were a new cylinder head and a 100 bar DI system using a GDI-type injector. Power is limited by carbon monoxide emission but smoke-free operation and $\text{NO}_x < 200\text{ppm}$ is achieved at all points of operation.

INTRODUCTION

The primary emission issues with CI four-stroke engines are particulates and NO_x . These emissions are related in such a way that the final design of such an engine is a trade-off between particulates and NO_x often incorporating some level of external EGR to lower combustion temperatures and thereby reducing NO_x .

Two-stroke engines are interesting in this respect since they have high levels of internal EGR which has also been proven to lower engine-out NO_x . This, combined with the fact that DME does not produce particulates during combustion, opens up an interesting scenario: A small two-stroke CI engine using DME with low fuel consumption, smoke-free operation and low engine-out NO_x .

This paper presents the development effort undertaken at the Technical University of Denmark to build a 50cc crankcase scavenged two-stroke engine with electronically controlled direct injection of DME through a GDI-type injector. Since DME injection is complicated by the low lubricity of DME it was decided to avoid spending

resources on designing a high pressure pump, the primary goal of the work being to evaluate the performance and emissions of a very small DI engine using DME. Therefore DME was supplied to the injector from a stainless steel cylinder which was pressurized to 100 bar with helium. The focus was on achieving satisfactory performance and low NO_x emissions without exhaust gas after treatment.

Cylinder pressure, brake torque and relevant emissions were measured on the engine and heat release analysis was performed in order to evaluate the combustion process. High-speed footage of the injection nozzle operating on DME was used to improve the design of the cylinder head.

DME

For ease of reference and for direct comparison some thermodynamic and physical properties of DME and diesel are listed in Table 1 [Ref. 1].

Table 1 – Selected thermodynamic and physical properties of DME and diesel fuel

| | Unit | DME | Diesel |
|--------------------------|----------------------|---------------------------|-----------------------------|
| Chemical formula | | CH_3OCH_3 | $\text{C}_n\text{H}_{1.8n}$ |
| Molecular weight | [g/mol] | 46 | >100 |
| Lower heating value | [MJ/kg] | 28.8 | 42.5 |
| Saturated liquid density | [kg/m ³] | 668 | 840 |
| Boiling point | [°C] | -24.9 | 180-350 |
| Viscosity at 25°C | [kg/m s] | 0.12 * | 2-4 |
| Vapor pressure at 25°C | [bar] | 5.1 | <0.01 |
| Critical pressure | [atm] | 52 | - |
| Critical temperature | [°C] | 127 | - |

* Sivebaek 2001 [Ref. 2]

TEST ENGINE

The simplest possible two-stroke engine was chosen as a basis for the work: A crankcase scavenged 2-port loop scavenging design with piston controlled inlet port. The specific engine is a carbureted gasoline Puch moped engine of 50cc displacement manufactured in Austria in the seventies and eighties.

Table 2 – Basic geometric properties of the test engine

| | | |
|-----------------------------|-------|-----|
| Bore | [mm] | 38 |
| Stroke | [mm] | 43 |
| Geometric compression ratio | [] | 19 |
| Trapped compression Ratio | [] | ~14 |
| Exhaust port opening angle | [deg] | 138 |
| Transfer port opening angle | [deg] | 104 |
| Inlet port opening angle | [deg] | 101 |
| Inlet port diameter | [mm] | 19 |

DIRECT INJECTION SYSTEM - The design aim was to be able to inject DME at 100 bars. This was believed to be the minimum acceptable pressure level in order to achieve sufficient penetration and mixing with air. Based on an evaluation of the properties of four different possible injectors, a Mitsubishi injector designed for a four cylinder 1.8l GDI engine was chosen - Figure 1.

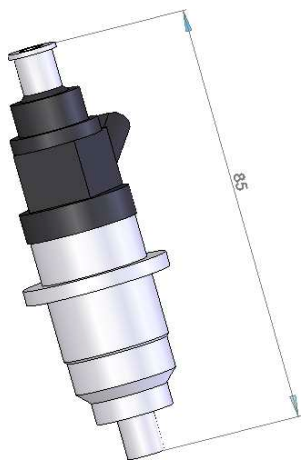


Figure 1 - Mitsubishi GDI injector nozzle

The primary difficulty with the application of this injector turned out to be compatibility issues between internal sealing components and DME. The rubber O-rings applied internally in the injector very quickly dissolved when they were exposed to DME. Figure 2 shows a cross section of the injector nozzle and the placement of the O-rings.

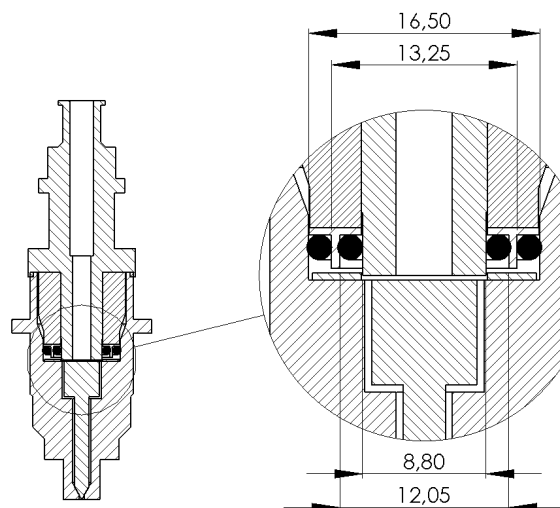


Figure 2 - Cross section of injector nozzle



Figure 3 - Photo of disassembled injector showing O-rings

The solution was a shift to KALREZ® O-rings. These have now been exposed to DME for more than 100 hours without any degradation that has influenced injector operation.

Table 3 – Dimensions and material of the new Kalrez O-rings used in the injector nozzle

| | ID | Dimension | Material |
|--------------|-------|-----------|-------------|
| Inner O-ring | 9,25 | 1.78 | Kalrez 4079 |
| Outer O-ring | 12,42 | 1.78 | Kalrez 4079 |

CYLINDER HEAD - The only change to the mechanical components of the test engine was the replacement of the standard air cooled cylinder head. A new cylinder head with a pronounced squish zone and higher compression ratio was manufactured. The cylinder head was axially symmetric with respect to the cylinder axis and had a squish area ratio of 0.85. The squish ratio is the ratio between the area of the squish zone and the cylinder bore area. The cylinder head is shown in Figure 4.

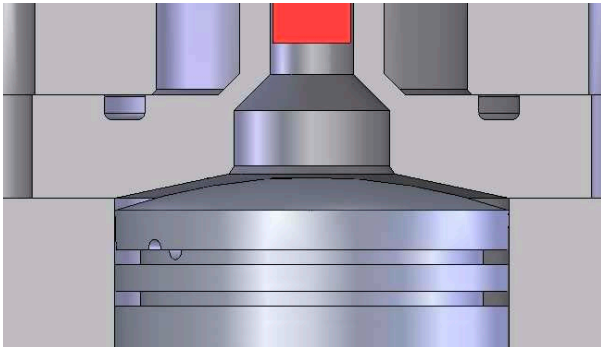


Figure 4 – Cylinder head 1

WATER COOLING - There was some concern that using an air cooled cylinder head would raise the temperature of the injector nozzle to more than 127°C. This is the critical temperature of DME. Injecting a supercritical fluid might give rise to uncontrolled variations in injected fuel mass especially when injection is regulated based on injection duration and not by changing the volumetric displacement of a plunger-type fuel pump. Water cooling was therefore supplied to the cylinder head as shown in Figure 5.

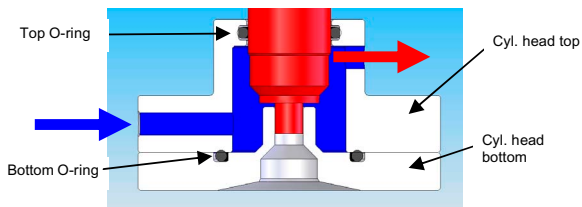


Figure 5 - Cylinder head 1 with water cooling arrangement

SEPARATE OIL INJECTION - Due to the change from carburetion to direct injection it was necessary to apply separate lubrication oil injection. This was achieved by means of a small solenoid type oil injector as used on modern scooters with direct injection of gasoline. The lubricating oil used was Shell Advance Ultra 2. A Synthetic oil.

TEST SETUP AND EQUIPMENT

The DME fuel tank was pressurized to 100 bars using Helium. Injection was controlled by an Atmel ATmega32 microcontroller based on crankshaft encoder signals. A

PID algorithm calculated the appropriate injection duration in order to maintain the specified engine speed independent of engine load. A LENZE MCA14L41 servo motor was used as brake. A Vibro Meter TG 1/B in-line torque transducer was mounted between engine and servo as shown on Figure 6. The servo motor is on the left and the test engine is on the right.

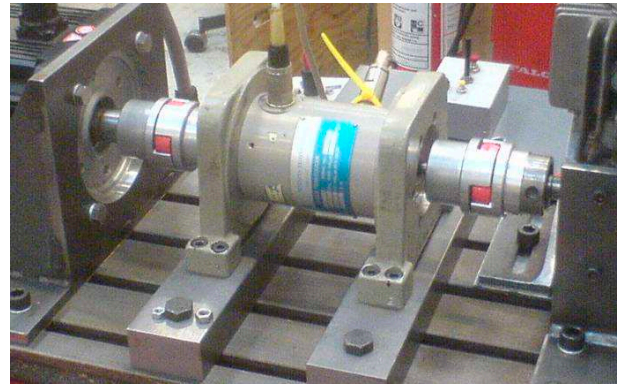


Figure 6 - In-line torque transducer

Static calibration of the torque transducer was performed using lever and weights.

PRESSURE - Cylinder pressure was recorded for every half crank angle degree using a Kistler 6052C piezoelectric pressure sensor. Crankcase and inlet pressures were measured at the same times using a Kistler RAG25A5BV 0 to 5 bar absolute pressure sensor.

TEMPERATURE - Exhaust, inlet and cooling water temperatures were measured using K-type thermo elements with electronic cold junction compensation and two-point calibration in freezing and boiling water respectively.

EMISSIONS - CO, CO₂, HC and O₂ were measured using a Bosch ETT8.55 exhaust gas analyzer. Output validation was done using certified calibration gas with component concentrations close to the expected measured values. NO_x was measured using a Horiba EXSA-240CL gas analyzer and heated pipes. Calibration gas with 101ppm NO₂ was applied to calibrate the instrument. Particulate emissions were not measured. In agreement with previous studies [Ref.³] there was no visible smoke produced from DME combustion. The exhaust pipe was also visually observed to be quite clean despite the addition of two-stroke oil to the engine inlet air.

FUEL - The fuel tank was mounted on a Mettler PE11 precision scale. Fuel and pressurization lines were arranged like opposed torsional springs so that the spring forces due to the small lateral displacements of the scale deck cancelled each other. Precision and repeatability was tested using weights while the fuel tank and lines were fitted and pressurized.

AIR FLOW - Hot wire anemometry in the form of a Honeywell AWM720P1 air flow sensor was employed to measure the air flow into the engine crankcase. In order to avoid reverse flow at the sensor a buffer tank was mounted between the engine inlet and the sensor. Calibration was performed using a Collins 120 liter chain compensated gas flow meter.

INLET AIR FLOW

Inlet air flow is very important, as it has a strong impact on the scavenging process and, therefore, the amount of air available for combustion. This also strongly influences the efficiency of the engine.

The inlet pipe length was chosen so that the optimum delivery ratio " R_d " was at 2000rpm.

$$R_d = \frac{\dot{m}_{air}}{\dot{m}_{air,ideal}} = \frac{\dot{m}_{air}}{\rho_{atm} \cdot V_d \cdot \frac{N}{60}} \quad \text{Eq. 1}$$

Nagao & Shimamoto [Ref.⁴] report, based on experiments with larger crankcase scavenged piston ported two-stroke engines, that the inlet pipe length should be 0.75 times a full inlet pulsation wavelength. This is equivalent to:

$$l_{inlet} = c_{sound} \cdot \tau_{in} \cdot 4 \cdot 0.75 \quad \text{Eq. 2}$$

$$l_{inlet} = 341 \cdot \left(\frac{101}{360} \cdot \frac{60}{2000} \right) \cdot 4 \cdot 0.75 = 0.538m \quad \text{Eq. 3}$$

The inlet pipe length that gave maximum delivery ratio in firing operation at 2000rpm was experimentally found to be 380mm. This is equivalent to 0.65 times a full wavelength. This difference to the observations of Nagao & Shimamoto can be attributed to differences in engine size, the ratio between crankcase volume and engine displacement and other scavenging related parameters compared to the experiments of Nagao & Shimamoto.

In order to better understand and improve the air exchange process, information was gathered from the pressure sensor in the inlet pipe and crankcase. The pressure-time history for one complete crank revolution at 2000rpm is shown in Figure 7. The vertical black lines at approx. 50 deg. before and after TDC indicate the opening and closing of the inlet port by the piston. The standing pressure fluctuations, that occur while the inlet port is closed, are clearly seen. The exponential decay of these fluctuations during the closed port period, from 50 deg. ATDC to -50 deg. ATDC, is also evident. The inlet

port opens just when the standing pressure wave is at its maximum. At the time where the inlet port closes 50 deg. ATDC the crankcase pressure is higher than in the inlet pipe indicating good crankcase filling.

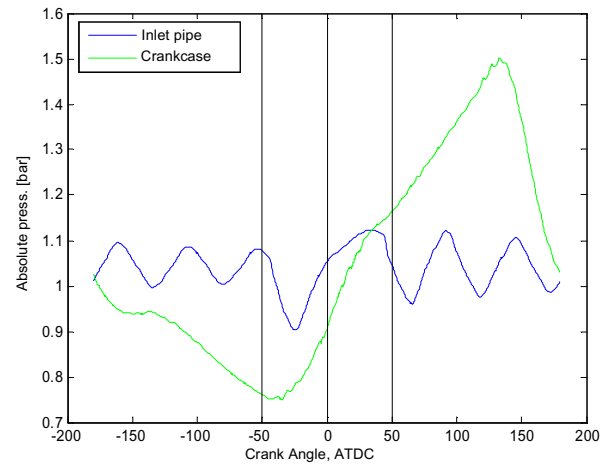


Figure 7 – Inlet and crankcase pressures for one cycle at 2000 rpm

The same parameters are shown in Figure 8 but this time recorded at 4000rpm. The pressure pulsations are larger in amplitude but the sequence of events is less desirable. The pressure in the inlet pipe is not at its maximum when the inlet port opens and the high pressure pulse from the inlet pipe arrives after the inlet port has closed. This gives rise to high pressure at the crankcase end of the inlet pipe just when the inlet port has closed but the pressure in the crankcase is significantly lower indicating poor crankcase filling.

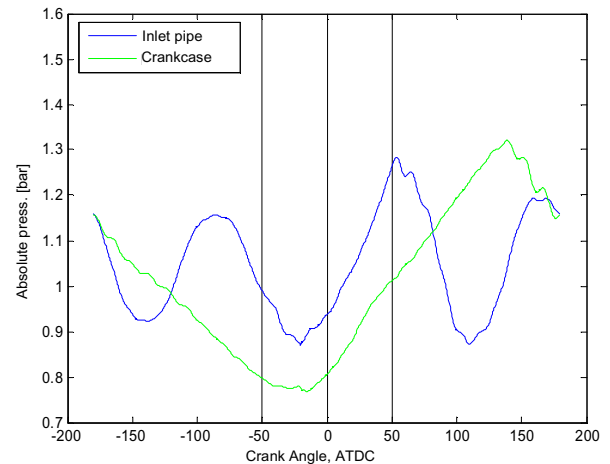


Figure 8 - Inlet and crankcase pressures for one cycle at 4000 rpm

These effects stand out clearly when the delivery ratio as a function of engine speed is plotted in Figure 9.

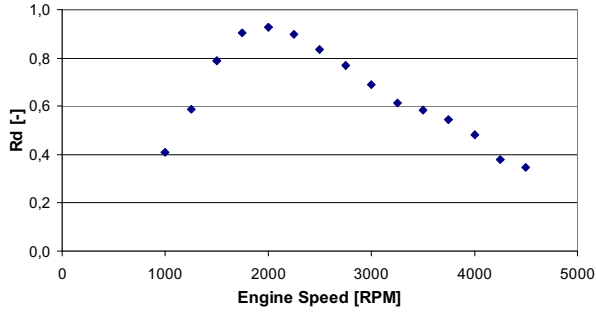


Figure 9 – Delivery ratio as a function of engine speed

The indicated mean effective pressure in the crankcase was also determined. As opposed to a four-stroke engine the pumping losses for a two-stroke engine are proportional to the air flow. Figure 10 shows the pumping work as a function of the delivery ratio for 2000, 3000 and 4000 rpm. The values are shown for three different engine load levels for each engine speed.

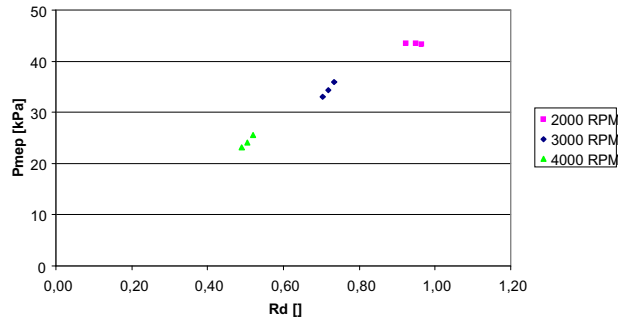


Figure 10 – Pumping mean effective pressure as a function of delivery ratio

This linear relationship, between flow and pumping work, results in reduced pumping losses during part load operation for SI two-strokes. If a throttling mechanism is installed this advantage can also be achieved on a CI engine. This would also increase exhaust gas temperatures during part load operation and thereby improve the performance of an oxidation catalyst in the exhaust if such a device is fitted. There is one drawback though. Throttling may reduce the indicated efficiency of the engine due to the higher fuel/air-ratio during the closed cycle. The positive effect of throttling on pumping losses may not be able to compensate for this. Since, in a two-stroke engine, the exhaust pipe pressure determines the cylinder pressure at the start of compression, throttling is not expected to have a significant negative influence on compression ignition at the time of injection. Throttling has not been tested in this study. The exhaust system was not tuned in this study. It consisted of a 560mm length of pipe with an inner diameter of 22mm.

MOTURING TESTS

High heat losses to the cylinder walls were expected due to the small size of the engine. Cylinder pressure measurements from motoring tests were used to evaluate heat loss since in this case there is no heat release from combustion and a heat release analysis will reveal the instantaneous heat loss during the portion of the cycle when the cylinder ports are closed. A pressure trace from motoring is shown in Figure 11. The vertical black lines indicate opening and closing of scavenging and exhaust ports. All pressure traces shown and used in calculations are the average of 20 consecutive pressure traces.

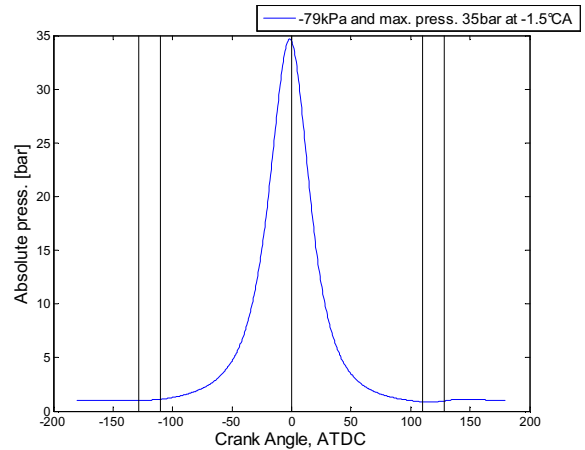


Figure 11 – Cylinder pressure during motoring at 2250rpm

A heat release analysis based on pure air with temperature dependant specific heats was chosen to investigate the combustion process [Ref.⁵]:

$$\dot{Q}_w = \frac{\gamma(T)}{(\gamma(T)-1)} p \frac{dV}{d\theta} + \frac{1}{(\gamma(T)-1)} V \frac{dp}{d\theta} \quad \text{Eq. 4}$$

Results from such a calculation is show in Figure 12 along with the values for heat transfer based on Annand's empirical model for heat transfer in two-stroke engines [Ref.⁶].

$$\frac{\delta Q}{dt} = A \left[a \frac{k}{B} Re^b (T - T_w) + c \sigma (T^4 - T_w^4) \right] \quad \text{Eq. 5}$$

$$Re = \frac{S_p B}{\nu} \quad \text{Eq. 6}$$

$$a = 0,76 \quad b = 0,64 \quad c = 0,54$$

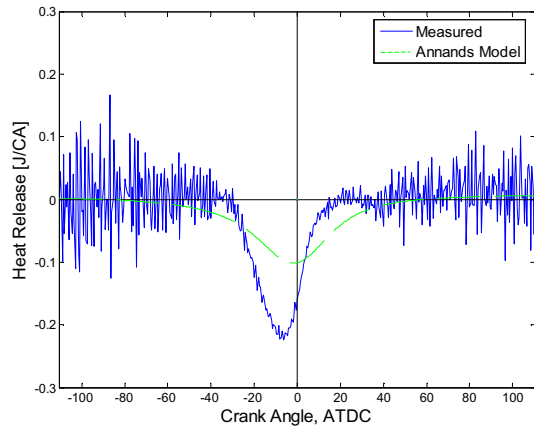


Figure 12 - Heat release analysis for motoring at 2250rpm

There is considerable difference between the measured instantaneous values and the predicted instantaneous values using Annand's expression. The accumulated heat loss for the full cycle on the other hand, shows good agreement between Annand's predictions and the measured values. The methods of Woschni and Eichelberg gives the same shape of the heat transfer curve as Annand but they predict only approx. half of the measured accumulated heat loss. See Table 4.

Table 4 - Measured and predicted accumulated heat loss

| Heat loss based on: | Heat loss expressed as mean effective pressure [kPa] |
|---------------------|--|
| Measurement | 75 - 85 |
| Annand | 79.9 |
| Woschni | 43 |
| Eichelberg | 44.6 |

The heat loss is quite high and this can also be acknowledged by simply looking at a log-log pressure-volume diagram of the motoring cycle. In such a diagram isentropic state changes will be connected by straight lines. Deviations from a straight line are seen especially on the compression stroke near TDC in Figure 13 – in accordance with the heat release analysis shown in Figure 12. A dashed line with an isentropic exponent of 1.35 is plotted on top of the pressure trace to ease interpretation. Again, the vertical black lines indicated opening and closure of transfer and exhaust ports:

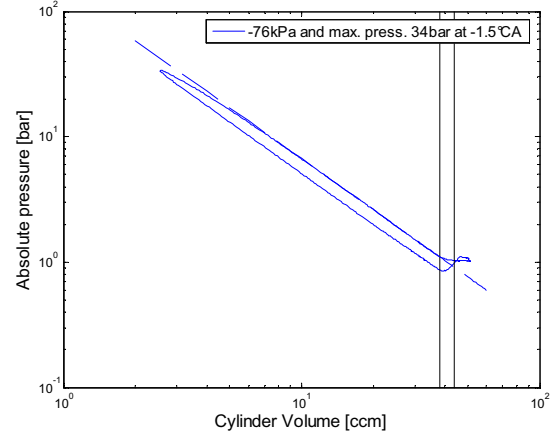


Figure 13 - Log-log pV diagram for motoring at 2250rpm

It is believed that the high heat transfer rates just before TDC on the compression stroke, indicated by the heat release analysis, are due to the very pronounced squish action which is a result of the cylinder head design. The squish area ratio is 85% and the squish clearance is only 0.5mm. Some effort was dedicated to test whether this high heat transfer rate could in fact be a mass transfer to the crankcase due to insufficient sealing between piston and cylinder. Estimates of flow area as a function of crank angle to achieve a flow giving the same effect showed that this was unlikely. This was also in agreement with experiments concerning piston ring design.

To test whether the squish action was actually the cause of the high heat transfer rates a new cylinder head was designed. This cylinder head was the simplest possible. The top edge of the cylinder is connected to the bottom edge of the injector mounting hole by a straight line giving a squish area ratio of 0. The test on this cylinder head gave a reduction in the heat loss of about 15%, indicating that squish induced velocities are at least a part of the explanation for the high heat losses. Cylinder head 2 is shown in Figure 14.

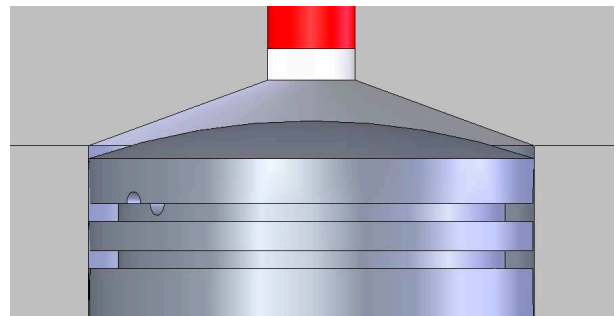


Figure 14 - Cylinder Head 2

Although the squish area ratio for cylinder head 2 is theoretically zero, there is still some squish action. The cylinder head does not have a squish zone incorporated in the design, but nevertheless the cylinder head and the

piston crown are parallel from the cylinder liner and approx. 5mm inwards. This creates a squish zone with an area ratio of 0.45 in praxis. The tests with cylinder head 2 has therefore not tested a zero-squish situation, but merely shown that a reduction in squish action translates directly to lower engines heat losses. The very small squish clearance could be another reason why the measured instantaneous heat transfer rate has a significantly higher peak value than Annand's model predicts. Assuming that the heat transfer boundary layer is larger than 0.25mm, which is the case according to [ref.⁷], the boundary layers on the cylinder head and on the piston crown will merge. This will create a new heat transfer situation that could justify these high heat transfer rates. A reason for the asymmetry of the measured heat transfer rates may lie in the different flow regimes on the compression stroke and expansion stroke. On the compression stroke the squish zone, which represents the largest heat transfer area, is the high pressure zone. On the expansion stroke the squish zone is the low pressure zone. This asymmetry in heat transfer rate is also found using more advanced computational methods like CFD [ref.⁸]. Annand's model does not allow for the consideration of these squish and flow effects and this is considered to be the reason why only the global, and not the instantaneous heat transfer, is comparable to Annand's predictions.

RESULTS FOR FIRING OPERATION

Optimum injection timing was first established for full load at 2000, 3000 and 4000rpm using cylinder head 1. 1% carbon monoxide, by volume, in the exhaust was chosen to define full load. This was difficult to achieve exactly due to the sharp response of CO to added fuel at high loads. The highest CO emission attainable without exceeding 1% was therefore defined as full load. 1% CO also constitutes the CO level that gives the highest brake efficiencies for the engine. Key values are shown in Table 5.

Table 5 - Performance using cylinder head 1

| Engine Speed | [rpm] | 2000 | 3000 | 4000 |
|--------------------------|--------|------|------|------|
| Optimum injection timing | [BTDC] | 8 | 16 | 26 |
| Delivery ratio | [] | 0.92 | 0.73 | 0.52 |
| Imep | [kPa] | 372 | 319 | 217 |
| Indicated efficiency | [] | 0.27 | 0.27 | 0.26 |
| Fmep | [kPa] | 101 | 97 | 82 |
| Brake efficiency | [] | 0.20 | 0.19 | 0.16 |
| CO emission | [%] | 0.80 | 0.89 | 0.97 |
| HC emission | [ppm] | 112 | 123 | 115 |
| NO _x emission | [ppm] | 40 | 57 | 65 |

The HC emission values shown may not be accurate since the infrared measurement method has not been verified for DME.

NO_x measurements of three different load levels and the three different engine speeds gave nine NO_x values for a variety of overall excess air ratios. Overall excess air ratio meaning the excess air ratio based on engine inlet air flow and fuel flow. The excess air ratio during combustion is significantly lower due to the loss of scavenging air to the exhaust.

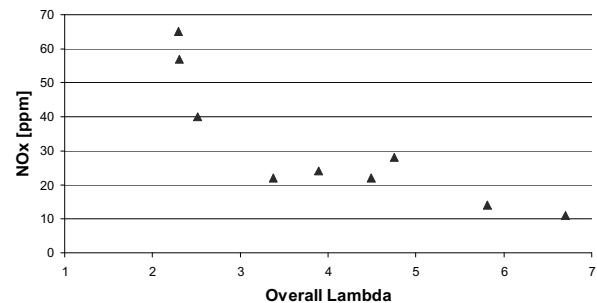


Figure 15 – NO_x emissions as a function of air/fuel ratio

The trend is as expected. Low excess air ratios give rise to increasing NO_x formation. The overall NO_x emission level is very low. This confirms one of the initial premises for this study: A two-stroke engine operating on DME should be able to achieve low NO_x emissions. That the NO_x emissions are as low as they are, indicate that it is not only a result of the high residual gas fractions inherent in the two-stroke principle. The analysis of the combustion process reveals another possible reason for the low NO_x levels.

COMBUSTION – The same heat release analysis based on pure air with temperature dependant specific heats, which was used for motoring, was chosen to investigate the combustion process. Heat transfer to the cylinder walls was based on Annand's expression that had shown the best agreement with motoring results.

$$\dot{Q}_{HR} = \frac{\gamma(T)}{(\gamma(T)-1)} p \frac{dV}{d\theta} + \frac{1}{(\gamma(T)-1)} V \frac{dp}{d\theta} - \dot{Q}_w \quad \text{Eq. 7}$$

To be able to determine the mean bulk gas temperature during the closed cycle it is necessary to specify the initial temperature of the cylinder contents at the start of compression. This was done using the measurements of delivery ratio as input to the scavenging model proposed by Blair [Ref.⁹]. The scavenging efficiency according to Blair is plotted as a function of engine speed along with the delivery ratio in Figure 16, both on a mass basis.

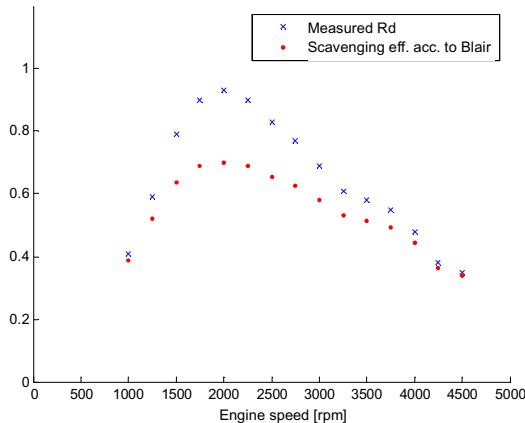


Figure 16 - Delivery ratio and scavenging eff. acc. to Blair

The scavenging efficiency expresses the ratio between the fresh air charge supplied from the transfer ports and trapped in the cylinder, and the total gas mass trapped in the cylinder. Knowing the charge air temperature and the exhaust gas temperature of the engine, it is then possible to calculate the mass averaged gas temperature at the start of compression, T_1 . The results are shown in Figure 17.

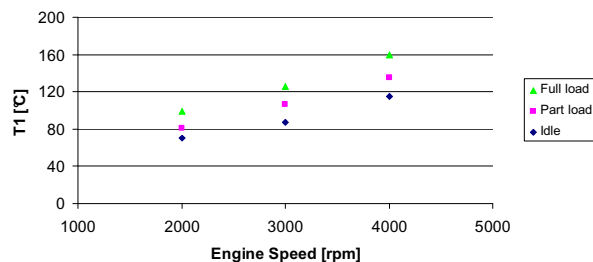


Figure 17 – Estimated gas temperature at the start of compression as a function of engine speed and load

The cylinder pressure, while the engine was operating at full load and 2000rpm using cylinder head 1, are shown in Figure 18.

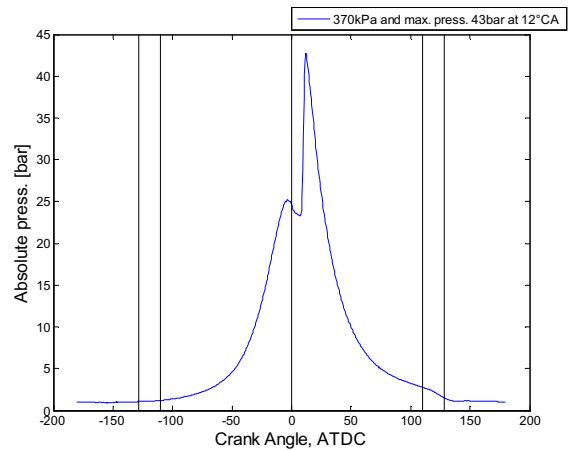


Figure 18 - Cylinder pressure - full load @ 2000rpm

The heat release curves obtained from analysis of this cylinder pressure curve is shown in Figure 19.

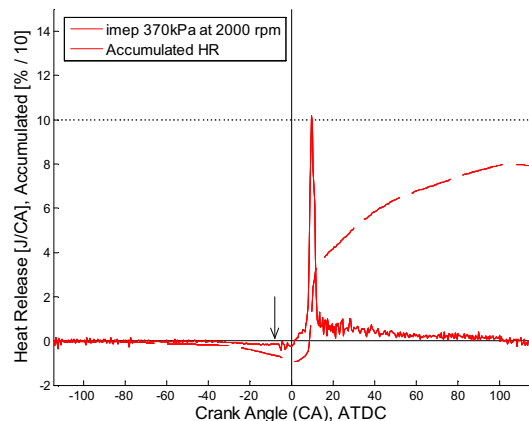


Figure 19 – Instantaneous and accumulated heat release – full load @ 2000rpm

The black arrow indicates start of injection. Because the injection nozzle is actually too large for this cylinder size injection is completed very quickly: 3 to 4 deg. CA at full load. Looking at Figure 19 it is clear that injection is completed before any positive heat release is registered.

Heat release starts approx. at TDC. At around 10 ATDC there is a sharp rise in the heat release rate. At the completion of this heat release peak approx. 50% of the fuel has burned. This occurs within 5 deg. CA. The remaining part of the fuel burns slowly and heat release is first completely over at 100 ATDC. The final accumulated heat released is 79% of the fuel lower heating value. 6% appears as carbon monoxide in the exhaust gas. The remaining 15% are due to higher heat loss than Annand's method predicts. This higher heat loss is believed to be a result of the rapid pressure rise around 10 ATDC. The last half of the combustion process is very different from normal diesel combustion. Figure 20 shows a schematic representation of the

combustion in a naturally aspirated DI engine compared to the DME engine of this study.

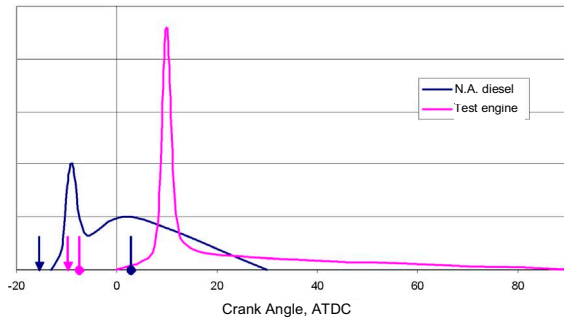


Figure 20 - Heat release for typical diesel combustion compared to the test engine

The vertical arrows pointing down indicate the start of fuel injection and the vertical pins with bullet bottoms indicate end of injection. In the case of the DME engine all of the fuel is injected within 4 deg. CA. This indicates that the very high heat release rate at the start of combustion is a result of premixed combustion. An ignition delay of approx. 10 deg. CA allows for 50% of the heat to be released shortly after the time of ignition. It is not known at which equivalence ratios this occurs. This produces the characteristic heat release peak observed. The remaining 50% of the heat release occurs slowly over the rest of the expansion stroke. According to Dec. [Ref.¹⁰] this last half of the combustion process is likely diffusion flame combustion.

According to Dec NO_x formation occurs in the diffusion flame and not during premixed combustion. Only in diffusion flames are the temperatures high enough for NO_x to form. Although this has been established based on observations of normal diesel combustion processes it may be a fact that the initial premixed combustion with high heat release rates does not produce any significant NO_x due to the excess of air that keeps temperatures down. During the last half of combustion the temperatures may be too low to form NO_x , since this occurs some way down into the expansion stroke, even though it proceeds as diffusion combustion. Assuming this explanation holds true the conditions for high rates of NO_x formation are never met and this results in the very low NO_x emissions that are observed. An uncertainty in this argument is the value of the equivalence ratios during the "premixed" combustion.

At 3000rpm, even though the indicated work is lower and the heat release peak is not so high, the same basic pattern exists. 50% of the heat is released during 5 deg CA. Heat release continues slowly until ending at approx. 100 deg. ATDC. The cylinder pressure and heat release analysis are shown in Figure 21 and Figure 22 respectively.

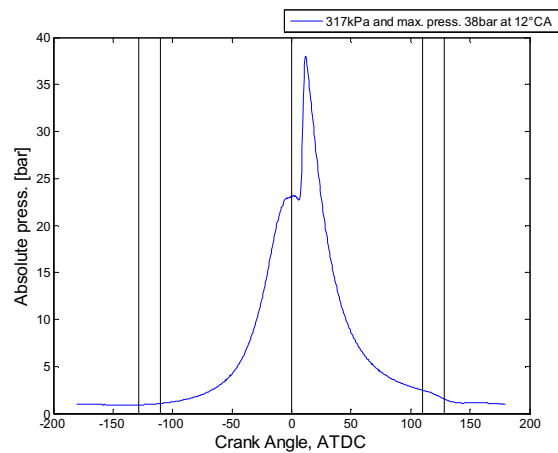


Figure 21 - Cylinder pressure - full load @ 3000rpm

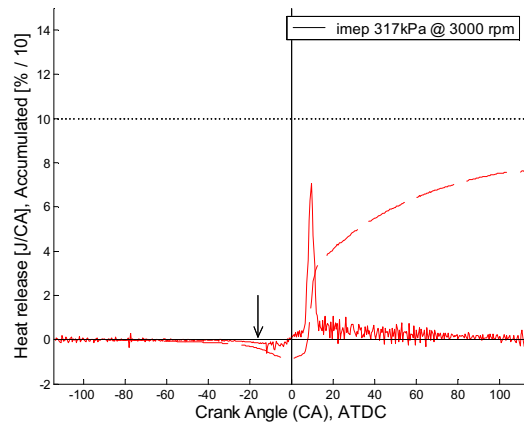


Figure 22 - Instantaneous and accumulated heat release – full load @ 3000rpm

At 4000rpm the only significant difference is that the peak has moved closer to TDC. The cylinder pressure and heat release analysis are shown in Figure 23 and Figure 24 respectively.

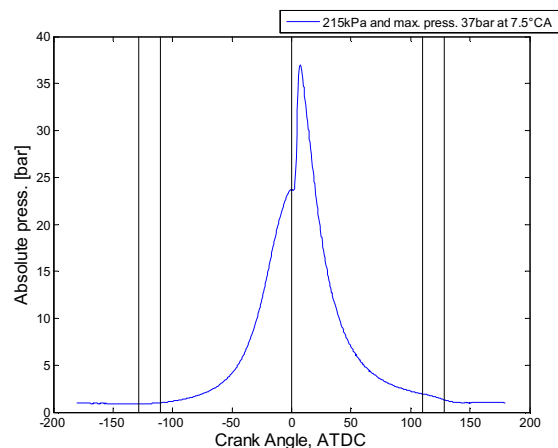


Figure 23 - Cylinder pressure - full load @ 4000rpm

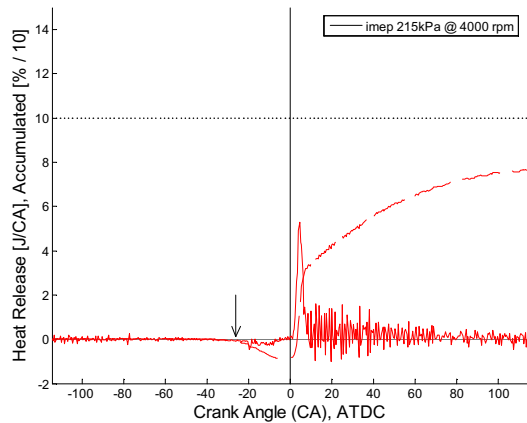


Figure 24 - Instantaneous and accumulated heat release – full load @ 4000rpm

Based on the heat release analysis a simple empirical heat release function was formulated for simulation purposes – see Figure 25. The function consists of three straight line segments. The area under the curve is equal to unity and half of that is within the peak that has a duration of 5 deg. CA.

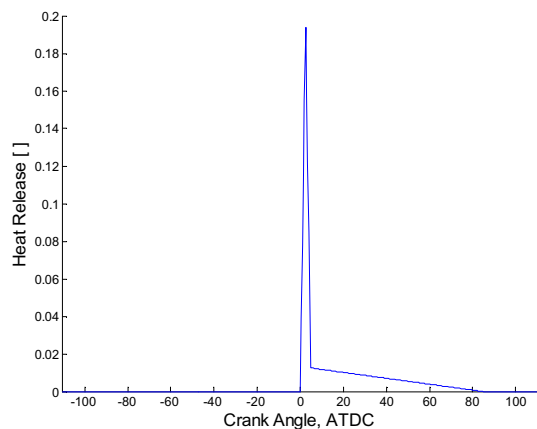


Figure 25 - Simplified heat release function

The modest indicated efficiency, shown in Table 5, is partly due to the high heat losses. Another reason is the slow heat release during the expansion stroke. A large portion of the heat is released at a significantly lower expansion ratio than is desirable. This equates directly to reduced indicated efficiency. Using a suitable simulation model it can be shown that a sinusoidal heat release function that starts at TDC and lasts 30 deg. CA has an approx. 5 percentage point's higher indicated efficiency than what is modeled using the heat release function shown in Figure 25 (assuming Annand heat loss). Thus, without reducing the heat losses, an indicated efficiency of 32% instead of 27% should be achievable if better control could be exercised over the heat release rate. A smaller injection nozzle is probably the key to this, though pilot injection could also be considered.

INJECTOR SPRAY PATTERN

The first cylinder head design, cylinder head 1, was based on qualified guesses. The high heat losses identified while analyzing motoring tests resulted in the design of cylinder head 2. Cylinder head 2 was designed to reduce squish velocities and thereby heat transfer rates to the cylinder walls. Until this point a very important piece of information was not available for the design of the cylinder head: The injector spray pattern while operating on DME.

HIGH SPEED PHOTOGRAPHY - The setup shown on Figure 26 was used to shoot digital backscatter images of the injector during operation. The equipment allowed a recording speed of 100.000 frames per second with a resolution of 128x80 pixels. The camera was triggered by the same output pin on the microcontroller which was used to trigger the injector.

The injection nozzle was mounted vertically in a pressure chamber with glass side walls that was pressurized with nitrogen to 11 bars at ambient temperature. In this way the gas density in the chamber was similar to the gas densities prevalent in the combustion chamber around TDC.

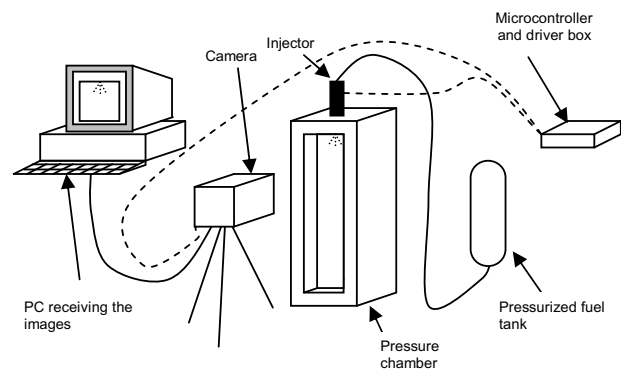


Figure 26 - High speed photography setup

The images in Figure 27 show the visible spray penetration after the injector has been activated electrically for 200, 300 and 500 μ s respectively. The circular collar surrounding the injector tip in the top of the images is 14mm in diameter. The visible spray had a spray angle of 45 deg.

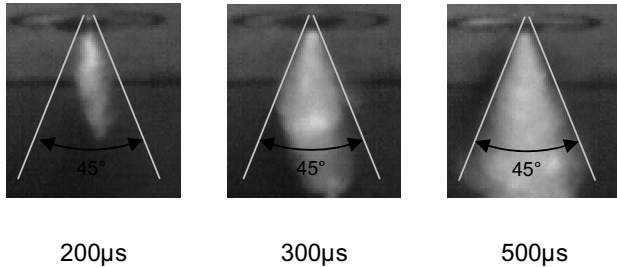


Figure 27 - Visible injector spray pattern

GAS PENETRATION - The images were also used to determine the speed and distance traveled of the visible spray. The distance traveled within short range of the injector can be expressed as:

$$S_{short} = C_{short} \cdot U_b \cdot t = C_{short} \cdot \sqrt{2 \frac{p_l - p_a}{\rho_l}} \cdot t \quad \text{Eq. 8}$$

According to Naber & Siebers [Ref.¹¹] the empirical constant for C_{short} should be 0.39. The results based on this calculation and the measured values obtained from the images are plotted in Figure 28. At time zero the injector is electrically actuated. It was found from the pictures that the mechanical delay is 300 μ s. The calculation of S_{short} therefore starts at 300 μ s. The measured and calculated values stop at 14mm's. This is because the tip of the visible spray at that point extends beyond the photographed area.

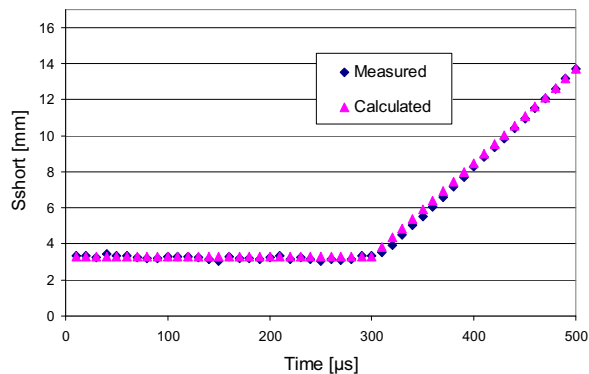


Figure 28 - Measured and calculated spray penetration

Very good agreement with Naber & Siemens is observed.

CYLINDER HEAD DESIGN

The information gathered from the high speed footage was used to design the third cylinder head. Several contradictory requirements must be met: Achieving the required trapped compression ratio (13 to 15), avoiding spraying excessive amounts of liquid fuel directly onto the piston and keeping squish velocities low to avoid high heat losses while still maintaining enough squish action to mix fuel and air fast enough. The end result is shown in Figure 29. Cylinder head 3 had a squish area ratio of 0.6 and a minimum distance from injector to piston of 11.3mm.

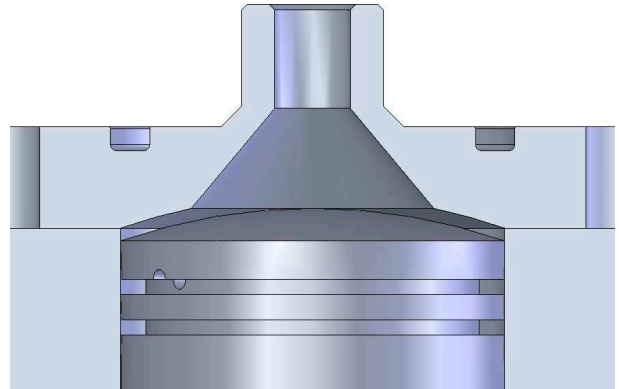


Figure 29 - Cylinder Head 3

The heat release rates for all three tested cylinder heads at full load and 3000rpm are shown in Figure 22, Figure 31 and Figure 33.

The equivalent cylinder pressure diagrams are shown in Figure 21, Figure 30 and Figure 32.

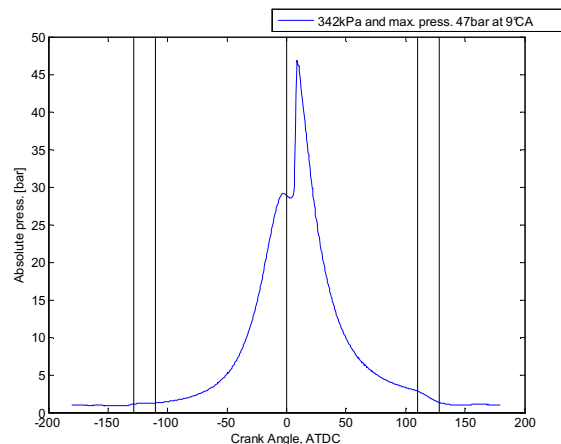


Figure 30 - Cylinder pressure - full load @ 3000rpm - cylinder head 2

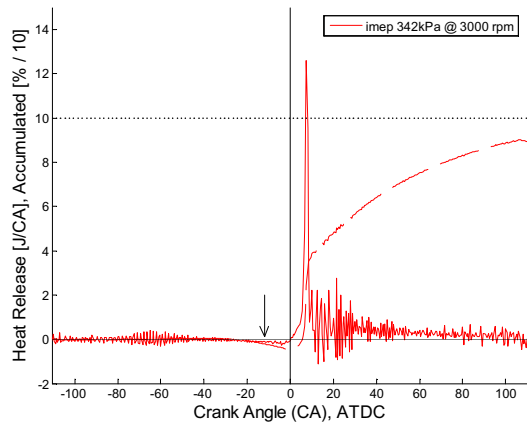


Figure 31 - Instantaneous and accumulated heat release – full load @ 3000rpm – Cylinder Head 2

The heat release peak for cylinder head 2 is higher than for cylinder head 1 and this could be the reason for the noisier combustion observed after the heat release peak. The accumulated heat released, using Annand's expression for heat transfer to the cylinder walls, accounts for 89% of the fuel energy. Of the remaining 11%, 7% is lost to the exhaust as carbon monoxide.

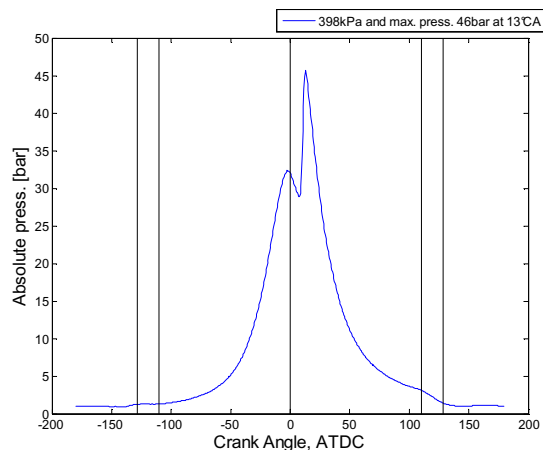


Figure 32 - Cylinder pressure - full load @ 4000rpm - cylinder head 3

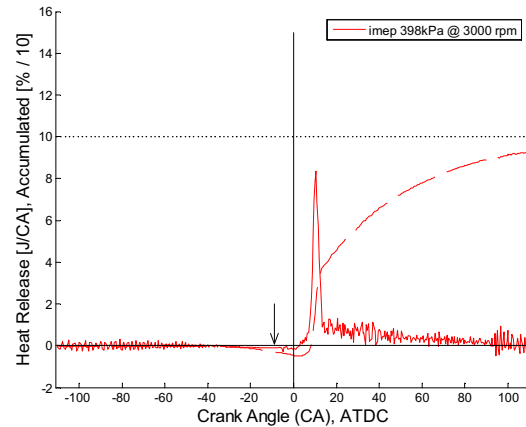


Figure 33 - Instantaneous and accumulated heat release – full load @ 3000rpm – Cylinder Head 3

Cylinder head 3 had the same overall heat release pattern as the other cylinder heads tested but allowed higher power output without producing excessive amounts of CO. Table 6 shows the performance of the three cylinder heads at 3000rpm.

Table 6 – Performance for three different cylinder heads

| Cylinder Head | | 1* | 2 | 3 | 3** |
|--------------------------|--------|------|------|------|------|
| Optimum injection timing | [BTDC] | 16 | 12 | 9 | 10 |
| Imep | [kPa] | 319 | 342 | 398 | 410 |
| Indicated efficiency | [] | 0.27 | 0.28 | 0.29 | 0.29 |
| Fmep | [kPa] | 97 | 120 | 127 | 101 |
| Brake efficiency | [] | 0.19 | 0.18 | 0.20 | 0.22 |
| CO emission | [%] | 0.89 | 0.80 | 0.82 | 0.97 |
| HC emission | [ppm] | 123 | 310 | 220 | 190 |
| NO _x emission | [ppm] | 57 | 18 | 48 | 25 |

* A different but similar cylinder was used in this test due to mechanical problems.

** Same configuration as "3" but at 2000rpm.

CONCLUSION

A 50cc crankcase scavenged piston ported engine with direct injection of DME at 100 bars was developed and tested.

Best performance at this very early stage of development was a bmep of 309 kPa at 2000rpm. Total efficiency at this point of operation was 22%. Soot free operation with $\text{NO}_x < 200\text{ppm}$ was achieved at all points of operation.

High heat losses at the end of compression were identified. Although Annand's heat transfer correlation agrees with measured values for global heat transfer during motoring, the instantaneous values differ significantly from the measured heat transfer values based on heat release analysis of motoring operation.

A Mitsubishi automotive type GDI injection nozzle was used to inject DME directly into the combustion chamber. As expected, the standard O-rings in the injector were not compatible with DME. They were replaced with Kalrez O-rings that performed successfully.

Heat release analysis showed a distinct pattern for all engine speeds at full load operation. The heat released from combustion is divided into two equal portions: A "premixed" phase which is very rapid and a "diffusion" phase which is quite slow. Heat release has only just finished at the time the exhaust port opens. This type of heat release combined with the high heat losses observed during motoring operation is believed to be the cause of the modest indicated efficiency ranging from 27 to 29%.

Simulation indicates that reducing the heat release duration to about 30 deg. CA would increase the indicated efficiency by about 5 percentage points assuming the same heat loss model.

Photographs of the injector spray while operating on DME were taken at room temperature. The visible spray penetration fits very well with the correlation of Naber & Siebers. The spray angle was 45 deg.

Combustion was improved by altering the squish zone and the shape of the combustion chamber in accordance with the photographs of the injector spray. These changes mainly allowed for higher indicated power but did not change the overall pattern of heat release as it is outlined above.

ACKNOWLEDGMENTS

The authors would like to acknowledge the assistance of MAN Diesel A/S and Doctor Bjarke Skovgård Dam in obtaining the photographs of the injector spray. The contributions of many members of the mechanical staff at the institute are also greatly appreciated.

DEFINITIONS, ACRONYMS, ABBREVIATIONS

A: Area [m^2]

ATDC: After Top Dead Center [deg.]

B: Cylinder bore [mm]

CA: Crank Angle [deg.]

CI: Compression Ignition

c_{sound} : Local speed of sound [m/s]

C_{short} : Empirical nozzle coefficient

DI: Direct Injection

EGR: Exhaust Gas Recirculation

GDI: Gasoline Direct Injection

HC: Hydrocarbons

ID: Inner diameter [mm]

k: Heat conductivity [J/K m]

l_{inlet} : Inlet pipe length [m]

m: Mass [kg]

N: Engine speed [rpm]

NO_x : Oxides of nitrogen

p: Pressure [Pa]

p_l : Liquid pressure [Pa]

p_a : Atmospheric pressure [Pa]

Q_{HR} : Heat released by combustion [J/CA]

Q_w : Heat transfer on cylinder walls [J/CA]

R_D : Delivery Ratio []

S_p : Mean piston speed [m/s]

SR: Squish Ratio []

T: Temperature [K]

t: Time [s]

T_i: Temperature at the start of compression [C]

TDC: Top Dead Center

T_w: Cylinder wall temperature

U_b: Speed of spray acc. to Bernoulli

V: Cylinder volume [m³]

V_D: Cylinder volume swept by piston [m³]

: Ratio of the specific heats of air

: Liquid density [kg/m³]

_{in}: Inlet port opening time [s]

: Crank Angle [deg.]

⁷ Heywood, J. B., "Internal Combustion Engine Fundamentals", McGraw-Hill, 1988.

⁸ Wu, H. W., Perng, S. W., "Numerical analysis of thermal turbulent flow in the bowl-in-piston combustion chamber of a motored engine", International Journal of Thermal Sciences, Vol. 43 Issue 10, 1011-1023, Editions Scientifiques Medicales Elsevier, 23 Rue Linois, Paris, France, 2004.

⁹ Blair, G. P., Design and Simulation of Two-Stroke Engines, SAE, 1996.

¹⁰ Dec, J. E., "A Conceptual Model of DI Diesel Combustion Based on Laser Sheet Imaging", SAE 970873, 1997.

¹¹ Naber, J. D., Siebers, D. L., "Effects of Gas Density and Vaporization on Penetration and Dispersion of Diesel Sprays", 960034, SAE, 1996.

REFERENCES

¹ Sorenson, S. C., Glensvig, M. and Abata, D. L., "Dimethyl Ether in Diesel Fuel Injection Systems", 981159, SAE, 1998.

² Sivebaek, I.M., Sorenson, S. C., Jakobsen, J., "Dimethyl Ether (DME) – Assessment of Viscosity Using the New Volatile Fuel Viscometer (VFVM)", SAE, 2001-01-2013, 2001.

³ Sorenson, S. C., Mikkelsen, S., "Performance and Emissions of a 0.273 Liter Direct Injection Diesel Engine Fuelled with Neat Dimethyl Ether", 950064, SAE, 1995.

⁴ Nagao, F., Shimamoto, Y., "The Effect of Crankcase Volume and the Inlet System on the Delivery Ratio of Two-Stroke Cycle Engines", SAE, 690136, 1969.

⁵ Hayes, T. K., Savage, L. D., Sorenson, S. C., "Cylinder Pressure Data Acquisition and Heat Release Analysis on a Personal Computer", SAE, 860029, 1986.

⁶ Annand, W. J. D., "Heat Transfer in the Cylinders of Reciprocating Internal Combustion Engines", Proceedings of the Institution of Mechanical Engineers, vol. 177 issue 36, 973-996, Institution of Mechanical Engineers, 1963.

Optimizing the Performance of a 50cc Compression Ignition Two-Stroke Engine Operating on Dimethyl Ether

2011-01-0144

Published
04/12/2011

Kim R. Hansen, Jakob D. Dolriis, Christoffer Hansson, Claus S. Nielsen, Spencer C. Sorenson
and Jesper Schramm
Technical Univ. of Denmark

Copyright © 2011 SAE International

doi:[10.4271/2011-01-0144](https://doi.org/10.4271/2011-01-0144)

ABSTRACT

The paper describes the optimization of a 50cc crankcase scavenged two-stroke diesel engine operating on dimethyl ether (DME). The optimization is primarily done with respect to engine efficiency. The underlying idea behind the work is that the low weight, low internal friction and low engine-out NO_x of such an engine could make it ideal for future vehicles operating on second generation biofuels.

Data is presented for the performance and emissions at the current state of development of the engine. Brake efficiencies above 30% were obtained despite the small size of the engine. In addition, efficiencies near the maximum were found over a wide operating range of speeds and loads. Maximum bmep is 500kPa. Results are shown for engine speeds ranging from 2000 to 5000 rpm and loads from idle to full load. At all speeds and loads NO_x emissions are below 200 ppm and smokeless operation is achieved.

Design improvements relative to an earlier prototype are described. The major alterations are related to air intake arrangement, exhaust tuning and the fuel injector. Comparison is made to the first prototype engine and the effects of fuel injection rate, injection pressure, cylinder head geometry and injection timing are evaluated at selected engine operating conditions.

Cylinder pressure, crankcase pressure and rate of heat release were determined. The engine uses an oversize fuel injector so that fuel delivery happens within a few crank angle degrees. Since DME is very volatile a large degree of premixing occurs before auto-ignition of the fuel. This results in

approximately 65% of the fuel being burnt rapidly in the premixed phase of combustion. The engine mode of operation can be characterized as premixed compression ignition (PCI).

INTRODUCTION

Most studies of the application of DME in internal combustion engines have focused on DME as a substitute for diesel in conventional diesel engines, typically with cylinder displacements larger than 500cc. In these studies DME is injected at relatively high pressures, typically 200 to 1500 bar. The results have been near-zero soot emissions, equal or slightly lower NO_x emissions than with diesel fuel and high wear rates in the fuel injection system [1, 2, 3, 4, 5].

This study was performed as a part of ongoing research work at the Technical University of Denmark where an attempt is made to rethink the compression ignition engine so as to fully exploit the chemical and physical properties of DME and to find applications where these properties give special advantages. Motivating the use of DME in the first place is the very high field-to-wheel efficiency that can be attained using DME, produced by gasification of biomass, in a vehicle with a diesel engine [6, 7, 8, 9].

An earlier publication on the subject [10] describes the engine concept chosen and the first engine test results obtained with an engine built accordingly. The engine was a 50cc piston ported crankcase scavenged two-stroke engine. It employed direct injection of DME through a GDI type electronic injector at 100 bar. Fuel line pressure was maintained by pressurization of the fuel tank with helium.

Deciding on a two-stroke engine in the first place was based on the line of thought illustrated in [Figure 1](#):

| Decision matrix | Four-stroke | Two-stroke |
|-----------------|----------------------|----------------------------|
| Diesel | High NO _x | Low NO _x |
| DME | Low NO _x | Very low NO _x ? |

Figure 1. Engine concept decision matrix

The reason why lower NO_x emissions were expected from a two-stroke engine concept was that the larger amount of residual gas dilutes the trapped cylinder charge. This can reduce the flame temperature and hence the potential for NO_x formation [11,12]. Since high pressure injection nozzles are not available for 50cc engines the injectors used are from automotive engines. This means that the fuel is injected within a few crank angle degrees. This is the case for both the first concept engine and the second engine which is described in this paper. For both engines the short injection period is followed by an ignition delay with a typical duration of 0.5 ms which is equivalent to 10 CAD at 4000 rpm. If the premixing that occurs before ignition is effective, this method of operation would lead to low NO_x emissions as long as the global air/fuel-ratio is high, due to the low resulting combustion temperatures.

The first engine design proved that it is easy to achieve smooth operation with a DI two-stroke engine operating on DME. The engine was tested at engine speeds ranging from 500 to 6000 rpm. The lower limit given by excessive heat losses that prevented compression ignition and the upper limit given by a limitation in the dynamometer used.

But engine torque was somewhat disappointing reaching a maximum bmep of only 309 kPa at 2000 rpm. Despite the low bmep, engine brake efficiency peaked at 22%, a value that is comparable to fuel injected gasoline two-stroke engines of the same size. That this was possible despite the low engine torque and accompanying modest mechanical efficiency is attributed to the higher compression ratios employed and the resulting higher indicated efficiencies as compared to SI operation. Geometric and trapped compression ratios were 19 and 14 respectively. No particulate measurements were taken but no visible smoke was observed regardless of engine load. NO_x emissions were below 200 ppm at all speeds and loads.

The reason for the disappointing power output was found to be a combination of three factors. Poor scavenging, poor mixture formation and high closed cycle heat losses.

SCAVENGING

Intake

The fixed geometry of the piston ported air intake arrangement in the original engine design only gave acceptable air flow in a narrow engine speed range and the maximum delivery ratio was measured to be 0.92. In the present study it was decided to change to a reed valve intake arrangement in order to widen the effective speed range of the engine and also increase the maximum delivery ratio.

Transfer Passages

The cylinder of the earlier engine had two scavenge ports having an area of 216 mm². Increasing the area and thereby lowering the maximum flow speed of the air jets entering the cylinder through the transfer passages can reduce short circuiting to the exhaust port and hence increase the trapping efficiency. It was therefore decided to change to a cylinder with a larger transfer port area.

Exhaust System

Tuned expansion chamber exhaust systems are used to great effect on SI two-stroke engines to improve scavenging. The first engine did not have a tuned exhaust system but simply a straight cylindrical exhaust pipe. It was decided to devote some effort in this study to experiment with an exhaust system inspired by SI two-stroke engine designs.

MIXTURE FORMATION AND CLOSED CYCLE HEAT LOSS

These two phenomena represent a trade-off relationship. Closed cycle heat loss can be reduced by reducing forced flow due to the piston movement relative to the cylinder head, the so called squish flows. Unfortunately, this will adversely affect the rate at which fuel and air are mixed and thereby the heat release rate. The optimal design will be the compromise that best suits the requirements of the engine application. One way to circumvent this trade-off relationship is to improve mixing by better matching the injector nozzle spray pattern to the combustion chamber geometry and air flow. Some progress in that respect has been achieved on the second engine by using a 7-hole injector instead of the single hole conical spray injector that was used on the first engine.

ENGINE DESIGN CHANGES

The second engine was built based on crankshaft, conrod, piston and an air-cooled cylinder from a 50cc Peugeot two-stroke SI scooter engine. The remaining parts were custom built based on the experience from the first engine. The primary mechanical changes introduced in order to improve the performance relative to the first engine are listed in [Table 1](#).

Table 1. Main parameters for the 1st and 2nd engine designs

| Feature | Unit | 1st | 2nd |
|-----------------------|--------------------|------------|-------------------|
| Bore | [mm] | 38 | 40 |
| Stroke | [mm] | 43 | 39.1 |
| Displ. | [ccm] | 48.8 | 49.1 |
| CR geo. | [-] | 19 | 22 |
| CR eff. | [-] | 14 | 16 |
| Squish ratio | [-] | 0.60 | 0.60 |
| Inlet port opening | CAD BTDC | 50 | Reed valve |
| Exhaust port opening | CAD ATDC | 111 | 109 |
| Transfer port opening | CAD ATDC | 129 | 132 |
| Transfer port area | [mm ²] | 216 | 372 |
| Fuel injector | [-] | Mitsubishi | Bosch |
| Fuel injector holes | [no.] | 1 | 7 |
| Exhaust | [-] | Cyl. pipe | Expansion chamber |

The compression ratio of the new engine was increased to improve cold starting. The new engine maintains the use of a solenoid activated plunger pump to supply lubricating oil to the air intake in the crankcase. It is beyond the scope of a paper to give all the details of the development work that went into the second version of this engine concept. The paper primarily lists the differences between the old and the new design and some of the results of the testing of the new engine design are presented and discussed.

METHODS

The engine was mounted on a dynamometer and the performance was characterized by measuring the parameters listed in [Table 8](#). A picture of the engine test setup is shown in [Figure 30](#).

For most of the tests, fuel rail pressure was provided by pressurization of the fuel tank with helium. However, a fuel pump that could supply up to 150 bar was designed and provided fuel rail pressure for some of the tests. The details of the fuel pump design and testing are not included in this paper. SAE J1088, the SAE recommended practice for utility engines less than 20 kW, has been followed when measuring the gaseous emissions.

DATA LOGGING

Data acquisition was performed using the CompactRio hardware platform and Labview software from National

Instruments. Cylinder and crankcase pressures were logged at intervals of 0.5 crank angle degrees. This high speed part of the data logging was programmed on the field programmable gate array (FPGA) available on the CompactRio platform.

The exhaust gas sample probe was manufactured according to SAE J1088 and was mounted in the center section of the expansion chamber exhaust. Immediately after the probe the sample passes through a glass fiber filter which was heated to 185 deg. C. From here the sample is led through a heated line to the gas analyzer.

TEST PROCEDURE

Tests were performed as steady state tests with engine load controlled by the dynamometer and engine speed governed by an engine control unit (ECU) developed on a PIC microcontroller for this purpose. The ECU regulated fuel injection duration on the basis of a PID algorithm with a manually chosen speed setting.

Unless otherwise stated, the fuel injection timing was chosen manually for every operating point so that the fuel injection duration, as regulated by the ECU in the manner just described, was at its minimum value. The purpose of this procedure was to find the injection timing giving highest engine efficiency. The idea was that the injected fuel mass should monotonically increase with increasing fuel injection duration. Fuel consumption was measured on a precision scale as the fuel mass consumed during five minutes of operation. The emission measurements presented are the averages of the emissions during at least two minutes during this period.

RESULTS AND DISCUSSION

More than 500 steady state tests of five minute duration were performed during the development period. Experiments with fuel injection rate, injection pressure, cylinder head geometry, injection timing and exhaust system design resulted in an engine that had significantly improved performance compared to the first engine. The results presented here are the performance and emissions of this design.

EXPANSION CHAMBER EXHAUST

Since the air flow through an engine to a large degree determines the engine performance, the first results presented are those for the tuning of the exhaust system. The expansion chamber exhaust systems typically used on SI two-stroke engines have a significant effect on their air flow. The change to a reed valve intake arrangement was expected to significantly increase air flow in itself, but the action of the tuned exhaust system and the reed valve is closely coupled and the results given below are for the combination of the reed valve and the exhaust system.

A custom made expansion chamber exhaust system inspired by the types used on two-stroke SI engines was tested. The purpose of such a system is to exploit the pressure wave created by the opening of the exhaust port. The pressure-time history in the engine cylinder during the scavenging period should be beneficial in terms of drawing in fresh air through the transfer passages while they are open and trapping that air in the cylinder at the time when the exhaust port closes. The goal is to increase the trapped mass of fresh charge. A principal sketch of such a tuned exhaust system is shown in [Figure 31](#).

The function of the down pipe and diffuser is to create a properly timed low pressure period in the cylinder that helps draw up fresh charge through the transfer passages. The effectiveness of the complete process leading to fresh charge flow into the engine is measured in terms of the delivery ratio:

$$R_d = \frac{\dot{m}_{air}}{\dot{m}_{air,ideal}} = \frac{\dot{m}_{air}}{\rho_{atm} \cdot V_d \cdot \frac{N}{60}} \quad (1)$$

The function of the nozzle is to act as a closed end and the initial pressure wave formed at exhaust port opening is reflected by the nozzle as a compression wave. This returning compression wave forces a portion of the fresh charge lost to the exhaust system back into the engine cylinder before exhaust port closure thereby increasing the trapping efficiency of the engine:

$$\eta_{tr} = \frac{\dot{m}_{air,trapped}}{\dot{m}_{air}} \quad (2)$$

The product of the delivery ratio and the trapping efficiency defines the charging efficiency of the engine, which is the mass of fresh charge available per cycle relative to the mass obtained by filling the engine displacement with air at ambient conditions:

$$\eta_{ch} = R_d \cdot \eta_{tr} = \frac{\dot{m}_{air,trapped}}{\dot{m}_{air,ideal}} \quad (3)$$

The ultimate goal is to achieve the highest possible charging efficiency so that as much fuel as possible can be burned effectively. This will enable high specific engine output and a high mechanical efficiency of the engine.

Expansion Chamber on a CI Engine

Whether an expansion chamber exhaust system would have such a significant positive effect on charging efficiency on a

CI two-stroke engine as it has on an SI two-stroke engine was uncertain for a number of reasons. In the case of an SI engine, which is not direct injected, the fresh charge will also contain fuel. Therefore, increasing the trapping efficiency of an SI two-stroke engine with a tuned expansion chamber exhaust will reduce the loss of unburnt fuel to the exhaust and hence increase both the power and the efficiency of the engine. In the case of a CI engine the fresh charge consists of only air and no fuel can be regained from the exhaust system. An increase in trapping efficiency will increase the mass of air available for combustion which, for the same global fuel-air ratio, will increase engine power but no efficiency increase due to a reduction of fuel short circuit will occur. There will be a secondary effect on efficiency though. For a given engine load the increase in excess air ratio due to an increase in trapping efficiency will serve to increase the indicated efficiency due to a higher specific heat ratio of the trapped charge. The greater indicated work produced in this way will also increase the mechanical efficiency.

A number of other factors contribute to the uncertainty regarding the effectiveness of an expansion chamber exhaust system on a CI engine. A CI engine burns fuel at a global fuel air ratio significantly leaner than stoichiometric. It also employs a compression ratio approximately twice as high as an equivalent gasoline engine. Both of these differences, relative to a gasoline engine, lower the cylinder pressure at exhaust port opening and hence lowers the potential for a strong pressure wave front to be created.

Due to these differences it was unclear if the increase in trapped air mass within the engine cylinder would be large enough to defend the added bulk and complexity of an expansion chamber exhaust system. It was also not possible to rely on the empirical design guidance that could be found in the literature for SI two-stroke engines. The expansion chamber exhaust system was therefore designed such that most geometric parameters could be changed easily.

Downpipe and Diffuser

Three different down pipe lengths and both a 2- and a 3-stage diffuser were tested. The effect of the different combinations of down pipes and diffusers was measured in terms of engine air flow. The result for the best combination is shown in [Figure 2](#).

It is clear that a properly tuned down pipe and diffuser combination does have a positive effect on engine air flow in the engine speed range it is tuned to work at but the improvement of about 15% is only approximately half of that typically achieved with SI engines of the same size and at the same engine speed [13]. [Table 2](#) summarizes the results.

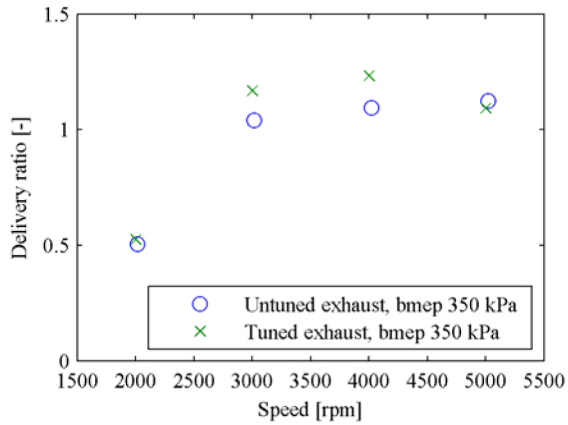


Figure 2. Engine air flow with and without tuned exhaust system

Table 2. Effect of intake arrangement and exhaust system on maximum delivery ratio.

| Intake | Exhaust | R_d |
|---------------|-------------------|-------|
| Piston ported | Cylindrical pipe | 0.92 |
| Reed valve | Cylindrical pipe | 1.04 |
| Reed valve | Expansion Chamber | 1.22 |

The increase in maximum delivery ratio from 0.92 to 1.22 was accompanied by a reduction in pumping work. Expressed in mean effective pressure the pumping work reduced from 44 to 18 kPa. This is testament to a significant improvement in pumping efficiency. The PV-loops for the two engines at maximum delivery ratio, 0.92 and 1.22 respectively, are plotted in Figure 3. A contributing factor to the lower pumping work was that the crankcase volume of the second engine was larger than that of the first engine.

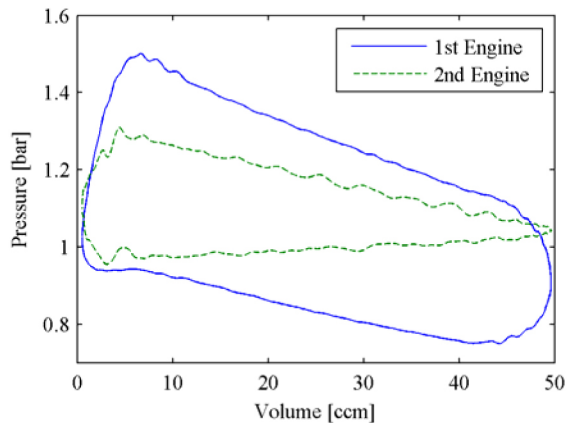


Figure 3. Crankcase PV-loops for the first and the second engine

In itself, an increased delivery ratio does not guarantee that a larger mass of air is retained in the cylinder at exhaust port closure. The increased air flow must be matched by an ability to trap that air in the engine cylinder. This ability is improved by the reflection of the compression wave at the nozzle.

Nozzle

The tuned length (L_t) of the exhaust system which is the distance from the exhaust port to the center of the nozzle was made continuously variable from 1 to 2 meters and adjustment was possible while the engine was running. The rod on the lower right corner of Figure 32 is the adjustment rod for that purpose.

The tuned length of the exhaust system determines the time at which the positive pressure wave returns to the engine cylinder. In the case of a CI two-stroke it is not possible to determine the actual trapping efficiency based on oxygen content in the exhaust gas as it is done on SI engines. The oxygen in the exhaust gas stream is not only a result of short circuiting air from the transfer passages into the exhaust but also excess air from combustion. Instead the carbon monoxide emission was observed and used as an indicator for trapping efficiency. For each down pipe and diffuser combination the tuned length was adjusted while the engine was running at constant load and constant speed. The tuned length setting that gave the minimum carbon monoxide emission at an intermediate engine speed was chosen as the optimum tuned length. The expansion chamber design chosen for the rest of the engine testing had the specifications listed in Table 3.

Table 3. Expansion chamber exhaust dimensions.

| Parameter | Units | Value |
|-----------------------------------|------------|---------|
| Down pipe ID and length | [mm, mm] | 22, 420 |
| Diffuser stage 1 length and angle | [mm, deg.] | 180, 4 |
| Diffuser stage 2 length and angle | [mm, deg.] | 80, 8 |
| Center section ID | [mm] | 70 |
| Nozzle | [mm, deg.] | 150, 10 |
| Stinger ID & length | [mm, mm] | 13, 200 |
| Tuned length (L_t) | [mm] | 1570 |

COMPARISON TO THE FIRST ENGINE

Comparison of the first and second engine was done at equal fuelling levels and with similar axisymmetric combustion chamber geometry. Injection timing was chosen as described earlier. The engines ran at 3000 rpm and with a fuel input energy equivalent to a fuel mean effective pressure (fume_p) of 1370 kPa. Cylinder pressure, accumulated heat release and average cylinder gas temperature is shown in Figure 4, Figure 5 and Figure 6 respectively. The differences between the first and second engines were outlined in Table 1.

The major difference between the first and the second engine is the increase in the heat released from the premixed phase of combustion. The first engine releases approx. 50 percent of the total heat release in the premixed phase of combustion. For the second engine this value is approx. 65 percent. This is believed primarily to be a result of an increase in trapped air mass and increased mixing of fuel and air due to the change of injector. Key values are summarized in Table 4.

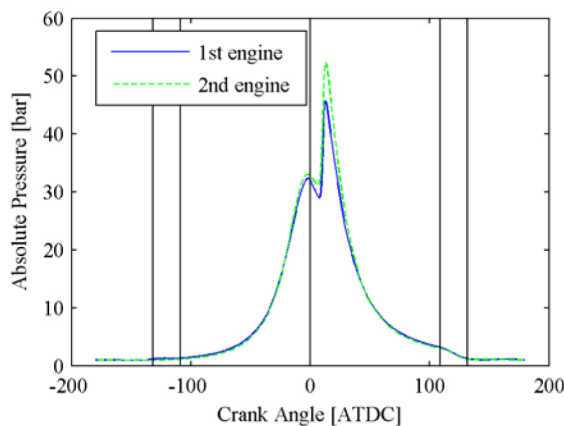


Figure 4. Cylinder Pressure for equivalent fuel input and cylinder head geometry

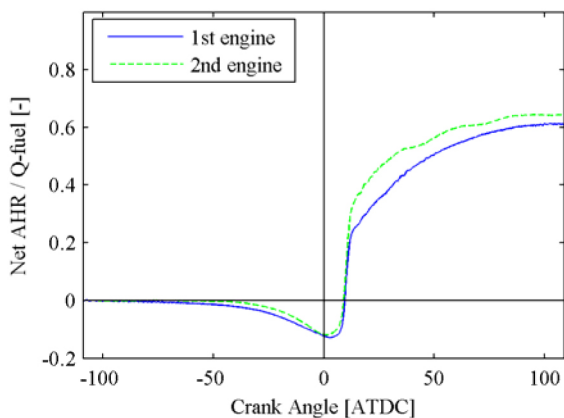


Figure 5. Accumulated heat release for equivalent fuel input and cylinder head geometry.

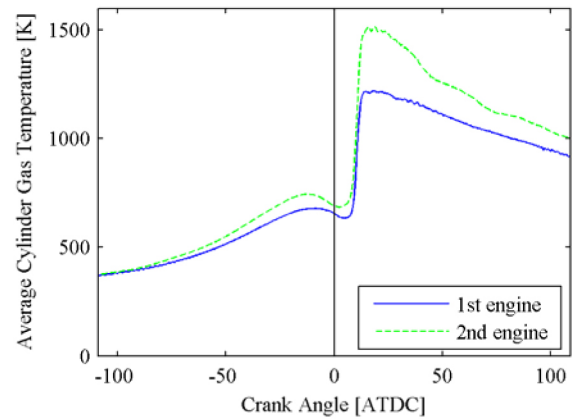


Figure 6. Average cylinder gas temperature for equivalent fuel input and cylinder head geometry

Table 4. Performance comparison for similar cylinder head geometry. Constant engine fuelling.

| | | 1st engine | 2nd engine |
|-------------------|-------|------------|------------|
| Injection press. | [bar] | 100 | 100 |
| Engine speed | [rpm] | 3000 | 3000 |
| Fume _p | [kPa] | 1370 | 1371 |
| Imep | [kPa] | 398 | 444 |
| Indicated eff. | [%] | 29.1 | 32.4 |

The indicated efficiency increased by 11 percent. Since the new engine has a larger fraction of nearly constant volume combustion and the combustion timing is unchanged, an increase in efficiency is also expected: A larger fraction of the total heat released experiences a larger expansion before exhaust opening and blow-down commences.

The premixed phase of combustion is more dominant compared to traditional diesel combustion [14]. The fuel injectors are both standard injectors from direct injected automotive gasoline engines. They were designed for a cylinder volume of approx. 500cc. Even though the density and mass specific lower heating value of DME are lower than for gasoline the injectors flow too much fuel for normal diesel operation in the 50cc test engine. Fuel delivery is completed within 2 to 8 crank angle degrees depending on engine load and speed. This, and the properties of DME, is the main reason for the high degree of premixed combustion.

Both engines exhibit a slow mixing controlled combustion phase following the premixed combustion. The mixing controlled combustion continues until approx. 90 CAD ATDC. This very slow combustion is not desired and reduces both the power and the efficiency of the engines. More development is needed in order to match injector and combustion chamber so that combustion is completed earlier. From this point and onwards all test results given are for the

second engine, with better scavenging, reed valves, tuned exhaust and the Bosch injection nozzle.

EFFECT OF INCREASED INJECTION PERIOD

It was decided to test what effect the short fuel delivery time had on engine performance by increasing the injection period. Ideally this should be done by reducing the size of the individual fuel injector holes but the type of injector used could not be delivered with smaller holes and reducing the hole size of the existing injector would be a very delicate job if at all possible. Instead the reduction of the injector flow rate was achieved by blocking 6 out of the 7 holes in the fuel injector. The result in terms of cylinder pressure, accumulated heat release and average cylinder gas temperature is shown in Figure 7, Figure 8 and Figure 9 respectively.

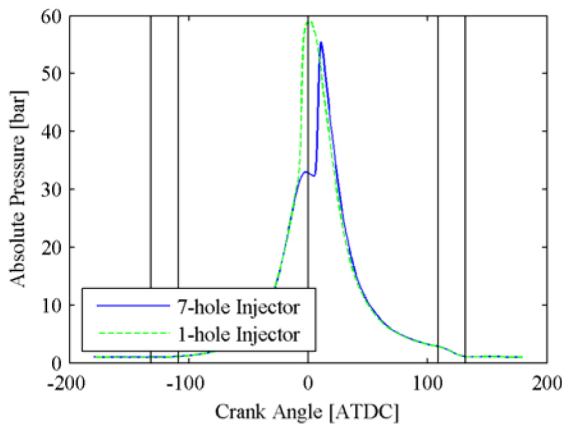


Figure 7. Effect of blocking 6 out of 7 injector holes on cylinder pressure. Injection timing set at maximum engine efficiency in each case.

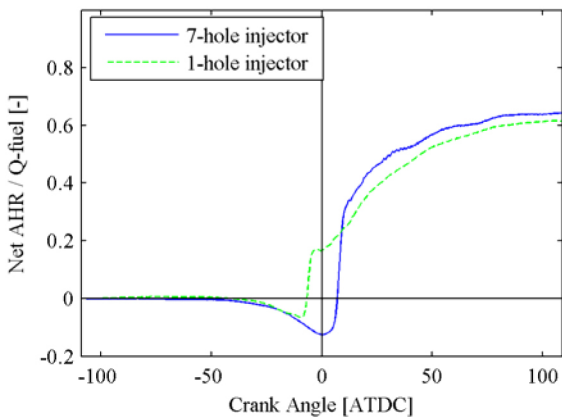


Figure 8. Effect of blocking 6 out of 7 injector holes on accumulated heat release. Injection timing set at maximum engine efficiency in each case.

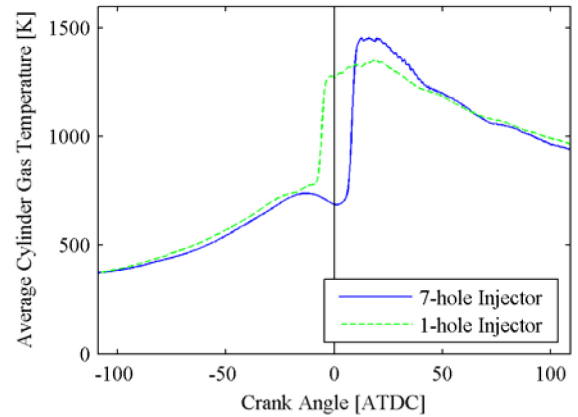


Figure 9. Effect of blocking 6 out of 7 injector holes on bulk gas average temperature. Injection timing set at maximum efficiency in each case.

The desired effect was achieved. The fuel injection period was increased from 4 to 37 crank angle degrees. The result is that there is less fuel available for combustion at the time of ignition and the premixed part of the heat release is therefore smaller. This is true even though the first portion of the fuel injected in the 1-hole case has significantly more time available for evaporation and mixing with air before the onset of combustion. This suggests that the reduction of the spray angle for the 1-hole injector is not compensated for by the longer time available for mixing. The sequence of events is shown in Figure 10.

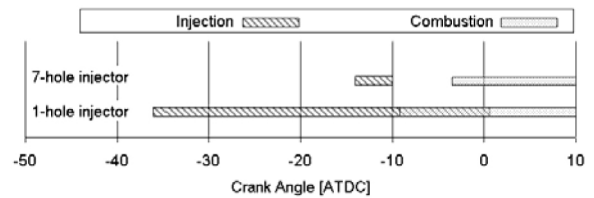


Figure 10. Timing of injection and combustion for the 7-hole and the 1-hole injector

The total net heat release is also lower for the 1-hole injector case. A contributing factor to this is the higher heat loss associated with the longer time at elevated gas temperatures in the combustion chamber for the 1-hole injector case. Both the smaller fraction of premixed combustion and the higher heat losses contribute to the lower indicated efficiency for the 1-hole injector as stated in Table 5.

Table 5. Comparison of performance for 7-hole and 1-hole injector. Constant engine fuelling.

| | | 7-hole inj. | 1-hole inj. |
|------------------|-------|-------------|-------------|
| Injection press. | [bar] | 100 | 100 |
| Engine speed | [rpm] | 3000 | 3000 |
| Fumep | [kPa] | 1280 | 1291 |
| Imep | [kPa] | 421 | 378 |
| Indicated eff. | [%] | 32.8 | 29.3 |

From this point and onwards all results are for the unmodified 7-hole Bosch injector.

EFFECT OF FUEL RAIL PRESSURE

The first engine used an injector that could not open at pressures higher than 110 bar. The injector for the second engine was operable up to 200 bar and experiments with higher injection pressures were therefore possible. Cylinder pressure and derived results for the second engine using 100 and 150 bar fuel rail pressure are shown in Figure 11, Figure 12 and Figure 13 respectively.

The effect of increasing the injection pressure from 100 to 150 bar is slightly higher premixed heat release resulting in a small increase in indicated efficiency as shown in Table 6. Increasing the pressure further did not show any performance improvement.

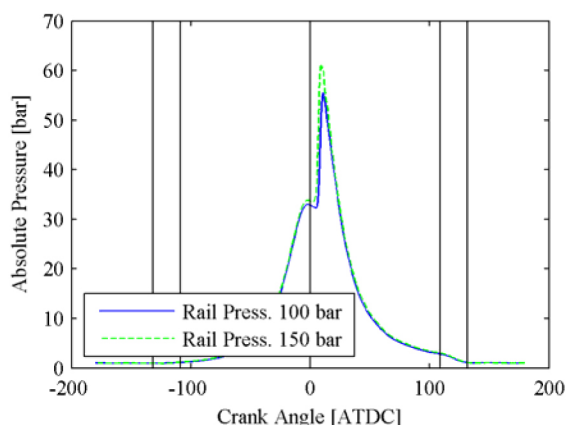


Figure 11. Effect of fuel rail pressure on cylinder pressure.

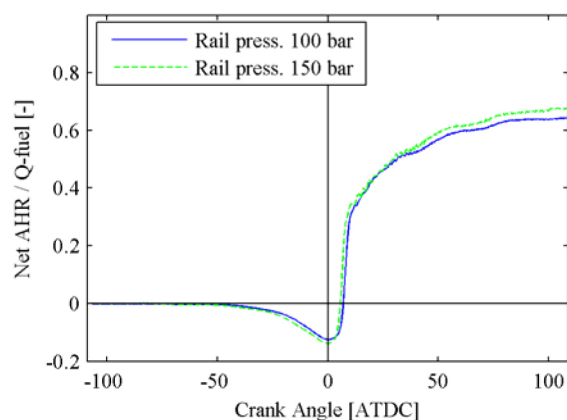


Figure 12. Effect of fuel rail pressure on accumulated heat release.

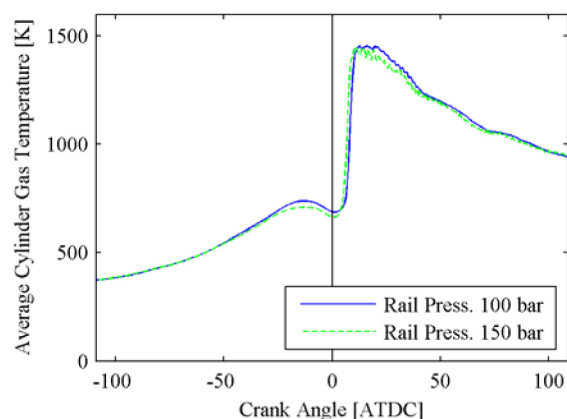


Figure 13. Effect of fuel rail pressure on average cylinder gas temperature.

Table 6. Performance comparison for different injection pressures. Constant engine fuelling.

| Injection press. | [bar] | 100 | 150 |
|------------------|-------|------|------|
| Engine speed | [rpm] | 3000 | 3000 |
| Fumep | [kPa] | 1280 | 1296 |
| Imep | [kPa] | 421 | 446 |
| Indicated eff. | [%] | 32.8 | 34.4 |

EFFECT OF ASYMMETRIC COMBUSTION CHAMBER GEOMETRY

To this point, a simple axisymmetric combustion chamber geometry was used. See Figure 14.



Figure 14. Axisymmetric cylinder head

Axisymmetric combustion chambers are typically used in four-stroke engines with inlet induced swirling flow around the cylinder axis [14]. The flow in a loop scavenged two-stroke engine is different. The arrangement of the transfer and exhaust ports give rise to a tumbling flow that has an axis perpendicular to the cylinder axis. See Figure 15.

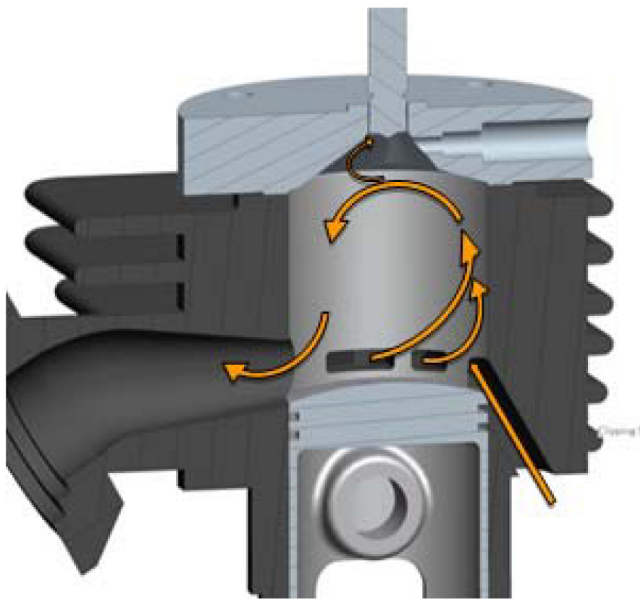


Figure 15. Tumbling flow in a loop scavenged engine. The picture shows the test engine with an asymmetric cylinder head mounted.

Since in-cylinder airflow is beneficial for the mixing of fuel and air it was decided to design and test cylinder heads that potentially could maintain or even accelerate the initial tumbling flow. Several different cylinder heads were manufactured and tested and the most successful of these is shown in Figure 16.

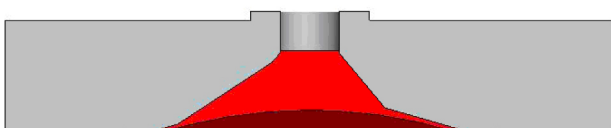


Figure 16. Asymmetric cylinder head.

The geometry between the fuel injector and the piston top was modified such that the squish zone on the left hand side of Figure 14 is eliminated and squish only occurs on the right

hand side as shown in Figure 16. The test results for the asymmetric cylinder head shown in Figure 16 are compared to those for the symmetric cylinder head in Figure 17 and Figure 18 at constant brake torque.

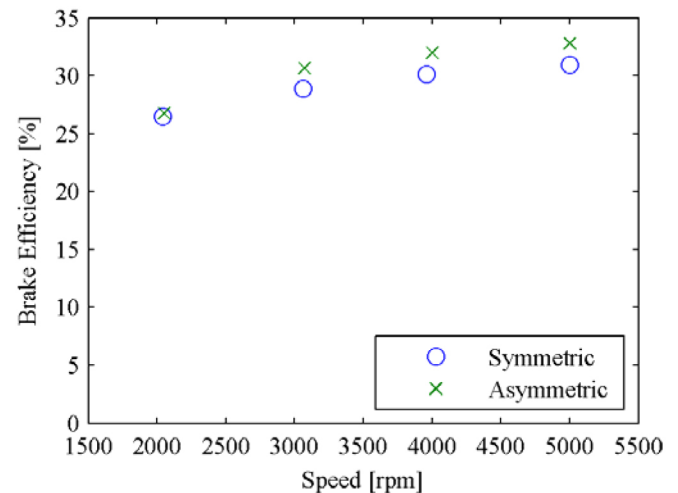


Figure 17. Comparison of brake efficiencies for symmetric and asymmetric cylinder heads. Bmep 350 kPa.

Except at 2000 rpm the engine brake efficiency is better with the asymmetric cylinder head. Injection timing was set for best engine efficiency in all cases. The tests at 3000 rpm are chosen for further comparison because they have the exact same injection timing.

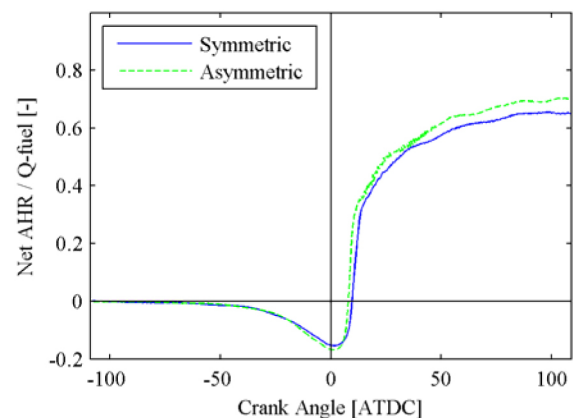


Figure 18. Comparison of net apparent heat release for symmetric and asymmetric cylinder heads. 3000 rpm and 350 kPa. Start of fuel injection at 12 deg. BTDC.

Figure 18 shows that before TDC the heat loss is slightly larger for the asymmetric cylinder head. This could be caused by higher flow speeds due to the asymmetric shape of the cylinder head. After auto ignition and premixed combustion the slow mixing controlled burn is more rapid and more complete in the case of the asymmetric cylinder head. This is

also evidenced by the emission levels for the two cases as can be seen from Table 7.

Table 7. Emissions and indicated efficiency for symmetric and asymmetric cylinder head.

| | | Symmetric | Asymmetric |
|----------------------|---------|-----------|------------|
| CO | [% vol] | 0.34 | 0.25 |
| HC | [ppm] | 135 | 88 |
| Indicated efficiency | [%] | 33.9 | 36.8 |

EFFECT OF TIMING VARIATION ON NO_x

Late injection is a widely used method in CI engine operation to reduce NO_x emissions. In an engine operating on diesel fuel, the ensuing lower combustion temperatures unfortunately also lead to increased soot emissions. In this way there exists a trade-off relationship between NO_x and soot. Replacing diesel with a non-sooting fuel like DME circumvents this trade-off relationship and it is therefore of particular interest to investigate the effect of late injection on an engine operating on DME. Figure 19 shows the results for an operating point close to maximum engine efficiency.

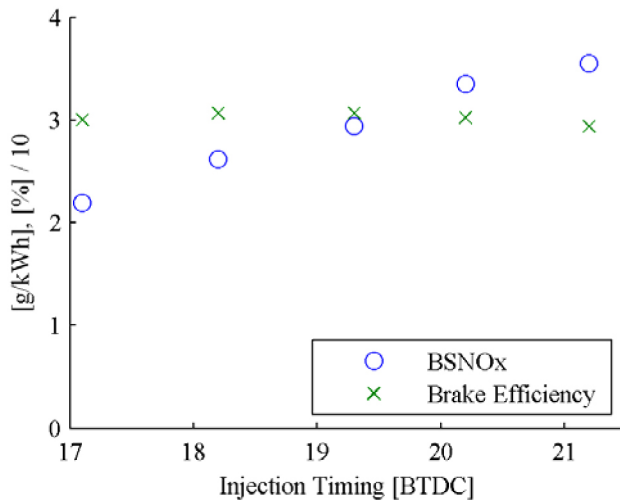


Figure 19. Brake specific NO_x and engine brake efficiency as a function of injection timing. 4000 rpm and 350 kPa bmep.

The range of injection timings tested may seem narrow but represents the operable range. Operation at more advanced injection timings result in knocking combustion and operation at more retarded injection timings result in misfires. The expected trend in NO_x emission was confirmed. Brake specific NO_x emissions are reduced as a function of

retardation of the injection timing. There is only a small variation in engine efficiency within the operable injection timing range but the in-cylinder conditions for the earliest and latest injection timings are quite different. This is illustrated by the cylinder pressure data for these two conditions shown in Figure 20, Figure 21 and Figure 22 respectively.

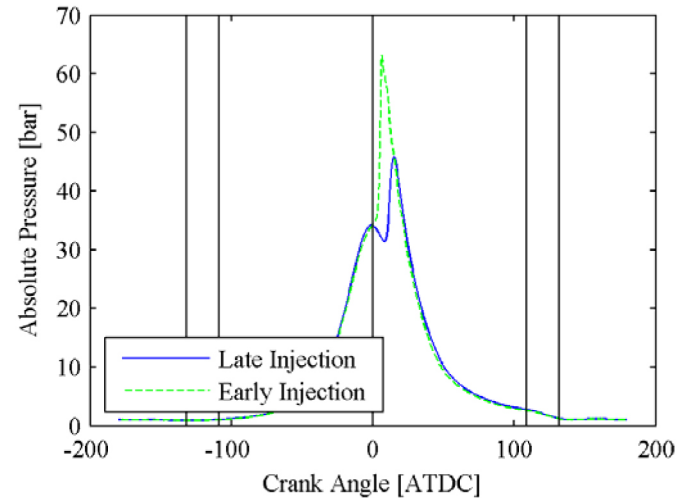


Figure 20. Cylinder pressure for start of injection at 21 and 17 degrees BTDC, shown in green and blue respectively. 4000 rpm and 350 kPa bmep.

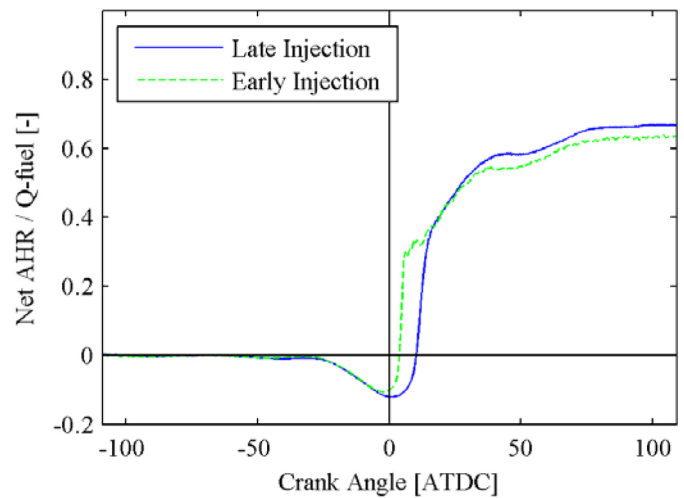


Figure 21. Accumulated heat release for start of injection at 21 and 17 degrees BTDC, shown in green and blue respectively. 4000 rpm and 350 kPa bmep.

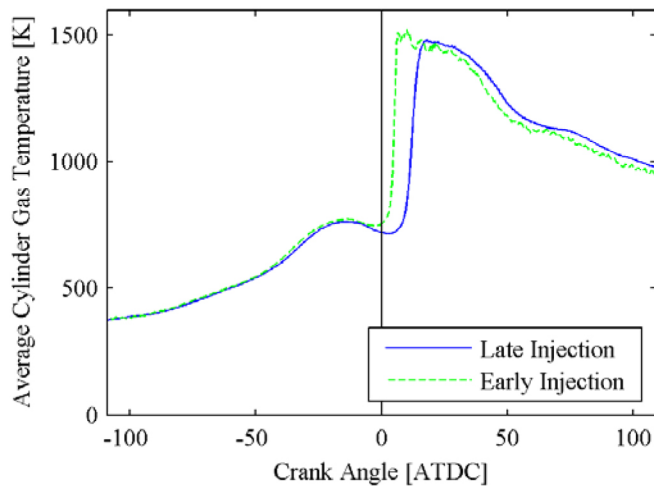


Figure 22. Cylinder bulk gas average temperature for start of injection at 21 and 17 degrees BTDC shown in green and blue respectively. 4000 rpm and 350 kPa bmep.

Early injection results in early combustion and hence a high effective expansion ratio which is favorable for the efficiency but the average in-cylinder temperature is high which results in increased heat losses to the walls. Late injection results in the opposite effects. Optimal injection timing is represented by the timing that produces the best compromise between these effects. For the operating point 4000 rpm and 350 kPa bmep, which is shown in Figure 19, this optimum occurs at 19 degrees BTDC. The experiments with injection timing indicate one of the challenges with PCI operation. In contrast to HCCI operation PCI operation is possible at all speeds and loads because fuel injection occurs late in the compression stroke and ignition timing is thus easier to control. But the fact that all the fuel is injected before ignition occurs removes direct control of the heat release rate. Early injection results in knocking combustion due to excessive pressure rise rates. Late injection gives the best engine efficiencies and smoothest operation but moving the fuel injection event only a few crank angle degrees later will result in misfires. Thus in terms of controllability the engine concept presented here is significantly better than HCCI but not as benign as the traditional diesel engine.

ENGINE MAPS

Indicated efficiency, brake efficiency and brake specific emissions are given in the form of engine maps for engine speeds ranging from 2000 to 5000 rpm and engine load ranging from idle to full load. The maps shown in Figures 23, 24, 25, 26, 27, 28 were made using the asymmetric cylinder head that gave best overall engine efficiency.

Performance Maps

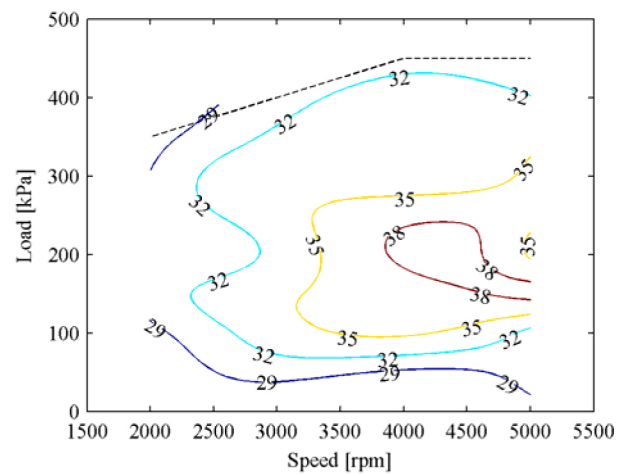


Figure 23. Indicated efficiency in percent

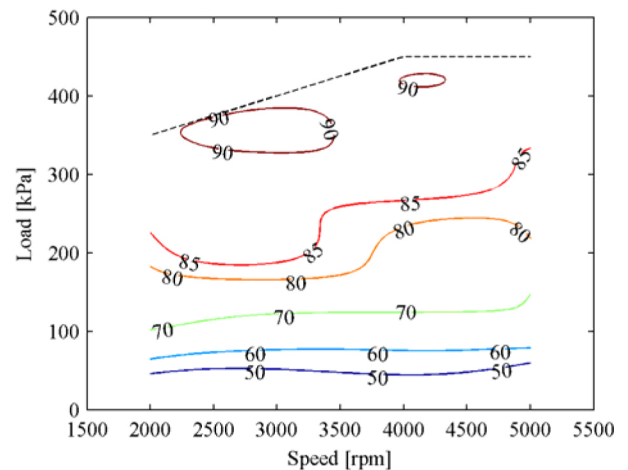


Figure 24. Mechanical efficiency in percent

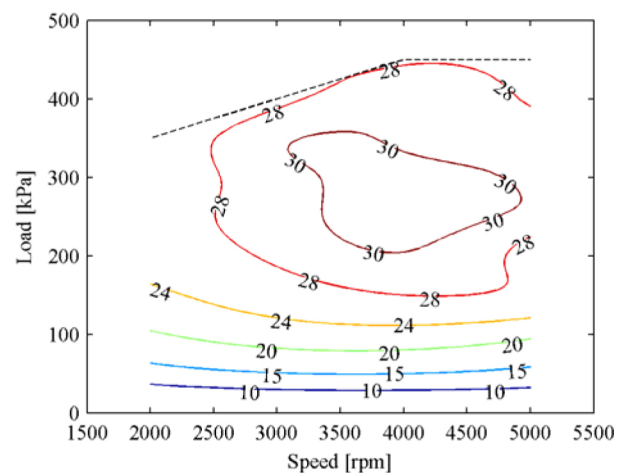


Figure 25. Engine brake efficiency in percent

Figure 25 shows that the engine brake efficiency is primarily load dependent. Except for the lowest engines speeds if the engine is operated at or above a bmep of 200 kPa the efficiency is higher than 28%. Also seen in the engine maps is the maximum bmep, which peaked at 450 kPa between 4000 and 5000 rpm. This is 46% higher than the maximum bmep achieved with the first engine design. The engine would operate up to 500 kPa, but the limit shown is based on a maximum CO emission of 1% in the exhaust gas. Above this value efficiency and emissions deteriorate fast.

Emission Maps

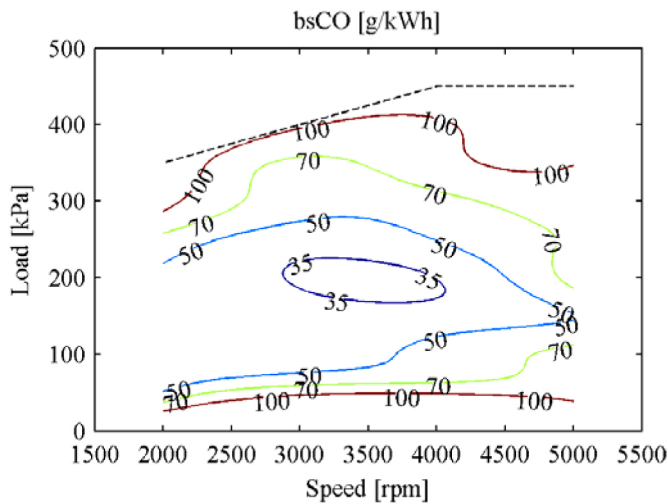


Figure 26. Carbon monoxide emission

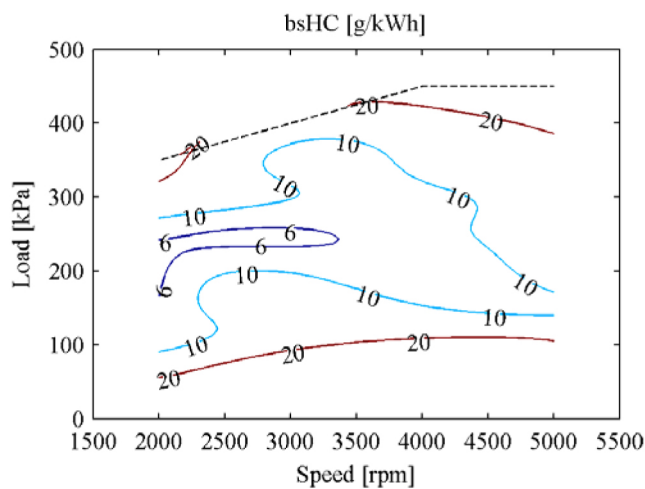


Figure 27. Unburned hydrocarbon emission

The emission maps of carbon monoxide and hydrocarbons were compared to the maps of an air-assisted direct injection SI gasoline two-stroke engine designed by Piaggio [15]. The Piaggio engine has similar size, port timings and layout as the test engine of this study. The emissions of carbon monoxide and hydrocarbons are on approximately the same level as

those of the Piaggio engine. The reference did not report NO_x emissions for the Piaggio engine.

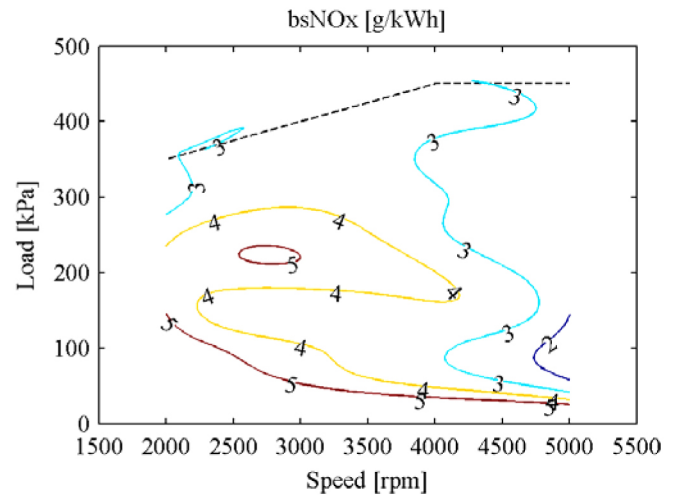


Figure 28. Nitrogen oxide emission

COMPARISON TO EU EMISSION LIMITS

The emissions were compared to the emission standards currently in force in the EU. Since only hot steady state testing of the test engine mounted in a dynamometer had been performed it was decided to compare with the emission standard valid for non-road engines (Stage III A). Assuming that the test engine is applied to drive an electric generator at 3000 rpm the five mode points that are given in the D2 test cycle of the ISO 8178 standard can be defined. Multiplying the measured emissions at each mode point with the given weighting of the mode points results in the values presented in Figure 29.

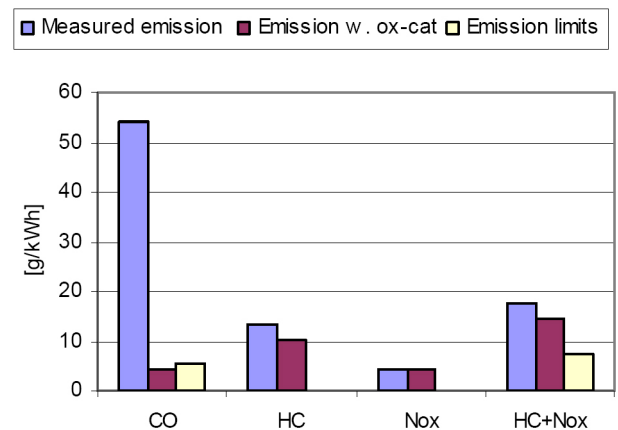


Figure 29. Comparison to EU emission limits with and without oxidation catalyst.

Figure 29 shows that the engine out carbon monoxide emission is a factor of ten higher than the emission limit. The sum of hydrocarbons and NO_x is also above the emission limit but only by about a factor of two. Clearly the engine could not be used without a catalyst. The effect of an oxidation catalyst was not tested but estimated by multiplying the measured emissions with the conversion efficiencies of an oxidation catalyst given as a function of exhaust gas temperature in [15]. Doing that shows that carbon monoxide can be reduced to a value below the emission limit. Unfortunately this is not the case for the combined hydrocarbons and NO_x emissions. The oxidation catalyst cannot reduce NO_x emissions and has poor conversion efficiency for hydrocarbons at the low exhaust gas temperatures of the test engine that range from 100 to 350 degrees Celsius. A fundamental question of this study was whether engine out NO_x emissions would be very low. Figure 28 and Figure 29 show that NO_x emission are low but still of the same order of magnitude as current emission legislation in the EU. The low levels obtainable in true HCCI operation are not achieved. This indicates that despite the fast fuel delivery and long ignition delays the premixing that occurs before ignition is not sufficient to reduce NO_x formation to the levels expected in HCCI-mode. Particulate emissions were not measured but visual inspection did not reveal any smoke formation.

PERFORMANCE IN A VEHICLE

In order to test the performance of the engine in vehicle conditions it was mounted in a car that participated in the Shell Eco-Marathon 2009. The Shell Eco-Marathon is a fuel economy competition for universities held annually in Germany. The engine was operated at constant load but varying speed, a method called “coast & burn”. While coasting the engine is turned off and while burning the engine is run at peak efficiency load while accelerating the vehicle. This method is used by all competitive participants using internal combustion engines in order to avoid running the engines at a low mechanical efficiency at the parts of the circuit that require little or no power to propel the vehicle. The car using the engine presented in this paper won the Urban Concept car competition with 589 km/liter (gasoline energy equivalent) as the result. Second place was awarded to a car with a four-stroke gasoline engine; their result was 343 km/l. The vehicles are not identical but they are built according to the same competition rules and vehicle mass, frontal area and drag coefficient for the two vehicles are very similar. The practical result reflects the high measured efficiency of the test engine.

CONCLUSION

The concept of a small two-stroke engine operating on dimethyl ether has been explored. The present study was conducted because a first prototype engine, described in an

earlier publication on the subject [10], had disappointing performance. A second version, also a 50cc crankcase scavenged two-stroke engine with direct injection of DME, was therefore developed and tested. The air flow of the engine was significantly improved by the application of a reed valve intake arrangement and a tuned expansion chamber exhaust system. Compared to the first version of the engine the improvement of the air flow combined with a new fuel injector resulted in a significant increase in maximum engine torque. Increasing the fuel injection pressure from 100 to 150 bar and applying an asymmetric cylinder head further improved engine performance. At the current state of development the maximum engine torque has increased by 46% relative to the first version of the engine. The new engine can operate up to a brake mean effective pressure of 500 kPa but efficiency and emissions deteriorate greatly above 450 kPa.

Approx. 65% of the charge is burnt in a rapid premixed phase and the remaining 35% of the fuel is burned in a slow mixing controlled phase. In the case of the previous engine version, the ratio between premixed and mixing controlled burn was 50/50. The increase in premixed nearly constant volume combustion was found to be the most significant contribution to the increase in indicated efficiency from 29% to 37%. Despite the use of direct injection late on the compression stroke injection timing is critical and too early injection results in knocking combustion and too late injection results in misfires. At typical operating conditions the injection timing has to be within ± 2 crank angle degrees in order to avoid those phenomena.

The engine was tested from 2000 to 5000 rpm with peak efficiency occurring at 4000 rpm and medium load. Higher engine speeds were not tested but engine power and efficiency are strongly related to engine air flow and tuning intake and exhaust system to a higher engine speed would most likely provide for increased power outputs at good engine efficiency because the premixed combustion is very fast.

Brake efficiency peaks at just above 30%. At loads above 200 kPa bmep and speeds higher than 2500 rpm the efficiency is higher than 28% providing a wide operating range at high engine efficiency. Practical experience with the engine mounted in a vehicle built for a fuel economy competition showed that the engine efficiency is superior to that of four-stroke spark ignition engines of similar size. By now the performance level of the engine corresponds to the initial expectations for the engine concept.

While engine-out NO_x emissions are low, compared to traditional diesel engines, they are still of the same order of magnitude as current emission limits for stationary engines in the EU. As is the case for HCCI engines carbon monoxide

and unburned hydrocarbons emissions were significantly higher than for traditional diesel engines. An oxidation catalyst could be considered. Such a catalyst would be effective in removing most of the carbon monoxide but due to the quite low exhaust gas temperatures effective hydrocarbon oxidation could be difficult to achieve. Future combustion

development should focus on the reduction of engine-out emission of hydrocarbons and/or oxidation catalyst performance with respect to hydrocarbons. If the HC emissions could be removed the combined HC and NO_x emissions would be below emission limits.

Table 8. Measurement equipment

| Measurement | Range | Type | Model |
|--------------------|-----------------|---------------------|---------------------|
| Torque | 0 - 10Nm | Strain gauge | HBM T22 |
| Crank position | 720 pulses/rev. | Optical | Scancon 2R720 |
| Cylinder pressure | 0 - 250 bar | Piezoelectric | Kistler 6052CU20 |
| Air flow | 0 - 400 SLPM | Hot-wire anemometer | Honeywell AWM720P1 |
| Crankcase pressure | 0 - 5 bar | Piezoresistive | Kistler RAG25A5VB1H |

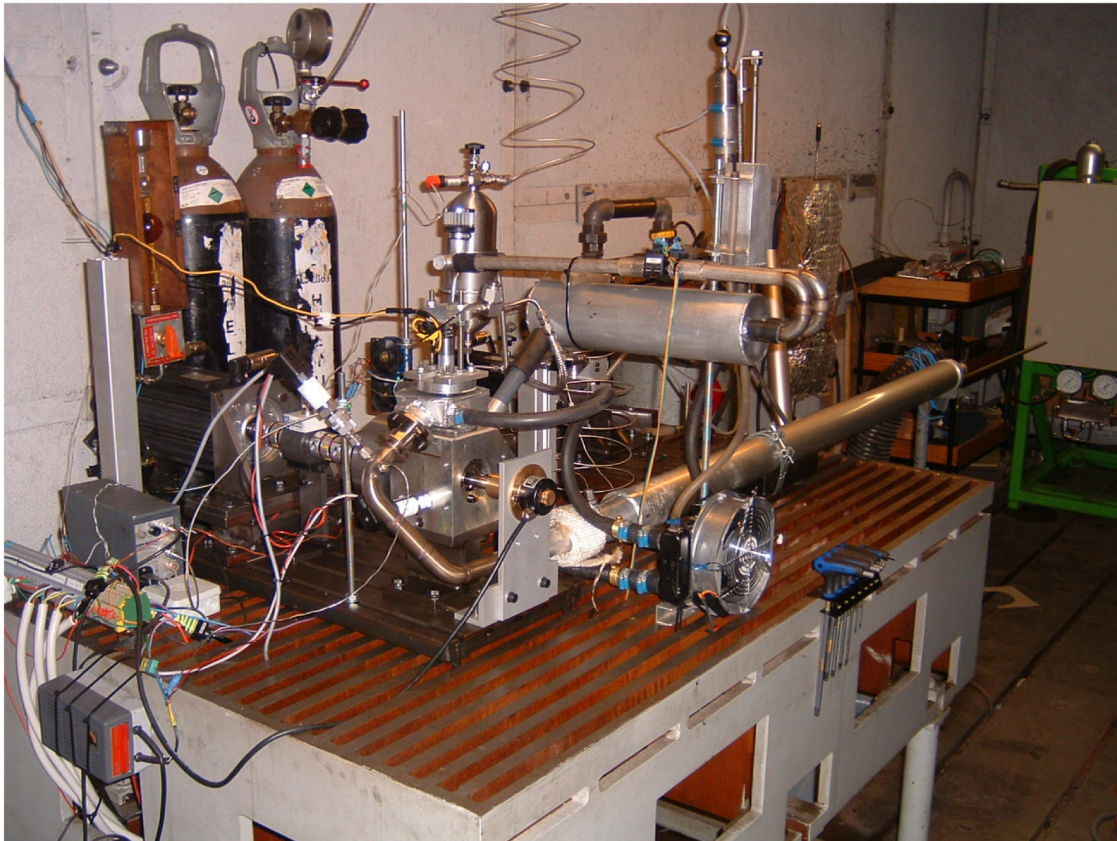


Figure 30. Engine test setup

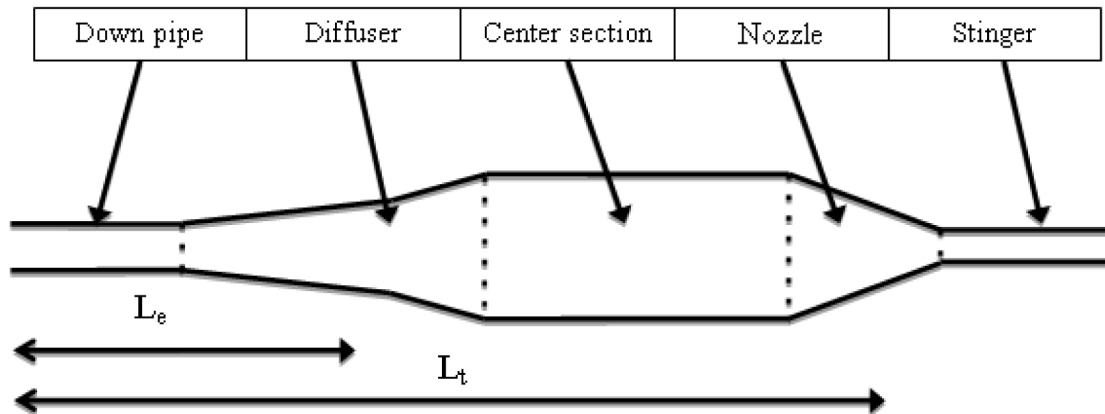


Figure 31. Principal sketch of an expansion chamber exhaust system

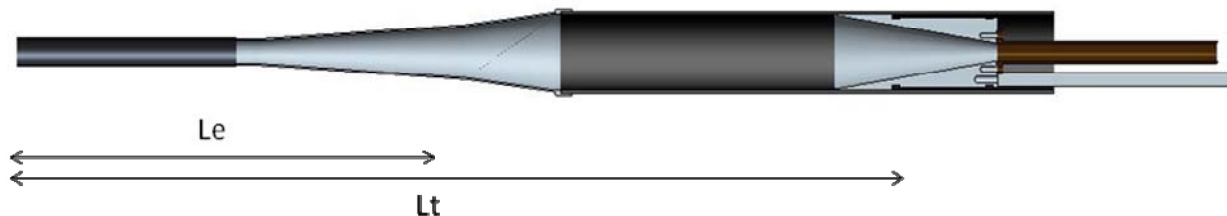


Figure 32. Actual expansion chamber design

REFERENCES

1. Arcounianis, C., Bae, C., Crookes, R., and Kinoshita, E. "The potential of di-methyl ether (DME) as an alternative fuel for compression-ignition engines: A review", *Fuel*. 87:1014-1030, 2008.
2. Egnell, R., "Comparison of Heat Release and NO_x Formation in a DI Diesel Engine Running on DME and Diesel Fuel," SAE Technical Paper 2001-01-0651, 2001, doi: 10.4271/2001-01-0651.
3. Zhang, J. J., Huang, Z., Wu, J. H., Qiao, X. Q., and Fang, J. H. "Combustion and performance of heavy-duty diesel engines fuelled with dimethyl ether", *Proceedings of the Institution of Mechanical Engineers Part D-Journal of Automobile Engineering*. 222:1691-1703, 2008.
4. Chen, Z. L., Konno, M., and Kajitani, S. "Performance and emissions of DI compression ignition engines fueled with dimethyl ether (Performance and emissions in retrofitted engines)", *Jsme International Journal Series B-Fluids and Thermal Engineering*. 43:82-88, 2000.
5. Sato, Y., Nakamura, A., Takada, Y., and Nakamura, K., "Development of DME Vehicles and Strategy of Practical Use Penetration", *Society of Automotive Engineers of Japan, Inc., Tokyo, Japan Technical Paper 2008-08-0165*, 2008.
6. DIRECTIVE 98/70/EC OF THE EUROPEAN PARLIAMENT AND OF THE COUNCIL. "Relating to the quality of petrol and diesel fuels and amending Council Directive 93/12/EEC", 1998L0070. 2009.
7. Zhang, W. N. "Automotive fuels from biomass via gasification", *Fuel Process Technol.* 91:866-876, 2010.
8. Consonni, S., Katofsky, R. E., and Larson, E. D. "A gasification-based biorefinery for the pulp and paper industry", *Chemical Engineering Research & Design*. 87:1293-1317, 2009.
9. Semelsberger, T. A., Borup, R. L., and Greene, H. L. "Dimethyl ether (DME) as an alternative fuel", *J.Power Sources*. 156:497-511, 2006.
10. Hansen, K., Nielsen, C., Sorenson, S., and Schramm, J., "A 50cc Two-Stroke DI Compression Ignition Engine Fuelled by DME," SAE Technical Paper 2008-01-1535, 2008, doi:10.4271/2008-01-1535.
11. Gentili, R. and Frigo, S., "What is the Future of the Two-Stroke S.I. Engine," SAE Technical Paper 1999-24-0069, 1999, doi:10.4271/1999-24-0069.
12. Millo, F., Mallamo, F., Arnone, L., Bonanni, M. et al., "Analysis of Different Internal EGR Solutions for Small Diesel Engines," SAE Technical Paper 2007-01-0128, 2007, doi:10.4271/2007-01-0128.

13. Zsiga, G., Kerres, R., Bach, M., and Fuoss, K., “Potential of Expansion Chamber Exhaust Pipes for Two-Stroke Powered Tools,” SAE Technical Paper 2010-32-0011, 2010, doi:10.4271/2010-32-0011.

14. Heywood, J. B., Internal Combustion Engine Fundamentals, McGraw-Hill, Singapore, ISBN 0-07-100499-8:930, 1988.

15. Nuti, M., “Emissions from Two-Stroke Engines”, Air-Assisted Direct Fuel Injection, Society of Automotive Engineers, Inc., Warrendale, U.S.A., ISBN 0-7680-0215-X: 198-203, 1998.

CONTACT INFORMATION

kimrh@mek.dtu.dk

ACKNOWLEDGMENTS

The authors would like to acknowledge the contributions of many members of the mechanical staff at the institute.

DEFINITIONS/ABBREVIATIONS

AHR

Accumulated Heat Release

ATDC

After Top Dead Center

BTDC

Before Top Dead Center

CAD

Crank Angle Degrees

CI

Compression Ignition

CR

Compression Ratio

fumep

$$fumep = \frac{m_f \cdot H_u}{V_d}$$
, where fumep denotes fuel mean effective pressure, mf denotes mass of fuel injected, Hu denotes fuel lower heating value, and Vd denotes the engine displacement volume.

GDI

Gasoline Direct Injection

HCCI

Homogeneous Charge Compression Ignition

ID

Inner Diameter

mep

Mean Effective Pressure

PID

Proportional, Integral, Differential (regulator)

PCI

Premixed Compression Ignition

R_d

Delivery ratio

SI

Spark Ignition

SLPM

Standard Liters Per Minute

\dot{m}_{air}

Mass flow of air into the engine intake

$\dot{m}_{air\ trapped}$

Mass flow of air trapped in the engine cylinder

ρ_{atm}

Density of air at the intake of the engine

V_d

Engine displacement

N

Engine speed in revolutions per minute

The Engineering Meetings Board has approved this paper for publication. It has successfully completed SAE's peer review process under the supervision of the session organizer. This process requires a minimum of three (3) reviews by industry experts.

All rights reserved. No part of this publication may be reproduced, stored in a retrieval system, or transmitted, in any form or by any means, electronic, mechanical, photocopying, recording, or otherwise, without the prior written permission of SAE.

ISSN 0148-7191

Positions and opinions advanced in this paper are those of the author(s) and not necessarily those of SAE. The author is solely responsible for the content of the paper.

SAE Customer Service:

Tel: 877-606-7323 (inside USA and Canada)

Tel: 724-776-4970 (outside USA)

Fax: 724-776-0790

Email: CustomerService@sae.org

SAE Web Address: <http://www.sae.org>

Printed in USA

SAEInternational®